University of Sheffield

Department of Civil and
Structural Engineering

Dispersion of Solutes in Sinuous Open Channel Flows

Ph.D. Thesis

Author: **Joseph B. Boxall**

Submitted: **May 2000**

Accepted: **2000**

Keywords

Pollution, Rivers, Mixing, Dispersion

Abstract

The research undertaken for this Ph.D. thesis concerns the dispersion of solutes in sinuous open channel flows. The aim of the work is to address the void in knowledge and understanding of mixing and transport processes in natural watercourses. The influences of plan form curvature and non-uniform cross sectional shape on transverse and longitudinal mixing are specifically addressed.

Experimental work was undertaken on the Flood Channel Facility at HR Wallingford Ltd. This involved creating a pseudo natural sand channel within the concrete meander plan form of the facility, and then stabilising the form. Tracer studies using instantaneous injection to investigate longitudinal mixing and continuous point source release to study transverse mixing were performed. Fluorescent tracer was used. Measurement was by six Turner Design Field Fluorometers in pump through mode and these were digitally logged. Detailed hydrodynamic measurements were made using a two-dimensional Laser Doppler Anemometer (LDA) fitted with a 14mm fibre-flow probe.

The resulting data has undergone robust analysis and detailed interpretation. The conclusions are that the dominant processes in mixing, in the natural channel form studied, are shear effects. Simple equations for the prediction of flow fields have been investigated and validated against LDA measurements. It has been possible to make accurate predictions of the transverse and longitudinal mixing coefficients from the predicted flow fields. These predictions have been shown valid for the variations in mixing coefficients over the meander cycle and with discharge.

Contents

List of Figures

List of Tables

Notation

A	area
b	channel width
C	Chezy coefficient
c	concentration
D_q	transverse dispersion coefficient in cumulative discharge notation
D_x	longitudinal mixing coefficient
D_f	dispersive fraction
e_m	molecular diffusion coefficient
e_t	turbulent diffusion coefficient
e	diffusion coefficient
g	gravity
h	depth of flow
J	flux
$K_{y/q}$	average transverse mixing coefficient used in Generalised Method of Moments
k_i	dispersion / mixing coefficient
k	roughness height
L	length scale
L_m	Prandtl's mixing length
M	mass
M_i	moment of distribution
m	metric coefficient
n	Manning's coefficient
Q	discharge
q	partial discharge
q_i	partial depth
R	hydraulic radius
Re	Reynolds number
r_c	radius of curvature
S_0	channel slope
T	residence time or temperature
t	time
$\bar{t}$	time of travel
U	cross section average velocity
u	longitudinal velocity
u_t	turbulent velocity
v	transverse velocity
w	vertical velocity
x	longitudinal distance
y	transverse distance
z	vertical distance
$\bar{y}$	centroid of distribution
u^*	bed shear velocity
z_0	bed roughness factor
κ	Von Karman's constant
f	Darcy-Weisbach friction factor
η	depth ratio z/d

ρ	density
τ_0	boundary shear stress
τ	viscous shear stress, or time delay
μ	mean
σ^2	variance
ν	kinematic viscosity
ν_t	eddy viscosity
φ	function of transverse variation
ν_t	eddy viscosity
Γ	volumetric mass transfer coefficient

Scripts

g	of gas
j	zone of interest
m	ensemble mean
x,y,z	component in associated direction
$'$	deviation from mean
$\langle\ \rangle$	average

Chapter 1 Introduction

Clean water has been dubbed 'the white oil of the 21st Century' and 'liquid gold'. Once considered a birth right, fresh water is now one of the most prized environmental assets in the world. The World Bank estimate that by the year 2025 the numbers of people facing water scarcity will rise from 1.2 to 3 billion.

- two thirds of people will live in water-stressed conditions,
- 70% of agricultural land will need to be irrigated,
- 15% of all nations will receive more than 50% of their water from upstream neighbours,
- Afghanistan, Egypt, Saudi Arabia, Pakistan, Israel, Jordan, Iran, Iraq, Kuwait, Syria, Tunisia, United Arab Emirates, Yemen, Singapore, South Africa, Oman, Libya, parts of India and China will face 'absolute water scarcity'.

Engineering to help realise fresh water supply opportunities is essential to modern society. Serious attention is required to minimise the impact of water pollution to downstream users.

The demands on water and watercourses are ever increasing. There is a serious need to improve the quality and accuracy of predictive water quality models, particularly pollutant processes, in natural watercourses. Addressing pollution in natural watercourses is an extremely complex task and the controlling processes are currently highly uncertain, unpredictable and economically uncontrollable. It is imperative for the survival of the modern world that there is considerable improvement in the understanding, management and use of our natural water resources. In recent environmentally aware times, because of public awareness and pressure, research in this area has been driven by water quality issues.

There is a growing need to better understand the fate of pollutants once they have entered natural watercourses. A waste discharge engineer must be able to quantify effluent mixing to be able to design and operate outlet structures that comply with water pollution criteria. Water resource scientists need to understand river mixing to monitor whether outfalls comply with their permits, and to design sensible chemical and biological monitoring systems. A fisheries scientist needs to consider the mixing of effluents and tributary inflows to predict their effects on fish stocks. The biologist wishes to predict, and quantify, the rate of mass transfer between the bed and the overlying flow to predict concentrations in pore water and overlying river water. Even short-term exposure to relatively low pollution concentrations can be damaging to microinvertebrate organisms. Hence, even intermittent Combined Sewer Overflow (CSO) discharges can have a significant impact on river ecology.

Once a pollutant enters a watercourse there are considered to be three fundamental processes at work which spread and mix the pollutant with the river water.

- Advection. The bodily movement of a parcel of fluid by the flow regime.
- Diffusion. Either molecular or turbulent, is the result of random short term fluctuations.
- Dispersion. Not a physical property of the flow, but an approximation to account for shear effects in depth or width averaged models.

The mechanics of river mixing defy complete mathematical description. Consequently, few mixing problems can be solved exactly using purely theoretical methods. There are, however, a number of simplifications and semi-empirical techniques that lead to approximate models for a number of important river mixing problems. These semi-empirical models need to be calibrated using field or laboratory data to check their validity and to evaluate model coefficients.

There are a few 'simple' requirements for water quality work, the prediction of the location, concentration and change with time of pollutants, see Figure 1.1. There are several types of model available based on various mathematical principles, but they all have the fundamental requirement of the specification of mixing coefficients which in some way define the rate of mixing.

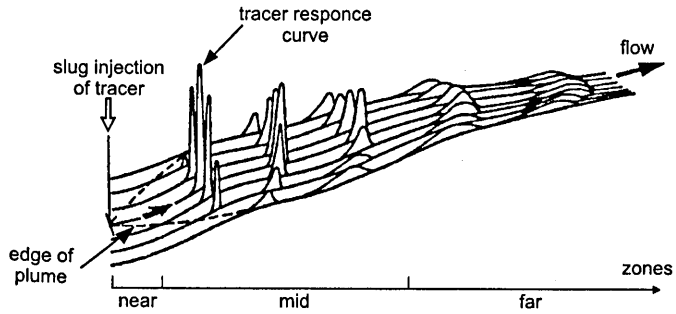

zone	dominant mixing
near field	vertical
mid field	transverse
far field	longitudinal

Figure 1.1 Pictorial representation of mixing in a river, highlighting the mixing zones and the dominant processes (adapted from Jobson (1997))

Every situation requires an appraisal of the most critical processes, and simplifying assumptions for models and the required coefficients must be made based on the knowledge of the critical processes. This procedure does not facilitate fast or accurate predictions, it is therefore desirable to improve understanding such that codes and guidelines may be produced to assisted the modeller or engineer.

There is a large gap in understanding over how and why results of experimental studies, which have concentrated on idealised open channel flow conditions, in regular shaped channels, cannot be expanded and applied to field conditions. The objective of this study is to investigate the impact and effects of this transition from idealised laboratory conditions to a natural channel environment. Both transverse and longitudinal mixing will be investigated, and the interdependence of the two processes highlighted. The transverse and longitudinal study will be backed by detailed velocity measurements to give a clear and accurate picture of the flow field. The longitudinal mixing study will be extended to investigate the impact of variations in channel form and discharge. This work is only concerned with neutrally buoyant pollutants.

Chapter 2 Background Theory

At some time in the future it may be possible to predict mixing coefficients from readily available channel and flow characteristics, negating the need for the expensive, and limited, field study calibration of models. The aim of this review is to draw together aspects of pollutant dispersion, with specific relevance to natural river channels, that is channels where plan-form curvature is present, as well as non-uniform bed profiles and roughness. The areas of transverse and longitudinal mixing are of particular interest. The extent of current understanding is examined and areas for investigation suggested.

2.1 Open Channel Flow

Open channel flow is characterised by the existence of a free surface. There are three major classifications of open channel flow:

1. Steady uniform flow in which depth is constant with time and distance.
2. Steady non-uniform flow in which depth varies with distance, but not with time.
3. Unsteady flow, in which the depth varies with both time and distance.

Steady uniform flow rarely occurs in natural channels, strictly the flow is unsteady and varying. Despite this deviation, uniform flow conditions are frequently assumed for flow computation in natural streams. The results obtained are understood to be approximate and general, however they provide a relatively simple solution to many practical problems.

In steady uniform flow gravity forces generated by water travelling down a channel slope are in equilibrium with the resistance forces of drag or shear. The forces between adjacent fluid layers are dependent upon viscosity and the channel boundary roughness.

A number of equations exist to describe flow in open channels. When considering the overall flow there must be continuity along the channel. This means that if there are no inputs or outputs along the channel, the discharge must remain constant. Considering this in the primary flow direction yields the continuity equation:

$$Q = UA \qquad \text{Equation 2.1}$$

here Q is discharge (m^3/s), A cross section area (m^2), and U cross section average longitudinal velocity (m/s).

In typical open channel flow the total energy level decreases in the downstream direction. This is due to the presence of flow resistance generated from the fluid viscosity and drag against the solid boundaries. The resistance generates a spatially varying velocity distribution. To explain this, envisage the flow as a series of adjacent layers. The layer immediately adjacent to the boundary is considered to adhere to the boundary and become stationary. Subsequent layers are slowed by a shearing action with the adjacent layers. The shear reduces with distance from the boundary, until some point where the boundary effect is negligible. The distance between the boundary and this point is defined as the boundary layer. The ideal definition of uniform flow is not accurate when spatial variations in flow conditions exist. Uniformity in open channel flows is therefore defined as no variation in average flow conditions in the longitudinal direction.

Open channel flows can be either laminar or turbulent, depending upon the fluid viscosity and the boundary roughness. A turbulent flow is defined as a flow that is not constant with time, but instead contains rapid random fluctuations. These fluctuations are generated by the presence of rotational motions and eddies occurring independently of the primary flow which promote the transfer of fluid mass between adjacent layers. In laminar flow, the fluid layers remain independent of each other and the velocity does not fluctuate with time. A turbulent flow can be defined as uniform provided the mean velocity values remain constant with time. Within the boundary layer the local velocity approaches zero, therefore, a laminar flow area is present close to the channel boundaries.

When considering the overall flow conditions within open channels, a balance of forces between gravity and friction can be applied to derive equations of motion.

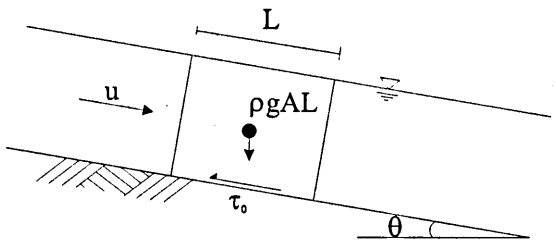

Figure 2.1 Force diagram for derivation of uniform flow equations

This derivation produces an expression for the mean boundary shear stress, see Chadwick and Morfett (1994):

$$\tau_0 = \rho g R S_0 \qquad \text{Equation 2.2}$$

where τ_0 is boundary shear stress (kg/ms^2), ρ density (kg/m^3), g acceleration due to gravity (m/s^2) R hydraulic radius (m), and S_0 channel slope (-).

From this the bed shear velocity may be defined as:

$$u^* = \sqrt{\frac{\tau_0}{\rho}} = \sqrt{gRS_0} \qquad \text{Equation 2.3}$$

where u* is bed shear velocity (m/s). Bed shear velocity is a measure of the shear stress and the velocity gradient near the bed.

In rough turbulent flow, bed shear velocity is proportional to velocity squared. Incorporating this relationship into Equation 2.2 yields:

$$U = C\sqrt{RS_0} \qquad \text{Equation 2.4}$$

This is known as Chezy's equation, Chadwick and Morfett (1994). C is the Chezy coefficient, which is dependent on both Reynolds number and the boundary roughness. Values for C can be obtained by an analogy with the Darcy-Weisbach friction factor. Alternatively, C can be estimated from the relationship:

$$C = \frac{R^{1/6}}{n} \qquad \text{Equation 2.5}$$

where n is a constant referred to as Manning's n. This is a coefficient which represents the roughness of the channel bed. Substituting Equation 2.5 into Equation 2.4 yields:

$$u = \frac{1}{n} R^{2/3} S_0^{1/2} \qquad \text{Equation 2.6}$$

This is known as Manning's equation. The value of n is an empirical value, which can be obtained for different channel conditions from tables such as those in Chadwick and Morfett (1994).

2.2 *Mixing Theory*

When a tracer is introduced into a river, advection carries it away from the source. The tracer is also spread by diffusion and / or dispersion. Advection is the bodily movement of a parcel of fluid resulting from an imposed current. The effects of diffusion have two fundamental bases, molecular diffusion and turbulence. When considering depth and / or width averaged forms of the equations describing diffusion and advection, it is necessary to take account of the effects of velocity shear. This is done through the inclusion of a dispersion term and is not a direct physical property of the flow.

Consider a body of fluid (the receiving fluid) into which a small volume of a second 'tracer' fluid is injected. The tracer is neutrally buoyant. If the receiving fluid is at rest, the tracer will gradually spread due to the effects of molecular diffusion. This process is very slow, for example a source of dye a few millimetres in diameter injected into a still body of water will take about 24 hours to disperse through a 1 metre diameter. If the receiving body of fluid is flowing and turbulent then a powerful diffusion process is present as well the effect of advection, the bodily movement of the pollutant by the flow regime. The processes of advection and turbulent diffusion are of a similar order of magnitude, while molecular diffusion is normally several orders of magnitude smaller, and is therefore often neglected, or included in a catch all term. Smith (1992) suggests the relative magnitudes of these processes.

Molecular diffusion	10^{-10} to 10^{-9} m^2/s
Turbulent eddy diffusion	10^{-3} to 10^{-1} m^2/s
Shear dispersion coefficients	1 to 10^{3} m^2/s

Table 2.1 Relative mixing rates, from Smith (1992)

Any comprehensive theory of mixing and dispersion processes in natural watercourses must include a number of complex factors such as turbulence, velocity gradients, secondary flow, and other non-uniformities that are associated with natural open channel flows.

The mixing of non-neutrally buoyant tracers and particles is not considered in this work.

2.2.1 Derivation of the advection diffusion equation

In 1855, the German scientist Fick drew an analogy between the diffusion of salt in water and the diffusion of heat along a metal rod. He hypothesised that the rate of transfer of tracer should be proportional to the concentration gradient between two regions. In a one-dimensional form this is:

$$J_x = -e_m \frac{\delta c}{\delta x} \qquad \text{Equation 2.7}$$

where J_x is mass flux (kg/m^2s) in the x direction, c is concentration (kg/m^3), and e_m (m^2/s) is the molecular diffusion coefficient. This is a mathematical statement of Fick's first law. It can be expanded in all co-ordinate directions. The negative sign denotes diffusion from areas of high concentration to areas of lower concentration.

If the ideas of conservation of mass are incorporated into the diffusion process, it is possible to derive a second descriptive relationship. A one-dimensional situation will be dealt with at present for the purpose of simplicity. Consider a parcel of fluid within a stagnant body of water, Figure 2.2.

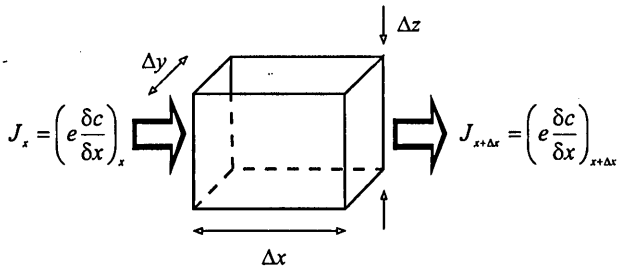

Figure 2.2 Diffusive flux into and out of small fluid element

As tracer passes through the surfaces the concentration within the parcel changes. Over a small time period this change can be written as:

$$\frac{(c_{t+\Delta t} - c_t)}{\Delta t}\Delta x \equiv \frac{\delta c}{\delta t}\Delta x \qquad \text{Equation 2.8}$$

where c_t and $c_{t+\Delta t}$ are tracer concentration within the parcel at times t and Δt respectively.

By considering conservation of mass along the x-axis, it must hold true that the rate of change of mass given by Equation 2.8 must equal the net diffusive flux into and out of the parcel. This change in flux can be written as:

$$J_{x+\Delta x} - J_x \equiv \frac{\delta J}{\delta t}\Delta x \qquad \text{Equation 2.9}$$

Equating Equation 2.8 and Equation 2.9 yields:

$$\frac{\delta c}{\delta t} + \frac{\delta J}{\delta x} = 0 \qquad \text{Equation 2.10}$$

This combined with Fick's first law gives:

$$\frac{\delta c}{\delta t} - \frac{\delta}{\delta x}\left(e_m \frac{\delta c}{\delta x}\right) = 0 \qquad \text{Equation 2.11}$$

The diffusion coefficient may be assumed constant with distance, such that Equation 2.11 becomes:

$$\frac{\delta c}{\delta t} = e_m \frac{\delta^2 c}{\delta x^2} \qquad \text{Equation 2.12}$$

This relationship defines the transport of mass by a Fickian diffusion process and is know as the diffusion equation. However, Equation 2.12 is not sufficient to describe open channel flow conditions. To extend the situation it is necessary to consider the same parcel within a steady, laminar, open channel flow and to consider all three co-ordinate directions. When this is done and an advective transport term is included, the expression for total flux in each co-ordinate direction can be written as:

$$J_x = uc - e_m \frac{\delta c}{\delta x} \qquad \text{Equation 2.13 a}$$

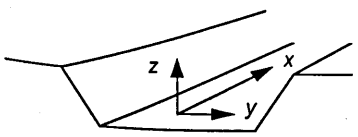

$$J_y = vc - e_m \frac{\delta c}{\delta y} \qquad \text{b}$$

$$J_z = wc - e_m \frac{\delta c}{\delta z} \qquad c$$

where u, v, w are velocity (m/s) in the x, y and z co-ordinates respectively, and uc, vc and wc are the advective flux in each direction (kg/m^2s). The change in mass within the parcel can now be expressed as:

$$\frac{\delta c}{\delta t}\Delta x\Delta y\Delta z \qquad \text{Equation 2.14}$$

Next, consider the net flux in each co-ordinate direction:

$$(\text{netflux})_x = \left(\frac{\delta J_x}{\delta x}\Delta x\right)\Delta y\Delta z \qquad \text{Equation 2.15 a}$$

$$(\text{netflux})_y = \left(\frac{\delta J_y}{\delta y}\Delta y\right)\Delta x\Delta z \qquad b$$

$$(\text{netflux})_z = \left(\frac{\delta J_z}{\delta z}\Delta z\right)\Delta x\Delta z \qquad c$$

The total flux is equal to the summation of the terms in Equation 2.15. As previously stated this change in net flux must be equal to the change in concentration within the parcel. Therefore, combining Equation 2.14 and Equation 2.15 yields:

$$\frac{\delta c}{\delta t} + \frac{\delta J_x}{\delta x} + \frac{\delta J_y}{\delta y} + \frac{\delta J_z}{\delta z} = 0 \qquad \text{Equation 2.16}$$

Then substituting the expressions for flux from Equation 2.13 produces:

$$\frac{\delta c}{\delta t} + u\frac{\delta c}{\delta x} + v\frac{\delta c}{\delta y} + w\frac{\delta c}{\delta z} = e_m\left(\frac{\delta^2 c}{\delta x^2} + \frac{\delta^2 c}{\delta y^2} + \frac{\delta^2 c}{\delta z^2}\right) \qquad \text{Equation 2.17}$$

This is known as the 'advection diffusion' equation, and is quoted in nearly all literature in this area. It is the form of the equation presented by Fischer *et al.* (1979), and Rutherford (1994). It should be noted that in this form, no account has yet been made for any turbulence effects, and that the molecular diffusion coefficient, e_m is assumed homogeneous in each co-ordinate direction.

2.2.2 Some properties of the ADE equation and concentration distributions

There are many solutions to the above equation, dependent upon the boundary conditions and release conditions. The solution for an instantaneous release into an isotropic unbounded flow is of the form:

$$c(x,y,z,t) = \frac{M}{(4\pi e_m t)^{3/2}} \exp\left(-\frac{(x-ut)^2 + (y-vt)^2 + (z-wt)^2}{4e_m t}\right) \qquad \text{Equation 2.18}$$

The solution of the above equation at any given time, distributed along the x, y or z axis is a Gaussian, or 'bell-shaped' curve, Figure 2.3.

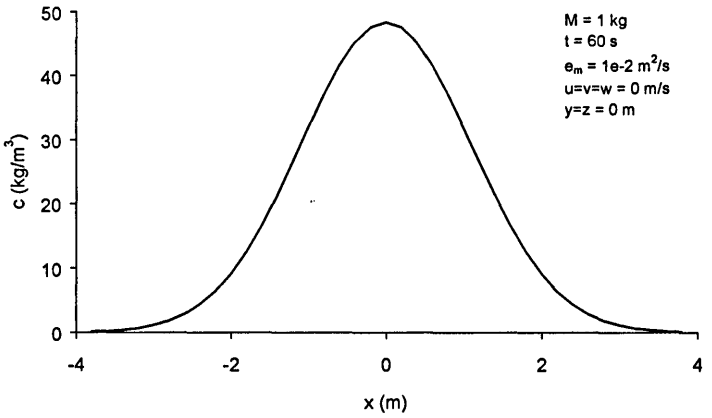

Figure 2.3 Tracer distribution predicted from Equation 2.18

The moments of such a distribution can be found:

$$M_0 = \int_{-\infty}^{\infty} c(x,t)dx \qquad \text{Equation 2.19 a}$$

$$M_1 = \int_{-\infty}^{\infty} xc(x,t)dx \qquad \text{b}$$

$$M_2 = \int_{-\infty}^{\infty} x^2 c(x,t)dx \qquad \text{c}$$

$$\vdots$$

$$M_p = \int_{-\infty}^{\infty} x^p c(x,t)dx \qquad \text{d}$$

Properties of the distribution can then be found from the moments, the mean μ and the variance σ^2.

$$\mu = M_1 / M_0 \qquad \text{Equation 2.20}$$

$$\sigma^2 = M_2 / M_0 - \mu^2 \qquad \text{Equation 2.21}$$

It can be shown for Equation 2.18 that:

$$\sigma_x^2 = \sigma_y^2 = \sigma_z^2 = 2e_m t \qquad \text{Equation 2.22}$$

It is a feature of Equation 2.17 that the variance increases linearly with time. Elder (1959) was the first to prove experimentally that the rate of increase in variance of a tracer with distance is linear for open channel flow. Therefore, Equation 2.22 can be re-written:

$$e_i = \frac{1}{2}\frac{\Delta\sigma_i^2}{\Delta t} = \frac{1}{2}\frac{\sigma_i^2(t_2) - \sigma_i^2(t_1)}{(t_2 - t_1)} \qquad \text{Equation 2.23}$$

where subscript i denotes co-ordinate direction. This can be rendered more practical by consideration of velocity and distance, rather than time. To calculate a transverse mixing coefficient from field measurements below a steady source, Equation 2.23 can be rewritten to become:

$$e_y = \frac{u}{2}\frac{\sigma_y^2(x_2) - \sigma_y^2(x_1)}{(x_2 - x_1)} \qquad \text{Equation 2.24}$$

This is known as the method of moments.

There are several restrictions on the use of these equations, care should be taken when applying them, especially to river mixing situations:

1. tracer diffusion must obey Fick's law with a constant rate;
2. tracer must not impinge on either bank;
3. for the above case, the tracer source must be steady;
4. the channel must be uniform so that the plume does not expand and contract with changes in bathymetry.

It is apparent from the limits of integration that the complete transverse tracer profile must be measured. This creates practical difficulty as the variance estimates are greatly affected by experimental errors in concentration measurements. At the edges of the tracer profile where c is small, but the lever arm squared is large, it is possible to obtain large errors in the estimation of second moment, and variance.

Another important feature of the ADE equation is that it is linear, so that solutions can be superimposed to account for reflections from channel boundaries, or from multiple releases.

2.3 *Turbulence*

So far, the situation considered has been one of laminar flow. However, the majority of open channel flows are turbulent in nature, except in the viscous sub-layer near the bed. Therefore, the role of turbulence must be addressed.

Turbulence and its relevance to mixing problems were first examined by Reynolds in 1895. He noted that a steady point source of dye release into a laminar pipe flow resulted in a single ribbon of dye along the pipe. The same source in a turbulent pipe flow results in rapid transverse and vertical mixing within the pipe. This is due to turbulent flow possessing random unsteady components. Turbulent flow may be defined by a Reynolds number:

$$\mathrm{Re} = \frac{uL}{\nu} \qquad \text{Equation 2.25}$$

where Re is Reynolds number, L turbulence length scale (m), defined as hydraulic radius or flow depth for open channel flow, and ν kinematic viscosity (m^2s^{-1}).

Turbulent flow is characterised by random short-term fluctuations about a steady mean. Figure 2.4 shows time domain traces of turbulent and laminar velocity measurements.

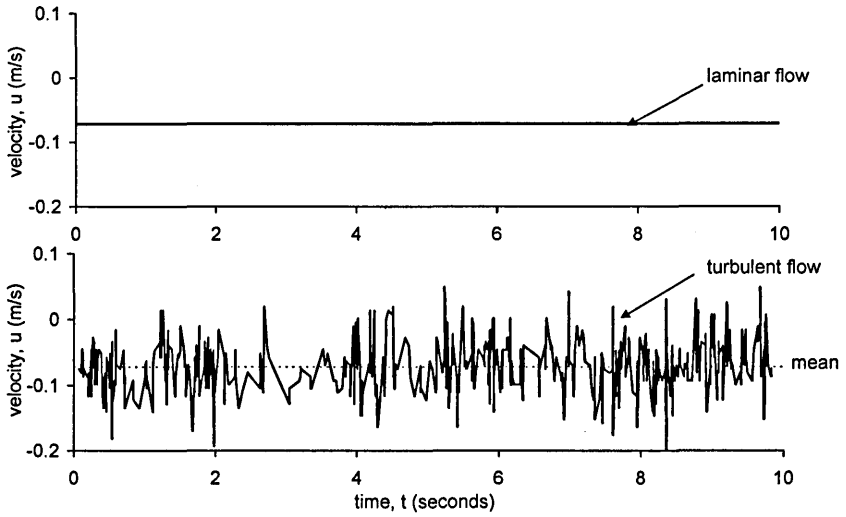

Figure 2.4 Examples of laminar and turbulent time domain velocity traces

In laminar flow particles follow predictable and repeatable paths. In turbulent flow, each particle follows a highly irregular path, particles with the same origin follow significantly different routes. If spectral analysis is carried out on time domain turbulent data then peaks are evident at characteristic length scales, provided that the full turbulence data has been collected at a sufficient data rate. These peaks relate to the scale of eddies present within the flow, the largest of which often occur at a scale similar to the depth to width ratio of the channel.

Turbulence is non-self-sustaining, in the absence of energy input the flow will revert to laminar flow conditions. In open channel flow energy is input from gravity. Turbulence is generated from velocity shear, hence turbulence is large at high shear areas such as bed irregularities and obstructions. Energy enters at the largest length scales and dissipates down to smallest eddies, finally being dissipated as heat energy. It is the largest eddies which have the greatest effect on momentum and mass transfer within the flow.

Although the presence of turbulence does not inherently cause greater mixing, the fluctuations in flow direction and magnitude cause differential advection, creating magnified concentration gradients, and therefore accelerating molecular diffusion.

Complete description of turbulence structures is very complex and requires solution of the Navier-Stokes equations for all three co-ordinate directions. The Navier-Stokes equations are derived from the continuity equations, but have intractable solutions.

It is theoretically possible to model turbulent flows with Equation 2.17, since the mechanism causing mixing is still driven by molecular diffusion. However, a very detailed evaluation of velocities both temporarily and spatially would be essential. Each tracer particle would have to be modelled individually, and then the mean concentration distribution calculated by means of superposition. This is due to the random nature of the flow, which causes each particle to follow a different path. Advances in computation power means that this is becoming possible, but requires very detailed accurate parameter definition, and simulations are time consuming to run. However, it is considered impractical given the requirements of speed and simplicity in modelling spills and accidental discharge.

Reynolds suggested that in turbulent flow velocities and concentrations can be expressed as:

$$u = u_m + u' \qquad \text{Equation 2.26}$$

where u is an instantaneous observed velocity, u_m temporal mean velocity, and u' deviation from the mean velocity.

It is necessary to define the mean as the ensemble mean, that is, the mean of a number of observations such that the results are independent of each other, and unbiased to the previous result. Good approximations of the ensemble mean can be obtained from temporal measurements, provided the time period for averaging is much greater than largest eddy scale. This definition can be applied to both velocity and concentration data. It is important to note that concentrations predicted by turbulence models are ensemble mean values, and that the peak instantaneous concentration may be significantly higher due to the fluctuating component. It should also be noted that the fluctuations from the mean value of a concentration are a function of the position within the plume.

The expression given in Equation 2.26 can be substituted into Equation 2.17 to yield:

$$\frac{\delta(c_m + c')}{\delta t} + (u_m + u')\frac{\delta(c_m + c')}{\delta x} + (v_m + v')\frac{\delta(c_m + c')}{\delta y} + (w_m + w')\frac{\delta(c_m + c')}{\delta z} = e_m\left(\frac{\delta^2(c_m + c')}{\delta x^2} + \frac{\delta^2(c_m + c')}{\delta y^2} + \frac{\delta^2(c_m + c')}{\delta z^2}\right) \qquad \text{Equation 2.27}$$

If Equation 2.27 is then simplified by taking ensemble means and considering continuity it can be shown that:

$$\overset{1}{\frac{\delta c_m}{\delta t}} + \left(u_m \frac{\delta c_m}{\delta x} + v_m \overset{2}{\frac{\delta c_m}{\delta y}} + w_m \frac{\delta c_m}{\delta z}\right) = e_m\left(\frac{\delta^2 c_m}{\delta x^2} + \overset{3}{\frac{\delta^2 c_m}{\delta y^2}} + \frac{\delta^2 c_m}{\delta z^2}\right) - \left(\frac{\delta(u'c')}{\delta x} + \overset{4}{\frac{\delta(v'c')}{\delta y}} + \frac{\delta(w'c')}{\delta z}\right) \qquad \text{Equation 2.28}$$

where expression 1 represents rate of change of mean concentration with time, 2 advection of ensemble mean concentration by mean velocity, 3 molecular diffusion, and 4 turbulent diffusion. In rivers turbulent, or eddy diffusion causes tracer to spread far more rapidly than could happen if spreading occurred due to molecular diffusion alone.

The cross product terms in expression 4, $u'c'$, $v'c'$, $w'c'$ are equivalent to the flux of tracer produced by the turbulent velocity fluctuations. It is necessary to obtain detailed records of velocity and concentration data to evaluate these terms. However, this was not possible until the recent advent of non-intrusive high definition measurement techniques, Shiono *et al* (1998), Guymer and Harry (1996), Harry, Guymer and Boxall (1998). These methods have not yet produced definitive results.

2.3.1 Taylor's analysis of turbulent diffusion

Taylor (1921) presented a paper on the theoretical analysis of the spreading of a cloud of tracer particles released into stationary homogeneous turbulence. This has long remained the basis for all analysis of turbulent diffusion. Taylor utilised a Lagrangian co-ordinate system, in which the system moves at the mean flow rate. Thus, the effect of turbulence is isolated. The result of this is that, after some time, the

rate at which the variance of the tracer increases is linear. Taylor went on to prove his hypothesis by investigation of longitudinal dispersion in turbulent pipe flow, Taylor (1954a). His work was further expanded by Elder (1959), to the application of open channels of infinite width.

By making the analogy between turbulent diffusion and Fick's first law:

$$J_x = u'c' = -e_t \frac{\delta c_m}{\delta x} \qquad \text{Equation 2.29 a}$$

$$J_y = v'c' = -e_t \frac{\delta c_m}{\delta y} \qquad \text{b}$$

$$J_z = w'c' = -e_t \frac{\delta c_m}{\delta z} \qquad \text{c}$$

where e_t is a turbulent diffusion coefficient, or eddy diffusivity. From this, following the same derivation as was used for Equation 2.17, an equation for turbulent advection diffusion can be written:

$$\frac{\delta c_m}{\delta t} + u_m \frac{\delta c_m}{\delta x} + v_m \frac{\delta c_m}{\delta y} + w_m \frac{\delta c_m}{\delta z} = \left(e_m + e_t\right)_x \frac{\delta^2 c_m}{\delta x^2} + \left(e_m + e_t\right)_y \frac{\delta^2 c_m}{\delta y^2} + \left(e_m + e_t\right)_z \frac{\delta^2 c_m}{\delta z^2} \qquad \text{Equation 2.30}$$

Although this analogy is supported by Taylor's analysis it should be noted that it is not conclusive proof of its validity. However, Rutherford (1994) reports a large body of empirical evidence to support the use of Equation 2.30 to describe turbulent mixing situations. Due to the nature of the derivation of this equation it should be applied with care in practical situations, particularly in the near field when it is imperative that sufficient time must elapse such that the effects of buoyancy and discharge momentum have been negated.

In Equation 2.30 the two separate coefficients for molecular and turbulent diffusion are included. However, it is common practice to simply include one term. This is because molecular diffusion is normally several orders of magnitude smaller than turbulent diffusion, see Table 2.1, and hence can be neglected, or assumed incorporated into the turbulent diffusion term, leaving:

$$\frac{\delta c}{\delta t} + u\frac{\delta c}{\delta x} + v\frac{\delta c}{\delta y} + w\frac{\delta c}{\delta z} = e_x \frac{\delta^2 c}{\delta x^2} + e_y \frac{\delta^2 c}{\delta y^2} + e_z \frac{\delta^2 c}{\delta z^2} \qquad \text{Equation 2.31}$$

It should be noted that all concentrations and velocities in Equation 2.31 and from this point onwards are ensemble mean values unless otherwise stated. Subscript m has been discontinued from this point forward for the sake of simplicity. The diffusion coefficient is stipulated separately in each co-ordinate direction. This reflects the importance of different governing factors in each direction.

2.3.2 Reynolds stress

Reynolds stress is often used to characterise turbulence levels in open channel flow and gives an indication of momentum exchange and mixing rates. Therefore, the derivation of expression of Reynolds stress will be undertaken.

Consider the simple situation of a channel with two distinct velocity regimes, Figure 2.5. From an expression for the momentum exchange between the two layers, it is possible to derive an expression for shear stress at the boundary between the two flow layers.

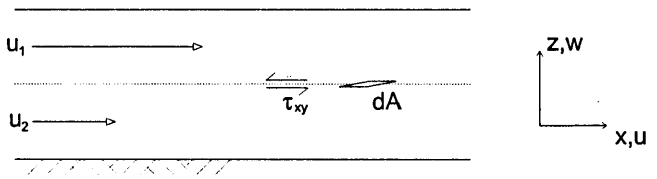

Figure 2.5 Idealised flow case

$$\begin{aligned} \text{momentum} &= \text{mass.velocity} \\ &= (\rho.w.dt.dA)u \\ \text{force} &= \frac{\text{momentum}}{\text{time}} \\ &= \frac{(\rho.w.dt.dA)u}{dt} \\ \text{shear stress} &= \frac{\text{force}}{\text{area}} \\ &= \frac{(\rho.w.dt.dA)u}{dt.dA} \\ \tau_{xy} &= \rho.w.u \end{aligned} \qquad \text{Equation 2.32}$$

This derivation is based on instantaneous point measurements of the associated velocities and yields an instantaneous value of shear stress.

Reynolds decomposition, the idea of decomposition of velocities into a stable time average component and a random time varying component, has been introduced. This decomposition was introduced to greatly simplify the description of mixing processes and the presence of turbulence. Using this decomposition Equation 2.32 can be re-expressed:

$$\tau_{xy} = \rho(w_m + w')(u_m + u')$$

$$\tau_{xy} = \rho u_m w_m + \rho w_m u' + \rho w' u_m + \rho w' u' \qquad \text{Equation 2.33}$$

This is still an expression for an instantaneous value of shear stress. It is desirable to time average this expression:

$$(\tau_{xy})_m = \rho(u_m w_m)_m + \rho(w_m u')_m + \rho(w' u_m)_m + \rho(w' u')_m \qquad \text{Equation 2.34}$$

Reynolds analogy states that the fluctuating component is random and homogeneous, therefore a time average of this component must be zero, leading to:

$$(\tau_{xy})_m = \rho(u_m w_m)_m + \rho(w' u')_m \qquad \text{Equation 2.35}$$

For the analysis of plane, turbulent two dimensional shear flow, the time average of the vertical component must be zero, as there is no net vertical movement of water, resulting in:

$$\overline{\tau_{xy}} = \rho\overline{w' u'} \qquad \text{Equation 2.36}$$

This expression, commonly called Reynolds Stress, has been used by many investigators to provide estimates of point values of shear stress within open channel flows. Its wide use has stemmed from the early velocity measurement devices, particularly hot wire anemometers as they provide a direct measurement of the time average of the fluctuating components. Point estimates of Reynolds stress have

often been used to define a vertical profile, such that a value can be interpolated to the bed and provide a direct estimate of bed shear stress / velocity. The shear stress through a vertical plane, τ_{xz}, has often been estimated by a similar expression of the cross products of transverse and longitudinal velocity fluctuating components.

2.3.3 Eddy viscosity

Equation 2.29 (a-c) is not new, it is helpful to consider its importance with respect to momentum transfer in turbulent flows. Turbulent eddies transfer both momentum and mass. Experimental work has shown the rates of transfer to be similar. Consider a two dimensional uniform laminar flow. The velocity is uniform along and across the channel. The no-slip condition requires that the velocity at the bed is zero, causing a vertical velocity gradient. In laminar flow random molecular movements cause a small exchange of flow between adjacent fluid layers. In turbulent flow a much larger exchange is affected by the turbulent eddies. Since the mean velocity of adjacent layers is different there is an exchange of momentum. From Newton's second law this results in a shear stress. In plain laminar shear flow the viscous shear stress is:

$$\tau = \rho\nu\frac{\delta u}{\delta z} \qquad \text{Equation 2.37}$$

where τ is viscous shear stress.

In turbulent flows the transfer of momentum by turbulent eddies is far greater than in laminar flow. The shear stresses which arise from turbulent velocity fluctuations are called turbulent or Reynold's stresses, Equation 2.36. It should be noted that Equation 2.36 contains the cross product of the velocity fluctuations, which is similar to the cross product of velocity fluctuation and concentration fluctuation defined in Equation 2.29.

It is suggested that by analogy with Equation 2.37 the Reynolds stress can be related to the gradient in the mean velocity. Thus:

$$\tau_t = \rho\nu_t\frac{\delta u}{\delta z} \qquad \text{Equation 2.38}$$

where ν_t is the eddy viscosity (m^2/s). Whereas the kinematic viscosity is a function of the fluid, the eddy viscosity is a property of the flow and depends on the intensity of turbulence and the length scale of the dominant eddies.

Reynolds noted that the turbulent eddies which transport momentum, also transport mass. Equation 2.38 states that the rate of transfer of momentum is proportional to the velocity gradient, and thus, so is the rate of change of momentum. This leads to:

$$J_z = -e_t\frac{\delta c}{\delta z} \qquad \text{Equation 2.39}$$

Note that e_t and ν_t have the same units (m^2/s). Reynolds analogy is that for tracer mass:

$$e_t = \nu_t \qquad \text{Equation 2.40}$$

2.3.3.1 Prandtl's mixing length hypothesis

Prandtl (1952) presents a theory for predicting the eddy viscosity in turbulent shear flow which has become known as the mixing length hypothesis. Prandtl noted that the kinetic theory of gasses gives rise to an expression for viscosity:

$$\nu_g = \tfrac{1}{3} L_g u_m \qquad \text{Equation 2.41}$$

where ν_g is the kinematic viscosity of the gas, L_g the mean free path of the gas molecules (the distance travelled between collisions) and u_m a typical molecular velocity. He drew an analogy between the kinetic theory of gasses and the eddies in turbulent flow and suggested that:

$$\nu_t = u_t L_m \qquad \text{Equation 2.42}$$

where L_m Prandtl's mixing length and u_t a turbulent velocity.

There are two potential deficiencies with Prandtl's theory. There is no proof that eddies interact in the same way as gas molecules and that there are a large range of eddy sizes associated with turbulent flow, such that the selection of the value of L_m is not easy. However, it is a useful result that indicates that the eddy viscosity is dependent on a turbulent length scale and a turbulent velocity.

2.4 *Simplifying the Advection Diffusion Equation*

The advection diffusion equation, Equation 2.31, forms the basis for much of the analysis of mixing problems in rivers. However, use of the full equations requires very detailed information about water depths, velocities and diffusion coefficients. This level of detail demands very expensive and time consuming field studies. Solutions of the full three-dimensional form of the equation for natural channels are also very complex. In certain situations some terms in Equation 2.31 are negligibly small and simplifications can be made.

If the co-ordinate system is aligned with the main flow along the x-axis such that net transverse and vertical velocity components are zero then Equation 2.31 may be simplified to:

$$\frac{\delta c}{\delta t} + u\frac{\delta c}{\delta x} = e_x \frac{\delta^2 c}{\delta x^2} + e_y \frac{\delta^2 c}{\delta y^2} + e_z \frac{\delta^2 c}{\delta z^2} \qquad \text{Equation 2.43}$$

If the tracer source is steady then the time varying term vanishes and the longitudinal concentration gradient will be negligibly small, such that:

$$u\frac{\delta c}{\delta x} = e_y \frac{\delta^2 c}{\delta y^2} + e_z \frac{\delta^2 c}{\delta z^2} \qquad \text{Equation 2.44}$$

If the tracer is released from either a vertical or transverse line source then the vertical or transverse concentration gradients are small, resulting in, for the case of a transverse source:

$$u\frac{\delta c}{\delta x} = e_z \frac{\delta^2 c}{\delta z^2} \qquad \text{Equation 2.45}$$

It should be noted that the form of this equation represents the case where the diffusion processes have been assumed constant over the channel, a more general form may be written:

$$u\frac{\delta c}{\delta x} = \frac{\delta}{\delta z}\left(e_z \frac{\delta c}{\delta z}\right) \qquad \text{Equation 2.46}$$

2.4.1 Depth averaging

In natural river channels the aspect ratio (width/depth) is often large, thus tracer from an instantaneous injection becomes vertically well mixed long before it becomes transversely well mixed. The region where vertical mixing occurs is often termed the near-field, Figure 1.1. In this region initial momentum and buoyancy effects are very important. The near field region is short and complex and not of importance in most cases, therefore, it can be ignored and with it vertical mixing effects. The advection diffusion equation may be depth averaged to simplify matters. Great care should be taken when depth averaging, as any errors will result in a model which is unlikely to correctly predict the behaviour of the depth average concentration distributions. The correct procedure is to integrate each term with respect to depth, taking careful account of any variations with depth, or velocity and concentration. The mathematics of this can be found in most textbooks and papers, for example Fischer *et al* (1979), Rutherford (1994), Holley *et al* (1972), Yotsukura and Cobb (1972). A full example of depth average is given later. In the standard orthogonal co-ordinate system the depth-averaged form of the advection dispersion equation may be written as:

$$h\frac{\delta c}{\delta t}+\frac{\delta}{\delta x}(huc)+\frac{\delta}{\delta y}(hvc)= \frac{\delta}{\delta x}\left(-h\langle u'c'\rangle+he_x\frac{\delta c}{\delta x}\right)+\frac{\delta}{\delta y}\left(-h\langle v'c'\rangle+he_y\frac{\delta c}{\delta y}\right) \qquad \text{Equation 2.47}$$

where c, u and v are now depth average concentration, primary and transverse velocities respectively, and angle brackets denote depth average products.

In Equation 2.47 uc and vc are the longitudinal and transverse advective fluxes, $e_x\frac{\delta c}{\delta x}$ and $e_y\frac{\delta c}{\delta y}$ are the diffusive fluxes longitudinally and transversely. The terms $-\langle u'c'\rangle$ and $-\langle v'c'\rangle$ arise as a result of depth averaging and quantifying the additional transport that results from non-uniformity over the depth of concentration and velocity. These additional processes are often termed dispersion, or more accurately shear dispersion. Shear dispersion is purely a result of averaging, by either width or depth.

2.4.2 Shear dispersion

Consider a vertical slice along a natural river channel with an idealised vertical velocity distribution as shown as shown in Figure 2.6. If a vertical line of dye is introduced at t_0 then the depth average concentration would be as in the bottom half of the figure. If we then consider the effects of advection and turbulence some time later, the tracer may have been transformed as shown at t_1, with an associated distance versus depth average concentration profile as shown, Figure 2.6.

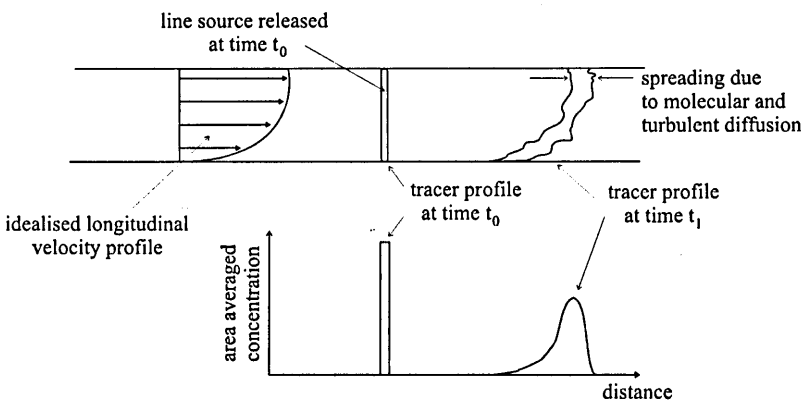

Figure 2.6 Sketch showing the combined effects of turbulent diffusion and vertical velocity shear on depth averaged longitudinal dye profile

If a horizontal slice is considered through the flow, the effects of the velocity distribution can easily be pictured as having a similar shearing effect on a transverse line source.

2.4.3 Taylor's analysis of shear dispersion

If the effects of diffusion were negligibly small then the shearing effects of the velocity profile would continue indefinitely. This suggests that the rate of growth is linear with time. It can be seen from Equation 2.21 that the variance is proportional to the square of the length. These two facts suggest that under infinite shear conditions the variance of tracer cloud would increase as the square of time. However, experiments show that the rate of increase of variance with time is linear, after an initial short period.

The reason that the rate of increase of variance with time is linear is the interaction between the velocity shear and diffusion. The distortion caused by the velocity shear increases the concentration gradient, thus promoting the effects of diffusion. Taylor (1921) is the primary paper investigating the interaction of shear and diffusion. Taylor (1953) and (1954a) specifically address the effects of radial velocity shear and diffusion in laminar and then turbulent pipe flow. His work was extended and proved for longitudinal mixing in open channel flows, vertically by Elder (1959) and transversely by Fischer (1966).

Using the ideas from Taylor's analysis it can be shown that at asymptotically large times the dispersive fluxes, that were unknown at the end of Section 2.4.1, are proportional to the longitudinal gradient in the depth average concentration. Hence:

$$-\langle u'c' \rangle = k_x \frac{\delta c}{\delta x} \qquad \text{Equation 2.48 a}$$

$$-\langle v'c' \rangle = k_y \frac{\delta c}{\delta y} \qquad \text{b}$$

where k_x and k_y are dispersion coefficients, which account for the effects on the depth average concentration profile of the depth variations in velocity.

Incorporating these terms into Equation 2.47 yields:

$$\frac{\delta c}{\delta t} + \frac{\delta}{\delta x}(huc) + \frac{\delta}{\delta y}(hvc) = \frac{\delta}{\delta x}\left(h(e_x + k_x)\frac{\delta c}{\delta x}\right) + \frac{\delta}{\delta y}\left(h(e_x + k_y)\frac{\delta c}{\delta y}\right) \qquad \text{Equation 2.49}$$

In natural open channels k >> e such that often only a k term is expressed, and assumed to incorporate diffusion and dispersion effects, a mixing coefficient. Using this and the ideas of continuity, Equation 2.49 may be rewritten:

$$\frac{\delta c}{\delta t}+u\frac{\delta c}{\delta x}+v\frac{\delta c}{\delta y}=\frac{1}{h}\frac{\delta}{\delta x}\left(hk_x\frac{\delta c}{\delta x}\right)+\frac{1}{h}\frac{\delta}{\delta y}\left(hk_y\frac{\delta c}{\delta y}\right) \qquad \text{Equation 2.50}$$

This equation is used extensively in situations where transverse mixing is an issue. Although, in the case where a continuous point source is present, the situation may simplified by neglecting longitudinal and time varying terms, as in Equation 2.44. When longitudinal mixing is dominant the above equation may be simplified by width averaging as well as depth averaging.

When tracer from an unsteady point source has been in the flow for sufficient time for the tracer to be considered cross sectionally well mixed, Equation 2.50 may be integrated over the channel width. Resulting in:

$$A\frac{\delta c}{\delta t}+\frac{\delta}{\delta x}(AUc)=\frac{\delta}{\delta x}\left(-A\langle u'c'\rangle+Ak_x\frac{\delta c}{\delta x}\right) \qquad \text{Equation 2.51}$$

Where c is ensemble mean cross-sectional average concentration, A cross sectional area and U cross sectional average velocity. In this case angle brackets denote cross sectional average.

The term $\langle u'c'\rangle$ is the longitudinal dispersive flux resulting from variations in velocity over the channel cross section. Taylor's analysis of turbulent shear flow suggests that at large times this term is proportional to the longitudinal gradient in cross-sectional average concentration, thus:

$$\langle u'c'\rangle=D_x\frac{\delta c}{\delta x} \qquad \text{Equation 2.52}$$

where D_x is a longitudinal dispersion coefficient. As with depth averaging substituting this back into Equation 2.51, considering continuity, and assuming $D_x >> k_x$ yields:

$$\frac{\delta c}{\delta t}+U\frac{\delta c}{\delta x}=\frac{1}{A}\frac{\delta}{\delta x}\left(AD_x\frac{\delta c}{\delta x}\right) \qquad \text{Equation 2.53}$$

This equation is often used as a basis in longitudinal mixing problems where the tracer is cross sectionally well mixed.

2.5 *Co-ordinate System*

The majority of the above theory is derived based on a Cartesian co-ordinate system, taking no account of channel curvature, which is found to some extent in all natural channels. Applying standard Cartesian co-ordinates to a curving channel leads to a very complex situation. As an approximation, the x-axis can be assumed aligned with the main flow path, this way the x-axis is no longer straight but follows the meander path. The y-axis is taken as orthogonal to the x-axis. Distance x is measured in the local down-stream direction. This leads to a curvilinear co-ordinate system, and the form of the above equations can be maintained.

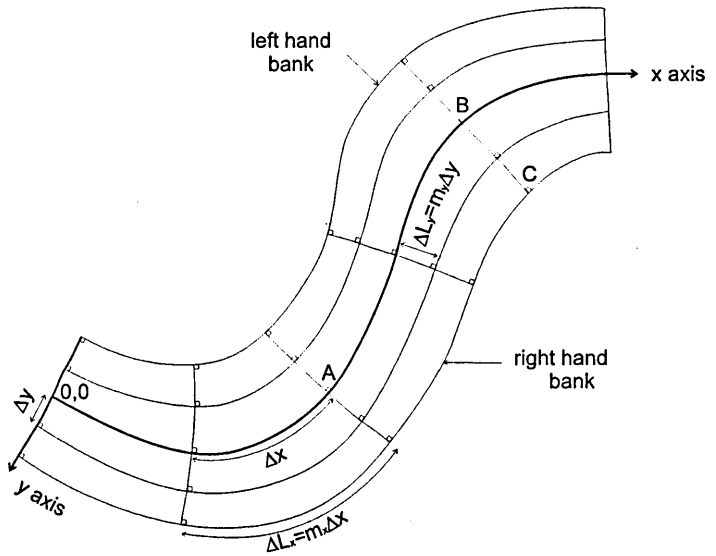

Figure 2.7 Orthogonal curvilinear co-ordinate system for natural channel

Due to the curvature in channel alignment and / or variations in width along the channel, measurements along different longitudinal (or transverse) co-ordinate surfaces are generally not equal. To account for this the metric coefficients m_x and m_y are introduced to accommodate the differences between distances along curved co-ordinate surfaces, and those measured along the co-ordinate axes. Thus in Figure 2.7 the horizontal distance along the longitudinal axis from A to B is given by $L_{AB} = \int m_x.dx$, and that along the transverse co-ordinate surface, the distance from B to C by $L_{BC} = \int m_y.dy$. The values of m_x and m_y may vary from point to point and are, in general, functions of both x and y, except that $m_x = 1$ along the x axis and $m_y = 1$ along the y axis. Horizontal surfaces are still defined as parallel, and therefore, the metric coefficient m_z is unity. If $m_x = m_y = 1$ everywhere, the co-ordinate system reduces to a regular Cartesian system. For a very sharp bend of the Missouri river Yotsukura and Sayer (1976) reference values of m_x ranging from 0.86 to 1.14.

For simplicity of calculation, the x-axis is defined as the point across the channel where the discharge is equally split. The y-axis is defined as the injection cross section.

2.5.1 Two dimensional ADE in curvilinear co-ordinates

Using these co-ordinate system ideas, the full three dimensional forms of the continuity equation and advection diffusion equation may now be written:

$$\frac{\delta}{\delta x}(m_y u)+m_x m_y\frac{\delta w}{\delta y}+\frac{\delta}{\delta z}(m_x v)=0 \qquad \text{Equation 2.54}$$

and

$$m_x m_y\frac{\delta c}{\delta t}+\frac{\delta}{\delta x}(m_y uc)+\frac{\delta}{\delta y}(m_x vc)+m_x m_y\frac{\delta}{\delta z}(wc)=$$
$$\frac{\delta}{\delta x}\left(\frac{m_y}{m_x}e_{tx}\frac{\delta c}{\delta x}\right)+\frac{\delta}{\delta y}\left(\frac{m_x}{m_y}e_{ty}\frac{\delta c}{\delta y}\right)+m_x m_y\frac{\delta}{\delta z}\left(e_{tz}\frac{\delta c}{\delta z}\right) \qquad \text{Equation 2.55}$$

The two dimensional depth average form of the above equations are obtained by integrating over the depth of flow, from the bed to the water surface, Holley *et al.* (1972). In carrying out the integration frequent use is made of Leibnitz's rule for reversing the order of integration and differentiation, and of the

zero mass flux boundary conditions at the water surface and bed. The resulting depth-integrated equations are:

$$m_x m_y \frac{\delta h}{\delta t} + \frac{\delta}{\delta x}\left(m_y h\langle u\rangle\right) + \frac{\delta}{\delta y}\left(m_x h\langle v\rangle\right) = 0 \qquad \text{Equation 2.56}$$

and

$$m_x m_y \frac{\delta h}{\delta t}\left(h\langle c\rangle\right) + \frac{\delta}{\delta x}\left(m_y h\langle uc\rangle\right) + \frac{\delta}{\delta y}\left(m_x h\langle vc\rangle\right) = \frac{\delta}{\delta x}\left(\frac{m_y}{m_x} h\left\langle e_x \frac{\delta c}{\delta x}\right\rangle\right) + \frac{\delta}{\delta y}\left(\frac{m_x}{m_y} h\left\langle e_y \frac{\delta c}{\delta y}\right\rangle\right) \qquad \text{Equation 2.57}$$

where angle brackets denote average taken over the depth. No simplifying assumptions have been made in progressing from Equation 2.54 and Equation 2.55 to Equation 2.56 and Equation 2.57. The product terms in Equation 2.57, such as $\langle uc\rangle$ and $\left\langle e_x \frac{\delta c}{\delta x}\right\rangle$ may be simplified by applying Reynolds analogy

$$\langle uc\rangle = \langle u\rangle\langle c\rangle + \langle u'c'\rangle \qquad \text{Equation 2.58}$$

and

$$\left\langle e_x \frac{\delta c}{\delta x}\right\rangle = \langle e_x\rangle \frac{\delta\langle c\rangle}{\delta x} + \left\langle e_x' \frac{\delta c'}{\delta x}\right\rangle \qquad \text{Equation 2.59}$$

where prime denotes deviation of local value from the depth average value. Following the dispersion theories of Taylor (1954) and Elder (1959), the cross product terms from Equation 2.58 may be approximated to a gradient dispersion term:

$$\langle u'c'\rangle = -\frac{k_x}{m_x}\frac{\delta\langle c\rangle}{\delta x} \qquad \text{Equation 2.60}$$

The covariance term on the right hand side of Equation 2.59 is eliminated under the assumption that e_x does not vary appreciably over the depth.

Combining Equation 2.59 and Equation 2.60 to yield a single longitudinal mixing term:

$$\frac{1}{m_x}\left\langle e_x \frac{\delta c}{\delta x}\right\rangle - \langle u'c'\rangle = \frac{k_x}{m_x}\frac{\delta c}{\delta x} \qquad \text{Equation 2.61}$$

where $k_x = \langle e_x\rangle + k_x$, the longitudinal mixing coefficient, which includes the combined effects of depth-average turbulent diffusion and advective dispersion. Similar approximations are applied for the transverse components. Hence, the two-dimensional advection-dispersion equations becomes:

$$m_x m_y \frac{\delta}{\delta t}(hc) + \frac{\delta}{\delta x}\left(m_y huc\right) + \frac{\delta}{\delta y}\left(m_x hvc\right) = \frac{\delta}{\delta x}\left(\frac{m_x}{m_y} hk_x \frac{\delta c}{\delta x}\right) + \frac{\delta}{\delta y}\left(\frac{m_y}{m_x} hk_y \frac{\delta c}{\delta y}\right) \qquad \text{Equation 2.62}$$

Using c, u and v to denote depth average concentration, primary velocity and transverse velocity respectively. In obtaining Equation 2.62 the only assumptions made were that velocity-concentration covariance can be represented as gradient-type dispersion terms, and that e_x and e_y do not vary appreciably over the depth. As stated in Taylor's analysis of shear flow this equation is only valid at asymptotic approximations and should only be applied when the tracer is well mixed over the depth.

2.5.2 Steady state curvilinear ADE

When the channel discharge and the tracer injection rate are both steady, the downstream plume will eventually become steady. The time derivative terms then be removed from Equation 2.56 and Equation 2.62. It has been extensively shown that the dispersive transport $(k_x/m_x)\delta c/\delta x$ is small, relative to the advective transport uc in a unidirectional flow. In the curvilinear co-ordinate system, the longitudinal co-ordinate surfaces will follow the main flow direction. For the previous reason the longitudinal mixing will contribute very little to the transport in the main flow direction and can thus be dropped. With these assumptions the continuity equation and the advection dispersion equation reduce to:

$$\frac{\delta}{\delta x}(m_y hu)+\frac{\delta}{\delta y}(m_x hv)=0 \qquad \text{Equation 2.63}$$

$$m_y hu\frac{\delta c}{\delta x}+m_x hv\frac{\delta c}{\delta y}=\frac{\delta}{\delta y}\left(\frac{m_x}{m_y}hk_y\frac{\delta c}{\delta y}\right) \qquad \text{Equation 2.64}$$

Equation 2.64 can be transformed into a more readily usable format by introducing a cumulative discharge term, $q_c=\int_0^y m_y hudy$ as defined in the curvilinear co-ordinate system, in the place of the independent variable y. First integrating Equation 2.63 with respect to y, from the left bank, y=0 to y, yields:

$$m_x hu=-\frac{\delta}{\delta x}\int_0^y m_y hudy=-\frac{\delta q_c}{\delta x} \qquad \text{Equation 2.65}$$

Making use of Leibnitz's rule and the conditions that u = v = 0 at the banks, and that y is independent of x, and then substituting Equation 2.65 into Equation 2.64 provides:

$$m_y hu\frac{\delta c}{\delta x}-\frac{\delta}{\delta q_c}\frac{\delta c}{\delta y}=\frac{\delta}{\delta y}\left(\frac{m_x}{m_y}hk_y\frac{\delta c}{\delta y}\right) \qquad \text{Equation 2.66}$$

Finally, let c(x,y) be replaced by $c(x,q_c)$ by use of the chain rule and partial derivatives so that Equation 2.66 may be reduced to:

$$\frac{\delta c}{\delta x}=\frac{\delta}{\delta q_c}\left(m_x h^2 uk_y\frac{\delta c}{\delta q_c}\right) \qquad \text{Equation 2.67}$$

This form of the ADE equation with $m_x=1$ is identical to the cumulative discharge form of the ADE that Yotsukura and Cobb (1972) first derived for a straight uniform channel.

The main advantage of using the cumulative discharge, for analysis purposes, is that there is no need for information about depth average transverse velocities. This is important, because although the mixing effects of the net transverse velocities can not be ignored, they are difficult to measure.

An alternative form of eliminating the depth average transverse velocities from Equation 2.64 is to align the longitudinal co-ordinate surfaces exactly with the depth average local velocity vectors, so that they form stream tubes. Under this condition the depth average transverse velocities are zero everywhere and Equation 2.64 reduces to:

$$m_x hu\frac{\delta c}{\delta x} = \frac{\delta}{\delta y}\left(\frac{m_x}{m_y} hk_y \frac{\delta c}{\delta y}\right) \qquad \text{Equation 2.68}$$

This is the analytical basis of the stream tube numerical models first derived by Fischer (1966) and subsequently refined by Chang (1971) and Yotsukura and Sayer (1976). Equation 2.67 includes Equation 2.68 as a special case. Equation 2.67 is a very useful result for obtaining simplified solutions to the ADE, however, if the evaluation of coefficients from tracer measurements is required, the cumulative discharge expression is most useful.

Several models and studies have been developed using the stream tubes ideas. Holley and Nerat (1983) proved the engineering application of the technique, and used it to provide a simple method of predicting the mixing effects at a river confluence. Luk *et al* (1990) presents results from a stream tubes model, and shows how the system can be used to accurately model longitudinal dispersion with time varying flows.

2.5.3 Cumulative discharge

Considering the mid-field region, where complete vertical mixing has occurred, but tracer is not yet cross sectionally well mixed, the situation as shown in Figure 2.8 can be envisaged. In such a situation, it can be seen that the dye plume is observed to expand and contract with variations in the channel cross section.

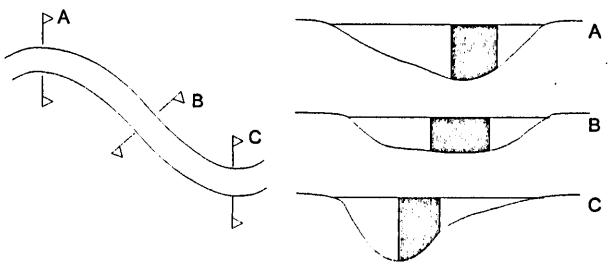

Figure 2.8 Effect of varying cross section on dye plume

If the depth average curvilinear Cartesian model was used with the change of moments method to estimate the transverse mixing coefficient in this situation errors would result. The calculated variance at section B would be greater than that at either A or C. This would result in an over estimate of the coefficient for the reach A to B, and an under estimate, possibly a negative dispersion coefficient, for the region B to C.

In Section 2.1 the continuity equation was given. Although a simple expression and its derivation apparent, it is an important expression and warrants further consideration. The two dimensional, depth average form of this expression may be written as:

$$\frac{\delta}{\delta x}(hu)+\frac{\delta}{\delta y}(hv)=0 \qquad \text{Equation 2.69}$$

If the curvilinear co-ordinate system as described above is adopted, i.e. the x-axis is aligned with the plan form curvature, and a situation assumed where cross sectional shape is not constant, Figure 2.8, it can be seen that over a finite distance, section A-C, there will be a net movement of water across the channel. This rate of flow, or net transverse drift may be evaluated from an expression derived by integrating Equation 2.69 across the channel:

$$v = -\frac{1}{h}\frac{\delta}{\delta x}\left(\int_{z=0}^{z} hudz\right) \qquad \text{Equation 2.70}$$

This net transverse drift velocity, v, can be included in the method of moments to account for the effects of expansion and contraction of the dye plume. However, the evaluation of this net transverse drift velocity is difficult to perform and leads to complex solutions. Alternatively, the transverse drift velocities can be negated by introducing the cumulative discharge expression as performed previously.

Luk *et al* (1990) and Luk (1991) have shown the versatility and simplicity of using the stream tubes approach for modelling both transverse and longitudinal mixing, including modelling river confluence and time varying flows.

2.6 *Generalised Method of Moments*

In Section 2.2.2 the method of moments was presented as a way of evaluating mixing coefficients from concentration distributions, based on the principals of linear increase in variance of Gaussian distribution with distance. Holley *et al.* (1972) discusses various factors which affect transverse mixing in rivers, such as changes in cross sectional shape and variations in transverse mixing rate, both transversely and longitudinally. One of the major results of their paper is the Generalised Method of Moments, used to evaluate transverse mixing coefficients from concentration profiles and velocity data. This includes terms to account for net transverse drift velocities resulting from changes in cross sectional shape, and impingement on the banks. This is potentially a very powerful tool, particularly when bank impingement and the reflections which this involves often negate the use of the standard method of moments.

2.6.1 Derivation of the Generalised Method of Moments

From Holley *et al.* (1972), taking the depth average form of the advection dispersion equation:

$$h\left(\frac{\delta c}{\delta t} + u\frac{\delta c}{\delta x} + v\frac{\delta c}{\delta y}\right) = \frac{\delta}{\delta x}\left(hk_x\frac{\delta c}{\delta x}\right) + \frac{\delta}{\delta y}\left(hk_y\frac{\delta c}{\delta y}\right) \qquad \text{Equation 2.50}$$

Considering a constant injection, longitudinal dispersion and time varying parameters may be neglected, leaving:

$$uh\frac{\delta c}{\delta x} + vh\frac{\delta c}{\delta y} = \frac{\delta}{\partial y}\left(hk_y\frac{\delta c}{\delta y}\right) \qquad \text{Equation 2.71}$$

Then multiplying through by $(y-\bar{y})^2$ and integrating from y = 0 to B, to give the second moment of the distribution, where $\bar{y}$ is the transverse position of the centroid of the concentration distribution, defined as:

$$\bar{y} = \frac{\int_{y=0}^{B} yhucdy}{\int_{y=0}^{B} hucdy} \qquad \text{Equation 2.72}$$

Yields:

$$\int_{y=0}^{B} uh\frac{\delta c}{\delta x}\left(y-\bar{y}\right)^2 dy + \int_{y=0}^{B} vh\frac{\delta c}{\delta y}\left(y-\bar{y}\right)^2 dy = \int_{y=0}^{B} \frac{\delta}{\delta y}\left(hk_y\frac{\delta c}{\delta y}\right)\left(y-\bar{y}\right)^2 dy \qquad \text{Equation 2.73}$$

(1) (2) (3)

The order of integration and differentiation of the x advective term (1) is then rearranged according to Liebniz theorem, and the transverse advective term (2) and transverse diffusive term (3) integrated once by parts. Applying zero flux boundary conditions and dividing the result through by the mass flux:

$$\text{mass flux} = \int_{y=0}^{B} huc\,dy \qquad \text{Equation 2.74}$$

Finally, introducing a variable to describe the variation of the transverse mixing coefficient in the transverse direction. The form of this variable is unknown.

$$k_y = K_y\varphi(y) \qquad \text{Equation 2.75}$$

where

$$\int_{y=0}^{B}\varphi(y)dy = 1 \qquad \text{Equation 2.76}$$

and K_y is a width average transverse coefficient, gives:

$$\frac{d}{dx}\left[\frac{\int_{y=o}^{B} uhc\left(y-\bar{y}\right)^2 dy}{\int_{y=0}^{B} huc\,dy}\right] - \frac{2\int_{y=0}^{B} vhc\left(y-\bar{y}\right)dy}{\int_{y=0}^{B} huc\,dy} = 2K_y\frac{\int_{y=0}^{B} h\varphi\frac{\partial c}{\partial y}\left(y-\bar{y}\right)dy}{\int_{y=0}^{B} huc\,dy} \qquad \text{Equation 2.77}$$

This is the standard form of the general method of moments given in many texts, although often written out as:

$$\frac{d\sigma_3^{\,2}}{dx} - g(x) = 2K_y f(x) \qquad \text{Equation 2.78}$$

where the definitions of σ_3^2, g(x) and f(x) can be seen by comparing the terms in Equation 2.77 and Equation 2.78. The main difficulty in evaluating Equation 2.77 comes from trying to define values for the depth average transverse velocity.

The variable σ_3^2 comes from the total spread of tracer due to mixing, primary and secondary velocities. The function g(x) includes the effects of net transverse velocities. Thus the difference ($d\sigma_3^2/dx$-g(x)) represents the effects of just the mixing, i.e. g(x) effectively removes the influence of the net transverse velocities from σ_3^2. The f(x) function allows for the bank impingement effects by factoring the length scale appropriately.

The use of the Generalised Method of Moments as an analysis tool was extensively explored and tested by Holley and Abraham (1973a) with a laboratory channel with groins, and by Holley and Abraham (1973b) and Verboon (1973) for field data. These studies concluded that the Generalised Method of Moments is a useful tool in analysing transverse mixing data. However, they also report considerable difficulty in obtaining accurate measurements of the net transverse drift velocities, and the large errors that inaccuracies in this evaluation can produce.

2.6.2 Cumulative discharge derivation of Generalised Method of Moments

Yotsukura and Cobb (1972) showed that the advection dispersion equation could be expressed in stream tube or cumulative discharge terms as discussed and derived in section 2.5. By using the cumulative discharge approach the need to accurately evaluate transverse velocities is removed.

From Equation 2.67, the ADE in cumulative discharge terms, for a continuous injection may be expressed as:

$$\frac{\delta c}{\delta x} = \frac{\delta}{\delta q}\left(D_q \frac{\delta c}{\delta q}\right) \qquad \text{Equation 2.79}$$

where

$$D_q = m_x h^2 u k_y \qquad \text{Equation 2.80}$$

Then following the derivation which was carried out by Holley (1972), multiplying through by $(q-\bar{q})^2$, where $\bar{q}$ is the transverse centroid of the concentration distribution, defined by:

$$\bar{q} = \frac{\int_{y=0}^{B} qcdq}{\int_{y=0}^{B} cdq} \qquad \text{Equation 2.81}$$

and integrating across the channel, from q = 0 to Q, to give the second moment of the distribution, yields:

$$\int_{q=0}^{Q} \frac{\delta c}{\delta x}(q-\bar{q})^2 dq = \int_{q=0}^{Q} \frac{\delta}{\delta q}\left(D_q \frac{\delta c}{\delta q}\right)(q-\bar{q})^2 dq \qquad \text{Equation 2.82}$$

Interchanging the order of integration and differentiation of the x advective term by Liebniz theorem, gives:

$$\int_{q=0}^{Q} \frac{\delta c}{\delta x}(q-\bar{q})^2 dq = \frac{d}{dx}\int_{q=0}^{Q} c(q-\bar{q})^2 dq \qquad \text{Equation 2.83}$$

and integrating the transverse diffusive term once by parts:

$$\int_{q=0}^{Q} \frac{\partial}{\partial q}\left(D_q \frac{\delta c}{\delta q}\right)(q-\bar{q})^2 dq = \left[\left(D_q \frac{\delta c}{\delta q}\right)(q-\bar{q})^2\right]_{q=0}^{Q} - 2\int_{q=0}^{Q} D\frac{\delta c}{\delta q}(q-\bar{q})dq \qquad \text{Equation 2.84}$$

Applying zero flux boundary conditions, noting that flux, from Fickian diffusion ideas, may be defined as, flux = $D_q \frac{\delta c}{\delta q}$, the expression in Equation 2.84 reduces to:

$$\left[\left(D_q \frac{\delta c}{\delta q}\right)(q-\bar{q})^2\right]_{q=0}^{Q} - 2\int_{q=0}^{Q} D_q \frac{\delta c}{\delta q}(q-\bar{q})dq = -2\int_{q=0}^{Q} D_q \frac{\delta c}{\delta q}(q-\bar{q})dq \qquad \text{Equation 2.85}$$

Working from Equation 2.82 and inserting the right hand side of Equation 2.85 and Equation 2.83 gives:

$$\frac{d}{dx}\int_{q=0}^{Q} c(q-\bar{q})^2 dq = -2\int_{q=0}^{Q} D_q \frac{\delta c}{\delta q}(q-\bar{q})dq \qquad \text{Equation 2.86}$$

Then dividing through by the mass flux:

$$\text{mass flux} = \int_{q=0}^{Q} cdq \qquad \text{Equation 2.87}$$

gives:

$$\frac{d}{dx}\frac{\int_{q=0}^{Q} c\left(q-\bar{q}\right)^2 dq}{\int_{q=0}^{Q} c dq} = -2\frac{\int_{q=0}^{Q} D_q \frac{\delta c}{\delta q}\left(q-\bar{q}\right) dq}{\int_{q=0}^{Q} c dq} \qquad \text{Equation 2.88}$$

Introducing a term for the variation for the transverse dispersion coefficient:

$$D_q = K_q \varphi(q) \qquad \text{Equation 2.89}$$

where

$$\int_{q=0}^{Q} \varphi(q) dq = 1 \qquad \text{Equation 2.90}$$

It should be noted that although the way in which the variation of the transverse mixing coefficient changes across the channel is an unknown, in the stream tubes definition this function must be included, and made proportional to $m_x h^2 u$, such that Equation 2.80 is complied with. Higher powers or other factors may be introduced depending on supporting arguments, to define the variation of mixing coefficient.

The result is:

$$\frac{d}{dx}\left[\frac{\int_{q=0}^{Q} c\left(q-\bar{q}\right)^2 dq}{\int_{q=0}^{Q} c dq}\right] = -2K_q \frac{\int_{q=0}^{Q} \varphi(q)\left(q-\bar{q}\right)\frac{\delta c}{\delta q} dq}{\int_{q=0}^{Q} c dq} \qquad \text{Equation 2.91}$$

Often expressed as:

$$\frac{d\sigma^2}{dx} = -2K_q f(x) \qquad \text{Equation 2.92}$$

Definitions of σ^2 and f(x) can be seen by comparing Equation 2.91 and Equation 2.92.

This derivation was suggested and performed by Rutherford (1994), however, his final equation incorrectly states q instead of (q-$\bar{q}$) on the right hand side of the final equation.

2.6.3 Evaluation of transverse mixing coefficient by the Generalised Method of Moments

In this section only the Generalised Method of Moments defined in stream tube notation is considered, although all ideas discussed in this section are equally valid for application to the regular Cartesian form. The main advantage of the stream tubes model over the Cartesian form is that it contains no net transverse velocity term, and therefore no g(x) term as in Equation 2.78, appears in Equation 2.92.

When tracer does not impinge on either bank, it can be shown by integrating the f(x) function in Equation 2.92 by parts from q=0 to Q that f(x)=1. From Equation 2.92, it then follows that:

$$K_q = \frac{1}{2}\frac{d}{dx}\left(\sigma_q^2\right) \qquad \text{Equation 2.93}$$

This is the standard method of moments solution as discussed in section 2.2.2. One of the main advantages of the Generalised Method of Moments is that it accommodates the situation where tracer impinges on the bank. In this case, it is necessary to evaluate Equation 2.92 by integrating along the

channel. To find a reach average transverse mixing coefficient Equation 2.94 may be used, where subscript one represents downstream measuring section and subscript 2 upstream.

$$K_q = -\frac{1}{2}\frac{\sigma_q^2(x_1)-\sigma_q^2(x_2)}{\int_{x_1}^{x_2} f(x)dx} \qquad \text{Equation 2.94}$$

Alternatively, if the coefficient is thought to be constant, a plot of σ^2 versus F(x) may be produced, and then K_q evaluated from half the gradient of this line. F(x) is defined as the integral of x.f(x) from injection to the point under consideration. The rate of transverse mixing is unlikely to be a constant with distance in natural channels. The function φ defines the variation of the transverse mixing rate over each cross section and with distance. φ should be defined as a local property or properties of the channel and/or flow, such that a straight-line fit is obtained when plotting K_q against F(x).

Once a value for K_q has been found it can be converted back to D_q by dividing by the average value of φ for the area under consideration. The value of the transverse mixing coefficient, usually quoted, k_y can be evaluated from D_q by dividing by the area average of h^2um_x.

2.6.4 Variation in transverse mixing coefficient

An average constant value of k_y is often used for a channel rather than considering possible variation within the cross section. It seems probable that a number of factors, such as depth and velocity, which vary over any given cross section may lead to significant changes in the rate of transverse mixing. Use of Equation 2.75 and Equation 2.89 in the Generalised Method of Moments allow for k_y to vary transversely. The question of which variation of k_y to use then arises. If a depth average value of transverse mixing is considered then this must stem from the characteristics of the turbulence regime responsible for the diffusion, and the shear effects of the flow regime.

It is common to find mixing coefficients normalised by the average flow depth and shear velocity. Holley *et al* (1972) suggested that the form of the transverse variation in transverse mixing coefficient, φ in Equation 2.75 and Equation 2.89 should follow a relationship based on the local variation of depth, shear velocity or velocity. They went on to show through numerical modelling that the effects of using local or width average values in their definition of φ, had a large initial effect near to the source, but that the differences in predicted and measured concentration profile decrease with distance.

Lau and Krishnappen (1981) present a predictive numerical solution to the ADE equation in stream tube co-ordinates. They investigated a number of relationships for D_q in their model, the results of which were compared to experimental data. The relationships investigated were:

1. $D_q = (uh^2m_x)\bar{k}_y(x)$ – local values for (uh^2m_x). The term $\bar{k}_y$ is assumed to be constant for a cross section but is allowed to vary with each cross section. Thus D_q varies with x and y.
2. $D_q = (uh^2m_x)\bar{k}_y$ – local values for (uh^2m_x). The term $\bar{k}_y$ is assumed to be a universal constant. D_q varies as (uh^2m_x).
3. $D_q = (\overline{uh^2m_x})\bar{k}_y$ – cross sectional average values of $\overline{uh^2m_x}$ are used. Hence D_q is a constant for each cross section.

4. $D_q = (\overline{uh^2m_x})\overline{k}_y$ – average values of $\overline{uh^2m_x}$ and $\overline{k}_y$ are used, D_q is a constant throughout.
5. $D_q = (uh^2m_x)(\alpha Y^*h)$ – k_y is assumed to vary as the product of local depth and the mean shear velocity U*. Local values of (uh^2m_x) are assumed.

It should be noted that in 2-4 above the relationship which is being investigated is the effect of averaging the uh^2m_x term, that is required in the stream tubes model, through a predictive numerical model. Relationships 1, 2 and 5 investigate the effect of the variability of k_y.

The conclusion from their work is similar to that of Holley *et al* (1972), little effect can be seen in the predicted distributions for the different relationships, except near to the source.

2.7 *Vertical Mixing*

Vertical mixing has the shortest time scale of the three co-ordinate directions. A suggested guide line is that neutrally buoyant contaminates become vertically well mixed, that is the difference between maximum and minimum concentration is less than 2%, in less than 50 water depths below the source. In many cases complete vertical mixing occurs considerably more quickly. The processes of vertical mixing are predominately governed by the turbulence generated by bed shear, although the rate of vertical mixing can be heavily affected by the presence of secondary circulations caused by obstructions, changes in shape or plan-form curvature.

Due to the speed with which vertical mixing occurs, and because of the large width to depth ratio of rivers, vertical mixing can often be neglected.

2.7.1 Theoretical derivation of vertical diffusivity

When considering plain turbulent shear flow, for example as generated by a river bed in an infinitely wide straight channel, Prandtl's mixing length hypothesis can be used in conjunction with a logarithmic velocity distribution to estimate reasonably accurately vertical eddy diffusivity.

In section 2.3.3, where eddy viscosity and Prandtl's mixing length hypothesis where introduced, it was shown that:

$$\tau_t = \rho \nu_t \frac{\delta u}{\delta z} \qquad \text{Equation 2.38}$$

$$e_z \approx \upsilon_t \qquad \text{Equation 2.39}$$

Where τ_t is turbulent shear stress, ρ density of water, u mean velocity, e_z vertical eddy diffusivity and υ_t eddy viscosity.

This should be considered in conjunction with the idea that in plain turbulent shear flow the shear stress varies linearly with depth and is zero at the water surface:

$$\tau_t = \tau_0\left(1 - \frac{z}{z_0}\right) \qquad \text{Equation 2.95}$$

Then, substituting Equation 2.95 and Equation 2.39 into Equation 2.39 and rearranging it can be shown that:

$$e_z = \left[\tau_0\left(1-\frac{z}{z_0}\right)\right] \Big/ \left[\rho\frac{\delta u}{\delta z}\right] \qquad \text{Equation 2.96}$$

If we assume the vertical distribution of primary velocities is described by a log law distribution:

$$u(z) = \frac{u^*}{\kappa}\log_e\left(\frac{z}{z_0}\right) \qquad \text{Equation 2.97}$$

differentiated with respect to depth:

$$\frac{\delta u}{\delta z} = \frac{u^*}{\kappa z} \qquad \text{Equation 2.98}$$

By substituting Equation 2.98 into Equation 2.96, and noting that $(u^*)^2=\tau_0/\rho$, the following expression is obtained:

$$e_z = \kappa u^* z\left(1-\frac{z}{h}\right) \qquad \text{Equation 2.99}$$

The implication of this is that the vertical diffusivity varies parabolically over the depth, being zero at both the free surface and the bed. Jobson and Sayer (1970) found that predicted concentration profiles were not sensitive to the vertical distribution of the diffusivity, and that for most cases the depth average value should be sufficient. Thus, by integrating over the flow depth a depth average expression can be obtained:

$$\langle e_z \rangle = \frac{\kappa u^* h}{6} \qquad \text{Equation 2.100}$$

taking $\kappa = 0.4$

$$\langle e_z \rangle = 0.067 u^* h \qquad \text{Equation 2.101}$$

Prandtl's analysis assumes that the flow is two-dimensional and that the eddies are in the x-z plane. Thus the eddies causing vertical diffusion also affect the longitudinal diffusion.

2.7.2 Published values of vertical diffusivities

There are relatively few published values of vertical diffusivity. This reflects the lack of importance associated with vertical mixing in rivers, and the centering of most practical problems upon transverse and longitudinal mixing. The speed with which vertical mixing occurs, coupled with the difficulties of separating the effects of momentum and buoyancy from turbulence effects in the near field, lead to serious difficulties in the experimental evaluation of the vertical eddy diffusivity.

Several laboratory studies quantifying the vertical diffusion in plain turbulent shear flow are reported by Rutherford (1994), Table 2.2.

The values of dimensionless dispersion coefficient in Table 2.2 show good agreement with the theoretical value of 0.067. It is particularly interesting to note that the field test results reported by Rutherford also show reasonable agreement. However, no information is given as to the character of the river and how well the situation conforms to the assumption of plain turbulent shear flow. It is suggested that most deviations from plain turbulent shear flow will result in an increase in the rate of vertical mixing, primarily through increased turbulence levels and secondary flows, as would be found around obstructions.

Width	Depth	Velocity	Shear Velocity	Diffusivity		Reference / Source
				e_y ($m^2s^{-1}x10^4$)	e_y/hu^*	
Laboratory Channel						
2.44	0.4	-	0.049-0.136	-	0.063	Jobson and Sayer (1970)
0.76	0.071	0.046	0.040	-	0.042	Jobson and Sayer (1970)
0.56	0.039-0.076	-	0.041-0.058	1.8	0.067	McNulty (1983)
0.56	0.05-0.065	0.024-0.028	0.014-0.016	-	0.067	Nokes (1986)
Waikato River						
80	2.0-2.75	0.90	0.066	86-155	0.055-0.099	Rutherford (1994)

Table 2.2 Published vertical diffusion coefficients (from Rutherford 1994)

2.8 *Transverse Mixing*

Transverse mixing is a very complex problem because of the number and disparity of the factors which affect it. Observations of the behaviour of pollutants and tracers have established that whilst vertical mixing is completed in a relatively short distance downstream, a much larger distance is required for the completion of transverse mixing in natural water courses. Problems of transverse mixing can often be treated using depth-mean concentrations and using a transverse mixing coefficient. The analogy of Fickian diffusion enables the transverse mixing coefficient to be ascertained from the relationship between longitudinal distance and increase in plume variance.

2.8.1 Transverse mixing distance

This is a simplified method of obtaining a preliminary estimate of the transverse mixing coefficient based on empirical values, derived from the distance required for tracer to become 'well mixed' (± 2%) throughout the channel cross section. Simply stated:

$$k_y = \frac{\beta u b^2}{L_y} \qquad \text{Equation 2.102}$$

where L_y = transverse mixing distance (m); b = channel width (m); u = longitudinal velocity (m/s) (assumed constant). β is an empirical value, based on data from past experiments, Yotsukura and Cobb (1972) give a list of such studies. β for a mid-channel injection point = 0.134, and for bank side injection is 0.536.

The main problem with this analysis is determining the transverse mixing distance, the distance from the point of injection to where the tracer is 'well mixed' across the channel. Various methods of defining 'well mixed' are suggested but no definition is universally accepted. Since Equation 2.102 was obtained from Rutherford (1994) it has been decided to use his definition, which states:- If $P_m = c_{min} / c_{max} = 0.98$, then the tracer is well mixed. However, it is often very difficult to resolve two-percent accuracy with field measurements.

2.8.2 Prandtl's mixing length

Prandtl's mixing length hypothesis provides theoretical predictions of vertical eddy diffusivity in plain turbulent shear flow which closely match experimental results. Unfortunately, there is no proved theoretical basis for predicting the transverse diffusivity. Prandtl's mixing length hypothesis relates the vertical diffusivity to the primary velocity gradient in the vertical. However, in the case of plain turbulent shear flow there is no primary velocity gradient in the transverse direction. In natural river channels with variations in local flow depth, there is a variation in the primary velocity over the channel width. Using the procedure adopted in Section 2.3.3, the following should hold true for the x-y plane:

$$\tau_{xy} = \rho \nu_y \frac{\delta u}{\delta y} = -\rho \overline{u'v'} \qquad \text{Equation 2.103}$$

where τ_{xy} is Reynolds stress in the x-y plane, ν_y transverse turbulent eddy viscosity (m^2/s).

From Reynolds analogy, ν_y can be taken as the transverse diffusion coefficient. By adopting this relationship an indication for the transverse distribution of transverse turbulent diffusion should be obtained. However, it should be noted that this value does not include any advection effects and thus does not represent the overall degree of transverse mixing.

Investigations performed by Shiono and Knight (1991) have analysed the transverse variation in eddy viscosity. However, their measurements were taken in compound channels with a sharp depth change in the cross section. One of the findings from this work was that the transverse shear generated by the bed topography was the main influence upon the transverse distribution of the eddy viscosity in the x-y plane. In the case of gradually varying bed topography it is unlikely that the same degree of bed shear will be generated.

2.8.3 Straight, rectangular laboratory studies

Elder (1959) was the first person to address transverse mixing. His work started from the basic ideas for mixing in pipes established by Taylor (1921 – 54). Elder performed his experiments in a straight laboratory flume with a two-dimensional flow. He showed that the transverse distribution of solute in two-dimensional flow is Gaussian, therefore the Fickian diffusion analogy is valid, and the value for transverse dispersion coefficient can be given by:

$$k_y = \beta h u^* \qquad \text{Equation 2.104}$$

Elder gave the constant β as 0.23. However, considerable variation in this value has been observed when dealing with non-plane turbulent shear flows.

Since the work of Elder (1959) a large number of laboratory experiments have been carried out in straight open channel flows, in an attempt to better define a value or method of predicting the value of β. Rutherford (1994) gives a review of past laboratory studies quantifying transverse mixing. The following plots are recreated from this review. To enable comparison of these data, the mixing coefficients have been normalised by the product of depth and bed shear velocity. The reason for normalising by these factors originates from the argument that turbulent diffusion (the dominant process in plain turbulent shear flow) is governed by the degree of turbulence. The turbulence level is directly related to bed shear

velocity, and the scale of the turbulent eddies is related to the depth. To illustrate the variation in coefficients obtained, Rutherford (1994) plotted the normalised transverse mixing coefficient against the channel aspect ratio, a non-dimensional representation of the channel shape. This relationship is recreated from Rutherford's summary data in Figure 2.9.

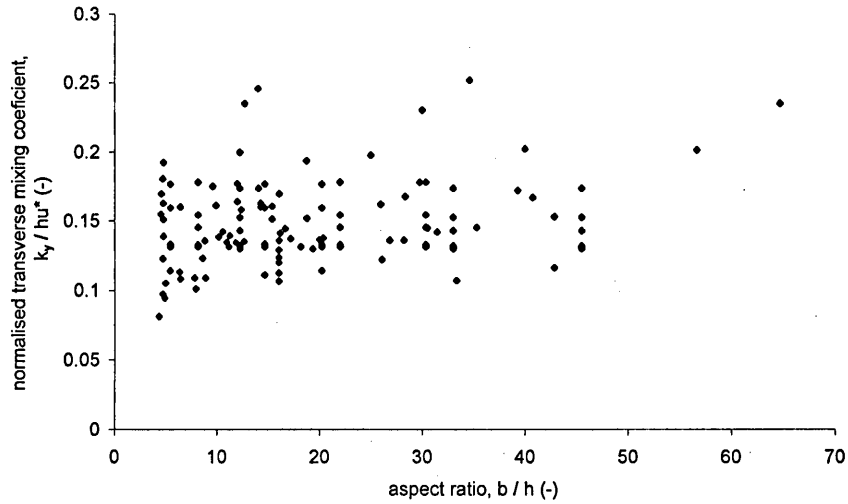

Figure 2.9 Experimental results quantifying transverse mixing for straight, rectangular laboratory flumes. (after Rutherford 1994)

From this data it can be suggested that for plain turbulent shear flow the transverse turbulent diffusion coefficient lies in the range:

$$0.10 < \frac{e_y}{hu*} < 0.26 \qquad \text{Equation 2.105}$$

From Figure 2.9 it can be assumed, as Rutherford (1994) did, that the transverse mixing coefficient is not influenced by the channel aspect ratio, since the overall trend of the data is horizontal. A lower bound estimate of the transverse turbulent diffusion coefficient could be given by:

$$\frac{e_y}{hu*} = 0.134 \qquad \text{Equation 2.106}$$

This is the value suggested by Webel and Schatzmann (1984), and Nokes and Wood (1988), but is lower than some published values. Elder (1959) reported a value for transverse turbulent diffusion coefficient of $e_y/hu*$ of 0.23. Fischer (1967) reports the same value of normalised transverse mixing coefficient for experiments carried out in a straight irrigation canal. However, he noted that the thalweg meandered within the channel and suggested that the secondary currents associated with this meandering were responsible for the increased rate of transverse mixing. Elder (1959) used overhead photography to measure plume development. It would not be possible to distinguish tracer at different elevations within the flow using this technique. Therefore the tracer would be pseudo depth averaged and lead to a mixing coefficient influenced by dispersion.

A comparison of this lower bound value with the value for vertical mixing given in section 2.7.1, shows that the rate of transverse turbulent diffusion is approximately twice that of the vertical.

Although the idealisation of straight rectangular open channel flow assumes no influence of secondary flow on the mixing coefficient, in reality secondary flows of varying degree, will always be present. The

secondary flows encountered in straight laboratory channels are markedly less than those found in straight natural channels. This is because the magnitude of the secondary currents is governed by the bed shear stress. The irregularities, higher and more variable roughness found in natural channels will generate higher bed shear stress levels, thus stronger secondary flows.

Three major papers presenting arguments about the main factors involved in determining the dominant processes which govern the rate of transverse turbulent diffusion are: Lau and Krishnappen (1977), Webel and Schatzmann (1984) and Nokes and Wood (1988).

Lau and Krishnappen (1977) carried out measurements and reviewed past data for straight laboratory channels of varying roughness and concluded that secondary circulations are the dominant contributor to transverse mixing. Consequently, Lau and Krishnappen (1977) suggest that normalisation of the transverse mixing coefficient should be by the product of bed shear velocity and channel width, as channel width governs the upper limit of the magnitude of the secondary flows. Lau and Krishnappen (1977) show that, for their data set, the transverse mixing coefficient normalised in this way varied inversely with channel aspect ratio, h / b. Webel and Schatzmann (1984) cast doubt on the findings of Lau and Krishnappen (1977). They claim that the shallow water depths adopted by Lau and Krishnappen to obtain a wide range of aspect ratios during their experiment were such that surface tension effects would influence the flow. However, from Figure 2.10 it can be seen that the relationship suggested by Lau and Krishnappen is followed by the data collated by Rutherford (1994).

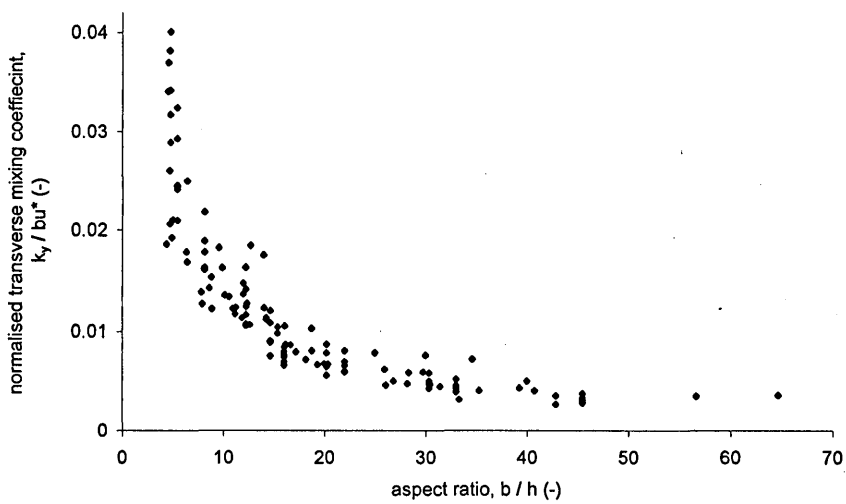

Figure 2.10 Experimental results quantifying transverse mixing for straight, rectangular laboratory flumes. Plotted after Lau and Krishnappen 1977 (data from Rutherford (1994))

Rutherford (1994) questions this result because of the presence of channel width within the ordinates of both axes. However, it should be noted that Rutherford's proposed relationship between normalised mixing coefficient and aspect ratio, represented in Figure 2.9, contains depth of flow, h within both ordinates. However, in Rutherford's relationship flow depth is the denominator in both ordinates. This anomaly can be addressed by adopting a modified aspect ratio, defined as depth / width, and investigating its relationship with normalised transverse mixing coefficient, as suggested by Potter (1999).

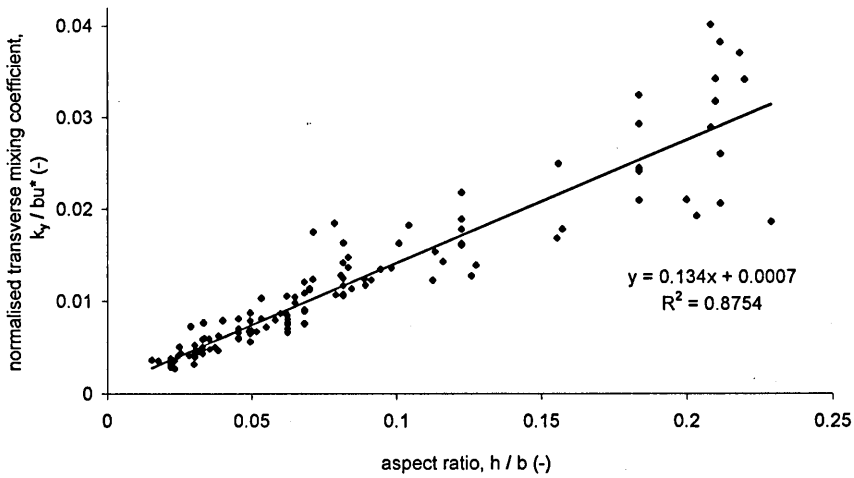

Figure 2.11 Experimental results quantifying transverse mixing for straight, rectangular laboratory flumes. Plotted after Lau and Krishnappen (1977) and Potter (1999), (data from Rutherford (1994))

The trend displayed in Figure 2.11 is independent of channel width as it is now part of the denominator of both axes. The data clearly show the influence of channel depth on the transverse turbulent diffusion coefficient. Similarly, the result shown in Figure 2.9 is independent of channel depth, and a lack of relationship to channel width can be seen. This suggests that it is the channel depth, and not the width that is the important length scale in defining the transverse turbulent diffusion coefficient for plain turbulent shear flow. This contradicts the ideas of Lau and Krishnappen.

It should be noted that the gradient of the linear regression plotted in Figure 2.11 has a value of 0.134. Analysis of the axis of Figure 2.11 shows that the gradient of the regression line is equal to e_y/hu^*, suggesting the same result as drawn by Rutherford (1994) and others. A lower bound to transverse turbulent diffusion coefficient for two dimensional plain turbulent shear flow can be found from the relationship expressed by, $e_y=0.134hu^*$.

It is worth considering the implications of the altered aspect ratio (depth to width) that has been used to create Figure 2.11. When the ratio is low, the channel is wide and shallow, such that the situation will truly be one of two-dimensional flow governed by the bed shear stress. At high depth to width ratio the channel is narrow and deep. In such a situation the flow is likely to be more three dimensional in nature. The situation at high aspect ratio is no longer one of plain turbulent shear flow, and no longer adequately explained by the simple relationship to flow depth and bed shear stress. This argument is supported by the increasing scatter around the trend line with increasing aspect ratio.

Lau and Krishnappen (1977) also attempt to quantify the effect of roughness on the mixing coefficient but with little success. In their conclusions, Lau and Krishnappen (1977) suggest that friction factor and Reynolds number may also be important factors, but that there is an insufficient range covered by the available data set to quantify the relationships.

Webel and Schatzmann (1984) conducted a series of experiments attempting to show that for strongly two dimensional flow, the transverse turbulent diffusion coefficient is independent of the aspect ratio. They also try to define the relationship with effective roughness and turbulence level within the flow. From the

Webel and Schatzmann (1984) data it is difficult to say whether the dependence of transverse turbulent diffusion coefficient upon aspect ratio was proved or disproved, the results table presents only average values of mixing coefficient for sets of varying aspect ratio. Little quality assurance is given in the paper. For example, no regression factor is given for the quality of the straight line fit between variance and distance. However, the results of Webel and Schatzmann's experimental study suggest there is a relationship to the Darcy-Weisbach friction factor, defined as $f=8(u/u^*)^2$, as shown in Figure 2.12. The Darcy-Weisbach factor was chosen as the research suggests that the transverse turbulent diffusion coefficient was dependent on both the effective roughness of the channel bed and the Reynold's number, both characterised by the factor. For all the cases studied Webel and Schatzmann (1984) show a strong relationship between normalised turbulent diffusion coefficient and Darcy-Weisbach friction factor, however, all the cases they investigated were two dimensional plain shear flows.

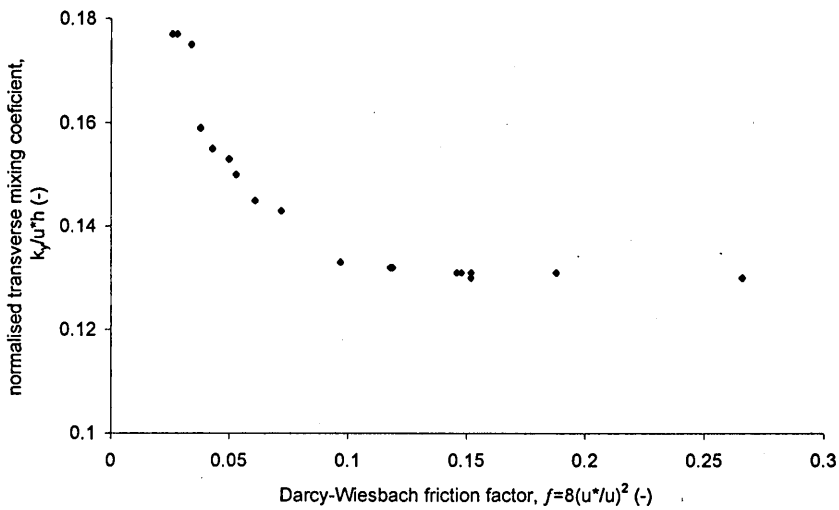

Figure 2.12 Experimental results of Webel and Schatzmann (1984)

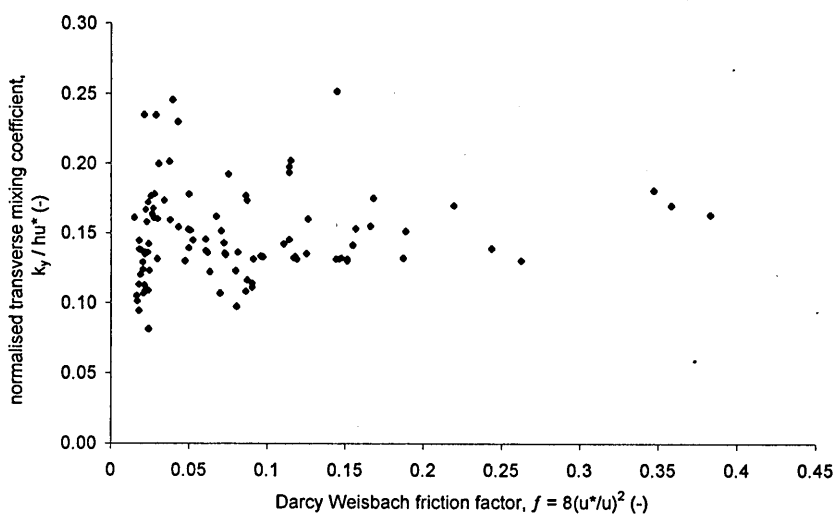

Figure 2.13 Experimental results quantifying transverse mixing for straight, rectangular laboratory flumes, plotted after Webel and Schatzmann (1984), (data from Rutherford (1994))

Using the data from Rutherford (1994), it is possible to create another version of Webel and Schatzmann (1984) figure investigating the relationship between transverse mixing coefficient and Darcy-Weisbach

friction factor. The data collated by Rutherford does include that data from Webel and Schatzmann's study.

As Figure 2.13 shows, the suggested relationship between normalised transverse mixing coefficient and Darcy-Weisbach friction factor is very poorly defined for the data set compiled by Rutherford (1994). The main conclusion to draw is that as the flow conditions deviate from idealised plain two dimensional shear flow, the influence of the Darcy-Weisbach friction factor is no longer significant.

Nokes and Wood (1988) present a definitive theoretical study of the above ideas, together with an investigation into the variation of the transverse mixing coefficient with lateral position. This variation was investigated by considering the 'coupling' of the vertical and transverse mixing processes. Nokes and Wood (1988) drew the following conclusions:

- Experimental results for vertical dispersion support the use of the solution with a parabolic diffusivity and logarithmic velocity distribution.
- The measurements of lateral diffusivity in the near field mixing zone and theoretical solution using a three dimensional eigen-function suggest that the vertical and lateral diffusion processes are uncoupled. This implies that the lateral diffusivity distribution has the same form as the velocity distribution.

Nokes and Wood (1988) reiterate the observation that for fully two dimensional plain shear flow, the transverse turbulent diffusivity can be estimated from the relationship:

$$\frac{e_y}{hu^*} = 0.134 \qquad \text{Equation 2.106}$$

2.8.4 Transverse mixing coefficients for natural channels

A number of publications report transverse mixing coefficients for natural channels. Rutherford (1994) presents a compilation of published values of transverse dispersion coefficients for natural channels from a number of different sources. However, the data table and figures presented by Rutherford are not in agreement. Several of the original publications have been checked and other values verified against other compilations of data, some values remained unchecked and have therefore been removed. Some of the reported values may be questioned, as the analysis methods have not used the rigorous Generalised Method of Moments.

From this checked compilation of data it is possible to create plots to investigate the relationships suggested above for natural channel data. It immediately becomes apparent that the magnitude of the transverse mixing coefficients obtained for 'real' river channels are considerably greater than for laboratory conditions. This can easily be attributed to the secondary flow patterns which are generated in the natural channels by a number of factors, for example irregularities, curvature, changes in shape and roughness.

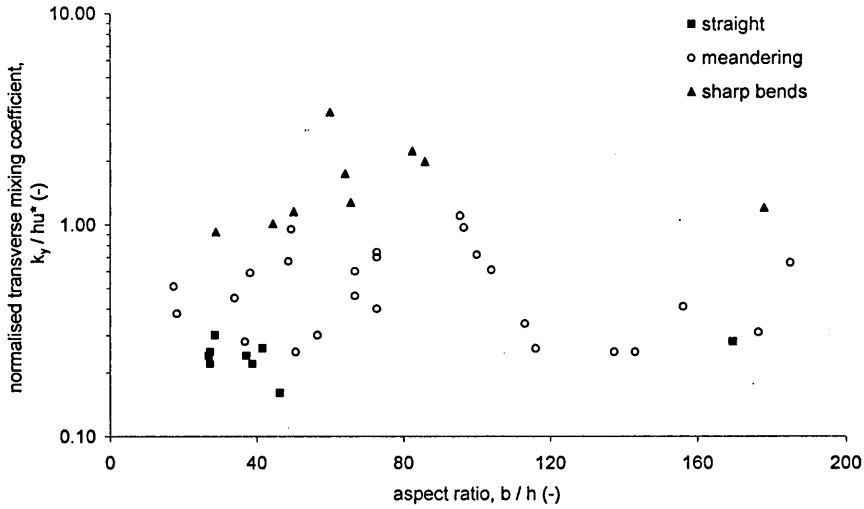

Figure 2.14 Normalised transverse mixing coefficient versus aspect ratio for field data (data from Rutherford (1994))

Figure 2.14 shows wide scatter in the normalised values of transverse mixing coefficients reported from the natural channel data. The variation is in orders of magnitude. However, approximate classification of the channels by the degree of curvature can lead to a banding of the results, suggesting:

'straight' channels	$0.15 < \frac{e_y + k_y}{hu^*} < 0.3$
'meandering' channels	$0.3 < \frac{e_y + k_y}{hu^*} < 1.0$
'strongly curved' channels	$1.0 < \frac{e_y + k_y}{hu^*} < 3.0$

Table 2.3 Classification of transverse mixing coefficients

The lower bound for the straight channel data set is approximately the same as the value previously found to characterise transverse turbulent eddy diffusivity in two dimensional plain turbulent shear flow. The increased upper range can be attributed to the presence of weak secondary currents induced by variations in the channel geometry and / or roughness. From the other two classifications it can be seen that as curvature increases so does the rate of transverse mixing.

Given the order of magnitude increase in values of normalised transverse mixing coefficients with increasing curvature, the turbulent diffusivity term could be considered negligible for curved channel cases and dropped. However, a more precise definition can be found if the decomposition of the above expressions were considered:

$$\frac{K_y}{hu^*} = \frac{0.134 + k_y}{hu^*} \qquad \text{Equation 2.107}$$

where K_y represents the catch all, or average of the diffusions and dispersion terms. K_y is often replaced by k_y, because of the relatively small value of e_y compared to k_y, values of k_y are assumed to encompass the effects of diffusion.

Following the work of Lau and Krishnappen (1977) and Potter (1999) a plot can be created to investigate the validity of hu* as the factor to be used to normalise transverse mixing coefficients. In Figure 2.15, the meandering channel data shows a reasonable fit to the straight-line regression suggesting that local flow

depth and bed shear velocity are valid for the purposes of normalisation of the transverse mixing coefficient.

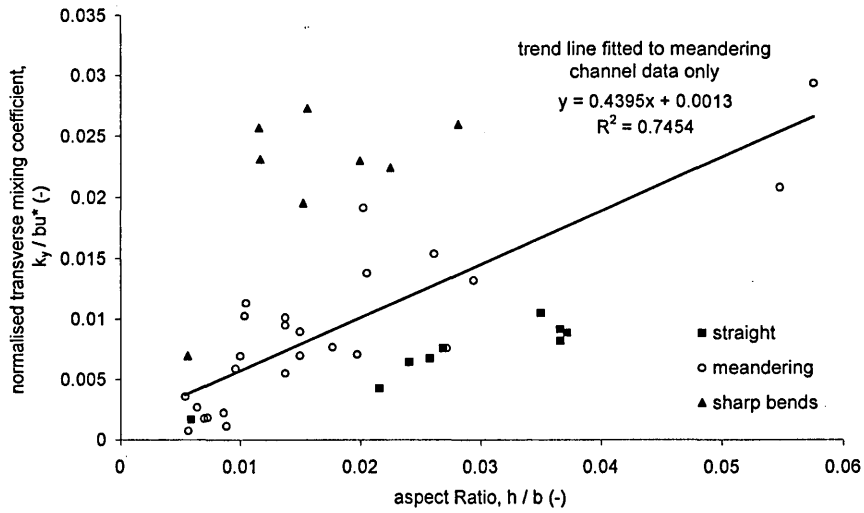

Figure 2.15 Normalised transverse mixing coefficient versus modified aspect ratio for field measurements (data from Rutherford (1994))

A significant change between the gradient of Figure 2.11 and Figure 2.15 can be seen, again reinforcing the increase in mixing rate between straight two dimensional laboratory experiments and natural channels. The increased gradient for the meandering channel data fits well in the middle of the range suggested above.

Following the work of Webel and Schatzmann a graph of normalised transverse mixing coefficient versus the Darcy-Weisbach friction factor has been produced for the natural channel data, Figure 2.16. However, as for the compiled straight laboratory channel data set, there is little relationship between the friction factor and the mixing coefficient.

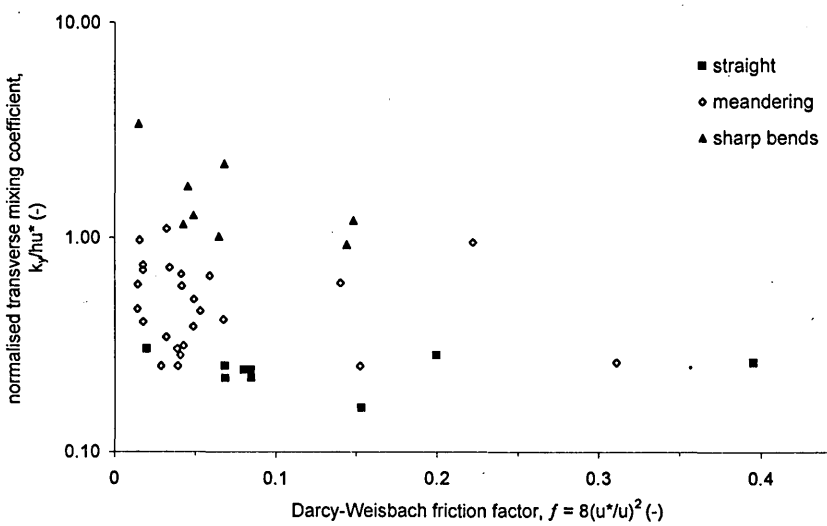

Figure 2.16 Normalised transverse mixing coefficient versus Darcy-Weisbach friction factor for field measurements (data from Rutherford (1994))

It is possible to produce an additional plot from the natural channel data set that investigates the relationship between discharge and transverse mixing coefficient. From Figure 2.17 there appears to be a

direct correlation between transverse mixing coefficient and flow rate. However, the trend breaks down if the relationship between normalised coefficient and discharge is investigated.

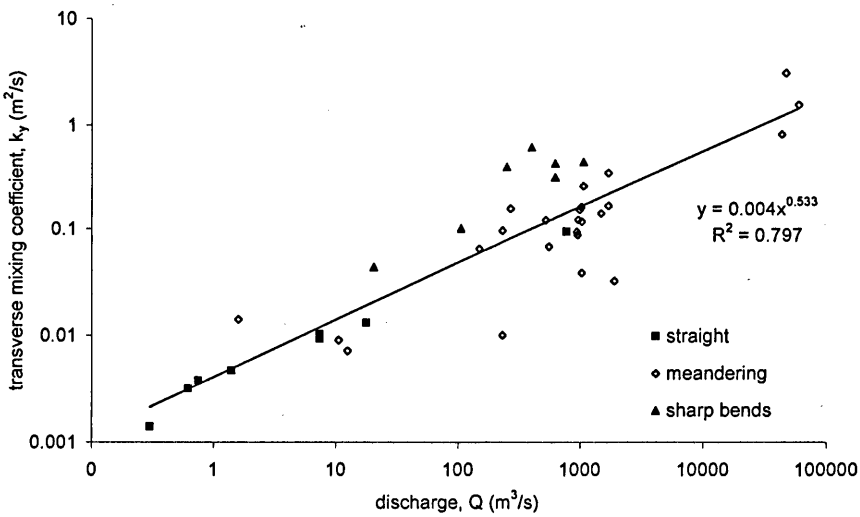

Figure 2.17 Normalised transverse mixing coefficient versus discharge for field measurements (data from Rutherford (1994))

Figure 2.17 shows a very clear trend between the logarithms of transverse mixing coefficient and discharge. This suggests that the nature of the relationship is a power law. The value of this is given by the gradient of the regression line and suggests that for natural river channels the nature of the variation of mixing coefficient with discharge is of the same form of the variation of cross-sectional average primary velocity.

2.8.5 Transverse mixing in channels with plan-form curvature

Fischer (1969), in his paper "The effects of bends on dispersion in streams" follows a similar line of reasoning as Elder (1959) used to compute an expression for longitudinal mixing from the vertical velocity distribution. Fischer derived a predictor for the transverse mixing coefficient in fully developed secondary flows. Fischer started from Rozovskii's (1957) theories and expressions for predicting fully developed secondary flows, and derived the following expression:

$$k_y = -\frac{U^2 h^3}{\kappa^5 r_c^2 u^*} I \qquad \text{Equation 2.108}$$

where κ is Von Karman's constant (0.41), and r_c is the radius of curvature (m). The value of I is obtained from the triple integration of Rozovskii's (1957) equation, or can be found from standard graphs with variables of friction factor and Von Karman constant.

Fischer tested this predictor by performing transverse mixing measurements in a circular flume. The flume consisted of a 330 degree bend, vertical steel sides and wooden base, and a centre line radius of curvature of 2.06m. Injection was 90 degrees around the bend, to allow secondary currents to develop, and the furthest down stream measurement was at 180 degrees, such that flow was not influenced by the perforated plate weir outlet at 330 degrees.

The results of Fischer's experimental study are shown in Table 2.4. The values for predicted and measured mixing coefficient show good agreement at low flow rates. However, there is some divergence at the higher flow rates. Fischer attributes this to the short development length. The fully developed secondary flow fields assumed in the analysis, had not had sufficient time to establish in the 90 degrees before injection.

Q (cm^3/s)	D (cm)	S_0 (-)	U_x (cm/s)	U* (cm/s)	Darcy-Weisbach factor (-)	Distance from injection, (m)	Variance (cm^2)	Predicted coefficient (cm^2/s)	Observed coefficient (cm^2/s)
720	3.02	0.0023	31.7	2.66	0.050	0.61 1.22 1.83	21.5 65.5 109	6.79	11.3
1063	5.28	0.0010	27	1.70	0.040	0.61 0.91 1.22	42.6 92.3 139	43.8	21.4
756	3.72	0.0012	26.8	2.13	0.050	0.61 1.22 1.83	22.0 68.5 118	11.8	10.6
290	2.03	0.0012	19.0	1.37	0.042	0.61 1.83	8.5 33.4	1.5	1.95
328	2.20	0.0013	19.7	1.68	0.058	0.61 1.83 3.05	8.9 32.2 61.8	1.66	1.88

Table 2.4 Fischer (1969), results of laboratory experiments

Fischer also compares his equation with field data from a study on a long bend on the Missouri River. Table 2.5 shows two sets of hydraulic conditions, firstly, the cross-sectional mean values from which a low value of transverse mixing coefficient is obtained and secondly, the observed combination of depth, velocity and radius of curvature from which the maximum value of mixing coefficient is predicted. From this Fischer concludes that as the maximum predictable coefficient is greater than the observed, therefore the secondary currents are at least partially responsible for the increase in mixing rate.

	Cross-section mean	Values to yield max. k_y
Depth mean velocity, u (m/s)	1.75	2.5
Depth, h (m)	2.7	4.9
Curvature Radius, R (m)	3400	1500
Bed Shear Velocity, u* (m/s)	0.074	0.074
Von Karman constant, κ (-)	0.4	0.35
k_y from Equation 2.108 (m^2/s)	22.2×10^{-4}	2740×10^{-4}
e_y from Equation 2.106 (m^2/s)	2.9×10^{-4}	5.3×10^{-4}
k_y observed (m^2/s)	1200×10^{-4}	

Table 2.5 Fischer (1969), results of field study

In Table 2.5, the values predicted for the transverse eddy diffusivity have been included. This shows the relative unimportance of the eddy diffusivity when compared to the dispersion processes brought about by the secondary circulations.

Fischer's work highlights the effect of bends and secondary circulations in dramatically increasing the rate of transverse mixing. He also shows that working from the relatively straight forward predictive equations presented by Rozovskii (1957) it is possible to derive an expression to predict the transverse mixing coefficient in fully developed secondary flows. He further shows that under ideal laboratory conditions this predictor is accurate. However, inaccuracies are experienced when applying the predictor to field data. This can be attributed to two main factors. 1. The difficulty of defining such parameters as

radius of curvature and mean flow depth for natural channels. 2. The suggestion could be made that under field conditions parameters vary around any given bend to such an extent that the flow is never truly fully developed. Fischer extended this paper by investigating the effects of bends on longitudinal dispersion through the interdependence of longitudinal and transverse mixing.

By considering the flow conditions in many lakes, sea and wide continental shelves, Fischer (1978) derived a 'tensor forms of the bulk dispersion coefficients'. Fischer's analysis was derived to predict the dispersion coefficients for uniform longitudinal velocity profiles and stepped transverse distributions. An important result from this work is a predictor of mixing coefficient in the presence of a stepped velocity distribution.

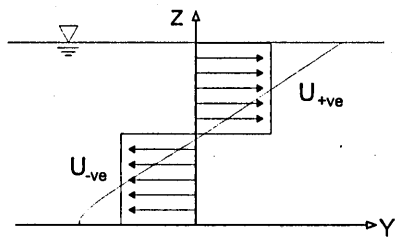

Figure 2.18 Step velocity profile as used in Fischer (1978)

$$k_y = \frac{(u_+ - u_-)^2 . h^2}{48e} + e_y \qquad \text{Equation 2.109}$$

However, the approximation of the secondary flow conditions to this idealised step function leads to an underestimate of mixing coefficient, due to under predicting the shear effects. In addition, the prediction of the magnitudes of the velocities associated with such step functions is left unexamined.

Chang (1971) was the first person to publish results from experiments carried out investigating transverse mixing in meandering channels under laboratory conditions. He used two laboratory channels, both of rectangular cross section. To obtain estimates of the transverse mixing coefficient from concentration measurements, Chang utilised the Generalised Method of Moments in Cartesian co-ordinates, see section 2.6. This necessitates the measurement of transverse velocity distributions. Chang also used a model fitting procedure to obtain estimates of mixing rates. The model is based on a stream-tubes approach, again necessitating some velocity measurements to define the stream tubes. From these two methods, he concludes that the results are remarkably similar, but that the construction and solution of the stream tube model is much simpler than the Generalised Method of Moments in regular Cartesian co-ordinates. Chang suggests a method to predict transverse mixing coefficients from measured lateral velocity distribution, however he found that his predictor is deficient for the meandering channel case.

The major conclusions which can be draw from Chang (1971) are that the depth average form of the ADE equation is adequate for analysing and predicting transverse mixing problems in meandering channels. Although some question is placed on the validity of the approximation near the banks, where the flow is more three dimensional, vertical velocities are not negligible in this region. Chang also showed that the transverse mixing coefficient varies periodically in the longitudinal direction, as can be seen in Figure 2.19. Figure 2.19 also attempts to show variation in rate of mixing, as a function of transverse position. From the results it does not seem to be a significant variation, but from Chang's method of integration of

the measured transverse velocity distribution, it seems that it may be possible to predict the variation in transverse mixing rate.

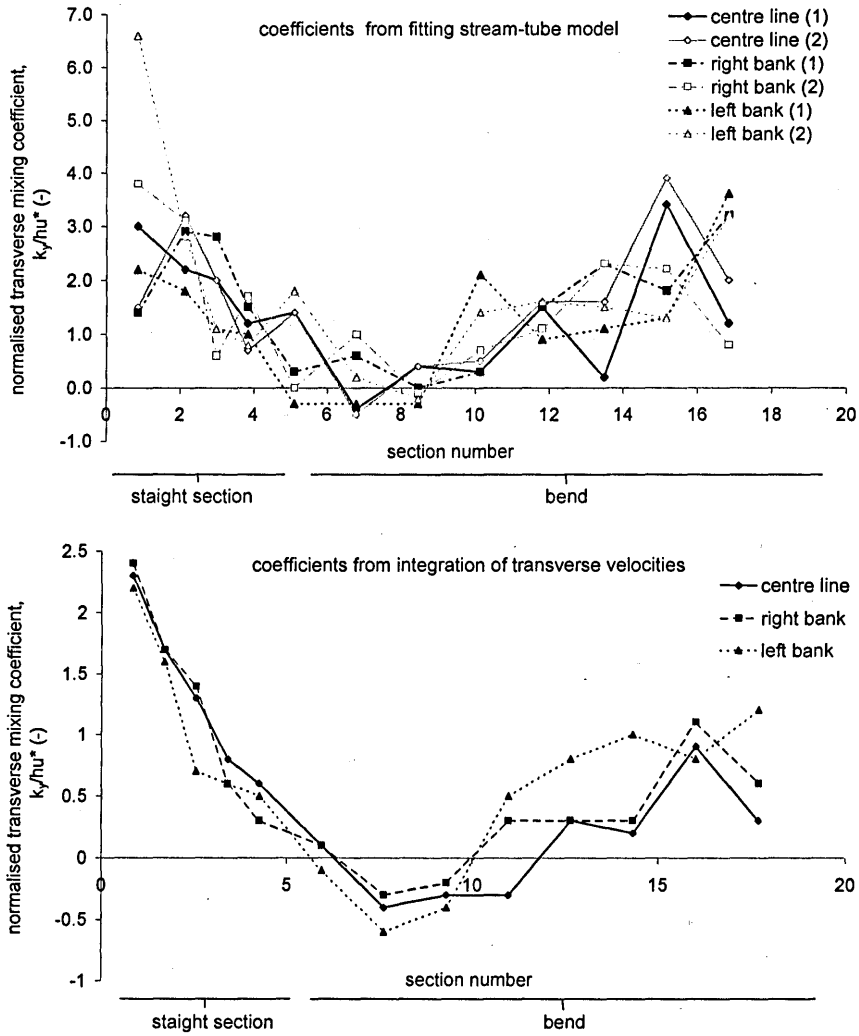

Figure 2.19 Longitudinal variation in transverse mixing coefficients for different injection points, from Chang (1971), large flume data only (b = 2.33m, straight length = 4.27m, r_c = 8.54m, θ = 90°)

Chang (1971) consistently reports negative values of transverse mixing coefficient, as can be seen in Figure 2.19. This poses serious question as to the validity of the data, and / or the analysis methods used.

Velocity measurements made and used throughout the analysis were made using a Pitot tube type device. The measurements were made over a reasonably spaced grid, given the dimensions of the flumes, 11 verticals with 9 points in the vertical for the large flume. However, the introduction of Pitot tubes causes disturbance of the flow, and the required measurement of static head can be highly suspect in the presence of strong secondary flows. This cast doubts over the quality of the results.

In both sets of experiments Chang used a continuous pass system to obtain transverse concentration distribution measurements. The measurement system, conductivity probe or fluorometer was continuously logged as the probe, or sample tube, was slowly driven across the channel. For the large flume case each pass over the channel width of 2.33m lasted 3 minutes. It is suggested that continuous

passes at this speed will have been too fast to provide good quality data. There would be insufficient time to average out longitudinal variations, allow for the response time of the instruments, spreading in sample pipes, or attenuation of peak. No mention is made of repeat passes or other checks on the repeatability of the measurements made. Passes were made at four depths in the large flume and three in the small flume. This suggests that the concentration data maybe poorly defined both vertically, leading to depth averaging errors, and transversely, leading to errors in the estimation of coefficients.

Krishnappen and Lau (1977) also investigate transverse mixing in meandering plan-form channels. Their investigation makes two steps forward from Chang (1971). Instead of using a rectangular channel, they allowed a bed form to generate freely under the flow condition to be studied. This bed-form was then fixed. However, the channel form development was restrained within fixed vertical side walls. Krishnappen and Lau (1977) also investigate the relationship between mixing coefficient and the ratio of meander amplitude to channel width. The laboratory channels were at a fixed width of 300 mm, so were small-scale experiments. The meander wavelength was constant. The amplitude was varied from 300 to 1500mm. Data analysis used the Generalised Method of Moments, again in a Cartesian co-ordinate system, necessitating measurements of longitudinal and transverse velocities. Krishnappen and Lau (1977) also use the Generalised Method of Moments to investigate the effects of transverse variation in the transverse mixing coefficient.

From their work, Krishnappen and Lau drew the following conclusions. The variation in the flow depth generated from the mobile bed is important in setting up secondary circulations. Therefore, variations in flow depth have a strong effect on the mixing processes. The advective transport is of the same order of magnitude as the transport due to dispersion. From the investigation of the transverse variation in transverse mixing coefficient, they conclude that k_y can be treated as independent of transverse location. This suggests that width only average values of transverse mixing coefficients are required for accurate predictions. Krishnappen and Lau (1977) also conclude that there is a strong, although un-quantified, link between dispersion coefficient and meander amplitude to channel width ratio.

Some questions may be raised over the work presented by Krishnappen and Lau (1977). The variance distance graphs presented show considerable scatter about the best-fit straight line used to calculate the mixing coefficients. This error may arise from inaccuracies in the evaluation of the variances of the distributions. The transverse concentration plots given suggest that each transect is only defined by eleven depth average point measurements across the channel. It is unclear how many, or at what spacing, measurements have been made over depth to obtain this average. This spatial resolution is insufficient to yield an accurate evaluation of variance. The concentration plots also show considerable skewness due to the meander in the main flow thalweg. Such meandering will have been exaggerated by the variable flow depth. This effect is only correctly accounted for by the Generalised Method of Moments once it has been adapted into cumulative discharge terms, as in section 2.5.1, and not by the Cartesian form of the method as used by Krishnappen and Lau.

The results presented by Krishnappen and Lau (1977) show no cyclic variation in the transverse mixing coefficient with longitudinal distance. Such variation was shown in the results of Chang (1971), and might be expected with the build up and decay of secondary currents along meandering channels. No

clear reasoning is given for the assumption that the change in the magnitude of the mixing coefficient should be related to the ratio of amplitude to width. Sinuosity may be better used to describe, or characterise the channel plan-form geometry. The results presented are somewhat confused, because of the attention paid to establishing the importance of transverse variation in transverse mixing rate. It is, therefore, not possible to attempt an investigation of the dependence of this data set on sinuosity.

Lau and Krishnappen (1981) investigate the use of the cumulative discharge approach to simplify some of the problems which are associated with modelling natural channels. A finite difference model solution of the advection dispersion equation in cumulative discharge terms is presented. They validated the model against a set of field data collected on the Grand River and show that the model could be used to accurately simulate the natural river channel system, once the transverse mixing coefficient has been evaluated.

The form of the solution developed facilitated an investigation into how transverse mixing varies across a channel. Results from the simulation, assuming different transverse variations were compared with the field measurements. The relationships investigated were given in section 2.6.4. This investigation concludes that other than at very short distances below injection, a constant value of transverse mixing coefficient could be assumed over the cross section, without loss of accuracy in the prediction.

In the final section of this paper attention is focused upon predicting values of the transverse mixing coefficient. The increase in mixing rate for natural channels over laboratory channels is again noted. It is suggested that the channel sinuosity may be the factor governing the change in mixing rate. In straight laboratory channels the rate of mixing is governed by the turbulent diffusion and dispersive transport due to secondary currents brought about by variations in bed shear stress. In natural channels, mixing is dominated by the dispersion brought about by secondary circulations, primarily induced by plan form curvature. Therefore, it seems reasonable to suggest that the mixing rate is not only dependent on aspect ratio and bed shear stresses, but also on some measure of the 'bendyness' of the channel.

Direct measurements of factors such as radius of curvature are difficult to define for natural channels. Any given river reach is usually characterised by straight sections joined by bends of different and varying radii of curvature. Therefore, the radius of curvature does not seem to be a practical method of characterising 'bendyness'. The suggested method of characterising meander configurations is a sinuosity factor, defined as the ratio of meander length to straight-line reach distance.

Lau and Krishnappen (1981) attempted to compile a data set of measured transverse mixing coefficients and sinuosity to investigate any potential relationship. Unfortunately, when past studies were undertaken measurement of sinuosity was not considered important. The majority of studies provide no information pertaining to sinuosity. In the data set compiled only two studies have significant sinuosity. It is therefore not possible to draw firm conclusions about the relationship between sinuosity and transverse mixing coefficient.

Since the work of Lau and Krishnappen (1981), no significant studies have been carried out to investigate the proposed relationship. It may be possible to carry out such an investigation using the field data set from Section 2.8.4. However, considerable time would have to be spent characterising the various test

reaches. In the future, it may be possible to do this from detailed maps, aerial photography and / or Global Imaging Systems. Unfortunately such systems do not currently provide sufficiently detailed information and are very expensive, therefore, it would be necessary to carry out very expensive site surveys rendering the project unviable.

2.9 Longitudinal Mixing

Longitudinal mixing occurs in the far field, which is once the tracer has mixed fully over the complete channel cross section. It is important to note that if tracer source and river flow are steady then for a conservative tracer concentrations in the far field will be constant.

Modelling longitudinal dispersion is most important where there is a sudden discharge, such as an accident involving a tanker on a bridge or combined sewer overflow resulting from summer storms. Such sudden discharges occur relatively infrequently. The majority of pollution incidents approximate steady state, with only gradual temporal variation. In these situations, transverse mixing is more important. However, the majority of work, particularly fieldwork, has concentrated on longitudinal mixing. This discrepancy arises because of the comparative ease with which the passage of the tracer can be monitored, and the time of travel information obtained. Time of travel data is vital for the calibration of all water quality models.

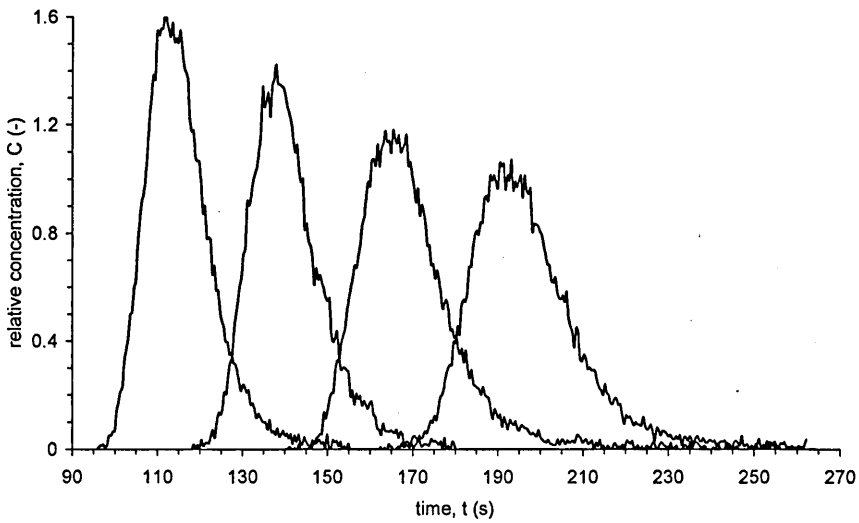

Figure 2.20 Typical time concentration profiles for longitudinal mixing tracer study

Figure 2.20 shows results from a laboratory based longitudinal mixing test. Typical time-concentration plume measurements can be seen for four sites along a channel. The decay of the peak concentration and increasing spread with distance / time can be seen.

2.9.1 Shear effects

In Section 2.4 the advection dispersion equation was simplified by depth and then width averaging, and through this the effects of shear dispersion introduced. Vertical and transverse shear dispersion are the two dominant processes causing longitudinal mixing. Fischer (1967) showed that for river channels the transverse shear effects make a greater contribution to the longitudinal mixing than vertical shear.

According to the ideas of Fickian diffusion, first presented by Taylor (1953, 1954), and as mentioned in Section 2.4.3, after an initial period, equilibrium between shear dispersion and turbulent diffusion exists. Once the tracer has had sufficient time to sample the complete flow field the effects become balanced, provided the effects are stationary random functions of time. In Figure 2.21 the initial effects of differential advection by the velocity field can be seen. In this period the tracer cloud will become negatively skewed, a shorter rising than falling limb. At the end of this purely advective zone the effects of shear dispersion and turbulent diffusion reach equilibrium. After this point the variance of the tracer profile will grow linearly with time / distance, and the skewness of the variation will slowly decease.

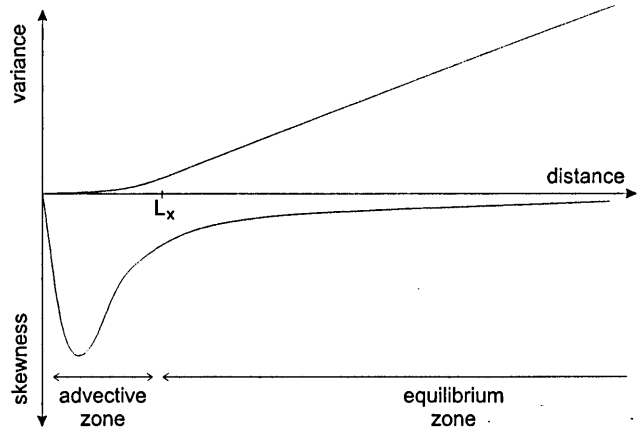

Figure 2.21 Fickian model of how skewness and variance of an instantaneous injection of tracer develops with distance

There is a misconception that in the equilibrium zone tracer concentrations are uniform over the cross section. However, velocity shear constantly creates concentration gradients that are continually, but never entirely, being removed by turbulent mixing. The prime effects of various river irregularities are to retard the onset of the Fickian dispersion process and enhance the rate of dispersion.

Elder (1959) derived an expression to predict the magnitude of the longitudinal mixing coefficient for two-dimensional flow where the vertical velocity distributions can accurately be predicted from the log law. Elder's solution involves the triple integration of the velocity distribution over the channel, yet yields the simple result:

$$D_x = \frac{0.4041}{\kappa^3} hu^* + \frac{1}{6} \kappa h u^* \qquad \text{Equation 2.110}$$

taking Von Karman = 0.41 $\qquad D_x = 5.93 h u^*$

By carrying out experiments in a very wide straight flume, where the flow is plain turbulent shear flow, Elder proved this expression accurate.

The work of Fischer (1967) shows that the rate of longitudinal mixing could be significantly altered by transverse variations in the primary velocity. Fischer's results are summarised in Table 2.6. The tests were carried out in straight trapezoidal laboratory channels.

Series	Banks	Flow depth (m)	Velocity U (m/s)	Channel width (m)	Longitudinal mixing coefficient D_x (m^2/s)	Normalised mixing coefficient D_x/Ru^*
3300	Smooth	0.034	0.483	0.39	0.0282	39
3000	Rough	0.035	0.451	0.38	0.4150	410

Table 2.6 Summary results from Fischer (1967)

The ten-fold increase in mixing coefficient can be attributed to the increase in the transverse shear brought about by the increase in channel bank roughness.

Based on the hypothesis that the processes governing the rate of longitudinal mixing are shear effects Fischer (1968) presented a theoretical expression for predicting the longitudinal dispersion coefficient:

$$D_x = -\frac{1}{A}\int\int_A u'dA\int_0^y \frac{1}{k_y d(y)}dy\int_0^y\int_0^{z(h)} u'dzdy \qquad \text{Equation 2.111}$$

where prime denotes spatial variation from cross-sectional mean.

This expression requires the integration of the shear effects over the complete cross section coupled with an estimate of turbulence and transverse mixing rate. The complete solution of this equation is very complex.

2.9.1.1 Approximate solution

Chickwendu (1986) presents the derivation of a method for calculating longitudinal dispersion coefficients, for contaminates in laminar or turbulent two-dimensional channel or pipe flow. The solution is based on the same ideas as Equation 2.111, but the solution is tractable. The method divides the flow into *N* zones of parallel flow each considered well mixed, and moving at a distinct uniform velocity. A dispersion equation is obtained for each zone and cross-stream mixing between the zones is taken into account, leading to a system of *N* coupled dispersion equations. The exact longitudinal dispersion rate at large times can be calculated for the *N*-zone model. Chickwendu (1986) notes that as *N* tends to infinity an integral expression can be obtained for the dispersivity.

After significant mathematical manipulation Chickwendu arrived at the following:

$$D(N)_x = \sum_{j=1}^{N-1}(q_1+q_2\ldots+q_j)^2\left[1-(q_1+q_2\ldots..+q_j)\right]^2.\left[u_{12\ldots j}-u_{(j+1)\ldots N}\right]^2/b_{j(j+1)}+\sum_{j=1}^{N}q_j e_{xj} \qquad \text{Equation 2.112}$$

where

$q_j = h/h_j$

e_{xj} = zone diffusivity in respective direction

$$b_{j(j+1)} = \frac{2e_{yj(j+1)}}{d^2(q_j+q_{j+1})}$$

$$u_{12\ldots j} = \left(\sum_{k=1}^{j} q_k u_k\right)\Big/\left(\sum_{k=1}^{j} q_k\right) = \text{mean velocity in the first j zones}$$

$$u_{(j+1)\ldots N} = \left(\sum_{k=j+1}^{N} q_k u_k\right)\Big/\left(\sum_{k=J+1}^{N} q_k\right) = \text{mean velocity in the last } (N\text{-j}) \text{ zones}$$

The form of the Chickwendu (1986) method can be considered analogous to the Simpson or Trapezium rules. The technique uses an approximation to provide a solution to a difficult or intractable integral function. The mathematics can be programmed on a spreadsheet, incorporating as many zones as required for sufficient accuracy.

2.9.2 Skewness

All field measurements of longitudinal concentration profiles exhibit deviation from a Gaussian shape. A Gaussian distribution is predicted by all solutions based on a Fickian model.

Day (1975) showed, through a Chatwin (1971) analysis, that the spread or standard deviation of an initially concentrated mass increases linearly with distance, but that the concentration profiles maintain a persistent asymmetry. These features suggest that the mean properties of the motion never become stationary random functions of time, as stipulated by a Taylor analysis of Fickian diffusion problems.

Ideally, concentration profiles would be presented as an instantaneous snap shot of the dye plume, concentration versus distance at a fixed time. However, this is extremely difficult to obtain experimentally. Most dye concentrations are temporal profiles, concentration versus time at a fixed site. Thus, skewness arises from the fact that longitudinal mixing occurs during the time taken for the tracer cloud to pass a fixed site. Therefore, asymmetry in temporal concentration profiles is not necessarily an indication of deviation from the Fickian model. Chatwin (1971) and (1980) presents mathematical tools to transform between temporal and spatial measurements, and methodologies to present and quantify the skewness. Results analysed using these transformation techniques still show skewness to varying degrees. Guymer (1998) presents longitudinal dispersion data from the Flood Channel Facility (HR Wallingford) from a 60 degree meander plan-form channel, with trapezoidal and 'pseudo natural' channel cross sections. Chatwin analysis of the results shows that both configurations yield negatively skewed concentration profiles. The analysis also shows an increase in skewness for the 'pseudo natural' channel over the trapezoidal channel.

Figure 2.21 suggests that the initial advective zone imparts considerable skewness to the tracer profiles. The Fickian dispersion model predicts that this skewness will gradually decay once the equilibrium zone is reached, and tracer profiles eventually become Gaussian. Estimates of the distance until profiles approximate a Gaussian form vary from Fischer *et al* (1979) $x > 2.5L_x$ to Lui and Cheng (1980) $x > 50\ L_x$. Where x is the distance from injection, and L_x is as defined on Figure 2.21. Thus, even in experiments where the conditions conform to the ideal of diffusion and dispersion effects being stationary random functions of time, skewness introduced during the advective zone may be present over the complete measurement distance.

In non-uniform channels it is unlikely that diffusion and dispersion characteristics are stationary functions of time. Thus, equilibrium between diffusion and dispersion is never likely to be established. Therefore, the use of equations based on Taylor's analysis of Fickian diffusion are not truly valid for natural channels. However, there is a large body of empirical evidence to suggest that the Fickian model accurately describes the processes of longitudinal mixing, given the correct mixing coefficients.

2.9.2.1 Dead zones

Natural river channels often exhibit regions of recirculating flow, or stagnant water. These features are often termed dead zones and effectively trap tracer.

Valentine and Wood (1977) studied the effect of dead zones under laboratory conditions. They investigated the effects of dead zones of various sizes uniformly distributed over the bed. A no dead zone situation was used as a control. From these studies they drew several conclusions:

1. The initial advective period, or time, when the effects of diffusion and dispersion are not in equilibrium is greatly increased by the presence of dead zones.
2. Where dead zones are uniformly distributed over the entire channel length, equilibrium between diffusion and dispersion becomes established.
3. The rate of increase of variance with time / distance becomes linear.
4. This rate of growth is significantly increased by the presence of the dead zones, the longitudinal mixing rate is increased.
5. The skewness of the measured profiles is increased by dead zones.
6. The trapping effect of the dead zones as the tracer first passes, and then the comparatively slow release of tracer back to the main flow considerably increases the initial skewness of the concentration profiles.
7. The rate at which the concentration distribution approximates to a Gaussian is decreased by the trapping effects of the dead zones.

The effects of dead zones are not allowed for in any of the theoretical derivations of the longitudinal mixing equations thus far considered. Given the high spatial variability of natural channels, it is very difficult to quantify and / or predict dead zones and their effects. The quality of fit obtained between measured and predicted profiles suggests that Fickian diffusion models are sufficient for most natural channel situations. However, if the measured concentration profile exhibits extreme skewness (large dead zone effects) the model fit becomes less accurate. Solutions of the Fickian model cannot predict skewed distributions.

2.9.3 Field data

A considerable number of longitudinal mixing tracer studies have been undertaken in the field. Rutherford (1994) provides a table of longitudinal mixing coefficients and all available channel property information. This data is from a variety of sources. The majority of the quoted values of longitudinal mixing coefficient have been found using the change of moments method. It is, therefore, possible that there is considerable error in the quoted coefficient values, arising from inaccuracy in the calculation of variance. Noise or inaccurate measurement at the plume edge can have a great effect on the calculated variance. Errors in calculated variance also arise from poor spatial resolution of plume measurement points. The quoted coefficients are reach specific.

2.9.3.1 Discharge

The data set facilitates investigation of the relationship between longitudinal mixing coefficients and discharge. Figure 2.22 shows the relationship in its simplest form. A direct correlation can be seen between the logarithms of longitudinal mixing coefficient and discharge.

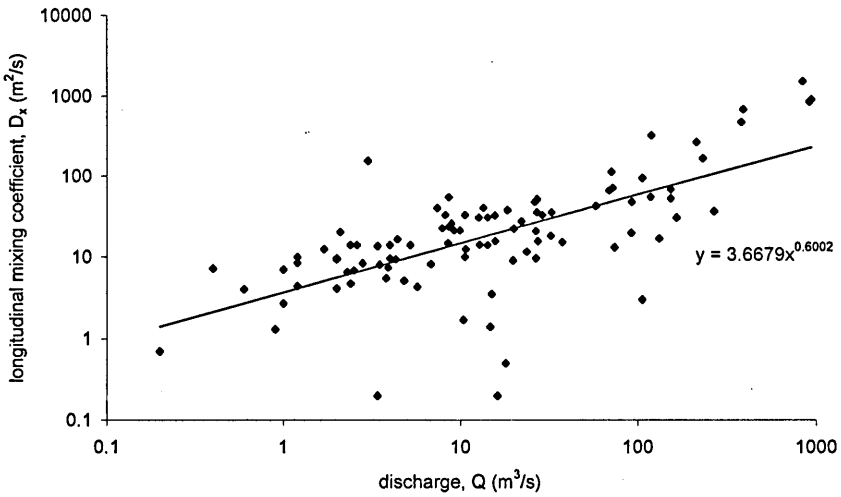

Figure 2.22 Longitudinal mixing coefficient versus discharge from field data set (data from Rutherford (1994))

Knowing no more than an estimate of discharge, it is possible to make an estimate of the longitudinal mixing rate from Figure 2.22. However, such an estimate will have a large degree of error associated with it. In the compiled data table, Rutherford (1994) presents results for the same reach at different discharges on four different English rivers. From this it is possible to specifically investigate the effect of discharge on dispersion rate. This is shown in Figure 2.23, and suggests that mixing rate increases as a power function with discharge.

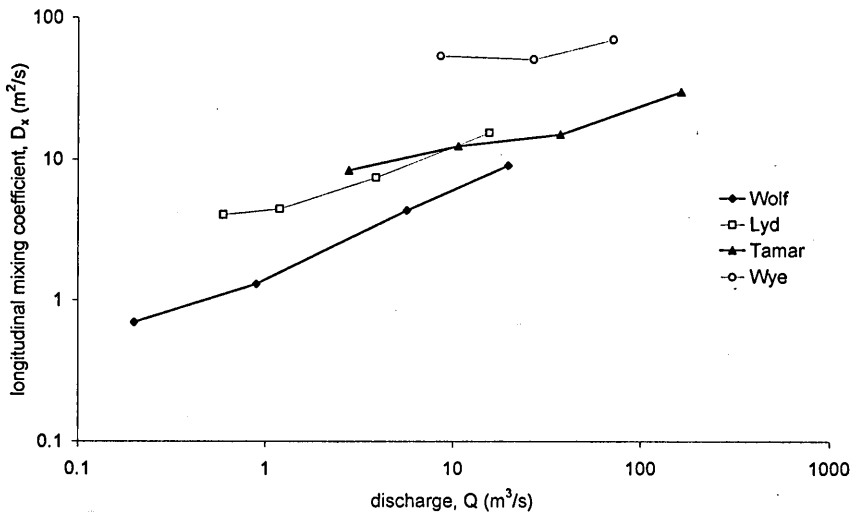

Figure 2.23 Longitudinal mixing coefficient versus discharge for four UK rivers reaches at different discharges (data from Rutherford 1994))

The data which is presented in Figure 2.23 is unpublished data from the Water Research council, U.K. Unfortunately, only final coefficient and discharge information is available for these reaches. Therefore, it is not possible to investigate the change of normalised coefficient with discharge for these cases, or further classify the reaches.

2.9.3.2 Aspect ratio

It is possible to investigate the relationship between normalised mixing coefficients and aspect ratio, as performed for the transverse mixing data.

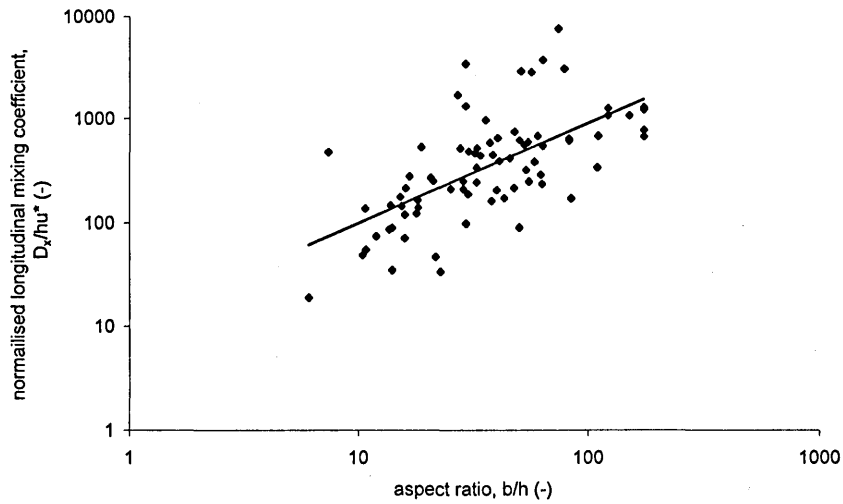

Figure 2.24 Normalised longitudinal mixing coefficient versus channel aspect ratio for field data set (data from Rutherford (1994))

Plotting the logarithm of longitudinal mixing coefficient, normalised by local depth of flow and average bed shear velocity, against the logarithm of aspect ratio, depth over width, Figure 2.24 shows an increase in coefficient with increasing aspect ratio. At low aspect ratio, narrow deep channels, secondary currents are strong, leading to smoothing of the primary velocity profile and thus to lower rates of longitudinal shear. With increasing aspect ratio, the secondary currents become less pronounced leading to an increase in the rate of primary velocity shear.

Figure 2.24 highlights the spread in normalised values of longitudinal mixing coefficient. Suggested upper and lower bounds are:

$$30 < \frac{D_x}{hu^*} < 4000 \qquad \text{Equation 2.113}$$

Following a similar line of reasoning as in section 2.8.4, a plot of longitudinal mixing coefficient normalised by channel width and bed shear velocity versus modified aspect ratio can be produced, Figure 2.25. The plot should highlight trends relating the rate of mixing to the upper bound of the turbulence and secondary flow structures, channel width. However, Figure 2.25 shows considerable scatter suggesting no direct relationship. The range of normalised values shows a similar order of magnitude variation as the previous method of normalisation.

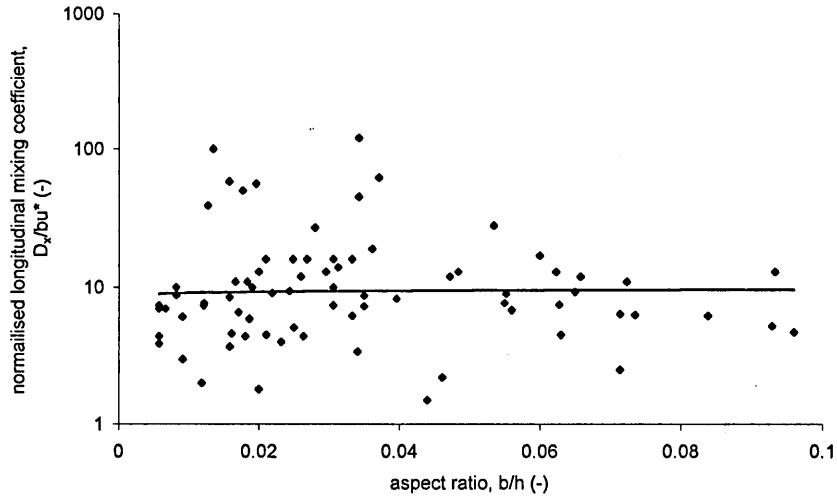

Figure 2.25 Normalised longitudinal mixing coefficient versus modified aspect ratio from field data set (data from Rutherford (1994))

2.9.3.3 Hydraulic radius

Several authors have utilised hydraulic radius and bed shear velocity to non-dimensionalise longitudinal mixing coefficients, Fischer (1967), Lui (1977), Beltaos (1980), and Guymer (1998). However, none of the authors provides specific reasons for adopting hydraulic radius, as opposed to depth or width as a normalising factor.

The hydraulic radius of a channel provides a length scale of the maximum size of turbulence and secondary flow structures. It also provides a measure of the channel shape. For wide shallow channels, the hydraulic radius approximates to the average channel depth. Whereas, for deep narrow channels the value is closer to the width, and thus variations in channel shape are accounted for.

The longitudinal mixing data set compiled by Rutherford (1994) gives no information on channel form, beyond average width and depth for each reach. However, by assuming rectangular channels, an approximation of the average hydraulic radius can be obtained for the various reaches. By doing this, the range of values suggested in Equation 2.113 can be reduced, to become:

$$40 < \frac{D_x}{Ru^*} < 3000 \qquad \text{Equation 2.114}$$

Although this decrease in range is not dramatic, it shows an improvement in narrowing the range of potential values. If more detailed information on the channel properties was available this range might be improved further.

Quantifying the variation in hydraulic radius over a given reach would give an indication of the variability of channel shape. The bigger the variations in channel shape, the more varied the flow regime, and potentially the greater the trapping or dead zone effects, leading to higher mixing rates.

Figure 2.26 shows longitudinal mixing coefficient normalised by bed shear velocity and hydraulic radius versus discharge for the field data set. As can be seen the relationship to discharge is not as pronounced as in Figure 2.22.

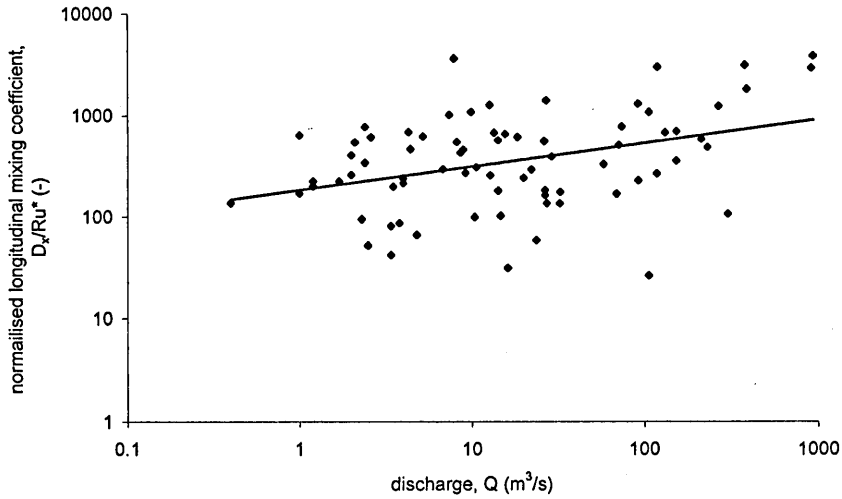

Figure 2.26 Longitudinal mixing coefficient normalised by hydraulic radius and bed shear velocity versus discharge for field data set (data from Rutherford (1994))

The US Geological Survey set up a research group to collect and disseminate dispersion data from all past studies on US rivers. The first work published from this is Jobson (1997). The paper represents a large volume of data, yet the results and conclusions are vague, concentrating on prediction of travel time. The characteristics of the various river reaches have not been conclusively linked to the variation in the travel times. A similar study has been attempted in the United Kingdom. The Environment Agency commissioned Dr. Ian Guymer to collate data from all past U.K. longitudinal tracer tests, together with reach characteristics. The data were then analysed using consistent techniques. At the time of writing, nothing has been published based on this database.

A definite trend has been shown between discharge and longitudinal mixing coefficient, and a range for values of normalised longitudinal mixing coefficient suggested. Although this section presents the results of a considerable number of past field tests, it is not possible to fully define the relationship between rate of longitudinal mixing and channel properties. This is predominately due to a lack of detailed information to classify the various reaches, such as bed slope, curvature, or variation in hydraulic radius. There could be considerable error in the data set. This is because of the variety and disparity of the analysis methods used to calculate coefficients from the tracer measurements, and the variety of methods used to obtain the tracer profiles.

2.9.4 Effects of channel curvature

Fischer (1969) presents results from investigations into the effects of bends on longitudinal dispersion. Fischer shows theoretically that the bends lead to a decrease in the rate of longitudinal mixing. Fischer (1968), Equation 2.111 suggests that the rate of longitudinal mixing is inversely proportional to transverse mixing.

The main effect of plan form curvature is to produce centrifugal forces in the water flowing around the bend. These centrifugal forces create a force imbalance in the transverse direction, which manifests itself as secondary, or helical, flow patterns around the bend. These secondary currents dramatically increase

the effects of depth average transverse velocity shear, transverse dispersion. Secondary currents also redistribute the primary velocities over the cross section, reducing the overall differences in maximum and minimum primary velocities. This reduces the effects of longitudinal velocity shear, and hence reduces the rate of longitudinal mixing.

Fukuoka and Sayer (1973), present longitudinal dispersion data from laboratory studies on a sinusoidal channel, with rectangular cross section. They took primary velocity measurements at several sections around two bends, and concentration measurements at bend apexes. Five conductivity probes were used to obtain concentration measurements. The probes were set in an array to provide plume variation information over each measurement cross section. Measurements only pertain to one cross section per injection. Plots are presented showing Gaussian concentration profiles, with little cross sectional variation in plume shape. The analysis undertaken shows that both the travel time and variance increase linearly with distance. The increase in variance is linear after only a short period, two bends, suggesting that an equilibrium between dispersion and diffusion is established quickly.

Longitudinal dispersion coefficients were evaluated by the change of moments method, a routing procedure, and through depth and width integration of measured velocities. The change of moments method and routing procedure gave similar results, although the change of moments method consistently yielded higher estimates of coefficient than the routing procedure. This is attributed to the undue weighting that the change of moments method gives to the tails of the distributions. The integration of measured velocities provides questionable results, even producing negative mixing coefficients. However, this method does render some idea of how the variation in primary velocities, caused by variation in secondary currents induced by the curvature, influence the mixing rate. The results suggest that the longitudinal mixing coefficient varies periodically in direct relationship to curvature. The coefficient attains a maximum at the end of the straight and a minimum at the end of the bend. Thus, longitudinal mixing may be directly related to the primary velocity shear, and inversely to the secondary currents. It should be remembered that this has not been calculated from concentration profiles, but from measurements of primary velocity.

Smith (1983) presents a theoretical study of the effects of channel variations on longitudinal mixing coefficients. He specifically addresses the effects of curvature and suggests that there are length scale implications for the size on the bend on the longitudinal mixing rate. He further proposes that these length scale effects explain why it has proved impossible to collapse field data onto a single empirical curve. However, Smith's study provides no direct method of evaluating longitudinal mixing rates.

Guymer (1998) presents results from longitudinal dispersion tests which were carried out at the Flood Channel Facility, HR Wallingford. The experiments were conducted on a 60 degree meander plan-form configuration, with a sinuosity of 1.374. The cross section was trapezoidal for the first tests. The channel was then modified to give an idealised natural cross sectional shape which varied around each bend, but had constant cross sectional area. The effect of different discharges on the longitudinal mixing was investigated for the second configuration.

The coefficients presented by Guymer (1998) are primarily the results of the change of moments analysis. The results are potentially more accurate than many previous studies due to several factors:

1. the large number of measurements used to define each profile.
2. use of standard deviation methods to locate the start end of each trace.
3. the measurement of multiple cross sections for each injection which greatly reduces temporal errors.

There is still some concern over the accuracy of evaluation of profile variance, particularly given the level of 'noise' on the traces. This concern over the calculated coefficients is reinforced when the quality of the fit between the results obtained from a simple routing solution are compared with the measured profile, as presented in the paper. Table 2.7 shows the summary results from Guymer (1998) and Fukuoka and Sayer (1973).

Study	Channel shape	Sinuosity	Flow depth, h (mm)	Hydraulic radius, R (mm)	Shear velocity, u* (m/s)	Longitudinal mixing coefficient, D_x/Ru^*
Fukuoka and Sayer (1973)	Rectangular	1.18	23.2 – 70.1	17.7 – 59.8	0.0133 – 0.0265	28.13 ± 11.4
Guymer (1998)	Trapezoidal	1.374	100	84.5	0.0246	39.2
Guymer (1998)	Idealised natural	1.374	60.5 – 95.4	41.5 – 67.8	0.0172 – 0.0220	99.8 ± 19.99

Table 2.7 Comparison of results of Fukuoka and Sayer (1973) and Guymer (1998)

The results for the rectangular and trapezoidal channels show similarity in the value of normalised coefficient. The trapezoidal channel shows an increase in longitudinal mixing rate, probably due to increased transverse variation in primary velocities, primary shear. The idealised natural channel shape with constant cross sectional area shows a dramatic increase in the normalised coefficient, probably due to another increase in primary shear, and increased dead zone trapping effects.

Guymer (1998) presents results of Chatwin analysis of the data from the trapezoidal and idealised natural channel. The difference in mixing rate represented by a change in gradient, and the large increase in, and persistence of, skewness for the idealised natural channel case become apparent from the analysis. The increased skewness supports the suggestion that the velocity shear effects are greatly increased and / or that the dead zone trapping effect is greatly increased. Unfortunately, there are no velocity measurements to quantify the change in shear or dead zone effects between the two cases.

The author presents no clear conclusions with regard to the variation in coefficient which was obtained for the different flow rates studied in the pseudo natural channel. Some suggestions are made between increasing longitudinal mixing and increased trapping, or dead zone effects which may be present on the 'shelf' forms at the bend apexes at lower flow rates.

2.9.5 Models

The Generalised Method of Moments, together with cumulative discharge or stream tube ideas, were introduced earlier in this chapter. These methods or approaches facilitate the evaluation of transverse mixing coefficients from dye concentration measurements below a continuous point source in natural channels. The situation can be simplified for longitudinal mixing to a one-dimensional model, such that the complex ideas of streams tubes and the Generalised Method of Moments are not needed.

Two longitudinal mixing models are presented for analysis purposes. The one dimensional Advection Dispersion Equation (ADE) routing procedure and the Aggregated Dead Zone (ADZ) model. By optimising the model fits, the best coefficients for each of the models can be found. A number of other models have been suggested by various authors, common forms use modifications of the ADE to enable prediction of skew. However, the majority of these solutions result in models requiring excessive parameters and are no longer considered simple.

The U.S. Geological Survey has extensively developed an OTIS model, One-dimensional Transport modelling with Inflow and Storage, to characterise the fate and transport of water-borne solutes in streams and rivers. The governing equation underlying the model is the advection-dispersion equation with additional terms to account for transient storage, lateral inflow, first-order decay and sorption. It has been developed with the ability to model transient storage in the riverbed. The bed exchange parameters, although of interest for biological interactions, are relatively unimportant for mixing problems, and are very difficult to quantify. The model is available free on the Internet, http://webserver.cr.usgs.gov/otis/.

The dispersion coefficient for the ADE model can be estimated from the change of moments method. There is often considerable error in the estimation, resulting from inaccuracies in the evaluation of the variance because of the 'noise' of measured profiles. Accuracy can be improved through averaging the results of a number of repeat injections. The ADZ model provides robust simple mathematics that can be solved using simple spreadsheets and can accurately predict concentration profiles, and can predict skew.

2.9.5.1 Advection dispersion equation

The solutions of Fickian diffusion models predict instantaneous spatial concentration profiles of Gaussian shape. In practice, a simple routing procedure can be used to predict the temporal concentration distribution c_2 at a downstream site, x_2 knowing the temporal concentration at an upstream site, x_1 (Fischer *et al*, 1979). This is summarised by:

$$c_A(x_2,t) = \int_{\gamma=-\infty}^{\infty} \frac{c_A(x_1,\gamma)u}{\sqrt{4\pi D(\bar{t}_2-\bar{t}_1)}} \exp\left[-\frac{u^2(\bar{t}_2-\bar{t}_1-t+\gamma)^2}{4D(\bar{t}_2-\bar{t}_1)}\right] d\gamma \qquad \text{Equation 2.115}$$

where $\bar{t}_i$ = the time of passage of the centroid of the tracer cloud at site i, given by:

$$\bar{t}_i = \frac{\int_{t=-\infty}^{\infty} tc(x_i,t)dt}{\int_{t=-\infty}^{\infty} c(x_i,t)dt} \qquad \text{Equation 2.116}$$

The dispersion coefficient can be initially estimated from the method of moments. γ is an integration variable.

This method effectively takes each individual upstream element of the temporal concentration distribution, advects it downstream by a fixed amount and spreads it assuming a Gaussian distribution. The down stream distributions can then be added to give the downstream concentration profile. This is illustrated in Figure 2.27.

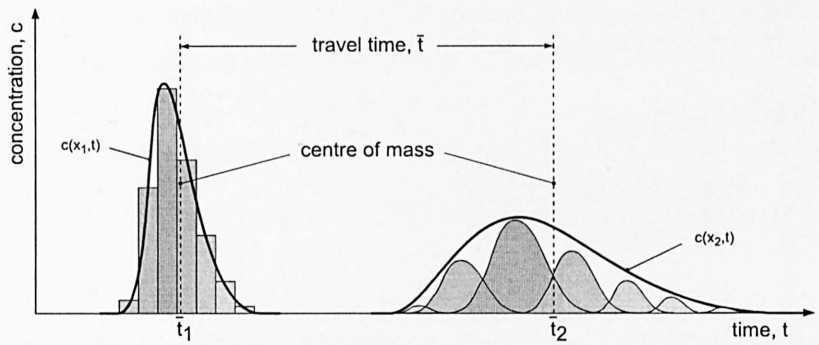

Figure 2.27 Sketch showing the process of the routing procedure solution of the one dimensional form of the ADE

Thus, to progress from the upstream profile to the downstream, two coefficients are required, the travel time, that is the amount each strip is moved downstream, and a dispersion coefficient, describing how spread each strip should be. The dispersion coefficient becomes a 'catch all' term for all the processes within the reach which work to spread the tracer longitudinally.

When dealing with longitudinal mixing problems concentration distributions often display a skewed profile, even after an initial period to allow sampling of the entire flow field. This is often attributed to dead zones and other trapping mechanisms. Solutions to the ADE and its derivatives provide Gaussian distributions and cannot predict skew.

2.9.5.2 Aggregated dead zone model

A development of the cells-in-series technique (chemical engineering), the ADZ model (Beer & Young, 1984, Wallis *et al*, 1989a) has gained favour by practitioners in the UK wishing to describe the longitudinal dispersion of solutes in river. This technique differs from the cells-in-series model by allowing both pure time delay and mixing to take place within a single cell or dead zone element.

Beer and Young (1984) demonstrate that a standard advective model can be modified to include a segregated mixing / retention zone. With the inclusion of this zone, the one-dimensional advection dispersion equation would take the form:

$$\frac{\delta c}{\delta t} + U\frac{\delta c}{\delta x} = D\frac{\delta^2 c}{\delta x^2} + \Gamma_c(s-c) \qquad \text{Equation 2.117}$$

which describes the dispersion within the main flow, and

$$\frac{\delta s}{\delta t} = \Gamma_s(c-s) \qquad \text{Equation 2.118}$$

describes the retention of a tracer within a dead zone, where c and s are tracer concentration entering and leaving the dead zone respectively, and Γ_c and Γ_s are volumetric mass transfer coefficient, in the main channel and dead zone respectively.

From these two equations, it can be seen that even if the Fickian dispersion coefficient, D, were zero, dispersion would still take place due to the retention within the dead zone. With this assumption, and through observation of riverine studies, it was postulated that the combined effect of all the dead zones within a reach provided the majority of the observed dispersion, whilst the shear flow dispersion was only secondary.

The model derived by Beer and Young (1984) differs from the cells-in-series. Instead of considering a chain of linked cells, this model assumes that a tracer is advected through the entire reach by a plug flow (i.e. advection with no dispersion), after which it passes through a single mixing cell that has the aggregated effect of all the dead zones within the reach (i.e. dispersion with no advection).

> *'The term dead zone is often misunderstood, although it implies a form of pocket that is separated from the main flow, it should be considered in a wider context as a bulk parameter that not only describes the effect of segregated regions of flow, but also other dispersive catalysts such as eddies, viscose sub layers and velocity profile' from Wallis, Young & Beven (1989a)*

To simulate an entire reach using the above model, the tracer must be advected through the reach prior to entering the dead zone. This can be done by entering a pure time delay (τ) into the input concentration term. By introducing these changes to the equation of a single dead zone, a model for an entire reach can be formed.

In practice, data is often acquired at discrete sampling times rather than as a continuous time varying fluctuation. Within Figure 2.29, the actual concentration / time distribution of a tracer at two locations (up and downstream) within a reach are shown. Superimposed over these temporal fluctuations are bars which illustrate the discrete time measurements of the data set. A discrete data set of this form is used when applying the aggregated dead zone model.

Wallis *et al* (1989b) give a simple discrete-time equation for predicting the temporal concentration distribution at a downstream site for a single cell:

$$c(x_2,t) = \underset{B}{-\alpha c(x_2,t-1)} + \underset{A}{(1+\alpha)c(x_1,t-\delta)}$$

$$\alpha = -e^{\left(\frac{-\Delta t}{T}\right)} \qquad \text{Equation 2.119}$$

$$T = \bar{t} - \tau \text{ (residence time)}$$

where $c(x_i,t)$ is concentration at longitudinal position, x_i at time t, with i equal to either 1 or 2 representing up or downstream locations respectively. $\bar{t}_i$ is the time of passage of the centroid of the tracer cloud at site i, t'_i is first arrival time at the location. $\bar{t}$ is travel time ($\bar{t}_2$-$\bar{t}_1$), τ is time delay (t'_2-t'_1). δ is the discrete-time interval equivalent of the time delay $\tau/\Delta t$. where Δt is the time step or sampling interval.

The equation can be considered in two distinct parts, reflecting the theory above. Part A represents direct advection of the tracer through the reach with linear decay. Part B represents exponential decay of the total predicted concentration at the previous time step. The result of this for a single time step upstream concentration profile is shown in Figure 2.28, and for a complete trace in Figure 2.29.

A first approximation for the residence time and the travel time can be obtained from first arrival times, and time of passage of centroid. Using these in Equation 2.119, a routing procedure can be carried out to fit upstream data to downstream data.

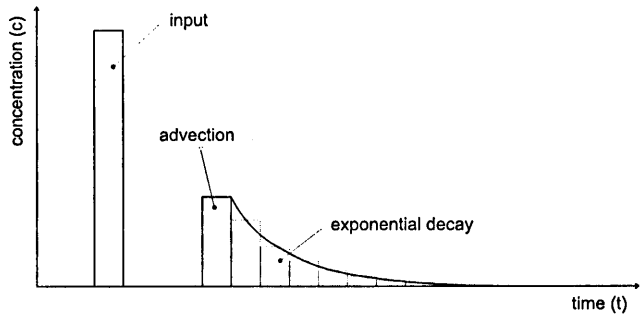

Figure 2.28 Simple representation of ADZ model

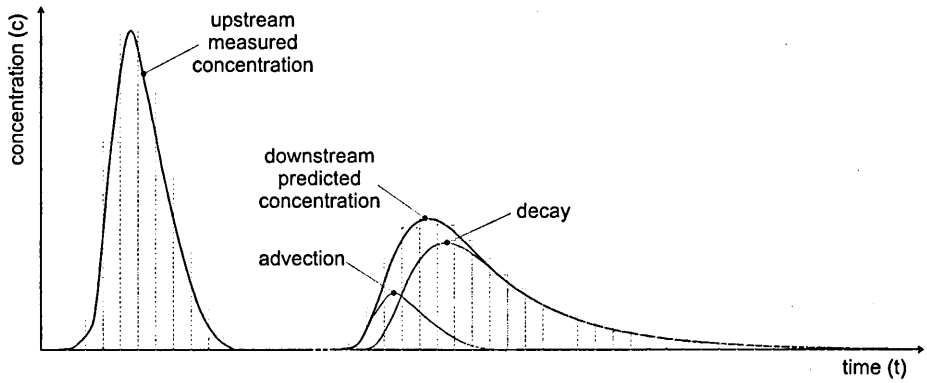

Figure 2.29 Graphic representation of ADZ model, showing discrete time steps, and advection decay elements

Wallis, Young and Beven (1989a), investigated modelling field data with the ADZ model. They studied four reaches on different rivers within a 20-mile radius of the University of Lancaster campus. The reaches were around 120 metres in length, with flow-rates up to one cubic metre per second. Various discharges were tested for each reach. The results of these studies show that the ADZ model can accurately predict the shape of the distributions obtained. However, this is not surprising given that the reaches were relatively short, with the upstream measurement section close to injection point, leading to skewed distributions particularly suited to the ADZ model.

Young and Wallis (1986) define a fraction, often called the dispersive fraction, D_f:

$$D_f = \frac{V_e}{V} = \frac{T}{\bar{t}} = \frac{\bar{t} - \tau}{\bar{t}} \qquad \text{Equation 2.120}$$

where V_e is the ADZ volume and V is the total volume in the reach.

The dispersive fraction is thus a measure of the ratio between the residence time and the total time a tracer spends in the reach.

The results of Wallis, Young and Beven (1989a) show dispersive fraction to be an approximate constant with discharge for the four river reaches tested. However, Green, *et al* (1994) present results for two reaches on the River Severn which suggest a slight decrease in dispersive fraction with increasing discharge, and one reach of the River Tonge where there is a marked decrease.

2.9.6 Environment Agency database

The Environment Agency has had a 'Time of Travel' database compiled by Dr. Ian Guymer. The analysis of the data contained within this database was carried out using the two models described above. No

findings have yet been published from the database, however it has been decided to present some preliminary results from the database. This will provide an idea of the values that are obtained for U.K. field data. Much of the input data used for the analysis was of extremely variable quality. Therefore, results from the database require extensive checking before any confidence can be given to the results. However, such quality control checking is beyond the time scale of this work. A simple criterion has been used to screen the data presented in this section. Only results providing optimised regression fit greater than 0.95 have been accepted. Due to the lack of quality assurance in the data, only two strong trends are presented.

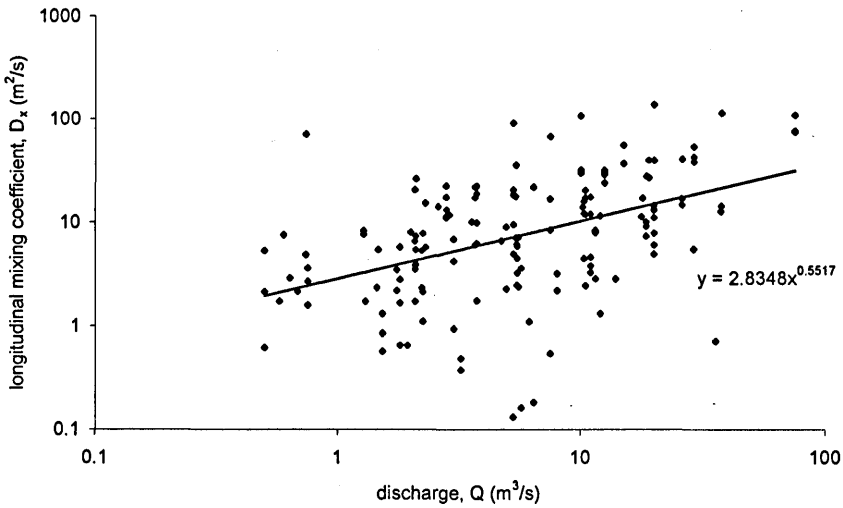

Figure 2.30 Longitudinal mixing coefficient versus discharge relationship from EA database

Figure 2.30 recreates Figure 2.22 for the EA data set, to highlight the relationship between longitudinal mixing coefficient and discharge. Both figures, for the two data sets, show a clear power law relationship between longitudinal mixing coefficient and discharge, at a power of about 0.5.

The EA database includes results of ADZ analysis. From this it is possible to investigate the relationship between dispersive fraction and discharge, which Wallis, Young and Beven (1989a) suggest should be constant. Figure 2.31 show the results of this investigation for the EA database. Although there is considerable scatter about the straight-line fit that is shown, the line clearly has a near zero gradient, concurring with Wallis, Young and Beven (1989a). The intercept, or average value, for the dispersive fraction is 0.15. Wallis Young and Beven (1989a) show results for four different channels where the dispersive fraction is constant with discharge for each channel. However, the four channels show a range of dispersive fraction from 0.372 to 0.121.

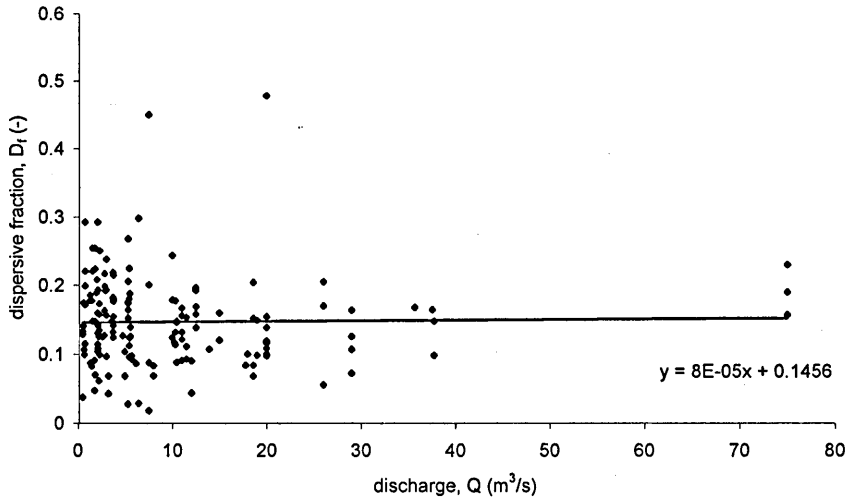

Figure 2.31 Dispersive fraction versus discharge relationship for EA database

The significant conclusion to draw from showing that dispersive fraction is constant with discharge, is that if travel time could be predicted, for example from $v \propto Q^?$ relationships or similar, then the residence time and thus concentration profiles can be predicted. However, some doubt is cast over whether the dispersive fraction is a universal constant. Therefore, at present it is recommended that a dye trace be performed to establish the value of dispersive fraction for the specific reach, and at several different discharges to ensure confidence.

2.9.7 Methods of predicting longitudinal mixing coefficient

A number of attempts have been made to derive semi-empirical formulae to predict the Fickian form of the longitudinal dispersion coefficient. Predominately this has been done through dimensional analysis and regression.

Following their laboratory investigation into the effects of channel sinuosity, Fukuoka and Sayer (1973), suggest:

$$\frac{D_x}{Ru*} = 0.8\left(\frac{r_c^2}{Lh}\right)^{1.4} \qquad \text{Equation 2.121}$$

where L is overall bend length (m).

This predictor seems to work reasonably well for the limited data set which they explored. However, their data set was limited to cases where strong curvature is presented, suggesting cases where the effects of curvature are pronounced. In cases where the radius of curvature is large, approximately straight channels, the coefficient predicted tends to be dramatically over estimated.

A series of equations have been developed as predictors of longitudinal mixing coefficients from readily available channel characteristics, starting from McQuivey and Keefer (1974), who suggested:

$$D_x = 0.058\frac{Q}{S_0 b} \qquad \text{Equation 2.122}$$

Fischer (1975), shows that this should be modified to:

$$D_x = 0.011\frac{U^2b^2}{hu^*}$$ Equation 2.123

Lui (1977) further improved this predictor, to become:

$$D_x = \beta\frac{Q^2}{u^*R^3}$$ Equation 2.124

where β can be estimated from:

$$\beta = 0.18\left(\frac{u^*}{u}\right)^{1.5} = 0.18\left(\frac{\sqrt{gRS_0}}{u}\right)^{1.5}$$ Equation 2.125

Lui (1977) concludes that this final form of the predictor offers the best fit to the data set that he used, although noting that errors in the predicted value could be as much as a factor of six.

The author has attempted to use this predictor with the Rutherford (1994) data set. Results show that longitudinal mixing coefficients are nearly always overestimated. The average of the over estimation is approximately a factor of 5.5, with a standard deviation of 4, showing considerable error in the prediction of the longitudinal mixing coefficient.

Lui (1977) suggests that improved accuracy in the estimates could be obtained by using a shape factor and a frictional factor in the estimate of β. Although in the discussion section of the paper, Lui suggests that the ratio of u/u* accounts for frictional variation as well as variations brought about by channel meanders.

Several other attempts have been made to derive a predictor such as Magazine *et al* (1988) although with little improvement on the work of Lui (1977). Seo and Cheong (1998) derive a predictor using dimensional analysis and the 'one-step Huber method'. The effect of vertical and transverse irregularities causing secondary currents and shear effects which affect the mixing rates are noted. The authors suggest that the channel sinuosity and bed shape factor govern these variations, however they are neglected in the dimensional analysis. The authors justify this by stating that these parameters are not readily available. However, sinuosity is as readily available as accurate assessments of average channel width or bed slope, from detailed maps.

Seo and Cheong (1998) propose:

$$\frac{D_x}{hu^*} = 5.915\left(\frac{b}{h}\right)^{0.620}\left(\frac{u}{u^*}\right)^{1.428}$$ Equation 2.126

Stating that the equation exhibits considerable improvements over previous predictors. This predictor has again been used with the data set presented by Rutherford (1994). For the complete data set, the average error was again an overestimate factor with an average of 5.5, but with a standard deviation of 3. The predictions showed considerable error for the man-made irrigation canals included in the data set. However, for the majority of natural river data the average error in predicted longitudinal mixing coefficient is reduced to a factor of 3, with a standard deviation of 2.5.

Further improvement could be made to the predictor if more information was available on the effects of shape variations, transverse mixing rates, and the effects of channel sinuosity.

Fischer (1969) and Jain (1976) both give predictors of the form:

$$D_x = \alpha \frac{Ub^2}{k_y} \qquad \text{Equation 2.127}$$

where (Jain 1976) $0.001 < \alpha < 0.016$

Both authors derive their equations with specific relevance to natural channels, with varying cross sections and platform curvature. Both papers highlight the relationship between transverse and longitudinal mixing. Equation 2.127 is limited in its applicability by the large inaccuracies in the prediction of transverse mixing coefficient.

Elhadi *et al* (1984) present a review entitled 'River Mixing – A state of the art report', which highlights the importance of the relationship between transverse and longitudinal mixing. The importance of plan-form curvature and secondary circulations in predicting the rate of transverse mixing is also expounded. Sinuosity is suggested as an ideal parameter to characterise the bendyness of a channel, and the suggestion made that it should be included as a factor in empirical predictors. The deficiency in data to attempt this is again pointed out.

2.10 Hydrodynamics

An understanding of open channel hydrodynamics is essential for a complete understanding of mixing processes. Understanding of mixing processes can be improved through study of the effects of flow regimes, especially secondary flows, and turbulence. There is much work published about the fundamentals of river hydrodynamics. Chow (1959) provides a comprehensive review. The knowledge which is required for mixing studies purposes is an understanding of flow patterns, including log law distributions, turbulent intensities and scales, Reynold's stresses, and energy exchange ideas. The ideas relating to turbulence and mixing processes have been dealt with in section 2.3.

Applications involving natural channels require further understanding of hydrodynamics with particular respect to flow around bends. Rozovskii (1957) is the definitive work describing the generation, propagation and decay of secondary currents around bends. Rozovskii (1957) gives detailed mathematical derivations and explanation of the theories of balancing centrifugal forces against bed generated shear effects, and presents results of extensive laboratory and field studies.

2.10.1 Definitions

Terms such as primary and secondary flow have been used in this chapter, as well as different definitions of co-ordinate systems. To avoid confusion in the following discussion, these definitions will be clarified. The co-ordinate system used will be a stream-tubes or cumulative discharge approach. The x-axes will be curvilinear, aligned with the local flow path, as discussed in section 2.5. From this definition of the co-ordinate system, it follows that the 'primary' flow is the flow down the channel, incorporating any net movement of water. 'Secondary' flows are defined as producing no net movement of water. Thus, at any given cross section there will be a net movement of water through the cross section, down the channel, the primary flow. Over the cross section there will be a circulation of water, but no net transverse or

vertical movement of water. For any horizontal slice through the cross section the net vertical movement will be zero, and for any vertical the net transverse movement will be zero. This definition has particular importance for calculation of velocity probe misalignment.

2.10.2 Flow distribution

Working from Manning's equation a number of attempts have been made to produce simple equations for predicting primary depth-average velocities.

Yotsukura and Sayer (1976) refer to Suim (1975), an Iowa University M.S. Thesis, for the proof of the use of Equation 2.128 for the prediction of discharge distribution:

$$\frac{q}{\langle q \rangle} = b_0 \left(\frac{h}{\langle h \rangle} \right)^{b_1} \qquad \text{Equation 2.128}$$

Values of $b_0 = 1$ and $b_1 = 5/3$ can be obtained from Manning's equation. Angled brackets denote cross sectional average values.

Rutherford (1994) suggests the use of Equation 2.129:

$$\frac{u}{\langle u \rangle} = \left(\frac{h}{\langle h \rangle} \right)^{2/3} \qquad \text{Equation 2.129}$$

where u is the depth average velocity

Smith (1983) suggests a slightly different equation for predicting depth average velocities from channel profile information, again the basis of the derivation is the Manning's equation, and the result is:

$$u = \frac{\langle u \rangle \langle h \rangle h^{1/2}}{\langle h^{3/2} \rangle} \qquad \text{Equation 2.130}$$

Smith also presents an equation to predict the transverse variation in bed shear stress, of the same form:

$$u^* = \frac{\langle u^* \rangle \langle h \rangle h^{1/2}}{\langle h^{3/2} \rangle} \qquad \text{Equation 2.131}$$

Together with a suggestion for the variation in the eddy diffusivity:

$$e_y = \frac{\langle e_y \rangle h^{3/2}}{\langle h^{3/2} \rangle} \qquad \text{Equation 2.132}$$

All of the above equations are derived for straight uniform channel flows, although Yotsukura and Sayre (1973) have shown that Equation 2.128 is reasonably accurate for a test reach of the Missouri River.

2.10.3 Bed shear velocity

Boundary friction generates turbulent eddies which cause solute transport and mixing within turbulent flows. For this reason, bed shear velocity has often been used to non-dimensionalise mixing coefficients. It should be noted that the procedure of non-dimensionalising is only theoretically valid for cases where the main driving force behind the mixing is boundary-generated turbulence. However, as has been shown,

this form of non-dimensionalising can be useful in three-dimensional mixing problems, where shear effects are also important.

For the simple case of a uniform rectangular channel, it is possible to obtain an average value of bed shear velocity:

$$u^* = \sqrt{gRS_0} \qquad \text{Equation 2.3}$$

In cases where the channel does not have constant depth over the cross section there will be transverse variation in the value of u*. Holley *et al* (1972) and Rutherford (1994) state that Equation 2.3 can be adapted to define a local value of u* by replacing the hydraulic radius with local depth, h. Holley *et al* (1972) also suggest that the magnitude of u* can be approximated from the expression:

$$u^* = \frac{\langle u \rangle}{20} \qquad \text{Equation 2.133}$$

However, the origins of this relationship are not reported. It seems to have been based on purely numerical reasons. Potter (1999) reports accuracy for the expression when compared to the results from detailed velocity measurements in a straight triangular laboratory channel.

The derivation of the universal log-law velocity distribution in the vertical is beyond the scope of this review of background theory, however the result of the derivation is useful for calculating bed shear velocity. The universal log-law can be represented as:

$$\frac{u}{u^*} = \frac{1}{\kappa} \ln\left(\frac{z}{z_0}\right) \qquad \text{Equation 2.134}$$

The derivations used to obtain this expression are based on assumptions that apply only to the near bed region. The solution relies on a linear shear stress existing over the water column under consideration. This is not the case for typical turbulent flow, where the shear stresses have been shown to vary with the vertical gradient of the primary velocity. An 'inner' region where the equation should theoretically hold is defined as 0.2δ, where δ is the height to maximum velocity. Measurements undertaken in straight channels with uniform flow have shown the log law distribution to hold up to the velocity maxima. Other expressions have been developed, such as Coles' law of the wake.

In situations where a number of velocity measurements have been made within a vertical profile, bed shear velocity can be ascertained from Equation 2.134. In order to evaluate Equation 2.134 it is necessary to first evaluate the constant z_0. Chow (1959) reports that for a channel with rough boundaries:

$$z_0 = mk \qquad \text{Equation 2.135}$$

where m is a constant and k is a roughness height for the channel.

For rough surfaces made of small particles such as sand or gravel, the roughness height is defined as the mean particle diameter. Experimental investigations of flows within rough pipes, performed by Nikuradse, produced values for the constant m of approximately 1/30. Although this value was determined using data from pipes, Chow (1959) suggests that the same value can be assumed when considering open channel flows. Graf and Kironoto (1994) investigated the structure of turbulent open channel flow. They report values of m in the range 1/20 to 1/45. Thus, it appears that Chow's suggestion of m = 1/30 is acceptable for open channel flow.

In many practical situations the scale of velocity measuring instruments and / or channel irregularities can lead to difficulties and errors in ascertaining the precise location of the measurement point with reference to the channel bed. Error in the vertical co-ordinates lead to the resultant logarithmic distribution not passing through the origin and consequently, calculations of bed shear velocity contain error. To account for this a correction factor, c, can be incorporated into Equation 2.134:

$$\frac{u}{u^*} = \frac{1}{\kappa} \ln\left(\frac{(z+c)}{z_0}\right) \qquad \text{Equation 2.136}$$

The magnitude of the correction factor is determined as the value giving a linear relationship through the origin on a logarithmic plot.

Using the log-law relationship it is possible to estimate bed shear velocity, by ascertaining the gradient of the linear relationship between u and $\ln((z+c)/z_0)$. The gradient should be equal to u^*/κ. However, the derivation and the majority of past work has been based on uniform turbulent open channel flow. The application to natural channels can be questioned.

Kironoto and Graf (1995) investigated the effects of accelerating and decelerating flows on the turbulent flow structure. Their work shows that under such conditions the vertical profile of the primary velocities is considerably altered, as can be seen in Figure 2.32.

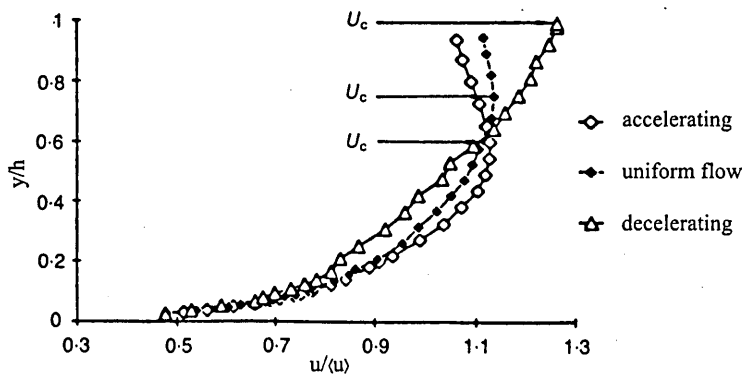

Figure 2.32 Vertical profiles of primary flows for accelerating, uniform and decelerating flows (from Kironoto and Graf (1995))

The work of Kironoto and Graf (1995) shows that for all the cases the log law explains the data in the inner region and a distance into the outer region.

Bathurst, Thorne and Hey (1979) investigated the effects of bends and secondary flows on shear stress through field measurements. However, their estimations of bed shear velocity are based on applying the log law distribution to measurements of primary velocity. Therefore, no comment can be passed on the validity of the application of the log law to the situation of curved channels. In the presence of curvature, secondary currents can be expected to have significant effect on the vertical profiles of primary velocities.

Bathurst, Thorne and Hey (1979) report that the bed shear velocity distribution is significantly altered by the presence of secondary currents. The bed shear velocity maxima associated with the core primary velocity is moved to the outside of the bend by the secondary currents. There is also another peak in bed shear velocity at the point of down welling, where the primary velocities are 'squashed' towards the bed.

An alternative method of ascertaining the bed shear velocity is by direct measurement, using a Pitot tube. This is accomplished by measuring the difference between dynamic and static pressures at the channel bed. Pitot tubes are often large so create considerable disturbance to the flow. Exact location on the bed, and alignment with the primary flow, is difficult and can lead to considerable errors. The presence of strong secondary flows causes errors in the measurement of static pressure. Pitot tube measurements are therefore unsuitable for laboratory scale studies, particularly in the presence of strong curvature and secondary circulations.

2.10.4 Secondary flows

Secondary currents caused by natural channel features, particularly curvature, have been shown to have a marked impact on mixing rates.

2.10.4.1 Channel forms

Any casual observer of a river will soon notice the sinuous channel pattern. In fact, rivers are very rarely straight for a length more than a few channel widths. This can be taken as evidence of rivers natural tendency to meander. Meanders are formed because of the close relationship between river flow and channel formation. Many river channel features and processes, such as meander plan-forms, bed topography, bank erosion and lateral migration are very much related to the dynamics of flow in curved channels. A number of different theories have been suggested to explain how and why meanders form. However, it is clear from their underlying regularity that meanders are not simply the result of random disturbances. Details of the various theories, together with further details of meander migration and general fluvial process can be found in 'Fluvial Forms and Processes - A new perspective' Knight (1998).

Rivers can be classified in terms of their sinuosity. Sinuosity is defined as the ratio of channel length to valley length. Rivers with sinuosity in the range of 1.1-1.5 are classified as sinuous and as meandering for the range 1.5-4.5.

The regularity of river meanders has often been noted in nature, and considerable material has been published on the subject. Langbein and Leopold (1966) is one of the earliest works investigating meander forms. One of their main conclusions is that meanders can all be accurately described by sine-generated curves.

Meandering channels are characterised by distinctive erosion patterns caused by secondary currents. Erosion occurs at the outside of the bend. Material is moved across the channel bed to the inside of the bend where it is deposited, resulting in pool riffle structures. Meander channel cross sections and plan-forms are never stable, however, migration slows after an initial development period, when the energy slope has been sufficiently reduced by the creation of meanders to approximate the valley slope.

2.10.4.2 Secondary flows

As water flows around a bend centrifugal forces are generated towards the outside of the bend. There is resistance to movement at the channel bed, friction, which is not present at the channel surface. Therefore, secondary currents can develop with flow towards the outside of the bend at the surface and

towards the inside at the bed. River channels normally meander therefore the water experiences a series of growth and decay of the secondary, or helical, currents as a series of bends are passed.

Rozovskii (1957) presents results from exhaustive studies into the nature and prediction of secondary flows, based on both laboratory and field studies, and theoretical derivation of predictive equations. Rozovskii theoretically derives formulae to predict the fully developed transverse velocities, and the build up and decay of these velocities around a bend. For relatively rough channels, C < 50:

$$v_0 = \frac{1}{\kappa^2} U \frac{h}{r_c}\left\{F_1(\eta) - \frac{g^{1/2}}{\kappa C}\left[F_2(\eta) + 0.8(1+\ln(\eta))\right]\right\} \qquad \text{Equation 2.137}$$

where v_0 is the fully developed transverse velocity and F_1 and F_2 can be found:

$$F_1(\eta) = \int \frac{2\ln\eta}{\eta - 1} d\eta \qquad F_2(\eta) = \int \frac{\ln^2\eta}{\eta - 1} d\eta \qquad \text{Equation 2.138}$$

where η is z/h.

F_1 and F_2 can be evaluated from the following graph:

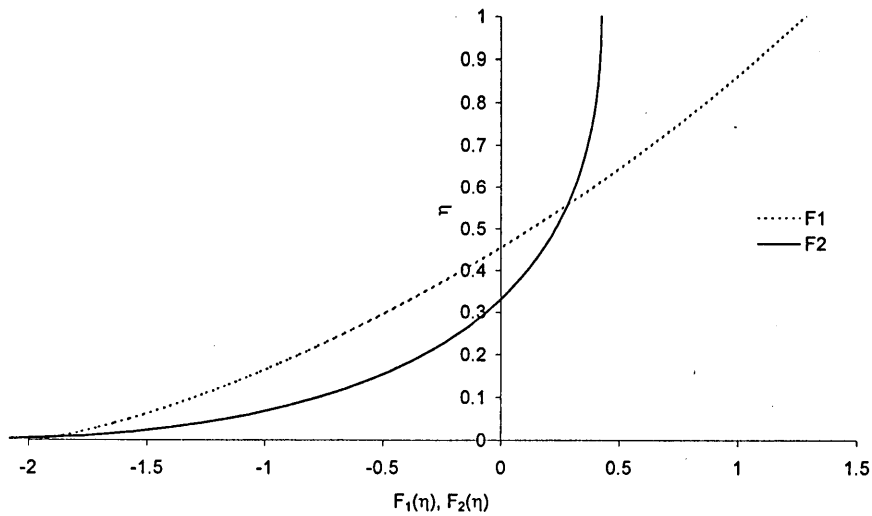

Figure 2.33 Graph of functions F_1 and F_2 by Rozovskii (1957)

The growth and decay of these velocities can be predicted from:

$$\text{Growth} \quad v = v_0\left[1 - e^{-\frac{g^{1/2}}{C}\frac{x}{h}\theta}\right] \qquad \text{Decay} \quad v = v_0 e^{-\frac{2\kappa g^{1/2}}{C}\frac{x}{h}} \qquad \text{Equation 2.139}$$

Rozovskii's theories state that growth commences at the entrance of the bend, and decay begins immediately the bend is exited. Rozovskii states that these formulae should hold for the majority of the channel width, except near the banks where the vertical component of velocity becomes important. Rozovskii suggests that vertical velocities may be significant over a region up to one flow depth from the channel banks. He recommends that the predictors should only be used to estimate the transverse velocity at mid-channel.

Rozovskii carried out a great deal of laboratory and field measurements covering a range of different bend and channel conditions. His final conclusions are that these formulae offer the capability to

compute, with an accuracy sufficient for practical purposes, the transverse velocity distribution in wide open streams having curvilinear plan form.

Since the work of Rozovskii, research into secondary circulations has progressed little, in terms of simple mathematical solutions. Several research projects have been attempted to make detailed predictions of the flow patterns around bends, and some have involved the collection of new velocity data. Demuren and Rodi (1986) present the results of a study carried out to try to calculate flow and pollutant dispersion in meandering channels. They use a three-dimensional model solution of equations of motion and the continuity equation together with a k–ε turbulence model, to predict the flow field. Transverse pollutant concentration profiles were then obtained from solution of solute transport equations. The model has been validated against the data of Chang (1971). Although the authors note the lack of quality in the data, they state no better data is available. Particular emphasis is put on the importance of the availability of data for natural channels so that future models can be accurately validated.

2.11 Concluding Remarks

Throughout this chapter an introduction to the ideas of mixing as applied to riverine situations has been provided. The fundamental ideas which are employed when describing river mixing have been introduced through the mathematics that are used to describe them. Further emphasis has then been placed on the processes and effects which dominate in each of the co-ordinate directions.

Through a detailed review of some of the most relevant research papers in this area, the limits of present understanding have been highlighted. The main area where understanding and knowledge have been shown deficient is concerned with making the progression from idealised laboratory conditions to natural river situations. The amount of published field data shows river mixing to be well-developed area, however, it is still necessary to carry out field studies if any accuracy is to be assured in water quality models.

The detailed review of transverse mixing shows that there is a lack of understanding beyond the bounds of regular laboratory channels. The derivation of mathematical tools to facilitate analysis of transverse mixing study results, from natural channels has been performed. It should therefore be possible to carry out rigorous studies investigating transverse mixing in natural or pseudo natural channels. This should further knowledge and understanding of the processes which govern transverse mixing.

The review of longitudinal mixing shows that the field of longitudinal mixing has been extensively investigated. However, the lack of understanding prohibits the prediction of mixing coefficients from simple parameters. A distinct but un-quantified link between discharge and rate of mixing has been shown. A link between the rate of transverse mixing and longitudinal mixing has also been suggested theoretically. However, this link remains un-investigated experimentally. Details of two mathematical approaches for the analysis of longitudinal dispersion data have been introduced.

Chapter 3 Experimental Work

This chapter covers the experimental work which has been undertaken to obtain the data used hereafter. Detailed descriptions of methodology and equipment are given.

3.1 Flood Channel Facility Background

A large scale Flood Channel Facility is available at Hydraulics Research Wallingford Limited. The Science and Engineering Research Council commissioned the facility in November 1985. Since this time, it has been used under numerous research grants to investigate various aspects of open channel flow. The scale of the facility particularly facilitates the study of strongly three-dimensional flows.

The facility has progressed through a number of plan-form configurations.

1. Initially, a straight channel (series A),
2. then 60 and a 110 degree meander plan-forms (series B)
3. and at the time of study, a sinusoidal meander plan-form within which mobile bed forms have been investigated (series C).

Each series has had a number of different studies undertaken, including investigations into stage discharge relationships, boundary shear effects, mixing studies, turbulence and sediment transport. The University of Sheffield has been specifically associated with dye dispersion tests. A considerable amount of data is available for comparison purposes, and as a knowledge base to build upon.

Between September and December 1996 a series of experiments investigating natural plan-forms and sediment transport were undertaken by Ian Benson of the University of Newcastle. During this study various channel configurations were formed and temporarily fixed. For brief periods within this testing program, these bed forms were made available to a group from the University of Sheffield. They performed a series of dye tracer experiments, investigating the effects of channel geometry and flow rates upon longitudinal dispersion.

The new experimental work which has been undertaken has been performed under the series C sinusoidal meander plan-form. A fixed 'natural' channel form was created. The flow case which created the channel was studied in detail. The work comprised two main elements, dye tracer studies, and hydrodynamic studies. Access to the facility was funded by the EC Commission, Directorate General for Science, Research and Development as part of the programme Training and Mobility of Researchers, Large Scale facilities, under control number ERB FMGE CT95 0082. The facility was available for a fourteen week period running from the 22nd June 1998 to 25th September 1998. The grant application was joint between the Mixing Studies Group, Department of Civil and Structural Engineering, University of Sheffield, England and the Department of Hydraulic, Maritime and Geotechnical Engineering, University of Padua, Italy. A Gantt chart of the working program is shown in Figure 3.1.

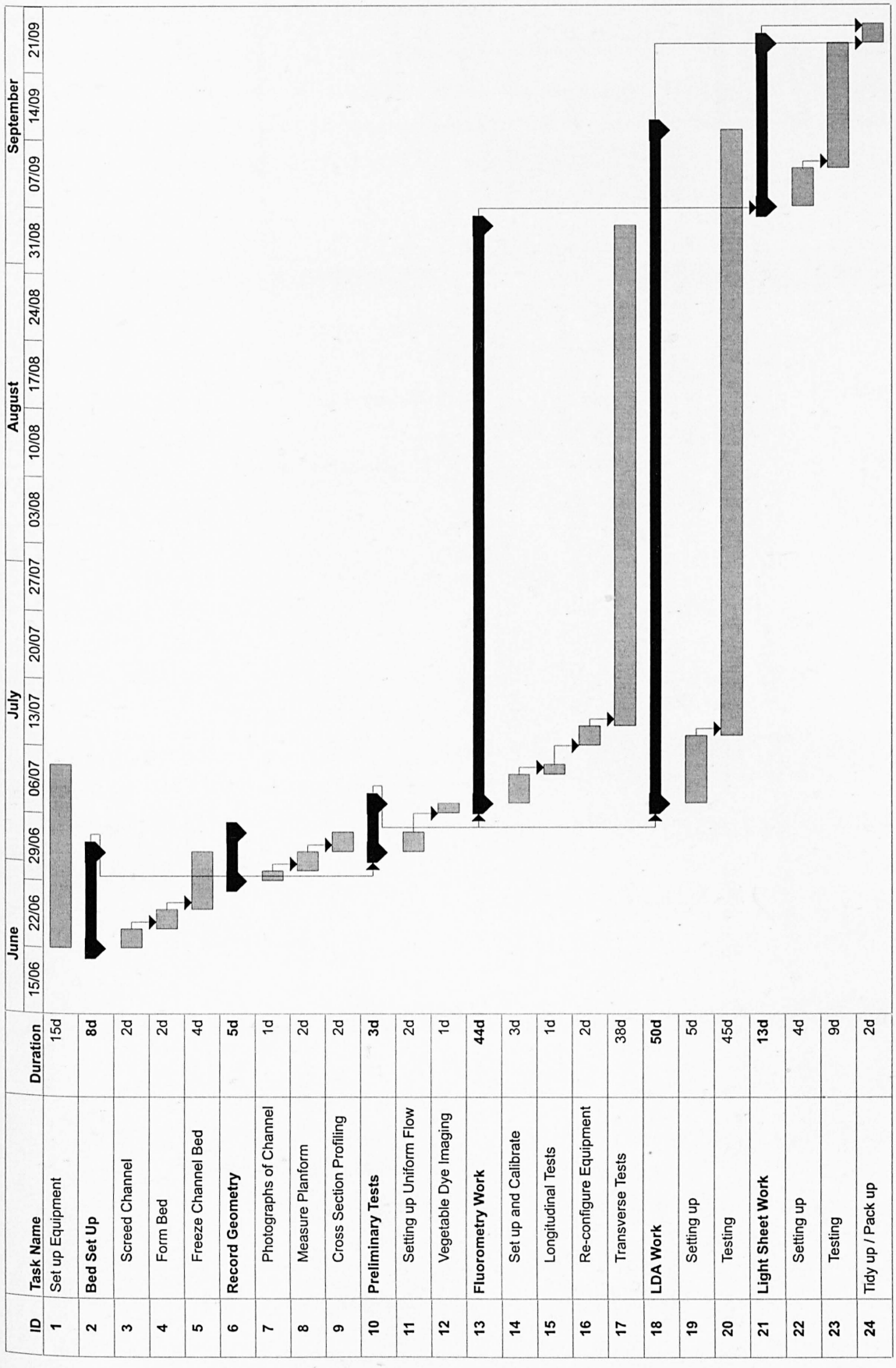

ID	Task Name	Duration
1	Set up Equipment	15d
2	**Bed Set Up**	**8d**
3	Screed Channel	2d
4	Form Bed	2d
5	Freeze Channel Bed	4d
6	**Record Geometry**	**5d**
7	Photographs of Channel	1d
8	Measure Planform	2d
9	Cross Section Profiling	2d
10	**Prelliminary Tests**	**3d**
11	Setting up Uniform Flow	2d
12	Vegetable Dye Imaging	1d
13	**Fluorometry Work**	**44d**
14	Set up and Calibrate	3d
15	Longitudinal Tests	1d
16	Re-configure Equipment	2d
17	Transverse Tests	38d
18	**LDA Work**	**50d**
19	Setting up	5d
20	Testing	45d
21	**Light Sheet Work**	**13d**
22	Setting up	4d
23	Testing	9d
24	Tidy up / Pack up	2d

Figure 3.1 Gantt chart of testing program

3.2 Flood Channel Facility Specification

The Flood Channel Facility shown in Figure 3.2 has an overall length of 56m, is 10m wide, and operates as a recirculating system. Flow conditions can be controlled by valves on the inlet pipes and downstream tailgates. Orifice plates allow the flow-rate to be monitored. For the purpose of this study only in-bank flows were investigated, therefore only the smallest pump (up to 0.0556 m^3/s) was used to generate the flow rate of 0.025 m^3/s.

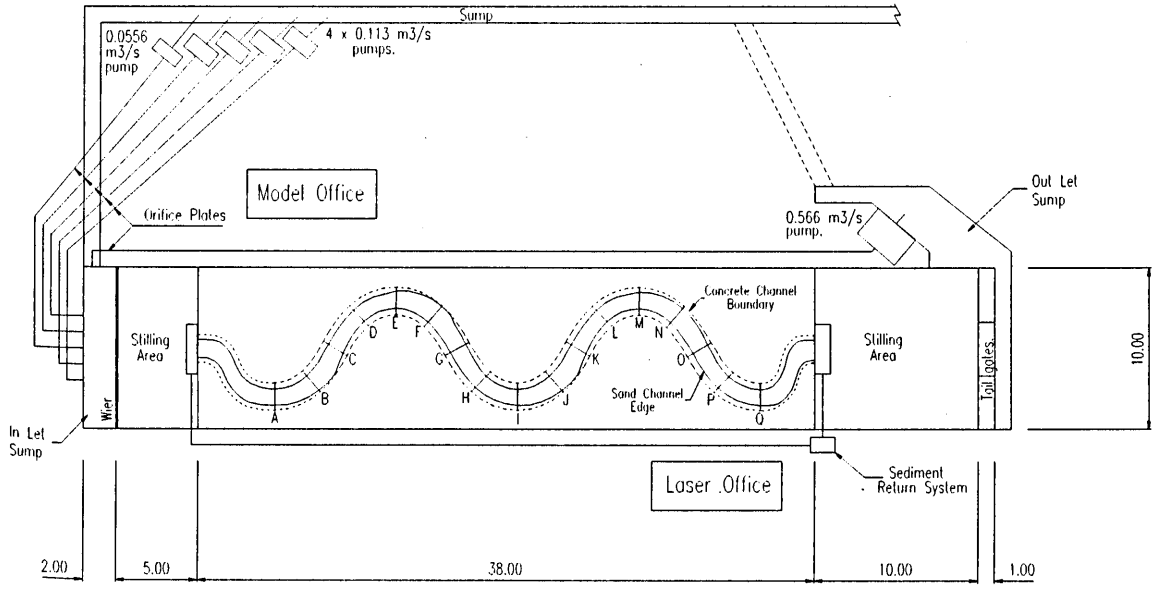

Figure 3.2 Schematic plan of Flood Channel Facility

Figure 3.2 shows that the series 'C' configuration has a sinusoidal concrete channel running the length of the facility. The channel has an overall curvilinear length of 55m, a sinuosity of 1.343, channel slope of 0.00125 and valley slope of 0.00168. The channel comprises a lead-in curve, two complete meander cycles, A to I and I to Q Figure 3.2, and a lead out curve.

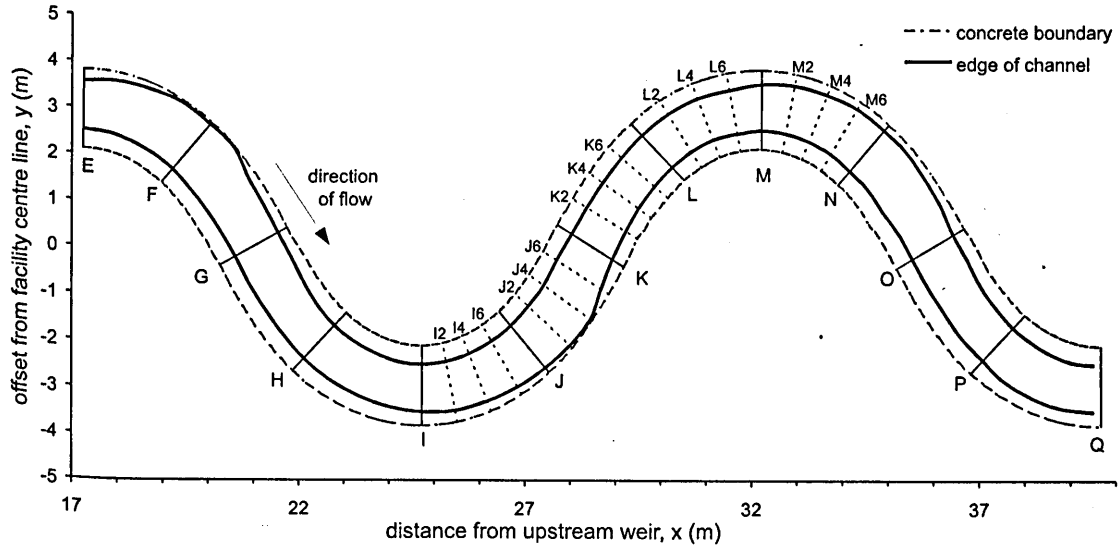

Figure 3.3 Plan view of channel showing channel form and indexing system used

3.2.1 Channel formation

For this study the concrete channel was filled with a uniform grain size material d_{50} = 0.85 mm. The size distribution for this material can been seen in Figure 3.4. A channel of trapezoidal cross section was screed into the sand, with a top width of 0.76m, a depth of 0.166m and a side slope of 33 degrees, conforming to the previous natural channel form studies. A flow rate of 0.025 m^3/s was generated from the smallest pump, and the sediment return system made operational. Water surface measurements were continuously taken during the formation period to ensure that uniform flow conditions were being achieved. The channel was allowed to develop for 1hour and 10 minutes before flow was stopped. At this point the migration of the channel towards the concrete boundaries, see section B, F, J and N Figure 3.3 was such that the generation of the channel had to be halted.

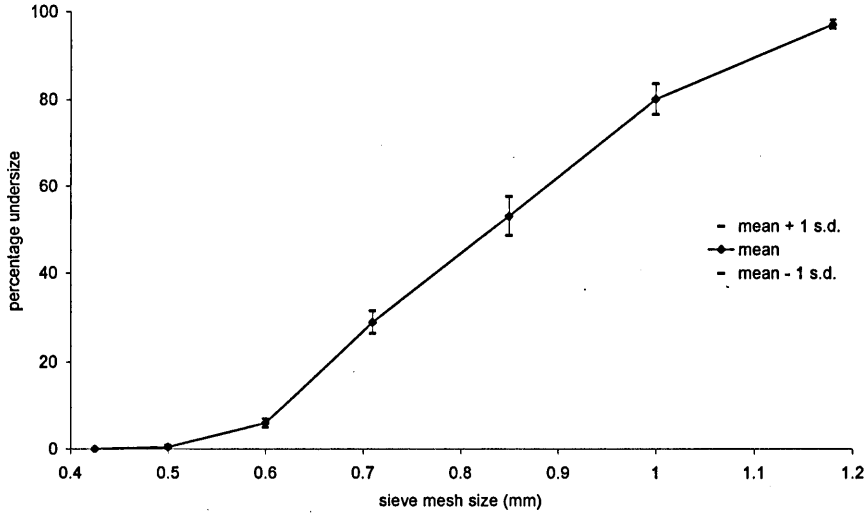

Figure 3.4 Sample size distribution of bed material, HR Wallingford sieve test results for fifteen samples

Water surface elevation measurements were plotted to show how the flow developed during the formation period and to ensure that uniform flow conditions had been present at the end of the formation period. Figure 3.5 shows the results of this:

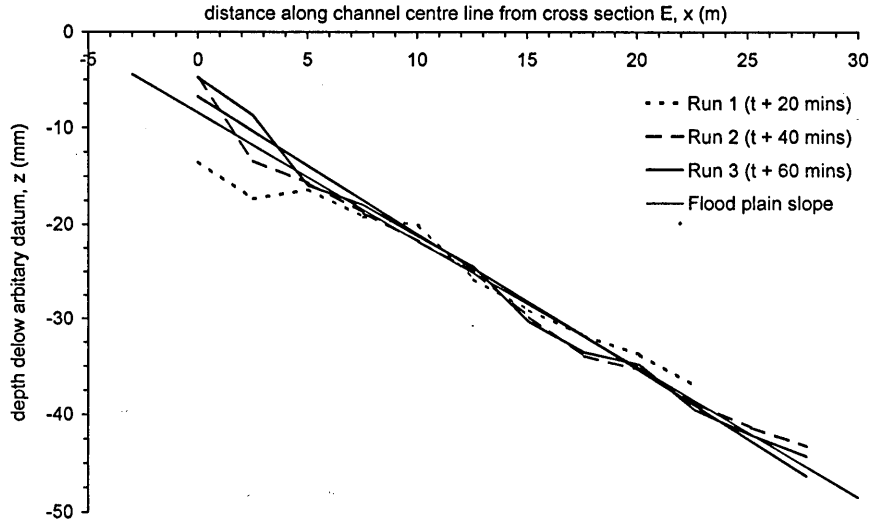

Figure 3.5 Results of uniform flow measurements, for final channel

Once the channel had been created bed profiles were taken at the apex cross sections E, I and M and plotted to ensure repeatability. Figure 3.6 shows the result of this and other cross sectional profiling data. The reversing and grouping of the profiles shows that the overall shape of the channel is repeating. The bed-forming period was recorded on video for future reference. Once a satisfactory channel had been formed, it was necessary to fix the channel bed.

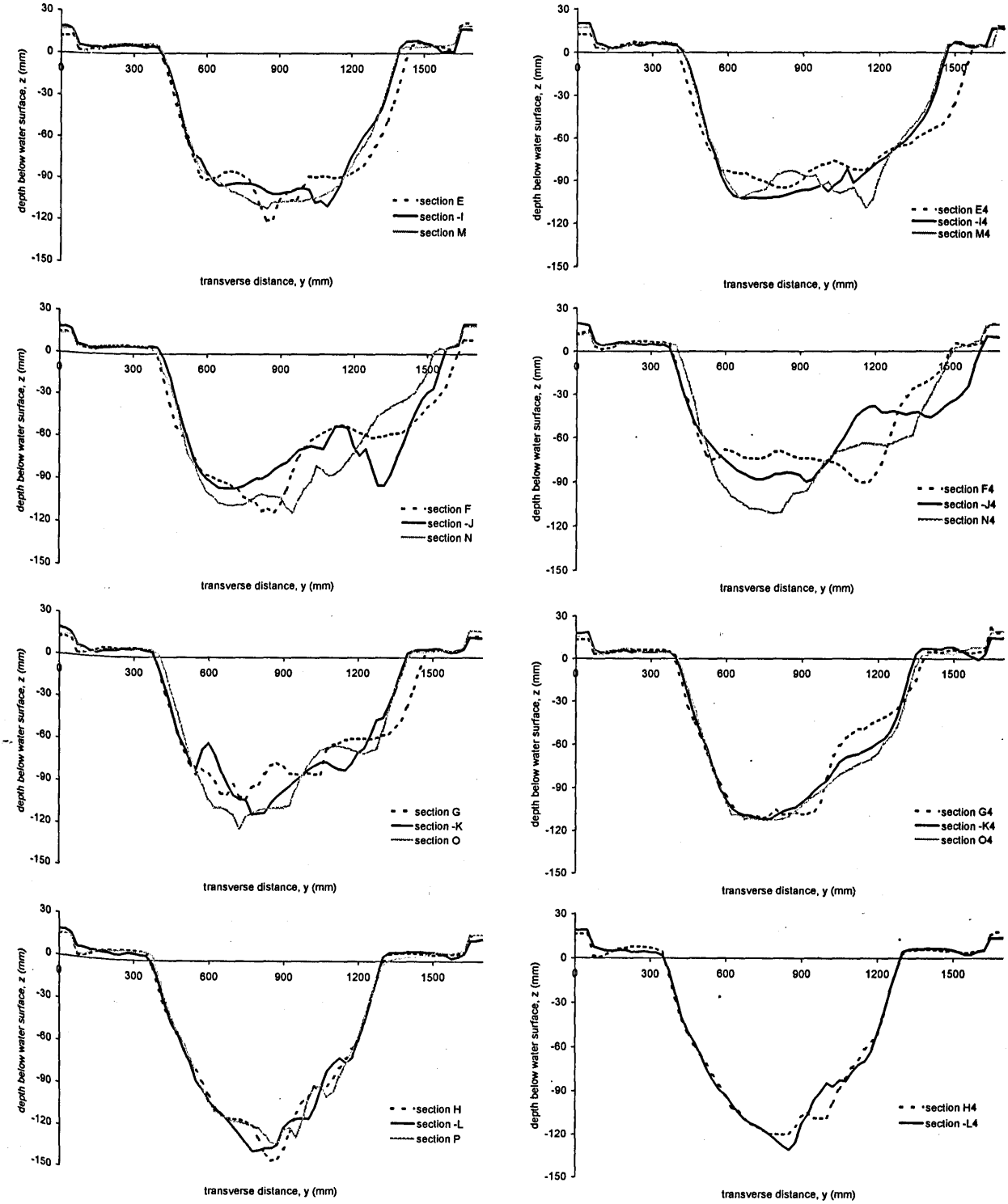

Figure 3.6 Cross-section profiling comparisons.
(cross-section profiles also taken at subsections 2 and 6)

3.2.2 Bed fixing

The bed was fixed using the method outlined by Kahlil (1972). The method used the application of a two-part system, a urea-formaldehyde adhesive (Aerolite 306) and a formic acid hardener (GBP.X Hardener)[1]. Aerolite 306 is commonly used as wood glue and is supplied in powder form, it has the important property that it remains as a solution with water until the hardener is introduced. The hardener sets up a chain reaction within the adhesive causing it to cure. Once in solution, the adhesive can be applied to the bed and allowed to percolate into the sand to the required depth. The hardener can then be introduced to the surface and the complete depth of adhesive cured.

Prior to formation of the bed, various concentrations of adhesive were tried together with several methods of application. The method found to be most robust used a mix of 1 part Aerolite powder to 4 parts water (by volume) application was by watering can fitted with a fine rose. The hardener was then applied via a horticultural backpack sprayer. This was the optimum method because it provided the least blockages and stoppage time, although it relied heavily on the skill of the operator to ensure a uniform application. The adhesive percolated into the bed providing minimal change to the channel roughness. This was checked by repeating measurements of the water surface slope, which showed no measurable difference from the end of channel formation measurements.

It should be noted that both the chemicals are toxic and the hardener highly corrosive. This meant that it was essential to obtain full and proper health and safety instruction. It was also necessary to perform the operation outside normal working hours to ensure the safety of other users of the building. The chemicals were applied on Friday evening and the facility left vented over the weekend. The bed was fully cured by Wednesday, although it was necessary to apply more adhesive and hardener to some areas which were thought to be weak. Throughout the test period, care was taken of the bed, as its final strength was unknown. This included very careful slow inundation of the channel after any drain down. At the end of the study the channel was removed. At this stage it was discovered that approximately the top 50mm of sand had been fixed. This was found sufficient to support the weight of a light person standing on the bed.

3.3 *Preliminary Tests and Surveys*

Once the bed had been fixed a number of preliminary studies and surveys were conducted. It was essential to create repeatable uniform flow conditions within the channel, with the same flow rate as used during channel formation. The control and pump settings from channel formation could not be used because a number of factors had changed:

1. There was no longer a mobile sediment load.
2. The sediment return system was no longer operational, which although designed to only return sediment did return some water, recorded as being approximately $0.005m^3/s$.
3. The backfill pump was switched off, this was used during channel formation to maintain the downstream stilling area water level.

[1] Chemicals supplied by Dynochem UK Ltd, Duxford, Cambridge, CB2 4QB

Once pump, control valves and tailgate setting had been found, which accurately recreated the flow rate and water surface profile, these were fixed for the duration of the study. There were some concerns over the durability and permanence of the bed form. Therefore, to ensure that the conditions were constant throughout the test period, up and downstream water surface monitoring points were set up at sections E and Q. These where checked at least twice daily throughout the programme. The bed proved to be very stable, and no adjustment of the settings was necessary.

An accurate survey of the plan-form geometry was carried out, as it was discovered that the actual geometry of the concrete channel deviates slightly from the idealised sine-generated form. This was performed by triangulation from the centre line of the facility and measurements made at every sixty-fourth of a meander. These measurements are plotted in Figure 3.3. An accurate level survey was also carried out. Detailed cross section profiles were taken every thirty-second of a meander cycle from sections E to P. These were plotted to check that the geometry of the channel was repeating. This was done by plotting up groups of profiles, for example, section G is plotted with section O, and the inverse of section K. The results of this are shown in Figure 3.6, and show that the geometry of the channel is repeating on a half meander wavelength level basis. This gave confidence in the validity of using one half-meander cycle as the test section for the transverse mixing study and the hydrodynamic measurements.

Once the geometry and the flow conditions had been established, some preliminary studies were carried out. Floater tests were performed by introducing a line source of small polystyrene balls at section A. The passage of these down the channel shows the route of the surface stream tubes. Instantaneous injections of vegetable dye were made at various points along, and across the channel, to provide a visual qualitative description of the longitudinal mixing. Various locations of continuous point sources of vegetable dye were then introduced to provide initial estimates for the rates and distance scales for transverse mixing. All of these activities were recorded on videotape for future reference.

3.4 *Fluorometery Work*

3.4.1 Adopted tracer

Rhodamine WT was used as the tracer. It is a pink fluorescent dye, which was developed in the 1960's especially for use as a tracer (U.S. patent 3, 367.946). Maximum excitation of Rhodamine WT occurs at 555nm and the peak-emitted wavelength is 580nm. Rhodamine WT was chosen for a number of reasons:

1. Highly detectable so low injection concentrations could be used, thus slowing the build up of background levels in the re-circulating system.
2. Long duration concentration profiles could be performed confidently with the knowledge that the levels of photochemical decay would be negligible for the test period.
3. The emission wavelengths do not interfere with the LDA system.

Other factors affecting Rhodamine WT are discussed in Smart and Laidlaw (1977). These properties do not affect the tests performed. By using the same water source for calibration as for the channel, any effects are encompassed within the calibration. The only other problem associated with Rhodamine WT is

that the fluorescence is temperature dependent. To obviate this, water temperature was monitored throughout testing so that corrections could be made by adopting Equation 3.1:

$$c_c = \frac{c_m}{e^{(-0.027T)}} \qquad \text{Equation 3.1}$$

where c_c = corrected concentration, c_m = measured concentration and T = temperature.

3.4.2 Fluorometers operation principals

Five Turner Design Model 10 Series Fluorometers were available to measure tracer concentrations. When exposed to particular wavelengths of light fluorescent tracers such as Rhodamine WT become excited and emit light of a different higher wavelength. The intensity of the emitted light is dependent upon the dye concentration and thus can be used to determine a concentration value for a tracer sample.

The Fluorometers use a mercury lamp with a broad band wavelength range as an excitation source. The light is filtered before being exposed to the test sample using a 10-056 dyed glass filter (ref. Turner Design filter selection guide) which cuts out all light above 546nm. Maximum excitation of Rhodamine WT occurs with light of wavelength 555nm, however, excitation will still occur to some lesser degree when exposed to light anywhere in the approximate range 480 to 610nm (Smart and Laidlaw, 1977).

The Fluorometers were used in continuous sample mode, using a 7mm-diameter glass cuvette positioned in front of the excitation light source. Sample water was continuously drawn from the abstraction point in the channel to the cuvette, and then fed to waste. As the sample was excited, any dye present emitted light of a different wavelength. The emission spectrum of Rhodamine WT is approximately 540 to 640nm, (Smart and Laidlaw, 1977) with maxima at 580nm. To measure the intensity of the emitted light the fluorometers used a 10-052 dyed glass filter (ref. Turner Design filter selection guide) which only allows light with a wavelength greater than 570nm through. This was set at 90 degrees to the excitation light source. The position had no effect on the amount of excited light reaching it, as fluorescence was equal in all directions, but cut down possible errors by minimising excitation light reaching it.

The intensity of light passing through the emission filter was measured as a voltage using a photomultiplier. In addition to measuring sample fluorescence, the photomultiplier also took a reading with no light present, to provide a zero level and a reading of the intensity of the light source. The latter is taken to account for any fluctuations in power supply to the lamp, as these would lead to fluctuations in the fluorescence levels of the sample, although concentration levels may be unchanged. The light source reference was passed through a 10-053 dyed glass filter which allowed all light with a wave length greater than 535nm to pass (ref. Turner Design filter selection guide). The fluorometers cycled the photomultiplier between these three readings every 0.0256 seconds, such that the sequence of three had a frequency of 13Hz. The fluorometers used the information from this sequence of readings to calculate a resultant fluorescence. A voltage representative of the degree of fluorescence was then output as an analogue signal.

Samples were extracted from the flow via 3mm-diameter brass tubing. Each brass tube was connected to a fluorometer by a length of similar diameter black plastic tubing. The sample was drawn into the lower end of the fluorometer, passed upward through the sampling cuvette and exited from the upper outlet. The

upward flow through the instrument was to ensure that no air bubbles were trapped in the system. Black plastic tubing was used to minimise extraneous light reaching the sample volume within the fluorometer. The length of tubing between intake and fluorometer was minimised to limit the effects of mixing within the pipe. A peristaltic pump was used to draw samples through the system. This was positioned beyond the fluorometer so that water was drawn through the instrument rather than pushed. This was a precautionary measure against the cuvette cracking, as in this event air would be drawn into the system rather than water being pumped into the fluorometer.

The abstraction ends of the brass intake tubes were bent through 90 degrees so that the intake faced upstream. This ensured that samples entered the tube from a discrete elevation, with minimal disturbance of the flow field. It was also important to ensure that water was being extracted at such a rate that the intake velocity was similar to the main flow velocity. This was to ensure that the disturbance was minimal and that only water from the point of interest was extracted. If the extraction velocity had been greater then water from a larger area would have been sampled.

The analogue output from the fluorometers was then fed via coaxial cable to a CED 1401+ data logger. The data logger is a computer-controlled device, which converts the analogue signal input into a digital signal, using 16bit conversion. The data can then be stored and analysed by computer. In this case the data logger was controlled by Spike2 for Windows. Both software and logger where supplied by Cambridge Electronics Design Ltd. (CED). Spike 2 allows the development of specialist scripts, which facilitates the automation of data collection.

3.4.3 Fluorometer calibration

Throughout testing, a bank of five fluorometers were used to measure concentrations at different points. For the results to be comparable, it was necessary to set the fluorometers to similar sensitivities, and then calibrate them. To encompass any changes to the fluorometers which may have occurred, such as lime-scale build up on cuvettes, it was necessary to recalibrate at weekly intervals throughout the test period.

The relationship between concentration and fluorometer output voltage should be linear. The fluorometers were calibrated in continuous flow through mode, using the same intakes and tubing as during testing. A sample was circulated through the fluorometers from a bucket initially containing 5L of clean water. As stated, temperature has an effect on the fluorescence of Rhodamine WT (Smart and Laidlaw, 1977), although it is possible to correct by adopting Equation 3.1. Water of a similar temperature to that in the system was used for calibration. A bucket of clean water was left in the sump over night, for the temperature to reach equilibrium before calibration. The brass intake tubes and the plastic outlet tubes were placed in the bucket and peristaltic pumps used to circulate the water through the fluorometers. Once the water was recirculating a micro-pipette, accurate to 50µl, was used to introduce known quantities of dye solution. Neat Rhodamine WT was not used, as the dilution would not have been sufficient for the sensitivity of the fluorometers. Instead, a solution with a concentration of $1x10^{-4}$l/l was mixed. Sufficient was made so that the same solution could be used for calibration throughout the test period, thus limiting potential errors. The dye was added to the bucket, and mixed with the water using a manual stirrer. Once the dye was mixed, the new solution was allowed to circulate and continue mixing

for a further 30 seconds (approximately the time for complete circulation through the pipe work). The fluorometer outputs at this concentration were then logged for 30seconds, at the same data rate as the present test. Temperature was also recorded.

Fluorometers scale settings are in steps of 3.16 (square root of 10). The minimum setting used during the tests was x1000 amplification. This is not the maximum setting available, but at the instruments highest sensitivity any small errors would be greatly magnified. Dye was added after each reading in sufficiently small quantities to ensure sufficient points were collected for each scale setting to well define the calibration curve. A minimum of six points were collected for each scale setting. Some overlap occurred between scale settings, and in these cases the solution in the bucket was logged twice, once on each scale setting. Only the scale settings used during testing were calibrated, these were x1000, x316, x100 and x 31.6. Typical calibration results can be seen in Figure 3.7:

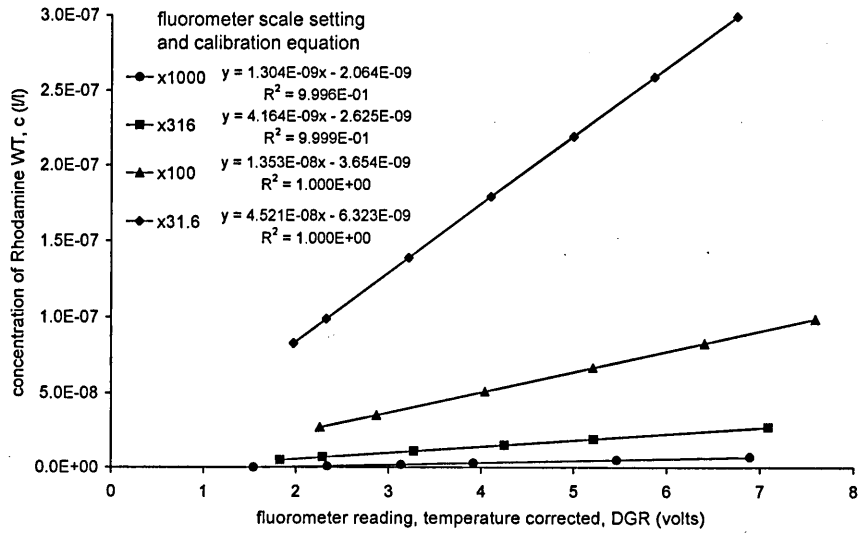

Figure 3.7 Typical fluorometer calibration curves

3.4.4 Longitudinal study

Longitudinal dispersion studies have been carried out by the Mixing Studies Group at the University of Sheffield in several pseudo natural channels created during a study carried out by the University of Newcastle. These studies investigated the effects of channel shape and flow rate upon longitudinal mixing. It was decided to repeat the longitudinal mixing tests for the current channel and flow rate.

During longitudinal tests, measurement of how an instantaneous of dye changes with distance must be obtained. An instantaneous injection system was introduced at the channel inlet, and the fluorometers sample tubes were positioned at discrete points down the channel. To negate near and midfield vertical and transverse mixing effects, as well cross-sectionally mixed a pulse of dye as possible was introduced into the channel. To achieve this a 'T' piece with a series of 1mm-diameter holes in the horizontal member was introduced on the bed at the channel inlet, shown in Figure 3.8.

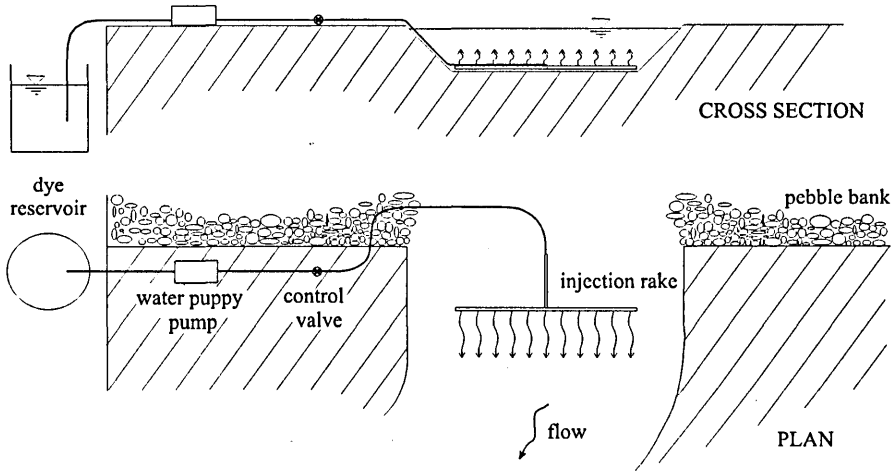

Figure 3.8 Longitudinal injection system

A control valve was introduced to the injection system to achieve an abrupt start and finish to the pulse injection. This minimised the spreading inherent to the injection system, thus maximising the measurable spread due to mixing within the channel. The high flow rate of the water puppy pump produces jets from the small injection holes such that vertical mixing is nearly instantaneous, the T piece promotes transverse mixing.

The fluorometers were positioned at sections E, I, K, M, Q, see Figure 3.3, the intakes were located horizontally at the velocity maxima of each cross section and at mid flow depth, as with the previous tests. The fluorometer at section E gave the initial upstream plume shape, E-I I-M and M-Q gave a measure of mixing over half meander cycles. I-K compared with K-M offers a chance to investigate longitudinal mixing at quarter meander cycle level.

The Flood Channel Facility is a re-circulating system, therefore, as dye is introduced there is an overall build up within the system. It is essential to be able to remove background from measured profiles. For the longitudinal tests, the fluorometers were set to log for fifteen minutes for each repeat injection. The dye was not injected until approximately five minutes after logging started. This meant that at least the first and last five minutes of each test recorded background concentration levels. It was found that a concentration of 2.5×10^{-5} l/l, injected for approximately 11 seconds produced near full-scale deflection on the times 316 sensitivity scale of the fluorometers.

The fluorometers have a fast and slow response settings. The slow response settings produce an element of data smoothing within the instrument. Experimentation with this, however, showed that the slow response resulted in attenuation of the peak and extension of the tail of the plumes. Slow response was abandoned in favour of obtaining accurate, but noisier results.

3.4.5 Transverse study

This study was performed in an attempt to quantify transverse mixing rates. As such, it was the second largest section of work undertaken. A sample section of the channel was adopted, running from cross section I to M. The cross sectional profiling work had previously shown good repetition in form, so it was assumed that this one half meander cycle could be considered representative for the channel as a whole.

Based on the work carried out with vegetable dye, a series of injection points and sampling cross sections were chosen. Table 3.1 gives a summary of the injection point locations and the sampling cross sections.

Injection cross section	Injection point	Sampling cross sections	No. sections
I0	Centre line bed	I2, I4, I6, J0, J2, J4	6
	Centre line surface	I4, I6, J0, J2, J4, J6	6
	Left hand side	I4, J0, J4, K0, K4, L0	6
	Right hand side	I4, J0, J4, K0, K4, L0	6
J0	Centre line bed	J2, J4, J6, K0, K2, K4	6
	Centre line surface	J4, J6, K0, K2, K4, K6	6
K0	Centre line bed	K2, K4, K6, L0, L2, L4	6
	Centre line surface	K4, K6, L0, L2 ,:L4, L6	6
	Left hand side	K4, L0, L4, M0, M4, N0	6
	Right hand side	K4, L0, L4, M0, M4, N0	6
L0	Centre line bed	L2, L4, L6, M0, M2, M4, M6	7
	Centre line surface	L2, L4, L6, M0, M2, M4, M6	7

Table 3.1 Transverse study, injection and sampling point locations

3.4.5.1 Injection system

Using a continuous point source injection and non-instantaneous transverse measurement it is possible to neglect any longitudinal mixing effects, since over a period of time continuity can be assumed in the longitudinal direction. Therefore, vertical and transverse mixing can be studied independently of longitudinal mixing.

Dye was injected from a point source located within the channel. This was via a 2mm diameter steel tube which was locally aligned with the channel centreline. A 300mm length was run along the channel before a 90-degree bend was present to bring the steel tube through the water surface. This was to minimise the effects of the injection on the flow, particularly at the point of injection.

It was noted that if a peristaltic pump was used to drive the injection, the oscillatory nature of the pump induced surges in the injection. Therefore, a constant head tank was used, shown in Figure 3.9. By setting the constant head tank at an elevation such as to induce similar injection velocities as the main flow, mixing due to injection momentum was minimised.

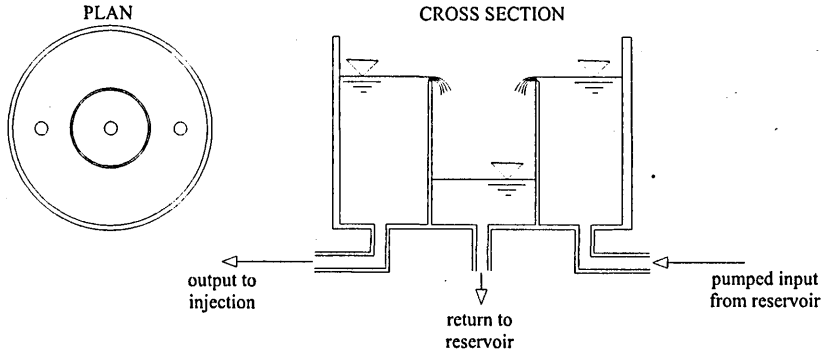

Figure 3.9 Constant head injection tank

3.4.5.2 Data collection

To optimise sampling within the average flow depth the fluorometer intakes were mounted in a vertical rake, with a vertical spacing of 18mm centre to centre. The sample rake was fixed to a traversing system that allowed accurate movement in the y and z directions. Movement was manually affected and monitored by potentiometers which were logged concurrently with the fluorometer outputs. The rake fixing was detachable from the traverser, but accurate relocation was ensured. This was to facilitate the taking of background readings.

A preliminary test was carried at each test cross section to ascertain the approximate plume width. From this, it was possible to select a step size to optimise data collection over the plume, whilst ensuring that a measure of background was made at each edge of the plume, where possible. Approximately 40 concentration measurements were made over the plume at each cross section.

At each step of the rake across the channel, the vertical position was checked with respect to the channel bed. The rake was moved in vertical steps of 18mm, ensuring that each level within the flow had a continuous trace. This meant, for example, the trace at surface –15mm would initially be logged with the fluorometer connected to the bottom intake. Then, when depth permitted, the traverser would be lowered and the bottom two intakes would be in the flow, thus intake one would now be measuring at surface –33mm and intake two at surface –15mm. This was repeated across the whole channel. Figure 3.10 represents this graphically.

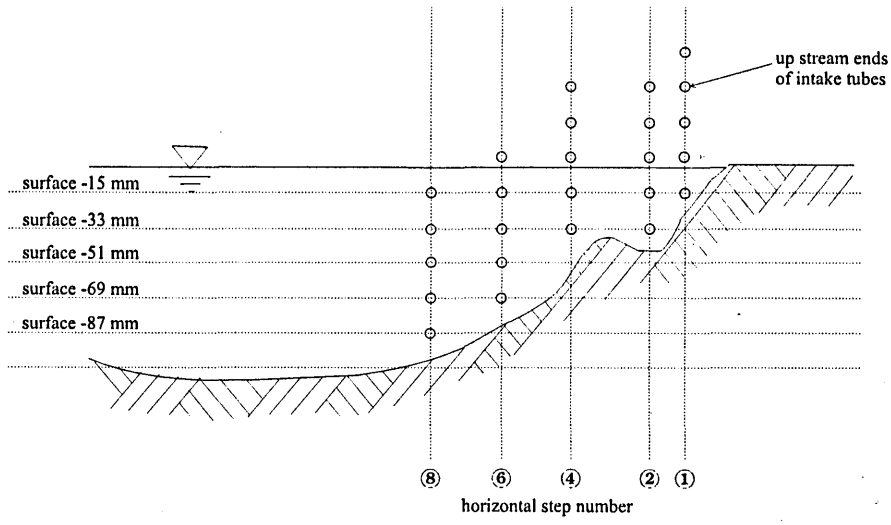

Figure 3.10 Transverse step system

To obtain a measure of temporal mean concentration at any given point from a continuous point source injection irrespective of longitudinal mixing effects, it is necessary to obtain a time average value. The period over which the concentration level should be logged to obtain a good average was investigated. The result of this showed that a two-minute period provides the optimum balance between accuracy and speed. Table 3.2 shows summary results of this study.

10 min		5 min		2 min		1 min	
average	% error	average	% error	average	% error	average	% error
2.951	-	2.961	0.37	3.054	3.40	3.136	5.91
		2.940	0.37	2.920	1.05	2.973	0.75
				2.886	2.22	2.880	2.43
				2.938	0.44	2.959	0.29
				2.955	0.14	2.859	3.20

Table 3.2 Results of log time study for transverse fluorometery testing

3.4.5.3 Background

Background concentration increase was important for the transverse study because of the time scale for collection of each profile. 40 points across a plume plus 15 background measurements with 2 minutes sampling, plus 30 seconds for the sample to pump through the fluorometer and 1 minute positioning, gives a minimum time per cross section of over 3 hours.

Preliminary tests were carried out to investigate re-circulation times for the facility. A fluorometer set to the highest sensitivity, logging at a low data rate, was positioned at the apex cross section A. A high concentration instantaneous injection of Rhodamine WT was then introduced at the channel inlet, such that the fluorometer over-scaled for a considerable period. The fluorometer was then logged for the next three hours to observe the re-circulation effects. The result was that after approximately thirty minutes a very gradual increase in concentration was recorded. After three hours, the trace was still gently rising but the rate of increase was minimal. This showed that the mixing through the sumps and re-circulation system was sufficient to smooth any irregularities in injection.

To facilitate background measurement the fluorometers were mounted on a trolley so that the intake rake could be detached from the traverser, and the complete measuring system moved upstream of the injection point. The sample tubes where then inserted into the flow and a reading of background concentration taken. A background reading was taken every fifth point through the profile, approximately every 15 minutes. A plot of a typical day's results is shown in Figure 3.11.

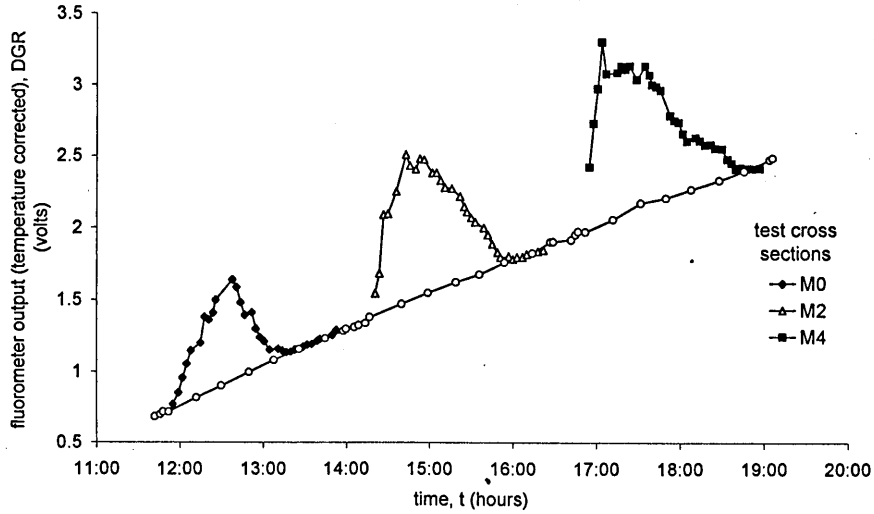

Figure 3.11 Example of testing results from a compete days testing, showing build of background concentration (injection was at water surface section L0)

A number of steps were taken to ensure that any changes in background level were not abrupt. Injection was started and the system allowed to run for half an hour before data was collected. The injection concentration was kept as low as possible, whilst still achieving reasonable deflection above background at the peak of the plume being measured. Injection was run continuously throughout the day.

At the start of each day sufficient injection solution was made up to last for all the proposed tests. The concentration of the solution had to be such that a satisfactory deflection on the selected scale setting of the fluorometer would be achieved for each cross section to be measured. A check had to be made to ensure that the peak concentration of the last cross section together with the end of the day background level would not cause the fluorometer to off-scale. Occasionally it was not possible to use a single injection concentration throughout the day. When a second injection solution was required the concentration was significantly increased, and again thirty minutes re-circulation time allowed before testing recommenced.

Once a trace as in Figure 3.11 was obtained, it was possible to order the data into plume measurements and background readings. From this, a line of best fit can be found for the rate of background increase, and the equation for this line used to remove background from the plume data points. Doing this corrects the concentrations to zero such that the intercept terms in the fluorometer calibration equations are unnecessary. The fluorometers can be compared simply by applying the calibration gradient factor.

The system was drained down over the weekends and refilled with fresh water, so that the overall build up of background levels could be limited. However, due to the depth of free sand under the frozen crust of the bed, the channel had to be kept permanently inundated to prevent consolidation which could have resulted in damage to, or movement of, the bed. Therefore, only around 50% of the water within the system could be changed at any one time, it was only possible to make one change of water per weekend because of time and water availability constraints.

Rhodolite was added to overcome the problem of increasing background concentrations. Rhodolite is a bleach based substance, of a free chlorine type solution. The free chlorine attacks the molecular structure of the dye, removing its colour and its fluorescent properties. This reaction has a finite time, therefore the chemical was added at the end of a day's testing. Care was taken with the amount of Rhodolite added, as any excess added would have meant that an active element would have been present in the system at the start of the following days testing. The result of this would have been decay even within the distance between injection and sampling cross section. An easy check on the amount added was to confirm that a residual level of Rhodamine WT was left in the system at the start of the day following dosing with Rhodolite.

3.5 *Velocity Measurements*

The aim of the testing was to obtain measures of mean velocities and turbulence parameters in the x, y and z co-ordinate directions. Measurements of near-bed turbulence were particularly important to gain a measure of the bed generated shear stress by adoption of the log law theory. Detailed measurements were made over a test section of the channel, sections I, I4, J, K, L, and M. The measurements were taken using a two dimensional Laser Doppler Anemoter (2D-LDA) system.

A LDA system was used for a number of reasons:

1. Of the possible measuring devices it provides the smallest measuring probe, thus minimising the disruption of the flow regime.
2. The measuring volume is very small, so providing good point data and good turbulence information, no spatial averaging.
3. It is possible to achieve very high data rates so turbulence data can be obtained.

However, the LDA system is one of the hardest systems to set up and operate, requiring very careful alignment and parameter selection.

3.5.1 LDA principles

This section refers to "Fibre Flow – Installation and User's Guide" Dantec 1994.

Laser Doppler anemometers use the principal of Doppler shifts, as first published by Christian Doppler in his paper "On the Coloured Lights of the Double Stars and Certain Other Stars of the Heavens". Simply stated Doppler's theory was that the light we receive from stars travelling away from us is shifted towards longer wavelengths, becoming redder. Light from stars travelling towards us is shifted towards shorter wavelengths, becoming bluer. Although LDA systems use this basic principal, the velocities of interest are many orders of magnitude smaller than those related to stars. Therefore, the wavelength shift is no longer measurable with standard spectroscopic devices.

A particle travelling through a laser beam will scatter light. The intensity of some of this light can be measured using a photo-detector. If the laser beam is split, and the two resulting beams made to cross at a given angle (the two beams being coherent to each other in the volume of their intersection), then a particle traversing this volume would scatter light, and a detector would receive light corresponding to each of the beams. Both components would have a Doppler shift, depending on the velocity of the particle, and on the direction of the light beam. Since the two beams are at an angle, the two components of scattered light would have different Doppler shifts. Therefore, at the surface of the photo-detector the two light components interfere, resulting in a pulsating intensity. Whilst the frequency of the electric field of the light is too high for the photo-detector to follow, the frequency of this pulsating intensity can be resolved and related to velocity.

Although the above description is accurate, it is difficult to grasp. Therefore, for LDA measurements the fringe model is introduced, as a first order approximation. When two coherent laser beams intersect they will interfere in the intersection volume, forming interference fringes. If the beams interfere at the beam waists, the wave fronts are nearly parallel, and therefore the interference fringes are parallel. This is important, as it means that a uniform velocity-frequency relationship exists over the measuring volume. As a particle traverses this volume the light received by the photo-detector will pulsate in direct proportion to the velocity component at right angles to the fringes. However, this is independent of direction. A positive and a negative velocity of the same magnitude will result in the same Doppler shift, to overcome this the frequency of one of the beams is slightly shifted. Consequently, the fringe pattern is no longer stationary but 'rolls' at a given velocity. This means that the photo-multiplier would detect the scattered light from a stationary particle as pulsating at a frequency equal to the frequency shift. Particles

travelling against the fringes produce Doppler bursts of a higher frequency than the shift. Particles travelling with the fringes produce a lower frequency Doppler burst. It is therefore evident that the higher the shift frequency, the greater the spread of velocity within a population of particles which can be accommodated, and larger turbulence intensities can be measured.

3.5.2 LDA system

The LDA system used a 50mW argon-ion laser to provide the light source. The laser was manufactured by AG Electro-Optics Ltd. The optical part of the system consisted of a series of elements that were supplied by Dantec Electronics. The laser beam is split into two (55x75 beam-splitter neutral) then phase shift is imposed on one beam by the bragg cell (55x29). The beams are then displaced (module 55x28). They enter the four-beam module (55x84) which splits each beam into its green (512nm) and blue (488nm) components. At this stage the light is ready to enter the transmitting optics system. The system thus far described was set up in the Laser Office, for location see Figure 3.2, to protect the delicate laser and optics from the damp and dirt of the main hall. To reach the channel the four laser beams were directed into a 20m long, 11.5mm diameter, fibre optic cable (60x30) by four fibre manipulators (60x24).

Ideally LDA measurements should be taken by non-intrusive bulk optic systems, this causes no disruption to flow regimes. It was not possible to use a bulk-optics system, as an interface through which the beams can enter the flow is required, such as a glass section of channel. This was not possible with the channel. Therefore, a fibre flow probe was used. The 14mm fibre-flow probe consists of a cylindrical, 14mm diameter, waterproof housing, inside which the ends of the fibre optic cable are mounted. The mountings are such that the beams are directed through a lens which focuses to a crossing point beyond the end of the probe. If this is inserted vertically into the flow, and aligned correctly, the longitudinal and transverse components of velocity are measurable.

A side looking section can be connected to the end of the probe. This contains a mirror mounted at 45 degrees to the axis of the probe. If this is correctly positioned it will direct the beams to a crossing point at the side of the probe, such that longitudinal and vertical velocity components can be investigated.

The beam separation was 8mm, focal length (in air) was 50mm, with an intersection angle was 0.160 radians. This, together with a beam waist of 0.27mm, gives a measuring volume of 113μm diameter and 1.41mm length, having a fringe count of 38 with a separation of 2.98μm.

The LDA system used a backscatter system. Reflected light is transmitted back up the fibre-optic cable, then split into its green and blue components before being directed onto to the photoelectric cells. The voltage output of the photoelectric cells is interpreted by an eight-bit processor unit. As the system has only an 8-bit register, equivalent to 256 bins, it was important to set the frequency range, the range of velocities the system is sensitive to, as accurately as possible. The system was design to measure unidirectional flow. This is fine for the primary flow case where the range can be optimised for the expected flow regime. However, for strongly alternating flows, transverse and / or vertical, the accuracy is reduced because the range that has to be used includes significant excess in the positive direction.

3.5.3 Near surface readings

When light crosses from one medium to another, such as air to water, there is a change in refraction angle. With LDA systems, such transition results in change in the location of the measuring point, and intersection angle. If transition through the free water surface was allowed to occur, ripple effects would result in a continuously moving measurement point, changing intersection angle and reflection problems. The focal length of the probe in water was measured as 72mm. This means that measurements in the downward facing configuration are limited to depth greater than 72mm below the free surface.

To overcome refraction effects and facilitate near surface readings in the downward looking configuration a 'collar' system was devised. This is shown in Figure 3.12. The collar was free to slide on the outside of the probe. With the probe underwater, the collar was slid onto the end of the probe. The probe was then raised to the required height, drawing a column of water up inside the collar. The position of the collar was then adjusted until it was just breaking the water surface. This eliminates the refraction and other water surface problems. The validity of the system was checked against bulk optic measurements in a compound straight channel at the University of Sheffield Water Laboratories. This showed that the collar had no discernible effect on the measured flow regime, and was shown to provide accurate readings to within 5mm of the water surface.

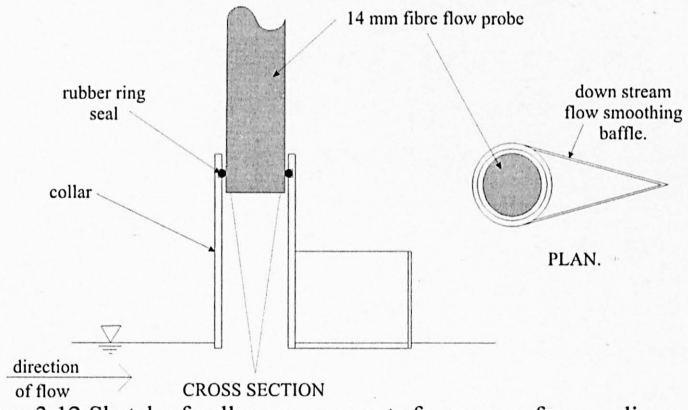

Figure 3.12 Sketch of collar arrangements for near surface readings with 14mm fibre flow probe in down facing configuration

3.5.4 Calibration

The calibration of the system was checked by taking readings on a rotating disk of known diameter, rotating at a specific velocity. The results obtained from a bulk optics system and those for the fibre flow probe system were compared, and showed favourable results.

3.5.5 Probe alignment

A procedure for alignment in both the downward and side looking configurations was devised. The main element assuring accuracy was the production of a specialist traverser system, see Figure 3.13. Any misalignment is an important consideration, since the primary longitudinal velocity is normally an order of magnitude larger than any secondary velocities. Therefore, any inclusion of a component of longitudinal velocity with either vertical or transverse readings caused by misalignment would lead to large errors.

The traverser had levelling points as indicated in Figure 3.13. Two sets of marks, one for side looking and one for downward looking configurations, were made on the end plates of the traverser. This was so that the traverser could be positioned in relation to the cross section marks on the channel sides to ensure longitudinal alignment with the required measuring sections. Thus, the longitudinal location of the measuring volume is correctly aligned, the probe mounted vertically, and the plane vertical and horizontal movement of the probe assured.

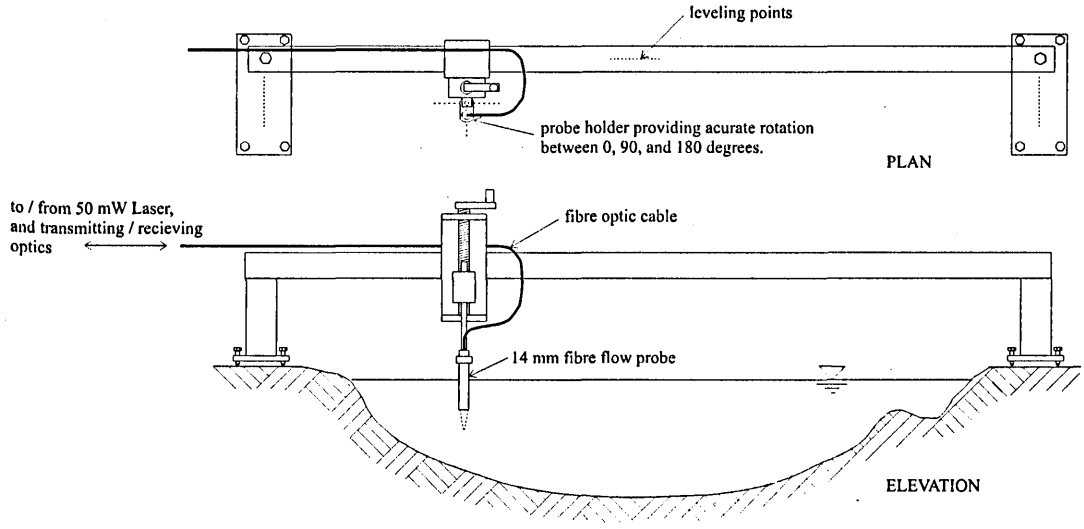

Figure 3.13 14mm fibre flow probe traversing system

Alignment of the side looking section onto the probe was set by removing the probe from all its fixings and then placing it on a large flat surface. The probe was then gently rotated, if the mirror was correctly positioned the beams measuring the vertical component aligned with the flat surface. This was checked over as long a distance as possible.

In the side-facing configuration it was essential that the probe could be rotated through exactly 180 degrees, to enable measurements near both left and right banks. This was facilitated by the traverser system which could be rotated and fixed in three positions, as indicated in Figure 3.13.

When in the side facing configuration the transverse location of the measuring volume was found by measuring the distance from the face of the probe to the pin, and subtracting the focal length in water. The focal length was predetermined by the use of a pin hole section. Vertical position was found in relation to the water surface at the channel centre line, by aligning the beams measuring the longitudinal component with the water surface.

For the down looking configuration, transverse location was found by positioning the probe over the pins such that the beams cross on the centre of the pin. This could not be used as the method to locate the probe vertically because the measurement is in air, and the diffraction angle is different in water. The water surface at the channel centre line was found with the end of the probe, and the focal distance, obtained from prior measurements with a pin hole section, added.

3.5.6 Misalignment angle

No accurate method of aligning the probe within the holder is given. Various steps were taken to ensure that alignment was a good as possible, but it was never perfect. A misalignment angle was present. However, using the above system the misalignment was a constant for each set of measurements. This means that post-data collection correction could be carried out to account for misalignment.

According to the definitions of primary and secondary flows, Section 2.10.1, and using the ideas of continuity, then for a horizontal slice within the flow the vertical mass flux must be zero. Similarly, for a vertical slice the mass flux must be zero in the transverse direction. Any deviation from this must stem from a component of the longitudinal velocity being incorporated in the secondary flow measurement. By considering the velocity data in a vector form, it was possible to derive Equation 3.2 to determine and correct for the misalignment angle:

$$\sum_{z=0}^{z=d}\left(v_z \cos\phi + u_z \sin\phi\right)=0 \qquad \text{Equation 3.2}$$

where ϕ is misalignment angle, u_z and v_z are primary and transverse velocities.

Once a misalignment angle had been found for each vertical and transverse profile, the velocity data was re-analysed to obtain the corrected mean and turbulence values.

3.5.7 Seeding system

For the LDA system to function it is essential that there are particles present in the flow to reflect the light. The level of particles is important. A lack of particles will result in no light scattering, too much seeding results in light being blocked and / or diffracted. The seeding used was Timiron Starluster MP-115, a very fine white powder of spherical particles, with a density close to that of water. A concentrated solution was made up in a stirrer tank and introduced into the flow via a peristaltic pump and an upstream point source. The concentration and the injection point location within the cross section were varied on a point by point basis depending on the re-circulating levels of Timiron, and the velocity field being measured. A study was carried out into the effect of distance upstream for introducing seeding. The optimum location of the injection point for the seeding was found to be one eighth of a meander cycle upstream of the measuring cross section, approximately 2.5m along the channel centre line. Using this distance it was found that the effect of the injection system on the flow regime was negligible, whilst providing good spread in the seeding cloud. To minimise the amount of seeding introduced, this distance was adopted as the standard for the remainder of the test.

During testing, over a period of about a week, there was a build up of very fine material upon the bed. Although this was not enough to significantly affect the water surface profile, through the alteration of bed roughness, the bed was swept clean weekly. This build up was attributed to the seeding, however, it was uniform along the entire channel length.

3.5.8 Data collection

As with the transverse Fluorometery work it was necessary to establish a log time which would provide representative results. With LDA measurements this was a complex process as the data rate of the system depends on a number of factors.

The system was set up with the blue beams as the primary velocity in the software, but measuring the weaker velocity component. The blue component gave the weaker signal, because of the lower power related to the shorter wavelength and the lower velocities producing a poorer signal. However, it was found that with the settings fine-tuned for this configuration, then when a good signal was obtained on the blue component, a good signal was nearly always present for the green secondary signal measuring the primary velocity. Adopting this set up was shown to produce the optimum data rates for the flow regimes being measured.

An average validated data rate of 50Hz was usually obtained, although, in the very fast moving flows using the side looking section where more power is lost with refraction on the mirror, this dropped to nearly 30Hz. The main limit on the data rate stemmed from the lower power output from the probe. This was limited by the 50mW laser input and the losses associated with fibre optic cables, normally stated as being in the region of 60-70%. Average validated data rates in excess of 500Hz where obtained at some points.

Once a procedure had been established and the settings finalised, a study was carried out into the log time required to obtain reliable measurements. The results of this are shown in Table 3.3 for two sets of readings representing the two extremes of the velocity fields measured:

Near-shore, cross section I															
Transverse Velocity (m/s x10-2)								Longitudinal Velocity (m/s x10-1)							
10 min		5 min		2 min		1 min		10 min		5 min		2 min		1 min	
Ave.	% error	Ave.	% error	Ave.	% error	Ave.	% error	Ave.	% error	Ave.	% error	Ave.	% error	Ave.	% error
-1.89	-	-1.90	0.56	-1.88	0.05	-1.98	4.79	3.65	-	3.65	0.07	3.66	0.19	3.67	0.51
		-1.87	0.57	-1.93	2.51	-1.79	5.35			3.65	0.07	3.65	0.11	3.65	0.13
				-1.85	2.08	-1.91	1.05					3.66	0.18	3.63	0.48
				-1.85	1.84	-1.96	3.88					3.65	0.06	3.66	0.26
				-1.91	1.29	-1.84	2.28					3.64	0.20	3.66	0.20
Channel centre line, cross section I															
Transverse Velocity(m/s x10-2)								Longitudinal Velocity(m/s x10-1)							
10 min		5 min		2 min		1 min		10 min		5 min		2 min		1 min	
Ave.	% error	Ave.	% error	Ave.	% error	Ave.	% error	Ave.	% error	Ave.	.% error	Ave.	% error	Ave.	% error
-4.83	-	-4.76	1.38	-4.76	1.53	-5.02	3.91	4.61	-	4.61	0.10	4.61	0.05	4.63	0.38
		-4.89	1.35	-4.78	1.02	-4.49	7.64			4.62	0.10	4.60	0.40	4.59	0.47
				-4.69	2.86	-4.72	2.36					4.62	0.23	4.60	0.26
				-4.95	2.52	-5.13	5.87					4.61	0.13	4.59	0.55
				-4.96	2.65	-4.74	1.81					4.63	0.35	4.63	0.41

Table 3.3 Investigation into log time for LDA testing

Comparisons of the percentage errors in the longitudinal and transverse velocities show that the transverse errors are much larger. This is because of the lower power of the blue beams and the

alternating nature of the secondary flows. This means that to cover the transverse velocity range it is necessary to select larger bin sizes in the 8-bit register than would ideally be used in the case of unidirectional flow, such as the longitudinal component. The difference between near shore and centre line measuring points showed remarkably little difference. The near shore region had a higher data rate, which had been expected to lead to lower errors. The higher data rate was attributed to the lower longitudinal velocities associated with the near-shore region, which result in better seeding. The table shows that a two-minute log time limits errors to less than 5%, and provides a good compromise between time and accuracy.

3.5.9 Noise removal from data

The presence of noise was noticed by examining time series data from the LDA measurements, that is occasional spikes which were of a magnitude that could not be part of the flow regime being studied. Where several of these spikes were present, they influence the mean velocity, and have an effect on the turbulence parameters. This noise could have a number of possible sources, for example interference from other equipment or vibrations. One source which was found, and minimised, was due to the backscatter configuration of the LDA equipment. With the irregular sand bed, it was possible for signals to be reflected back to the photomultiplier that had no association with the flow regime. This was particularly apparent with the downward facing configuration when taking near bed readings. To minimise this the bed was sprayed with matt black paint at the test sections.

Section 3.5.1 briefly discusses the principals of Doppler shift and its use in determining velocity. The following summary explains the source of noise and why it can not be removed by frequency analysis techniques, with reference to Drain (1980). Once the back scattered light signal has reached the photo-detector there are several ways of interpreting the signal. The two most common are spectrum analysis and counts.

1. Spectrum analysis uses an instrument with a selective response to sweep through a range of frequencies, recording in succession the components of various frequencies present in the signal. However, this method is limited to situations of continuous signal.
2. Counts, utilises the idea of counting cycles to determine the Doppler shift. This can operate with intermittent signals but a good signal to noise ratio is required so that individual signals can be detected. This method depends on accurate selection of validation settings, which are a compromise between limiting the data rate and accepting noise.

With turbulent flow the signal received is often intermittent, but, given a reasonable set-up a good signal to noise ratio can be achieved. Turbulent open channel flow favours the use of a counts based system. When a frequency-based system is used, noise can be eliminated on frequency bases, Shiono and West (1987). However, with the counts system, the data is not collected on a regular time basis so spectral type analysis cannot be readily performed, therefore, an alternative method must be used to remove noise.

The removal of the noise spikes from the velocity data was achieved using a FORTRAN program. This program examined each time series of data independently, and then removed 'noise' on a number of bases. Initially, a cut off was made on the vertical / transverse data so that the range was made uniform

about zero. This removed any noise which was interpreted as data because of the large unidirectional velocity range settings. Points lying beyond plus or minus three standard deviations of the mean were then removed. When data points failed the noise checks for either the transverse / vertical or longitudinal tests the corresponding point was also removed. It was possible to repeat the mean and standard deviation cut off several times. The effects of this noise removal could potentially be very large, therefore, an investigation into the 'smoothing' operations was conducted. It was carried out with four sets of point measurements from apex I. Vertical and side facing configurations time series data from a point at the channel centre line at approximately mid depth, represents data from a fast moving point in the flow where seeding was difficult, but reflections and noise levels low. Vertical and side facing configurations time series data from a point near the bed at the left-hand side of apex I, a point with slow primary velocity, therefore easy to seed, but incorporated extensive reflection effects.

The results of this investigation are shown in tabular form in Table 3.4 to Table 3.7 and visual representations of the data and smoothing processes in Figure 3.14 to Figure 3.21. The figures show the dramatic increase in turbulence levels for the near bank reading in the downward facing configuration. This visually confirms the effects of bed reflections on creating 'noise' effects in the time series. Visual inspection also shows that the secondary velocity components have a high degree of noise associated with them. Turbulence theory and past measurements suggest that the turbulence level of secondary velocities is around 70 percent of the primary. This 'noise' probably results from the lower power of the blue beams used to measure these velocities. The raw data histograms for the transverse and vertical measurements show that signals have been interpreted to fill the entire range which was set. The 0.4 cut off to obtain an equal range about zero is therefore deemed valid. The histograms after the 0.4 cut off still show excessive noise. Therefore, the first pass using the ± 3 SD criteria was deemed valid. Histograms of further cleaning showed distortion of the distribution away from the expected, the ends of the distributions were given sharp cut off. Inspection of the data tables also supports the use of the 0.4 cut off and the first pass. The 0.4 cut off and first pass show correction of the mean value. The second and third passes show little change in the mean value, suggesting no improvement in the removal of noise. A 'noise' removal system incorporating a 0.4m/s cut off on the secondary velocity component and a single pass of ± 3 standard deviations was adopted.

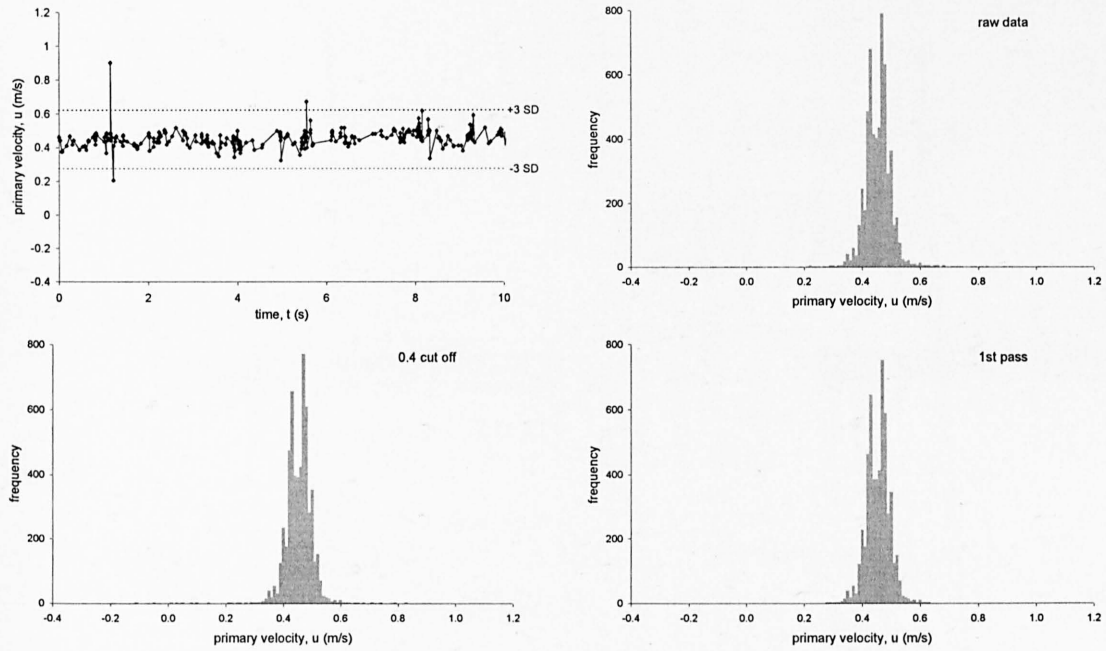

Figure 3.14 Section I centre line - longitudinal data from downwards facing configuration

	raw data	after 0.4 pass	after 1st pass	after 2nd pass	after 3rd pass
long mean	0.4481	0.4480	0.4497	0.4493	0.4495
long S.D	0.0609	0.0576	0.0398	0.0373	0.0367
transverse mean	-0.0062	-0.0313	-0.0351	-0.0354	-0.0356
transverse S.D.	0.1512	0.0634	0.0444	0.0393	0.0377
points removed	0	197	202	146	66

Table 3.4 Section I channel centre, downwards facing configuration, initial data points = 5800

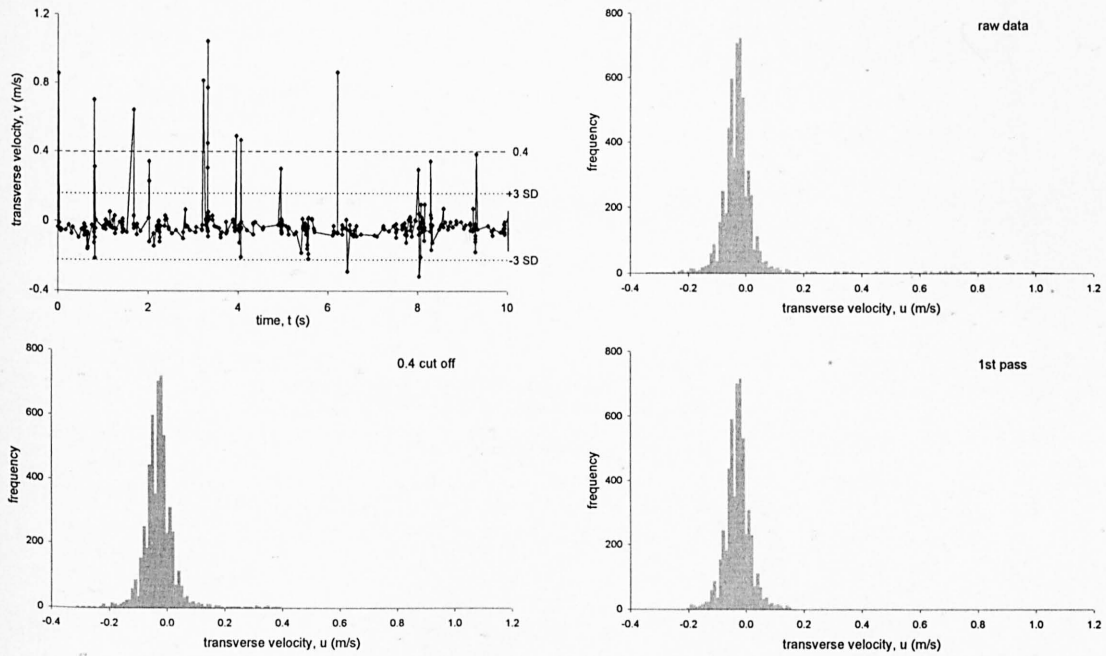

Figure 3.15 Section I centre line - transverse data from downwards facing configuration

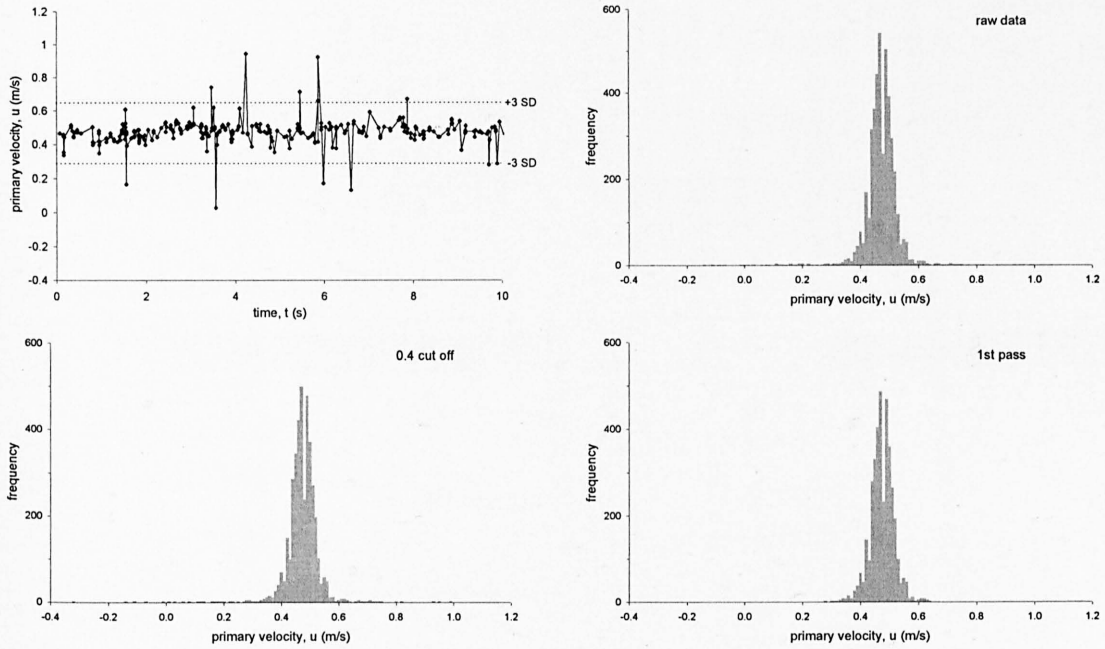

Figure 3.16 Section I centre line - longitudinal data from side facing configuration

	raw data	after 0.4 pass	after 1st pass	after 2nd pass	after 3rd pass
long mean	0.4679	0.46769	0.469752	0.47007	0.470149
long S.D	0.06137	0.05944	0.040268	0.03709	0.03637
vertical mean	0.03735	-0.009	-0.01592	-0.0171	-0.01745
vertical S.D.	0.18861	0.08333	0.060373	0.05032	0.04626
points removed	0	309	187	141	71

Table 3.5 Section I channel centre, side facing configuration, initial data points = 4283

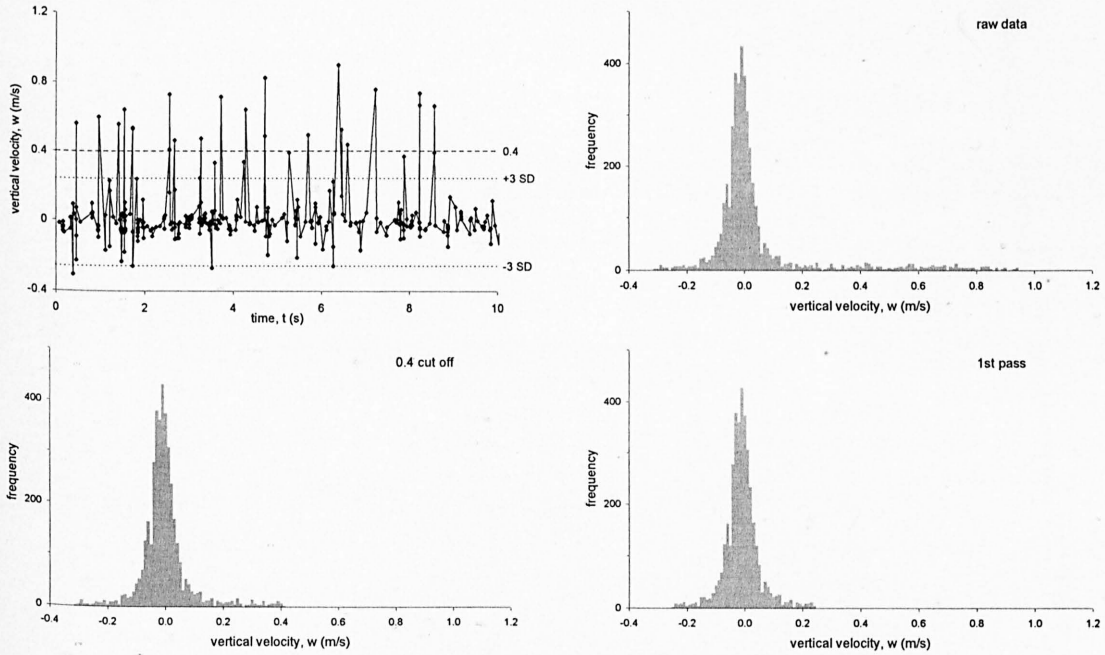

Figure 3.17 Section I centre line – vertical data from side facing configuration

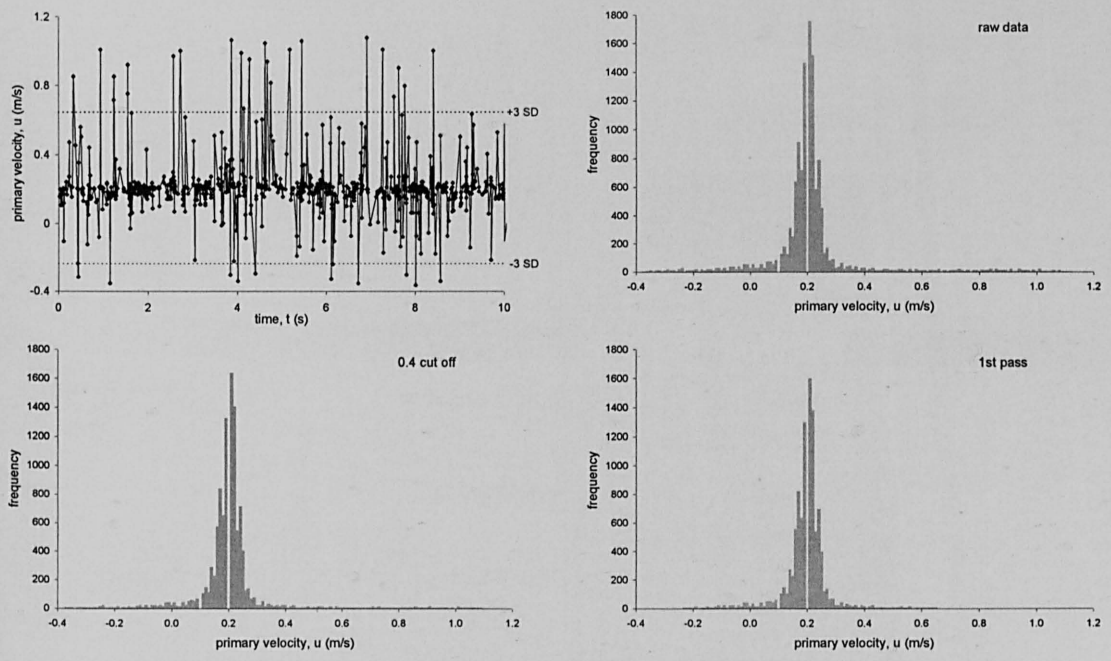

Figure 3.18 Section I L.H.S. - longitudinal data from downwards facing configuration

	raw data	after 0.4 pass	after 1st pass	after 2nd pass	after 3rd pass
long mean	0.2073	0.2034	0.1908	0.1926	0.1943
long S.D	0.1684	0.1469	0.0846	0.0580	0.0445
transverse mean	0.0670	0.0078	-0.0001	-0.0031	-0.0047
transverse S.D.	0.2533	0.0972	0.0751	0.0626	0.0557
points removed	0	1671	842	554	470

Table 3.6 Section I L.H.S., downwards facing configuration, initial data points = 12737

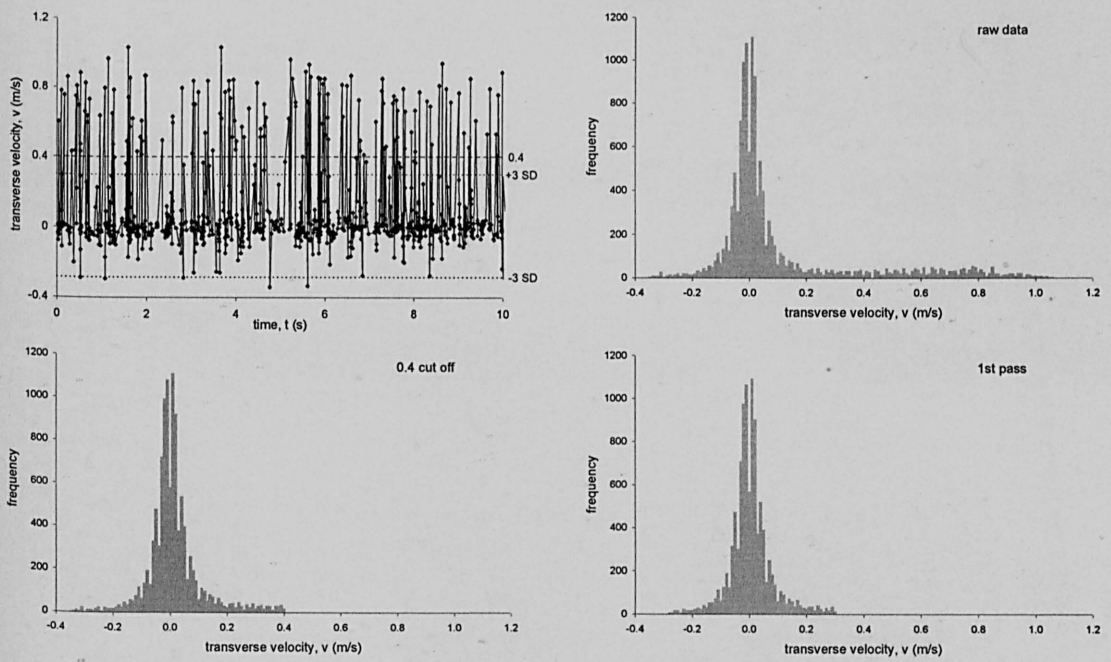

Figure 3.19 Section I L.H.S. - transverse data from downwards facing configuration

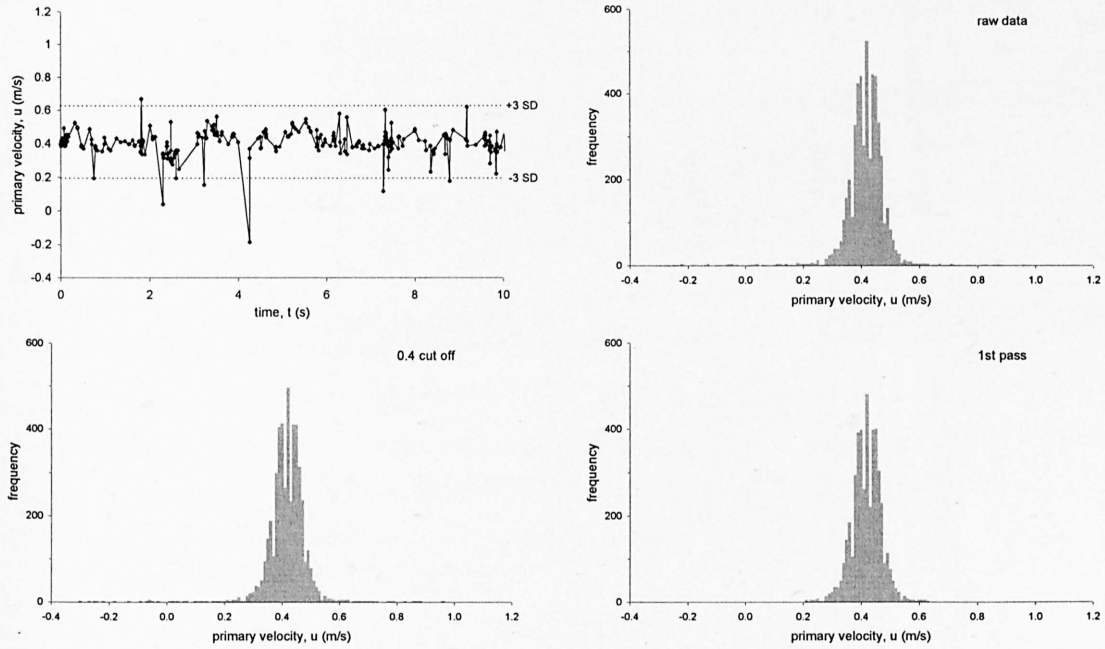

Figure 3.20 Section I L.H.S. - longitudinal data from side facing configuration

	raw data	after 0.4 pass	after 1st pass	after 2nd pass	after 3rd pass
long mean	0.41058	0.41101	0.413568	0.41351	0.413301
long S.D	0.07325	0.07189	0.050264	0.04687	0.046191
transverse mean	0.02263	-0.0238	-0.03055	-0.0314	-0.0312
transverse S.D.	0.19019	0.07831	0.05633	0.04712	0.043881
points removed	0	354	211	148	73

Table 3.7 Section I L.H.S., side facing configuration, initial data points = 5119

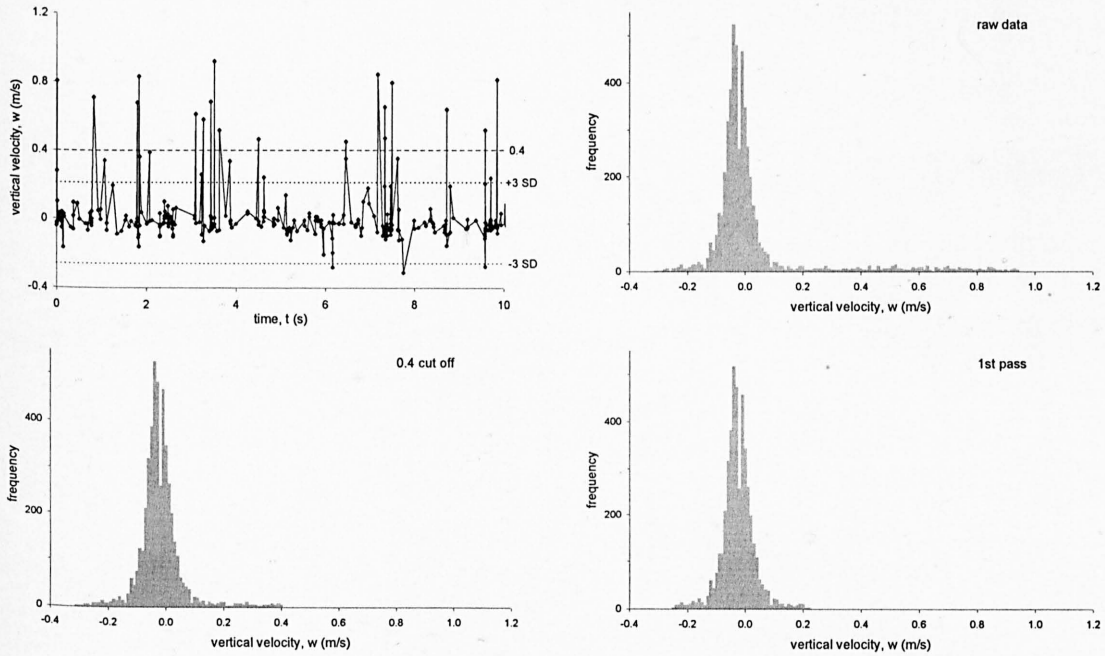

Figure 3.21 Section I L.H.S. - vertical data from side facing configuration

Chapter 4 Experimental Data

The results of the experimental study carried out at HR Wallingford during the summer of 1998 are detailed here. The data is presented in a form ready for further analysis, for example, the dye data has had background concentrations removed and calibrations applied as described in section 3.4.5. Details are also given of other longitudinal dispersion tests and data, which have been analysed.

4.1 Channel

The channel formation, bed fixing method and final shape were discussed in Section 3.2. Figure 3.3 shows details of the meander plan-form, and the cross sectional indexing system that was used. The half meander cycle that was used for the majority of the testing is shown in a three-dimensional form highlighting the variation in depth as well as plan form geometry in Figure 4.1.

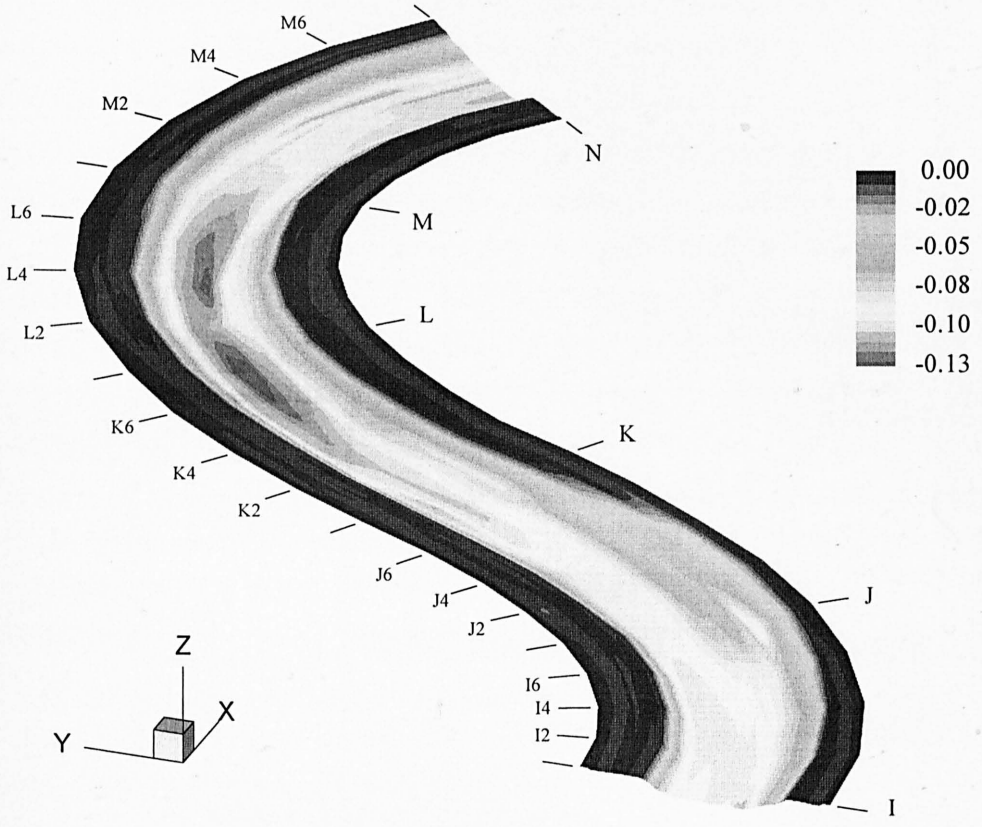

Figure 4.1 Three-dimensional contour flood plot of the final channel form showing cross section referencing system. X:Y:Z scale =1

4.2 Velocity Data

Velocity data was collected at six cross sections over the test meander half cycle, I0, I4, J0, K0, L0 and M0, see Figure 4.1 for details of cross section identification system. Within each cross-section data was collected at around 200 points, depending on the size of the cross section. As discussed in Section 3.5 a two-dimensional LDA system was used to measure velocities. This meant that every point within the cross section had to be measured twice. In the downward facing configuration, longitudinal and transverse velocities were measured, and in the side looking configuration longitudinal and vertical components were recorded. To facilitate correction for misalignment of the probe, vertical velocities were measured in horizontal slices, and transverse velocities measured in vertical slices. For each cross section around 13 vertical sections were measured, with spacing and exact number of slices dependant on the cross section dimensions. Between 15 and 20 points were then measured over each vertical for the downward configuration, and 2 to 15 points over each horizontal slice for the side-facing configuration.

Careful programming of the experimental timetable was necessary because of the selection of a single half-meander cycle test section for all the transverse dye dispersion test and velocity measurements. The order of velocity data collection was not sequential. The order was I, J, I4, L, M and finally K. Time did not allow testing of further #4 sections.

In chapter 2 the importance of bed generated shear effects and theoretical methods of evaluation of bed shear velocity were discussed. This resulted in a requirement to collect detailed velocity data in the inner, near bed region, so that bed shear velocity can be evaluated using the assumption of a vertical log-law distribution of the primary velocities. To facilitate this, readings from the downward configuration were concentrated near the bed. Near bed readings were not possible with the side facing configuration as measurements are limited to locations greater than 20mm from the bed, due to the mounting of the 45 degree mirror on the end of the probe.

At every measurement point, velocity data was collected for 120 seconds so that a reliable mean value and representation of the turbulence fluctuations could be obtained. The time traces were then signal 'cleaned' as detailed in Section 3.5.9 and a correction angle found in accordance with Equation 3.2. The correction angle was typically in the range of ± 5 degrees.

The following figures are intended to highlight a number of factors through examples of the data collected at section I. Figure 4.2 shows the profile of cross section I with the vertical and horizontal transects used marked. Figure 4.3 shows the results of the vertical profile measurements made, transverse and primary velocity. Figure 4.4 shows primary and vertical velocity components for the horizontal profiles. In both Figure 4.3 and Figure 4.4 the velocity data has undergone noise removal and had correction angles applied.

From this data, the volume and detail of the measurements made for each of the six test cross sections can be seen, as well as the pattern of the velocity structures measured. The concentration of the measurements in the vertical slice in the near bed region can be seen. Each of the approximately 200 points in each cross section is measured twice for 2 minutes, with considerable time required to set up seeding position, check data rate and signal validation for each point measured.

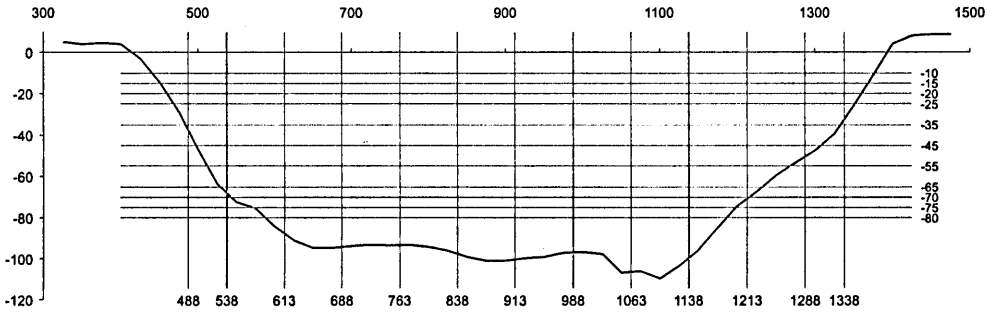

Figure 4.2 Section I cross section showing location of sampling transects (looking down-stream)

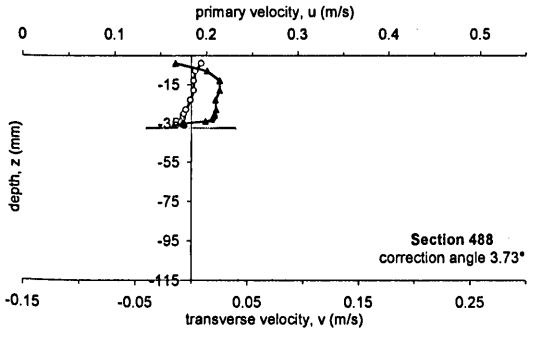

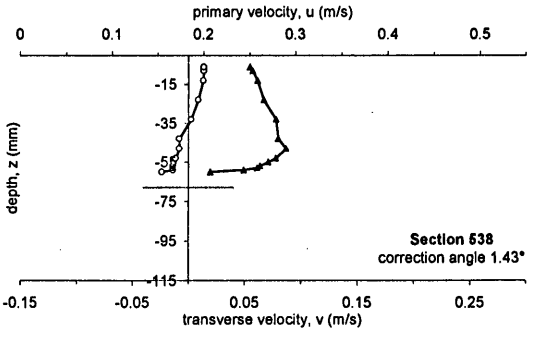

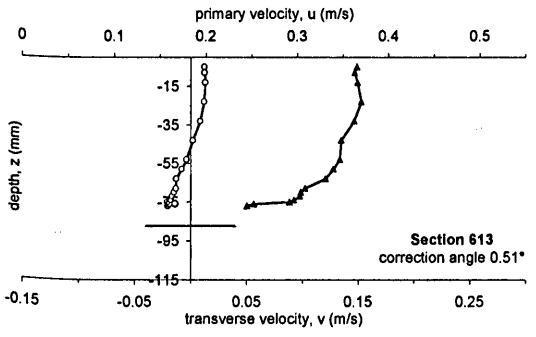

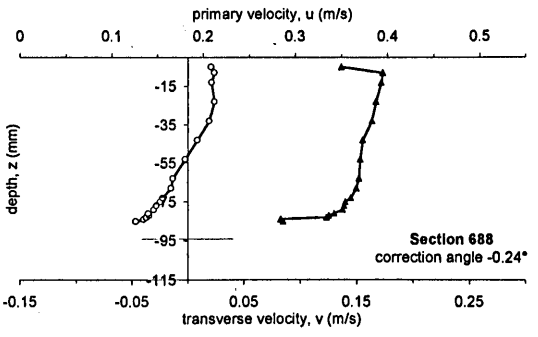

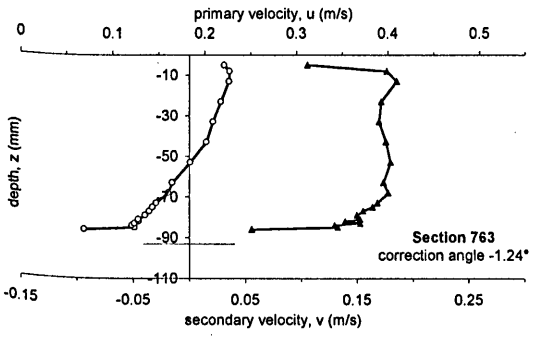

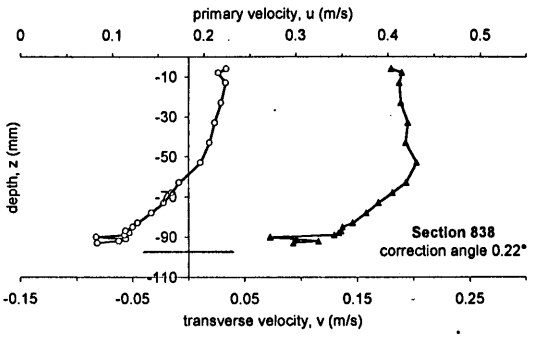

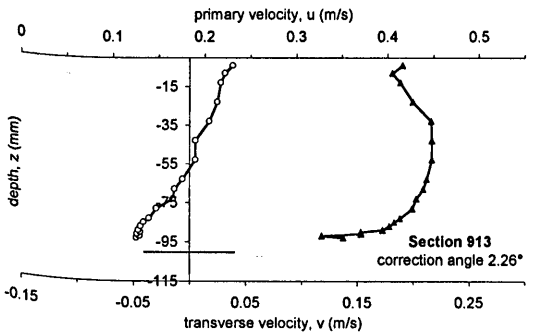

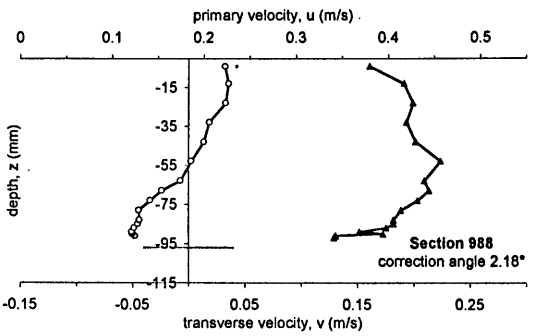

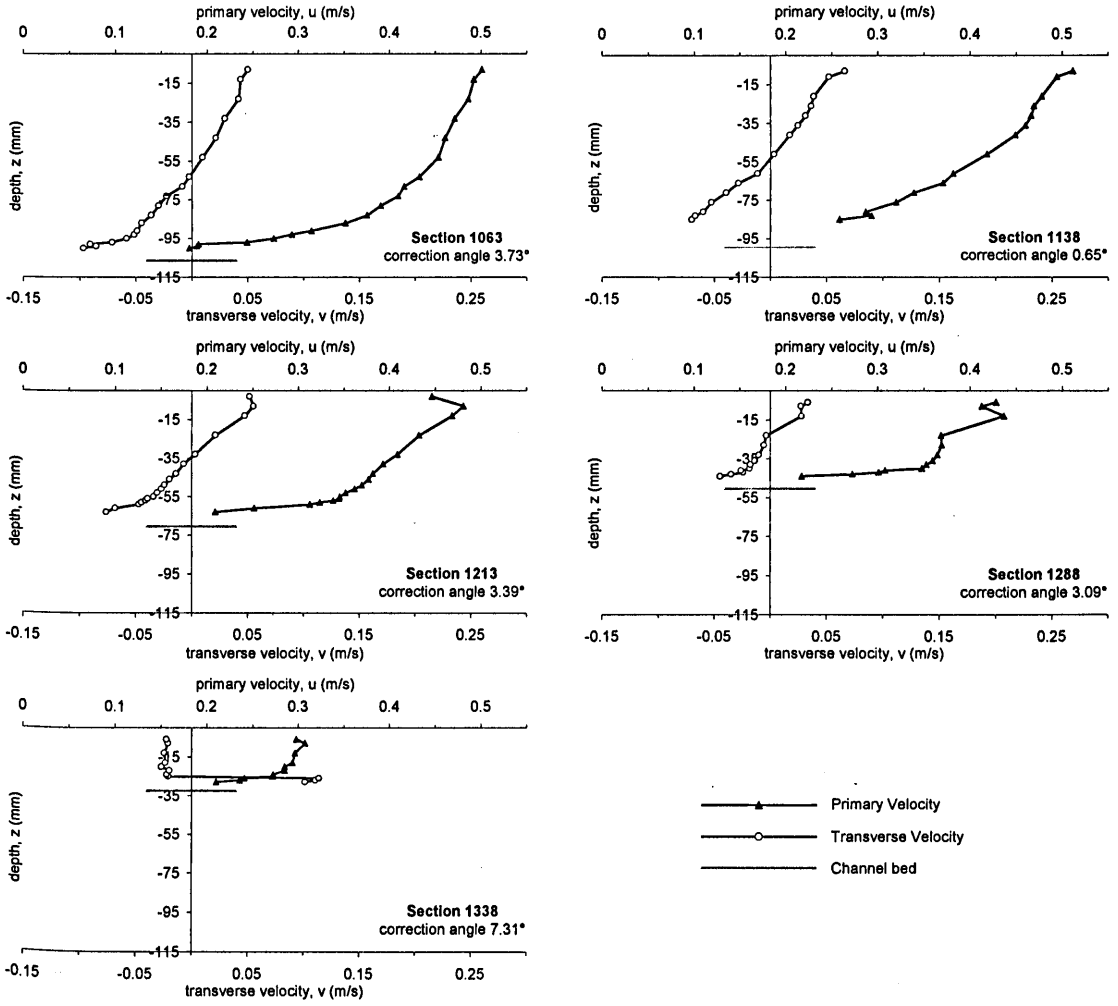

Figure 4.3 Vertical profiles of primary and transverse velocities collected at section I, correction angle and noise removal applied

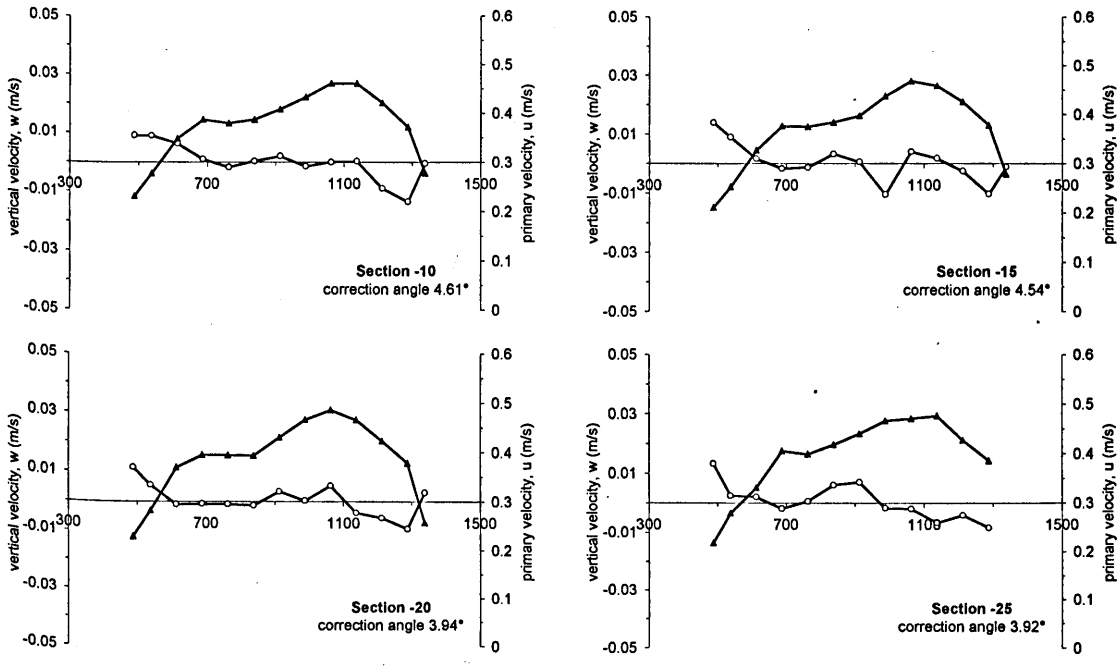

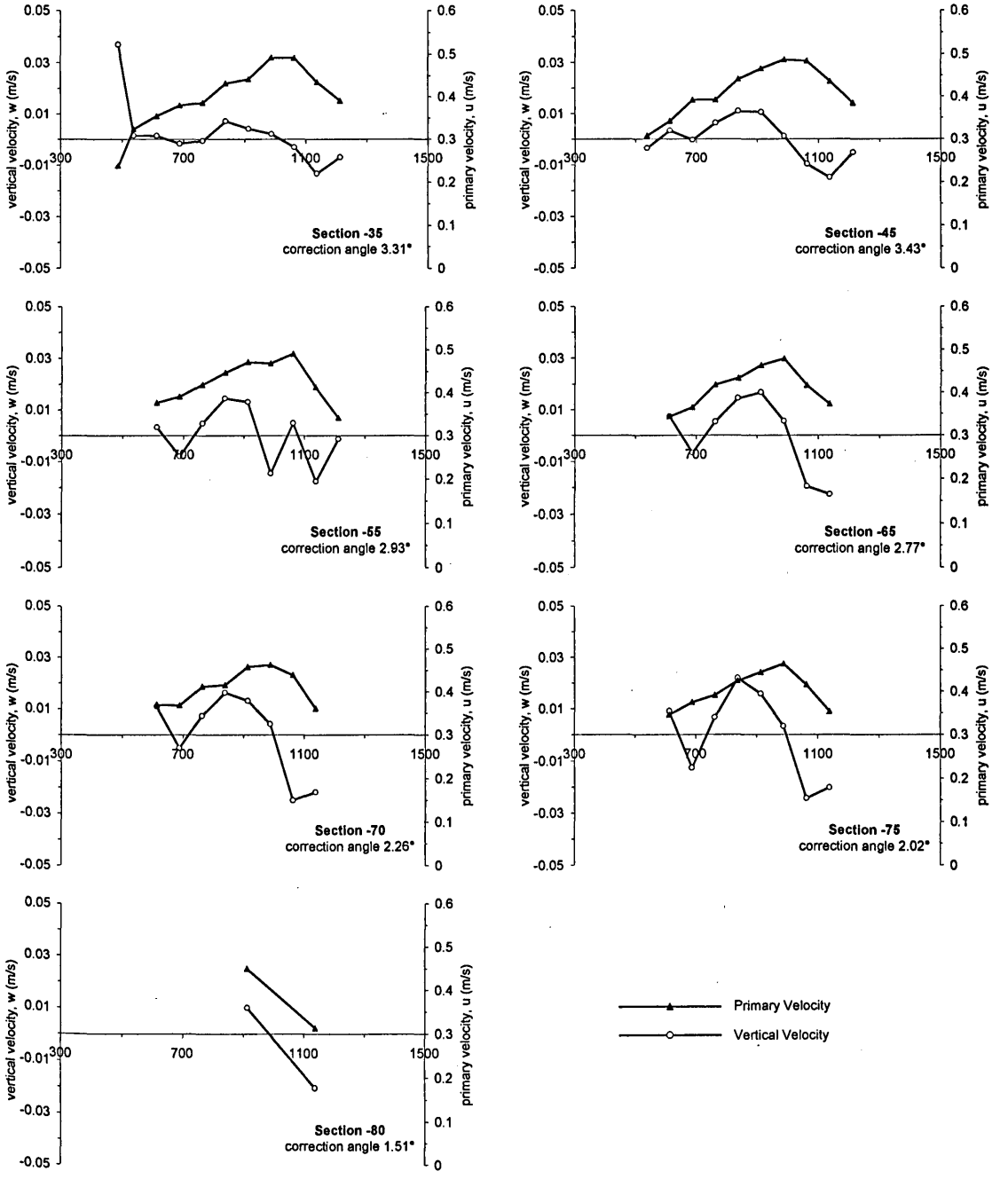

Figure 4.4 Horizontal profiles of primary and vertical velocities collected at section I, correction angle and noise removal applied

Figure 4.2 to Figure 4.4 are examples of the data collected at section I. The same volume and detail of data has also been collected for sections I4, J, K, L and M.

4.3 *Transverse Dispersion Data*

In chapter 3 the experimental procedure for obtaining transverse profiles of dye distributions below a continuous point source injection was detailed. Descriptions of procedures for removal of background and cross calibration of fluorometers were also given.

Twelve different injection points were used. Six or seven sampling cross sections were measured below each injection point. Details of these are given in Table 3.1. As with the velocity measurements, because

of the use of a single half cycle for all measurements the order of work was not alphabetical, injections were at K, L, I and then J. The sampling cross sections were equally spaced between an initial short distance below injection, to allow some vertical mixing, and a distance down stream where the dye was observed to have completely crossed the channel. Distance to cross the channel was set as the down stream limit, as it was believed that the calculation of variance and change of moments beyond this distance became susceptible to errors. Beyond the crossing distance the change in dye concentrations over the cross section would be reduced to a level where the accuracy of the readings would have an influence on the calculated variance. This was the case even with the use of the Generalised Method of Moments to account for bank impingement. Within each cross section, the spatial resolution of the measuring points across the channel was such that at least forty points were defined across the dye plume. As discussed in section 3.4.5.2 the vertical spacing of the sample rake was set to 18mm to optimise the vertical resolution with the five fluorometers over the average depth of flow.

Three cross section traverses could be completed per day, using the background sampling system and two-minute readings as specified. As was shown in Figure 3.11 the background increase in the system was appreciable over this time, so background concentration removal was necessary. The fluorometers were cross calibrated and the re-ordering of the point measurements made to obtain height ordered, not fluorometer ordered, data. Different injection concentrations were used for each day's testing because of the changing background level and the desire to optimise the days testing over one scale range of the fluorometers. Each day's measurements were normalised by the relevant injection concentration. The exact injection concentration was found using a similar system to that used during calibration.

After these procedures had been carried out, the data was considered ready for further analysis. An example of the data which was obtained after these procedures, for centre line bed injection at section I, is given in Figure 4.5. The traces clearly show the spreading of the plume away from the point source and the mass movement of the dye to the left hand side of the channel.

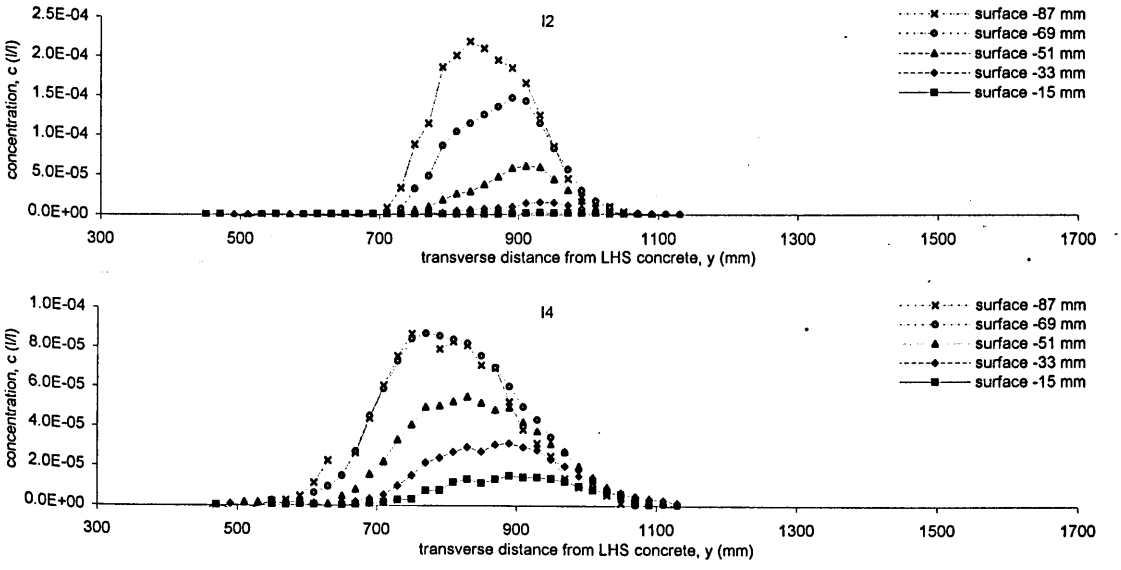

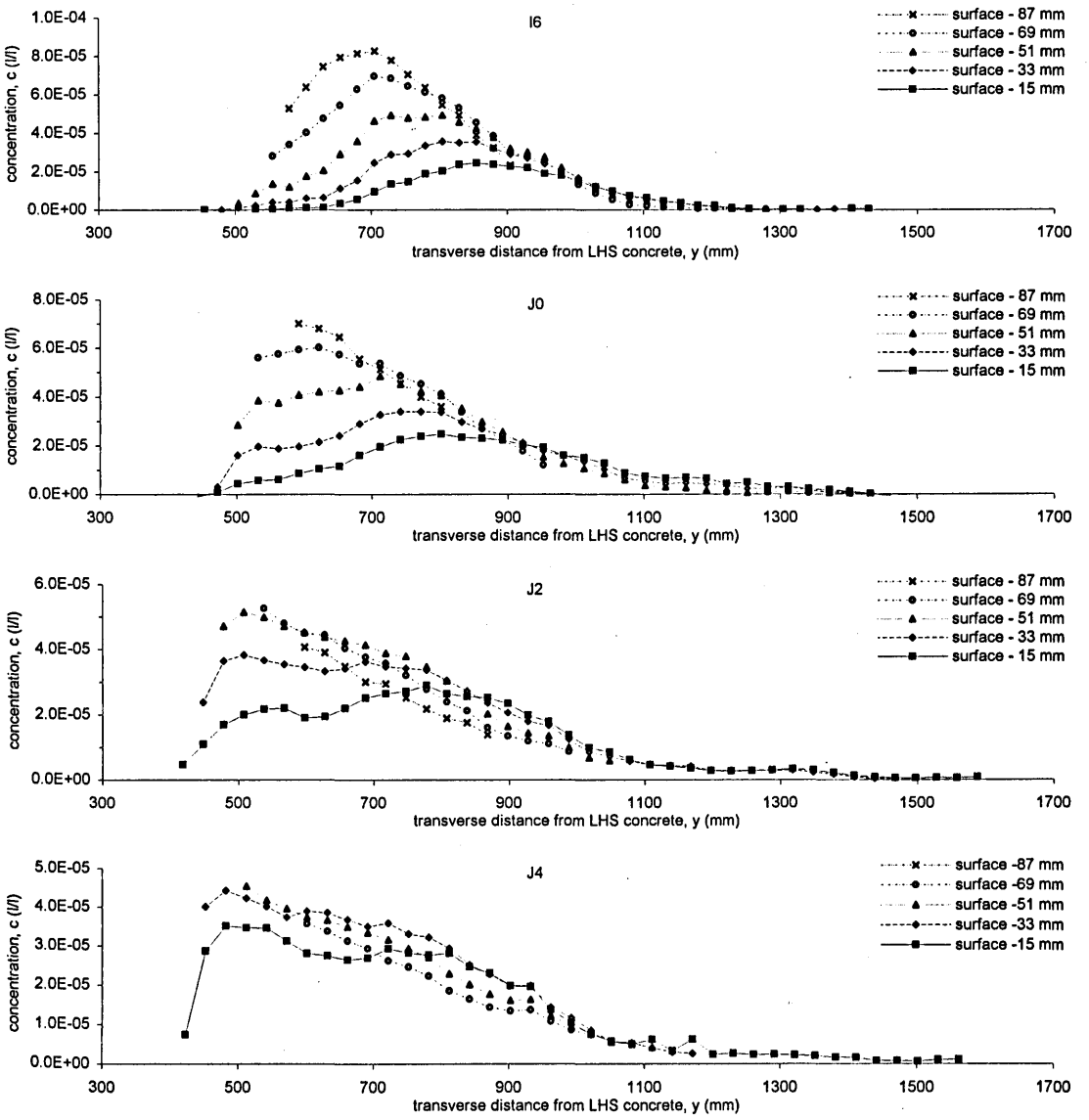

Figure 4.5 Example of transverse mixing data after calibration, background removal and normalisation by injection concentration, injected at section I0 bed

4.4 *Longitudinal Dispersion Data*

Longitudinal dispersion tests are less time consuming than transverse mixing experiments, because it is only necessary to measure the concentration profile of the dye as it passes a given series of points. It is not a prerequisite to obtain two minute point averages. Details of the injection and sampling systems that were used for all the longitudinal test was given in Section 3.4.4.

During 1996, the Flood Channel Facility was in used by the University of Newcastle to undertake channel-form and sediment transport studies. During these experiments, a team from the University of Sheffield was given access to perform longitudinal dispersion tests using the in-bank channel forms. Three in-bank channel forms were created by three different flow rates. 25l/s and 40l/s channel forms were developed exactly as the 25l/s channel which was detailed in Section 3.2.1, with formation halted when channel migration reached the channel boundary. A 97l/s channel was also formed, however, due to

the size of the channel required to convey this discharge, formation only ran for a short period before impingement of the channel on the concrete boundaries occurred. This flow rate was run, constrained by the concrete boundary, until the rate of change of channel form was negligible.

The study performed by the University of Newcastle was predominately aimed at investigating channel forms. Therefore, long term fixing of the bed forms was not required. The beds were temporarily stabilised by the application of caustic soda, for survey purposes and the longitudinal dispersion tests. The survey data has been manipulated to provide 3D representation of these channels, shown in Figure 4.6, to highlight the differences in the channel forms.

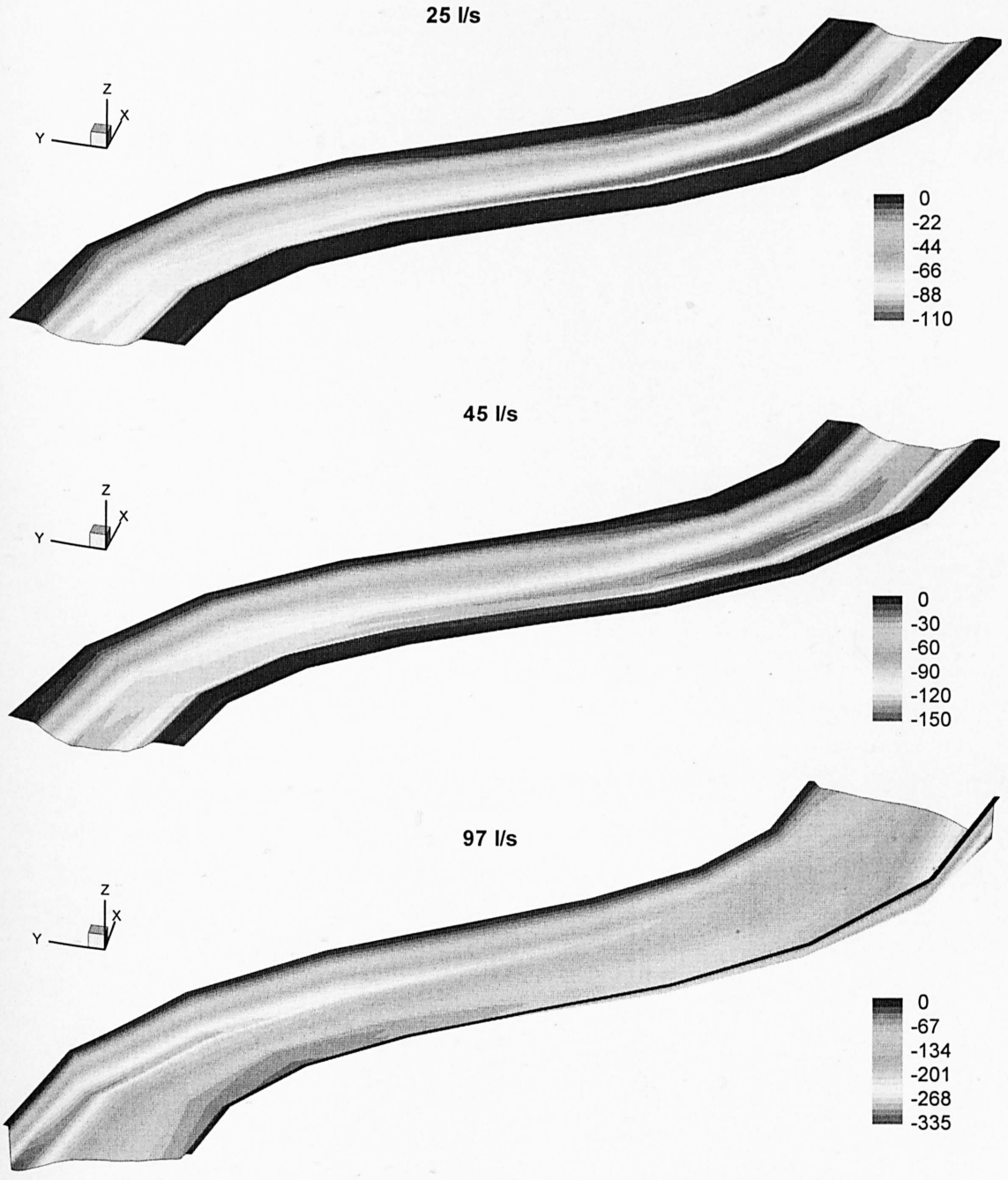

Figure 4.6 Profiles of 1996 channels used for longitudinal dispersion tests, flow direction is up the page, section shown is from apex E to I. X:Y:Z scaling = 1

The longitudinal dispersion tests carried out in these channels were undertaken to investigate the effects of the differences in channel form and discharge on longitudinal mixing rates. Tests were performed for a series of flow rates from bank full to low discharge, for each channel.

The longitudinal dispersion experiments performed during the testing period in the summer of 1998 were predominately a check on the repeatability of the data and channel form of the 1996 25l/s channel. This enabled the transverse mixing and velocity measurements to be linked to an extensive data set.

All the longitudinal tests were conducted in a similar manner to the description in Section 3.4. Each flow rate in each channel had 10-12 repeat instantaneous injections made. This was to ensure smoothing of any errors and thus confidence in results. Table 4.1 gives details of the flow rates studied in each of the channels, the locations of the fluorometers, and the possible reaches resulting from the sampling points.

Channel	Flow rates studied (l/s)	Sample points	½ cycle reach	¼ cycle reach
25 l/s Sept 1996	25, 20, 10, 15, 5	A, E, I, M, Q	A-E E-I I-M M-Q	-
40 l/s Dec 1996	40, 35, 30, 25, 20, 15, 10, 5	E, G, I, K, M, Q	E-I I-M M-Q	E-G G-I I-K K-M
97 l/s June 1997	97, 90, 80, 70, 60, 50, 40, 30, 20, 5	E, G, I, K, M, Q	E-I I-M M-Q	E-G G-I I-K K-M
25 l/s 1998	25	E, I, K, M, Q	E-I I-M M-Q	I-K K-M

Table 4.1 Longitudinal mixing tests details

Fluorometer output was logged directly to a PC, as detailed in Section 3.4.2. Results for each set of repeat injections for each flow rate were logged to a single file. A FORTRAN program was written to analyse these files. The program removed background by fitting a straight-line between the start and end 30 seconds of the trace. The peak of each trace was located, the program then searched forward and backwards from each peak for a 30 second section of data where the change in concentration was less than 0.5 percent of the peak. Each section around the peak was then separated, and fluorometer calibrations applied. All logged channels were analysed concurrently, and the results for each injection grouped together. A typical result for four fluorometers equally spaced along a channel, after this analysis was shown in Figure 2.20.

Chapter 5 Analysis

5.1 Channel Data

From the profile survey data it is possible to define cross sectional properties of the channel and present their variation over the test half meander cycle.

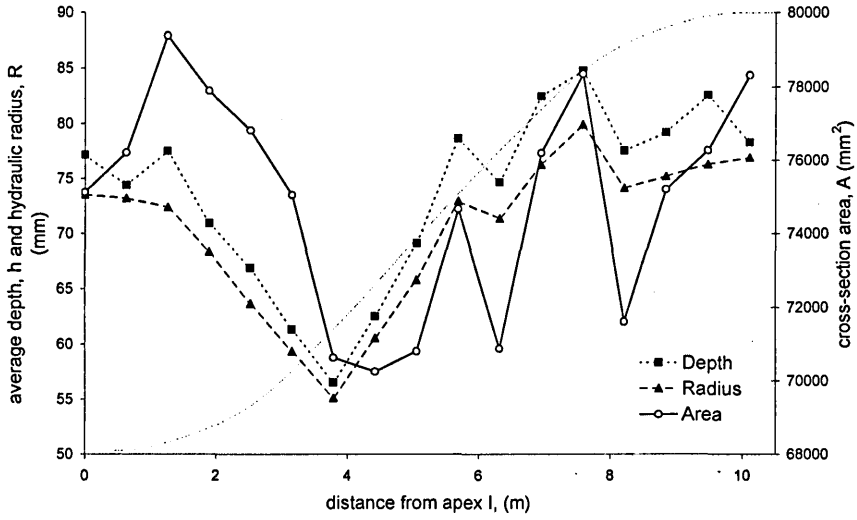

Figure 5.1 Longitudinal variation in cross section properties

The three properties presented in Figure 5.1, average depth, hydraulic radius and area, follow predominately the same pattern, although the area exhibits greater variation about the trend than the others. The light line on Figure 5.1 indicates the channel curvature. From the figure it can be seen that area, average depth and hydraulic radius all have a minimum at the end of the bend / start of the straighter section, and maximum values occur around the bend apex.

5.2 Velocity Data

Velocity information was collected at six cross sections over the test meander cycle (figure 4.1), using a two dimensional LDA system. The resulting data has been 'cleaned', correction angles found and applied. From this, quality assurance checks can be conducted, and trends illustrating the measured flow regime presented.

5.2.1 Mass balance

At each cross section a check can be made on the quality and consistency of the data by performing a mass balance. When the primary velocity component at any given point is multiplied by its associated area, and these multiples summed over a complete cross section, the result should be consistent with the channel discharge. The channel flow rate was set to $0.0255m^3/s$ using the control orifice plates on the facility inlet pipe, according to the calibration curves for the facility, provided by HR Wallingford Ltd. The channel areas were approximated using trapeziums. The results of these calculations are shown in

Table 5.1, together with the results of mass balance calculations based on the depth average value of primary velocity multiplied by its respective area.

	Calculation based on individual primary velocities		Calculation based on depth average primary velocities	
Cross-section	Q (m^3/s)	% change from average	Q_d (m^3/s)	% change from average
I	0.0271	0.68	0.0268	-0.92
I4	0.0268	-0.48	0.0268	-0.79
J	0.0255	-5.47	0.0252	-7.28
K	0.0286	5.94	0.0284	4.88
L	0.0270	0.26	0.0273	1.24
M	0.0265	-1.62	0.0276	2.06
Average	0.0269		0.0270	

Table 5.1 Results of mass balance calculations for velocity data

The results of the non-depth averaged mass balance checks show that the deviation of the total flow at each cross section has a maximum variation of ± 6% from the average value, with 3 of the measurements less than 1%. As may be expected the depth average calculations lead to a slight increase in errors. These values are good given the irregular nature of the channel form, the complex flow regime being studied and the time scale of the data collection. The average calculated discharge is 5% larger than the value given from the calibration curves for the inlet conditions. As the name suggests, the Flood Channel Facility was primarily intended for the study of over bank flows using larger discharges than during this study. Thus, the inaccuracies between calculated and set discharge may stem from running the facility controls at low flow rates.

A below average value for channel discharge is obtained at section J. An investigation of profile data from section J shows a dip on the right hand side of the channel, photographs revealed this to be a localised hollow. The flow field in this region is likely to be strongly three-dimensional and very complex. Over this hollow the ideas of correction to primary and secondary flow may be invalid. This is borne out by visual inspection of Figure 5.2, where directly over the hollow there are very large secondary flows which appear to be inconsistent with the rest of the cross section.

The discharge calculated for section K, the last section tested, is some 5% greater than the average value. This may be due to wear of the fibre flow probe, during testing of section K, a slight 'halo' was noticed on one of the green beams. This was due to the ingress of moisture into the fibre-probe head. When the effect was first noticed the probe's accuracy was checked using the calibration method detailed in Section 3.5.4, this showed that the system was still accurate. During the completion of section K measurements it was noticed that the halo effect had increased. At the end of the test, the accuracy of the probe was again verified. However, the method of checking the accuracy using a rotating disc may have been overcoming the errors of the halo effect. Measuring a signal from a perfect reflector, with the reflector passing exactly through the centre of the measuring volume may have been compensating for the effects of the halo. The 'halo' may have been influencing the readings, resulting in a slight over estimate of the primary velocity. The 'noise' level of the time series obtained at section K was visually compared with other traces but no significant difference was observed.

5.2.2 Data presentation

From the data in the form presented in Figure 4.3 and Figure 4.4, it is possible to create composite plots for the complete flow field over each cross section.

5.2.2.1 Flow field

Representations of the main flow fields at the measured cross-sections are shown in Figure 5.2. The contours represent primary velocities, as measured in the down facing configuration. This was used in preference to the data from the side-facing configuration because of the 20mm blind spot area above the bed associated with side-facing configuration. The vectors represent secondary velocities. At all the points where the two sets of readings, transverse/primary and vertical/primary, coincide it is possible to correlate the vertical and transverse components to produce these vectors.

The sequence of images in Figure 5.2 show a number of features of the average flow field. The build-up, decay and reversal of the secondary currents over the half meander cycle can clearly be seen. Redistribution of the primary flow field is evident. In straight uniform open channel flow the primary flow maxima are expected to be at the centre of the channel below the water surface. At sections I, I4 and M the maxima are moved across the channel and towards the bed by the strong secondary currents. However, at section K where the secondary currents are much reduced, the maxima are shown at the channel centre. Section K also shows a marked increase in the overall primary velocity, beyond the errors associated with the mass balance checks. This increase can be related to the decrease in flow resistance in this region, due to the reduced curvature. As with the bed profile data, the repeatability and regularity of meander features can be highlighted by comparing the inverse of repeated cross sections. Comparison of section I with the reverse of section M shows remarkable repetition of the overall flow fields.

5.2.2.2 Comparison of primary velocities

The quality of the velocity data can be further verified by comparing the differences in the two sets of measurements of the primary velocity. This is possible at all the points where the two sets of readings coincide. The results of this are shown in Figure 5.3, as percentage errors between the pairs of two-minute average readings, $(1-(u_{trans}/u_{vert}))100$. The error plots show good agreement between the two sets of readings, the majority of the errors are under 5% and the errors vary randomly between positive and negative values. Occasional points show greater error, this is expected because:

- the duration over which readings were averaged;
- variable data rates;
- natural bed form;
- effects of the probe on the local flow regime;
- time between compared readings.

This check provides confidence in the velocity data, and the repeatability of the hydrodynamic conditions throughout the test period.

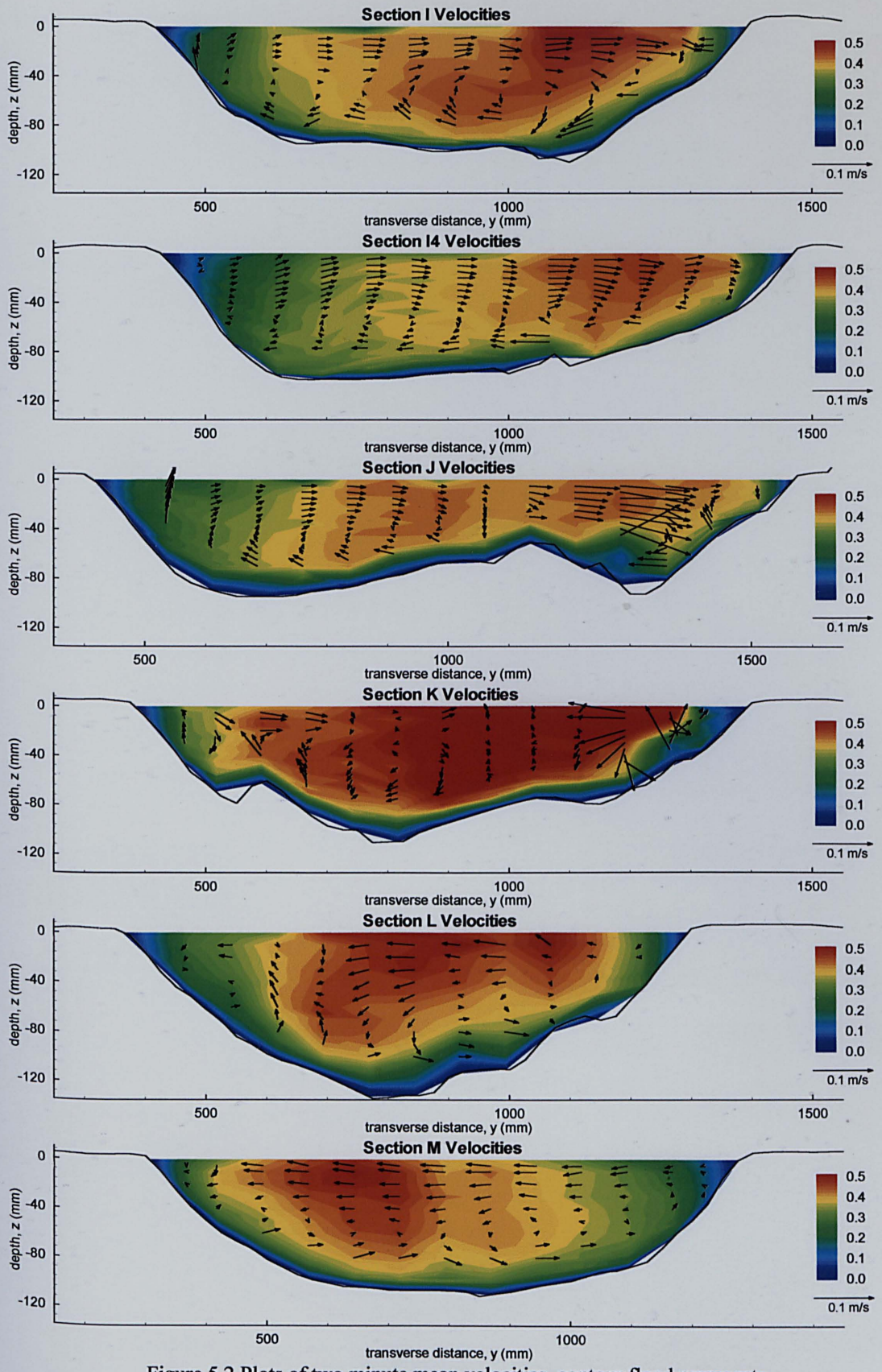

Figure 5.2 Plots of two minute mean velocities, contour flood represents primary velocity and vectors depict secondary flow (looking downstream)

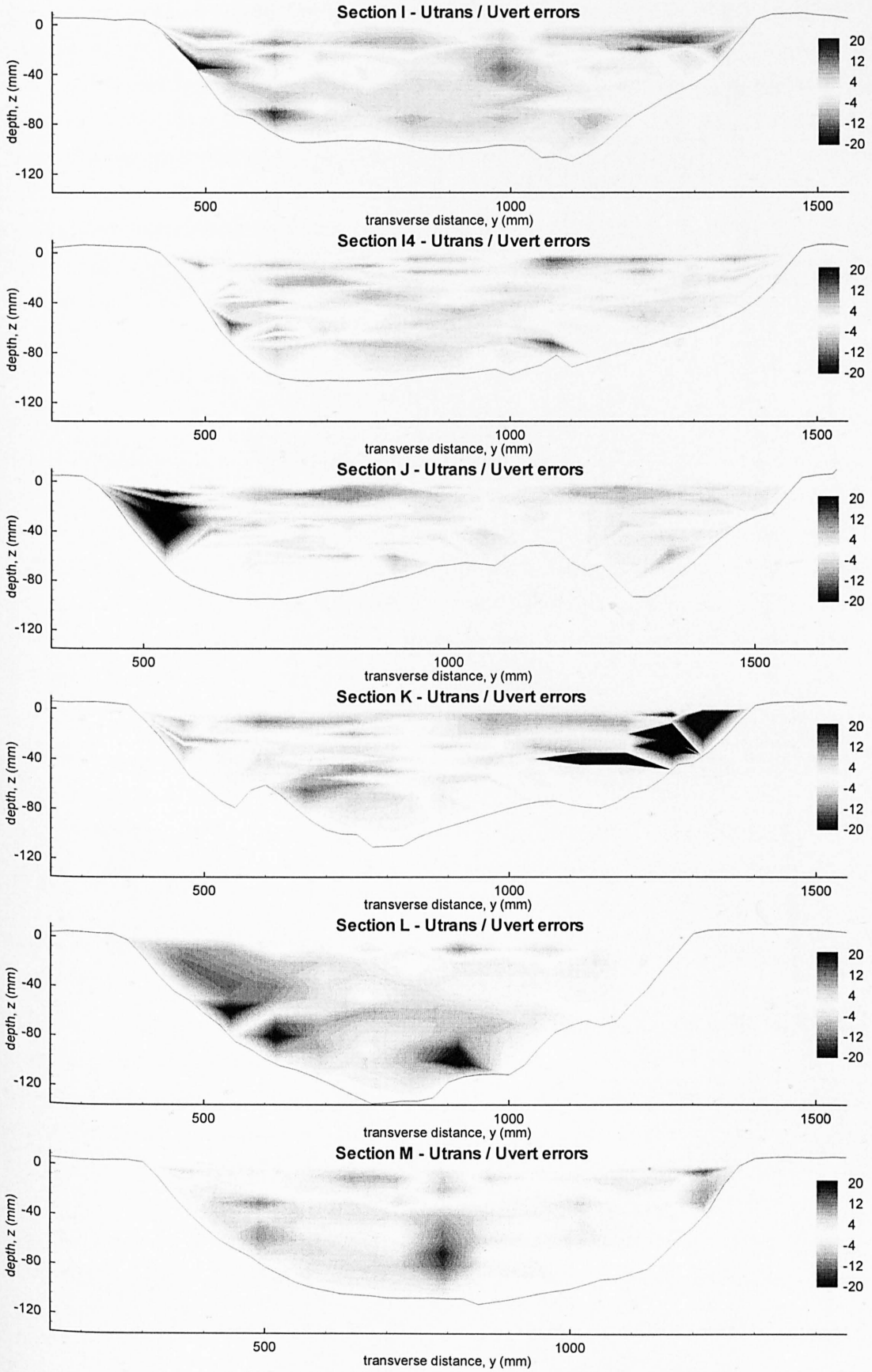

Figure 5.3 Plot of U_{trans}/U_{vert} percentage errors (looking downstream)

The plots for sections J, K and L in Figure 5.3 show point values with large errors when compared with the mean values. The area in sections J and L show no clear trend towards positive or negative, and the errors in both reach point maxima of around 20-25 percent. Both sets of errors are near the channel edges and probably result from excessive noise, due to reflections off the bed or disturbance of the flow by the probe. Investigation into section K showed that the area of error on the right-hand-side had predominately negative errors of large magnitude, up to several hundred percent. This suggests an overestimate of velocity component measured in the down facing configuration, as compared with the side facing velocity measurement. This discrepancy at section K could account for the high value of discharge calculated for this cross section, and could be a direct result of the 'halo' effect mentioned previously.

5.2.3 Bed shear velocity

In Chapter 2 bed shear velocity was introduced, and its importance in characterising the flow resistance of channel regimes and as an indicator of turbulence levels was shown. In Section 2.10.3 a method of estimating bed shear velocity from near bed measurements of primary velocity was detailed. Using this method and the two minute average values of primary velocity which have been presented, it is possible to obtain point estimates of the bed shear velocity. This can be done at the location of each vertical slice for all the test cross sections. Thus, it is possible to obtain an indication of how bed shear stress varies transversely and longitudinally over the test half meander cycle. The bed shear velocities are related to the direction of the primary velocity and are not aligned longitudinally.

In Equation 2.137 the need for a depth correction factor, c, was introduced. This factor is required to correct for any errors in location of the measuring volume with relation to channel bed, which can lead to large errors in the calculated value of bed shear velocity. The correction values which ensure the fitted lines pass through the origin are presented in Figure 5.4. The values for elevation correction show that the error in the location of the measuring volume was small and irregular. This suggests that the probe location procedure was accurate and repeatable. However, the correction is still required by the calculation, as even small errors in bed location lead to large variations in the calculated value of bed shear velocity.

Past investigations have suggested that the log-law distribution is only valid over an inner region, defined as one twentieth of the depth to the velocity maxima. However, inspection of Figure 4.3 shows the difficulty in accurately defining the point of maximum primary velocity. Unfortunately, no consistent method has been found to define how much of each profile should conform to the log-law distribution. The straight line fits shown in Figure 5.4 have been obtained based on conservative estimates of the location of the velocity maxima. Given that the log-law is only valid over the inner region points have been removed when the fit is poor. This method is not ideal and the resulting values may be questioned, however the resulting data is useful to give an indication of the overall variations in bed shear velocity.

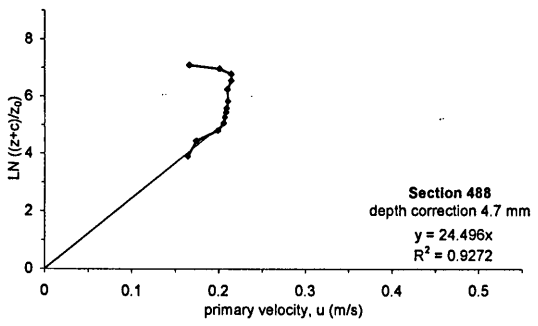
LN ((z+c)/z0)
primary velocity, u (m/s)
Section 488
depth correction 4.7 mm
y = 24.496x
R² = 0.9272

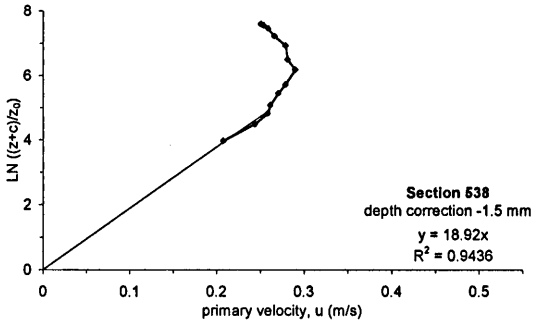
LN ((z+c)/z0)
primary velocity, u (m/s)
Section 538
depth correction -1.5 mm
y = 18.92x
R² = 0.9436

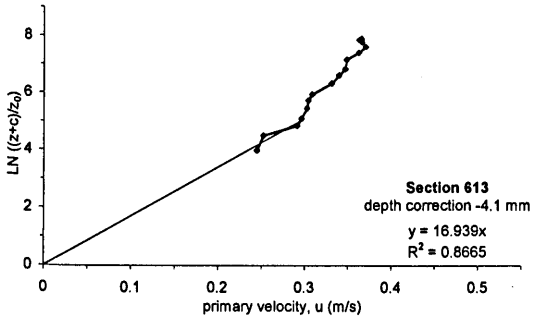
LN ((z+c)/z0)
primary velocity, u (m/s)
Section 613
depth correction -4.1 mm
y = 16.939x
R² = 0.8665

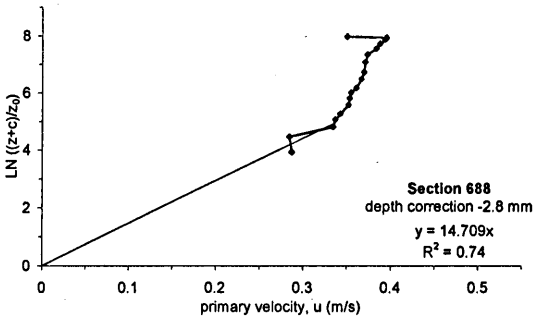
LN ((z+c)/z0)
primary velocity, u (m/s)
Section 688
depth correction -2.8 mm
y = 14.709x
R² = 0.74

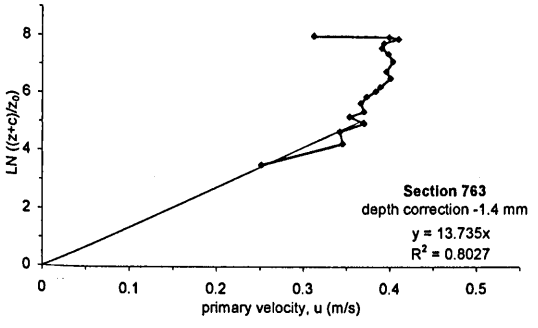
LN ((z+c)/z0)
primary velocity, u (m/s)
Section 763
depth correction -1.4 mm
y = 13.735x
R² = 0.8027

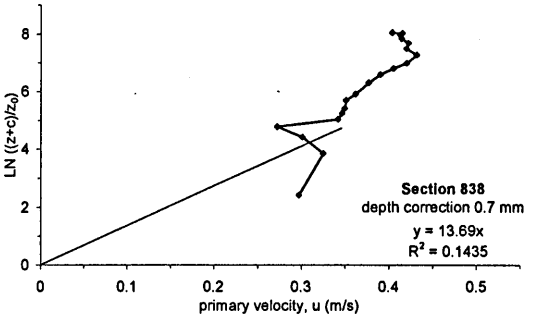
LN ((z+c)/z0)
primary velocity, u (m/s)
Section 838
depth correction 0.7 mm
y = 13.69x
R² = 0.1435

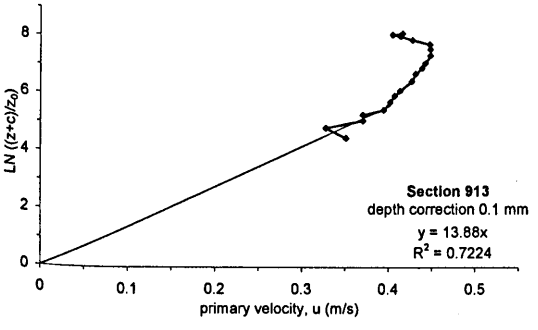
LN ((z+c)/z0)
primary velocity, u (m/s)
Section 913
depth correction 0.1 mm
y = 13.88x
R² = 0.7224

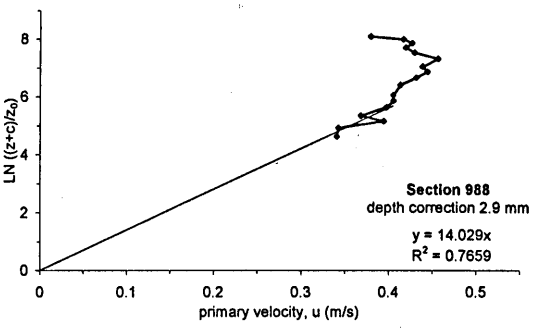
LN ((z+c)/z0)
primary velocity, u (m/s)
Section 988
depth correction 2.9 mm
y = 14.029x
R² = 0.7659

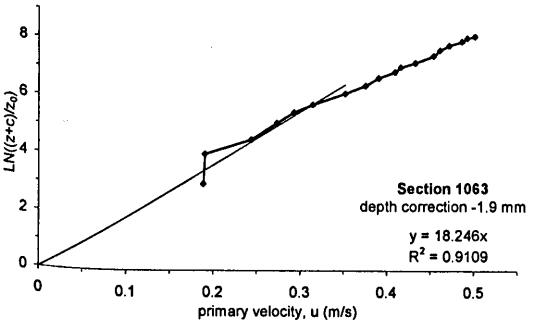
LN((z+c)/z0)
primary velocity, u (m/s)
Section 1063
depth correction -1.9 mm
y = 18.246x
R² = 0.9109

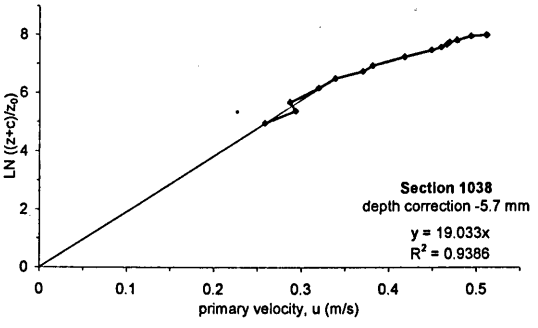
LN ((z+c)/z0)
primary velocity, u (m/s)
Section 1038
depth correction -5.7 mm
y = 19.033x
R² = 0.9386

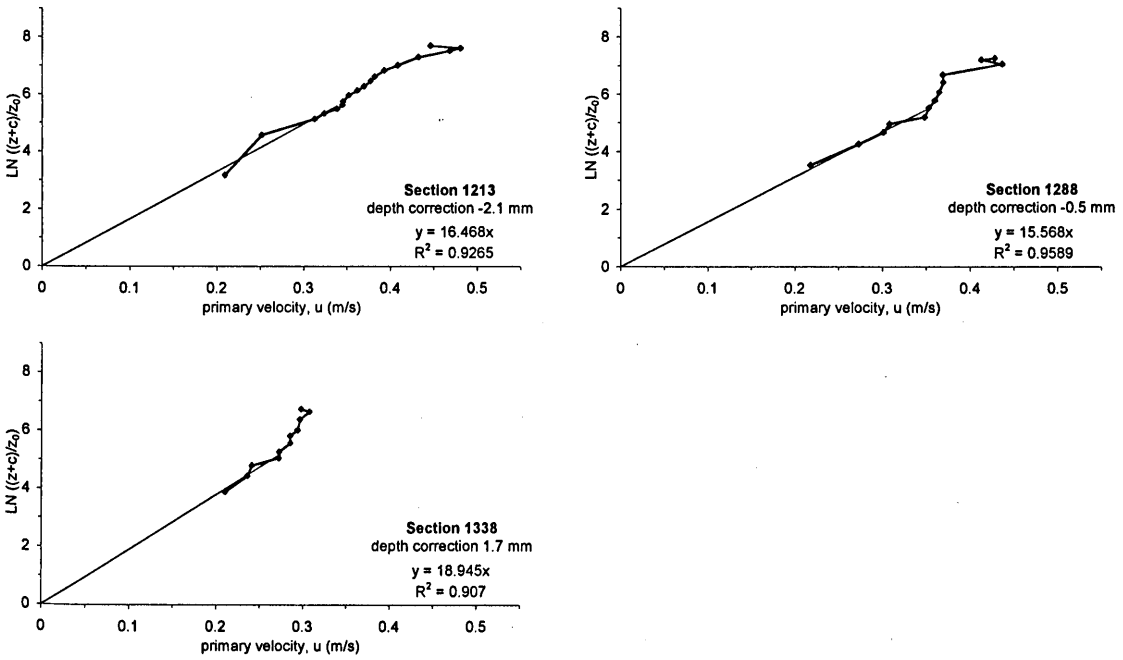

Figure 5.4 Plots showing fit of log-law distribution to measured velocity data for calculation of bed shear velocity

The derivation of the expression for evaluating bed shear velocity from primary velocity distributions is based on the assumptions of uniform plain two dimensional shear flow. Some evidence was presented in Sections 2.10.3 to show that log law distributions are valid over an inner region for accelerating and decelerating flows. No prior evidence exists to validate the fitting of log law distribution for strongly three-dimensional flows, however, the quality of fit obtained in Figure 5.4 suggests that the procedure is valid in this situation.

Figure 5.5 shows the transverse variation in the calculated value of bed shear velocity for each of the velocity test sections. One of the major features that this highlights is the dependence of the bed shear velocity on local bed features. Local dune, ripple and hollow features have a very strong influence on the local value of bed shear velocity. The overall cross sectional variation is roughly parabolic.

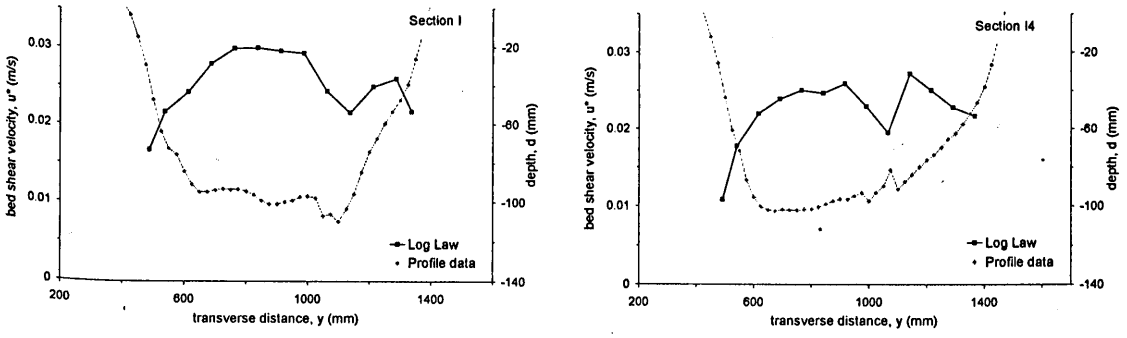

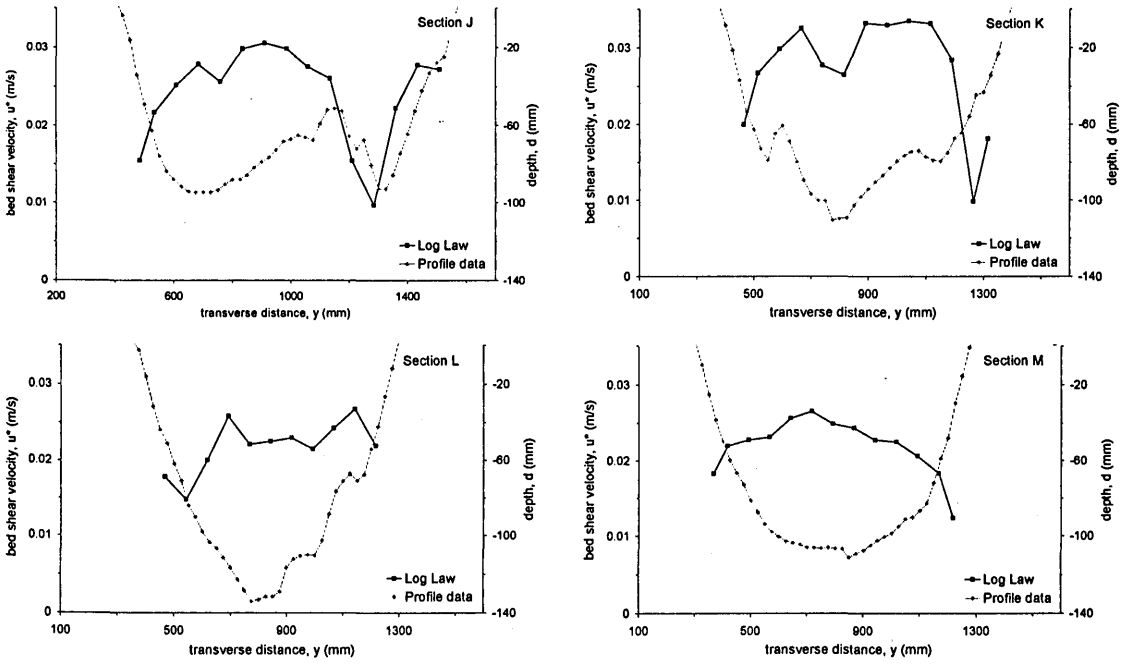

Figure 5.5 Transverse variation in bed shear velocities

5.2.4 Velocity predictions

It is beneficial to predict depth average velocity distributions for the construction of stream tube or cumulative discharge models. Past research, as presented in Chapter 2, suggests that an understanding of the variation of mixing coefficients may be obtained from an understanding of the variation of bed shear velocity over a given channel. It is, therefore, desirable to attempt to predict the variation in bed shear velocity.

Predicting the vertical variation and distribution of primary velocities would be useful, however, all simple theory, as presented in Section 2.10 are based on log-law distribution, or Cole's law of the wake and make no account of acceleration, deceleration or the influence of secondary flows. To attempt vertical distribution predictions it would be necessary to construct a fully three dimension model, this is outside the scope of this thesis.

5.2.4.1 Cross sectional average properties

It is useful to characterise the longitudinal variation in two velocity-based features, cross section average velocity and bed shear velocity, and to predict these values.

Figure 5.6 shows the variation in measured and predicted cross sectional average primary velocity. Predictions were made using the depth and width average form of the continuity equation, Equation 2.2. The agreement between measured and predicted values is good. Comparison of Figure 5.6 and Figure 5.1 shows the inverse relation between velocity and area.

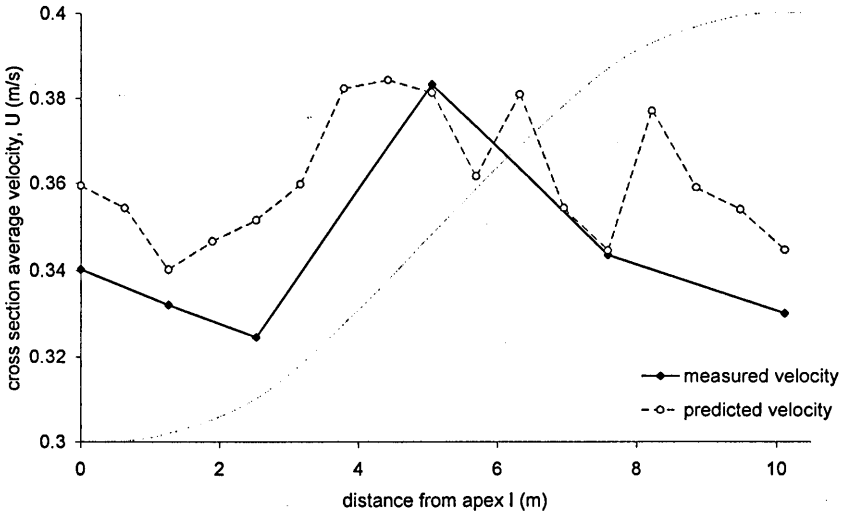

Figure 5.6 Longitudinal variation in and prediction of cross section average velocities

Predictions of bed shear velocity have been made using Equation 2.3. This was derived assuming bed shear stress is a product of the flow resistance generated at the boundary interface, and plain turbulent two dimensional flow. However, in natural channels flow resistance is influenced by channel irregularities and curvature. Figure 5.7 shows that the bed shear stress is reasonably accurately predicted in the straight region of the channel, however, when there is strong curvature the prediction over estimates the calculated bed shear stress. This suggests that the curvature is having a strong influence on the flow resistance.

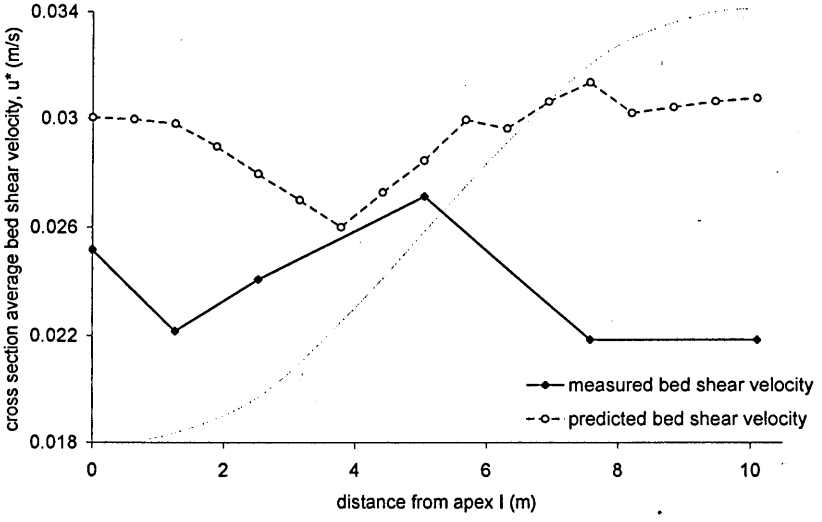

Figure 5.7 Longitudinal variation in, and prediction of cross section average bed shear velocities

5.2.4.2 Depth average velocity

In section 2.10.2 three equations were suggested from literature to predict depth average velocities in plain turbulent open channel flows, Suim (1975) Equation 2.128, Rutherford (1994) Equation 2.129 and Smith (1983) Equation 2.130. All these equations relate transverse variation in depth average velocity to local flow depth. They have been applied to each of the cross sections where velocity data have been

collected and the results compared. Figure 5.8 shows an example of the variation in measured and predicted depth average velocities over apex I cross section.

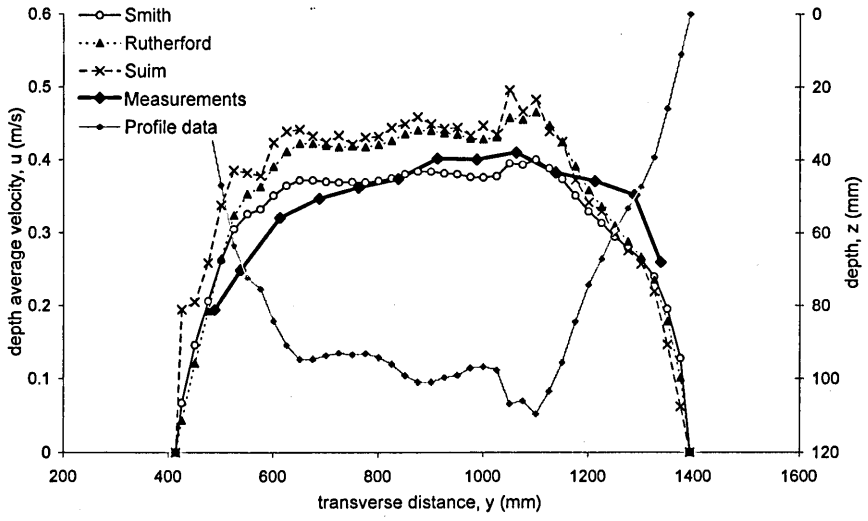

Figure 5.8 Example comparison of predicted and measured depth averaged velocities at section I

Table 5.2 quantifies the errors in predictions over all six measured cross sections. All three equations require the same input survey and discharge data. The continuity equation has been used to obtain cross sectional average values.

	Smith (1983)		Rutherford (1994)		Suim (1975)	
Section	% error Q	U ave |% error| max % error	% error Q	U ave |% error| max % error	% error Q	U ave |% error| max % error
I	-0.13	12.1 30	10.8	12.3 23	13.1	19.1 36
I4	-0.17	15.5 33	9.2	17.4 33	11.4	22.0 42
J	-0.19	13.7 39	9.5	14.9 43	11.5	16.3 43
K	-0.15	14.7 25	10.4	12.6 35	12.6	16.4 28
L	-0.16	11.7 29	13.2	12.4 22	15.5	19.9 38
M	-0.16	13.7 22	11.1	12.6 23	13.4	9.0 20

Table 5.2 Comparison of percentage errors from measured and predicted depth average velocities, and discharges

From Figure 5.8 and Table 5.2, it can be seen that none of the equations recreate the transverse variation in the primary velocity perfectly. However, this is unsurprising given the simple nature of the equations used for the predictions, and the complexity of the factors governing the actual distributions. All three of the equations show good accuracy in the areas of greatest velocity shear at the channel edges.

The formula suggested by Suim (1975) gives the greatest average modulus and maximum errors in the magnitude of predicted velocity. The average modulus and the maximum percentage errors predicted by Rutherford's and Smith's equations give very similar errors in the magnitudes of the predicted velocities, Smith's equation being slightly better. The equation of Smith (1983) shows no closure errors for the input discharge values.

For the purposes of prediction of stream tubes and cumulative discharge models, it is the variation in cumulative discharge which is important to predict, rather than the absolute magnitude of the velocities. From Figure 5.9, it can clearly be seen that the variation in cumulative discharge is best predicted by the Smith (1983) equation. This is because of the accurate closure to the input discharge achieved by the equation, which is not present with the other two. This can also be seen on Table 5.2.

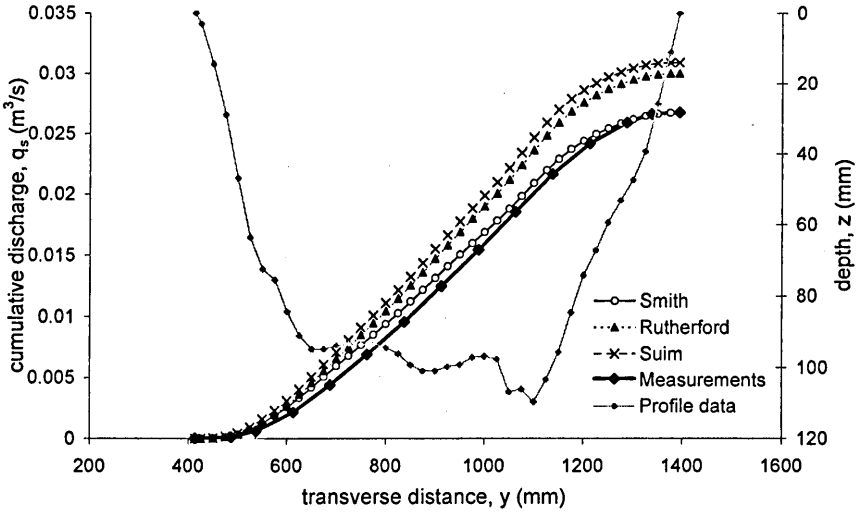

Figure 5.9 Example comparison of predicted and measured cumulative discharge at section I

The maximum spatial error in cumulative discharge predicted by the equation of Smith (1983) occurs at section I4 and is of the order of 50mm, or 5 percent of the average channel width. This is very good considering that this prediction is based simply on variation of flow depth across the channel, and only profile data and discharge are required for the prediction. No account is taken of curvature or its effects.

Smith (1983) also presents an equation to predict the transverse variation in bed shear velocity, which it is possible to investigate. Figure 5.10 shows the results of using Equation 2.131 to predict bed shear velocity distributions at section I.

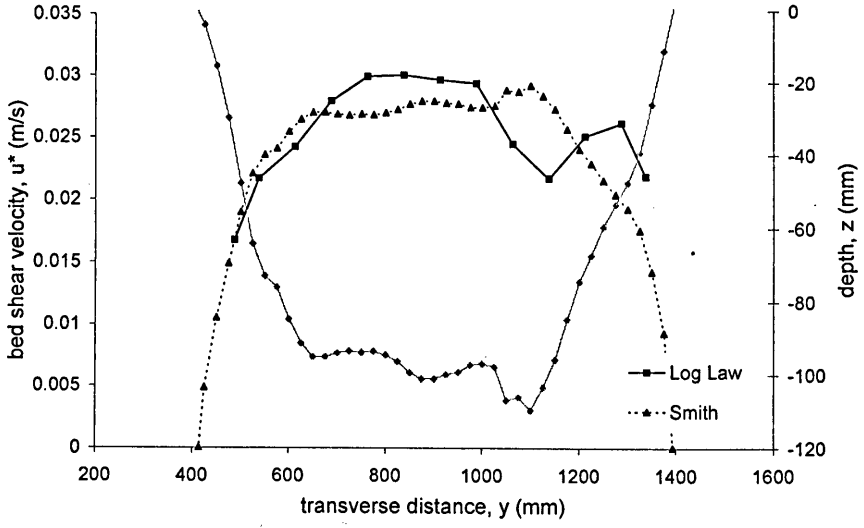

Figure 5.10 Comparison of predicted and calculated depth averaged bed shear velocities at section I

The predicted bed shear velocities in Figure 5.10, show reasonable agreement to the values of bed shear velocity calculated assuming a log law distribution near the channel bed. However, Equation 2.131 requires that the cross sectional average value of bed shear be known for the prediction. The equation is unable to predict the local variations brought about by the bed features. The prediction of cross sectional average bed shear velocity by equation 2.3 has been shown limited in Figure 5.7.

5.2.4.3 Secondary flow prediction

In Section 2.10.4.2 equations for the prediction of fully developed transverse velocities caused by plan form curvature were presented. Equations to predict the build up of these velocities from the start of a bend, and their decay after the end of the bend were also presented.

The application of the predictive equations to natural channel situations requires the approximation of natural channel plan-forms to idealised straight and uniformly curved sections. Figure 5.11 shows the quality of fit which has been obtained when approximating the 'natural' channel form generated within the facility sinusoidal plan form, to straight and curved sections. The largest errors appear to be in the regions of change from curve to straight, where the actual curvature is under predicted.

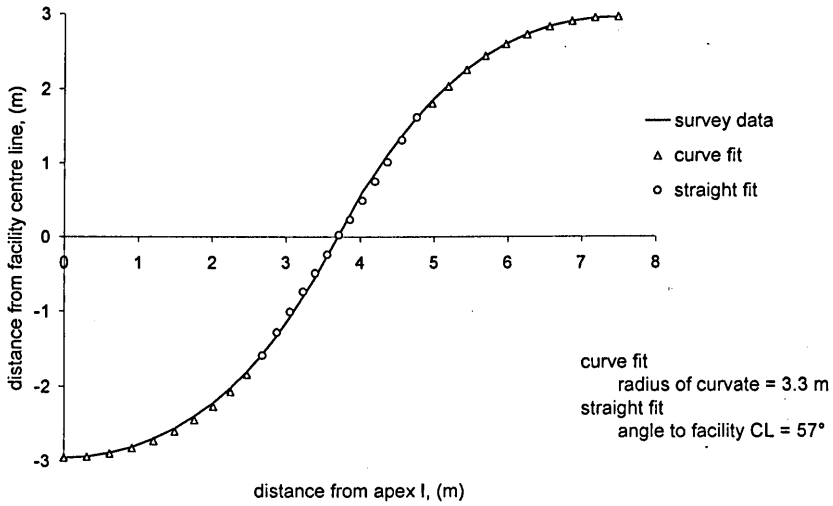

Figure 5.11 Curve fitting to survey data, channel centre line

From this information, and using the F1 and F2 functions found from Equations 2.139, evaluated and presented in Figure 2.33, it is possible to make a prediction of fully developed transverse velocities using Equation 2.138.

Figure 5.12 shows the predicted fully developed transverse velocities from the given values. Chezy C was found from equation 2.5, the average hydraulic radius and a Manning's n value of 0.02. This value of Manning's n was obtained from tables in Chadwick and Morfett (1994).

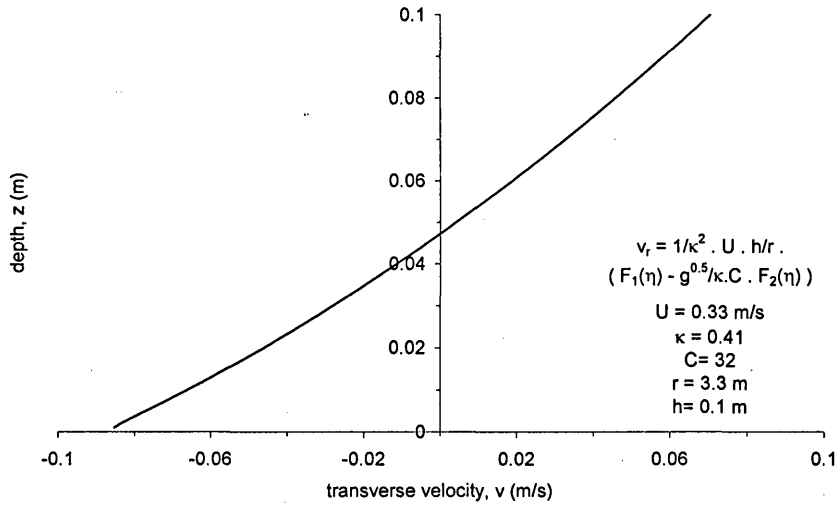

Figure 5.12 Predicted fully developed transverse velocities

It is possible to make predictions of the build up and decay of secondary velocities from this predicted fully developed transverse velocity. The transverse velocities are assumed to be zero at the entrance to the bend and grow exponentially, Equation 2.140. The velocities are then assumed to be fully developed at the end of the bend and to decay as distance increases down the straight, as described by Equation 2.140.

Figure 5.13 shows the predicted transverse velocities near the bed and surface and at mid depth, an indication of the channel curvature is shown. It can be seen that the assumption of fully developed secondary flow at the end of the bend, and complete decay at the end of the straight, are valid, given that the rates of growth and decay are approaching asymptotic values.

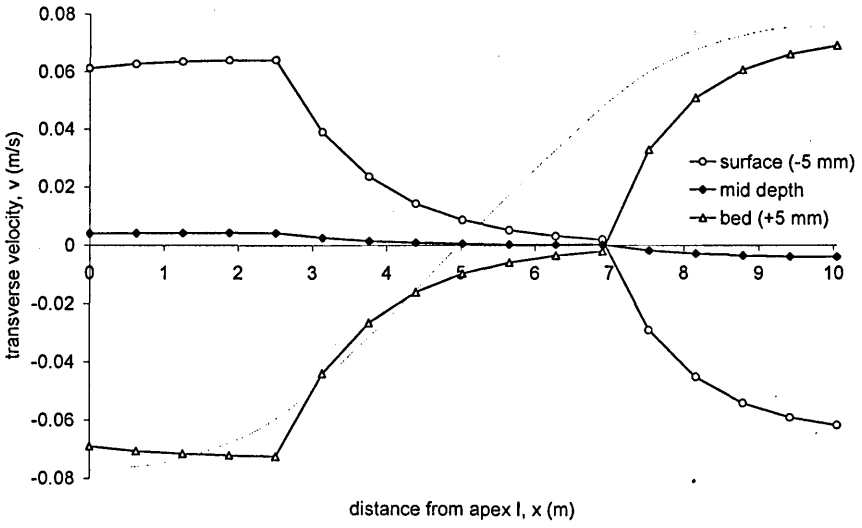

Figure 5.13 Predicted growth and decay of transverse velocities

Although Rozovskii (1957) validated these predictive equations with data collected in natural channels, they were developed assuming idealised conditions. Rozovskii (1957) stated that the equations should be valid at the channel centre line, extending to a maximum region up to one flow depth from the bank. For this reason, comparison of the predicted and measured transverse velocities has been performed around the channel centre line, Figure 5.14. In the near bank regions transverse velocities will be less. No method of predicting this decrease, or the magnitude of vertical components is suggested.

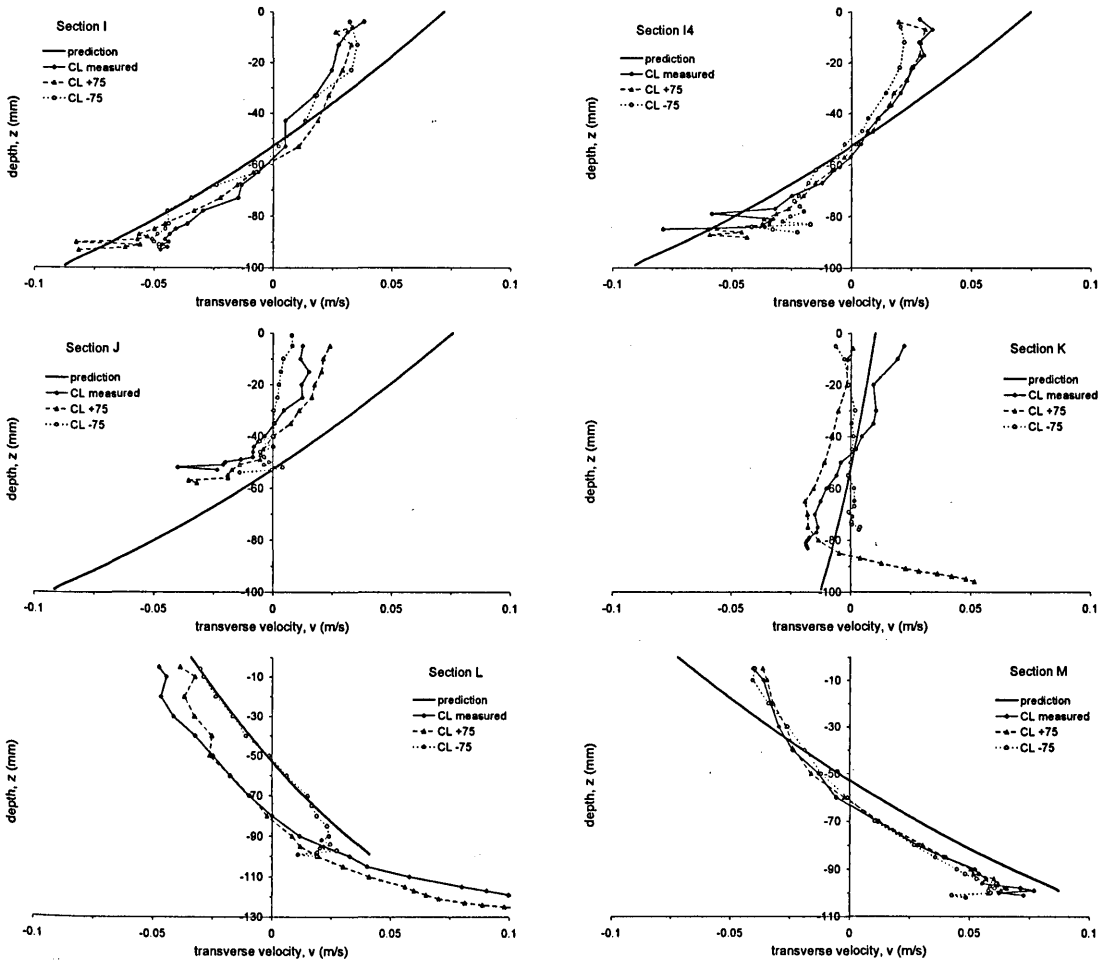

Figure 5.14 Comparison of measured and predicted transverse velocities

The agreement between predicted and measured velocities in Figure 5.14 is good. The fact that the predictions are always made over the average flow depth of 100mm is apparent. However, comparison of the gradients of the slopes at each cross section shows agreement. This suggests that the magnitude of the variation in velocity over depth, with respect to curvature is accurately predicted. The major errors which occur are at the regions of the interface between straight and curved sections (sections J and L), and coincides with the errors in approximated geometry. Figure 5.2 shows small multiple secondary circulations cells which these predictions are unable to recreate.

5.2.5 Channel average properties

Table 5.3 gives channel average properties which have been used in the preceding predictions, together with some average values resulting from these predictions. These values will be used in all further calculations.

Property	Measured	Predicted
bed slope, S_0	0.125×10^{-3}	-
cross sectional area, A	74704 (mm^2)	-
average depth, h	73.5 (mm)	-
average channel width, b	~ 1000 (mm)	-
approximated radius of curvature, r_c	3300 (mm)	-
hydraulic radius, R	69.9 (mm)	-
primary velocity, U	0.342 (m/s)	0.362 (m/s)
bed shear velocity, u*	0.024 (m/s)	0.029 (m/s)
average fully developed transverse velocity magnitude, v (at channel CL)	0.038 (m/s)	0.040 (m/s)
reach average transverse velocity magnitude, v (at channel CL)	0.024 (m/s)	0.026 (m/s)

Table 5.3 Channel average properties

5.3 *Turbulence Data*

The use of an LDA measurement system provides the opportunity to investigate the turbulence levels of the measured flow regime. As stated in Chapter 2, the turbulence level is very important in defining the eddy viscosity and diffusivity, as these have a significant effect on mixing rates. A number of factors and considerations need to be investigated when considering turbulence data.

5.3.1 Measurement system

The system used is an LDA system offering the potential for very high data rates with very small measuring volume, and a small probe head. These factors combine to provide accurate point evaluation of time average stable velocity components. The system also offers the potential to investigate the turbulence levels within the flow. For these mixing studies, turbulence data and the variation in turbulence levels over the channel could lead to an improved understanding and quantification of mixing coefficients.

5.3.1.1 Data logging rate

Consider a turbulence bursting event, as represented by Figure 5.15, where a representative, eddy length scale for the near bed events may be taken as one tenth of the flow depth. Considering this turbulence event as it travels past a measuring point at the mean primary velocity, u, and ten measurements to provide a complete description of the turbulence event, Figure 5.16, it is possible to calculate the required data rate.

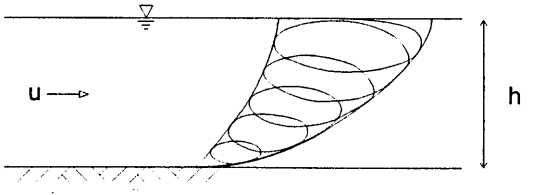

Figure 5.15 Turbulence bursting event

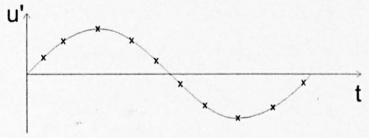

Figure 5.16 Measurement distribution over eddy

h = 0.1 m

u = 0.3 m/s

eddy scale = h/10

$$(\Delta t)_{min} = \frac{1}{10}\left(\frac{h/10}{u}\right)$$

$$= 0.003 \text{ s}$$

frequency $\approx$ 300 Hz

From this simplified calculation, it can be seen that to define individual turbulent events, a validated and cleaned data rate of 300 Hz or higher is required. It could be suggested that provided the logging period is great enough, a slower data rate would provide enough information to describe turbulence events through measurement of successive events. However, this approach could lead to serious errors if the data rate at which measurements were made matched the frequency of turbulence events.

The average validated data-rate obtained with the LDA measurements was around 50Hz. In Section 3.5.9 three time series of data were investigated in detail with respect to noise removal. Using these time series it is possible to investigate the overall data rates which were obtained during the measurements. The investigation was conducted by calculating the time interval between consecutive readings (drop out period), and plotting histograms of the results. Figure 5.17 shows the resulting histograms for one of the time series. All the time series analysed yielded very similar distributions.

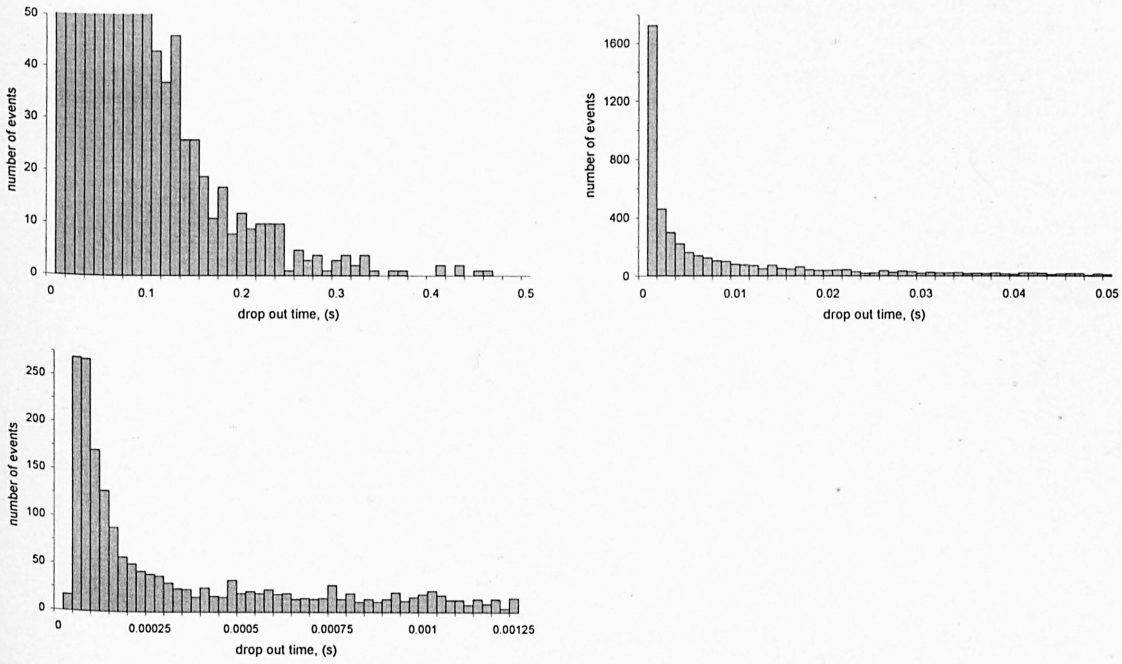

Figure 5.17 Drop out time histogram for CL section I mid depth, downward facing configuration

This analysis highlights the strongly skewed nature of the drop out periods. Although the mean data rate is 50Hz (0.02s drop out), the majority of the data was collected at far higher data rates. The peak in the distributions is around 20,000 Hz. 55% of the data were collected at a data rate greater than the 300Hz

calculated above. However, the average data rate is only 50 Hz due to occasional long drop out periods of up to 0.5 seconds. The results show that information has been collected at a sufficient data rate for valid turbulence data to have been collected, suggesting the data could be used to define eddy diffusivity. However, the causes and effects of the drop out periods are unknown and could bias the resulting turbulence calculations.

5.3.1.2 Seeding

With the LDA system used, it was necessary to introduce seeding particles upstream of the measuring point. It is possible that the data 'drop outs' result from a lack of seeding of certain eddy events.

If the turbulence events were assumed to be regular or repeating features of the flow regime then a regular frequency of occurrence of drop out periods, concurrent with the frequency of un-seeded eddy events could be expected. This was not apparent during data collection, or subsequent analysis. Visual inspection of Figure 3.14 to Figure 3.21 also confirm this.

5.3.1.3 Resolution

The digital interface used for the LDA measurements utilises an 8 bit register. The equipment was manufactured for the measurement of unidirectional flows, therefore the ranges available are set non-equally around zero. It is possible to work out the sensitivity of the system.

Range =	-0.3 to 1.1	= 1.4 m/s
Register (8 bit) =	256 bins	
bin size =	1.4 / 256	= 0.006m/s

This means that the maximum resolution of the measuring system was 6mm/s. The ranges for each component of velocity were the same, ensuring uniform resolution. This resolution should be sufficient to provide turbulence information.

5.3.1.4 Noise removal

Section 3.5.9 gave details of how and why 'cleaning' of the raw time series velocity data was necessary. This process although necessary to ensure that reliable means of the velocities were obtained, could raise questions about the nature of the resulting turbulence information. Visual inspection of the figures in Section 3.5.9 clearly illustrates that noise was present in the data. However, as discussed, defining the boundary between data and noise was not a simple process. The shape of the histograms presented in Section 3.5.9 suggests that the noise was removed "to a sensible degree". The raw data shows extensive scatter over the complete range. After the 0.4 m/s secondary component cut off and the first pass, the histograms exhibit gently curved start and finish to the distributions. Further passes produce erroneously abrupt curtailment of the distributions. The results obtained after the cut off and one pass seem concurrent with past measurements in two-dimensional flows, such as Grass (1971). Given the normally distributed nature of the histograms in Section 3.5.9 a change in the mean and variance of the distributions would be expected as erroneous data is removed. The data tables in section 3.5.9 show dramatic change in the calculated means and standard deviation of the data sets with the 0.4 cut off and the first pass, suggesting that noise was being removed. The information about further passes show very little change in the mean

and standard deviation values, suggesting little improvement in the removal of noise, and therefore suggesting the removal of valid data.

5.3.1.5 Interpolation

In Section 3.5.9, the possibility of signal cleaning by high and low band frequency pass was briefly discussed. However, this technique was discounted due to the random frequency of data collection associated with the signal interpretation system used. Included in the software provided by the manufacturer of the LDA system is the capacity to carry out spectral analysis. This may be desirable so that the frequency of turbulence events could be investigated. The system uses a complex algorithm to interpolate the data into a regular time-period data set. However, given the duration of the data drop out periods that have been observed, little confidence is held in this system, either for use as a means of cleaning the data or interpolating for improved average data rates.

Given these considerations about the quality and nature of the turbulence data, insufficient assurance can be given to the data to present definitive point by point variation of the turbulence levels. However, the turbulence data are a very valuable set of information and overall trends can still be established from the measurements. The turbulence data cannot be used for calculation of bed shear stress from Reynolds stresses, or for establishing eddy viscosity.

The data set is unique and may prove to be very important in the future, for example with the calibration or validation of computational fluid dynamic models of open channel flow.

5.3.2 Data presentation

5.3.2.1 Reynolds stress

In section 2.3 some of the ideas of turbulence and Reynolds decomposition were introduced, together with the derivation of expressions of Reynolds stress. Reynolds stress is often used to characterise turbulence levels in open channel flow, and to give an indication of momentum exchange and mixing rates.

The derivation of Equation 2.36 from Equation 2.32 was made on the assumption that the time average of vertical velocity components at any given point is zero. In three-dimensional flow this is not a valid assumption. Estimates of shear stress should, therefore, be made including the stable time average velocity components from Equation 2.35 or before the velocity is decomposed, time average of Equation 2.32. However, the resulting expressions of Reynolds stress would include the effects of the time average components.

Reynolds decomposition was used to simplify the solution of the advection dispersion equation and is important in attempting to predict mixing coefficients. Any classification of the turbulence levels within the channel should be based on these decompositions. The use of Reynolds stress expressions does not facilitate this. It may be necessary to look at the magnitude of the fluctuating components about the mean stable component in each co-ordinate direction individually, to provide a method of comparing the level of turbulence at given points within the channel.

Reynolds stress is an important expression if there is cross correlation between the fluctuating turbulent components of the velocities. The presence of cross correlation would have significant impact on the momentum exchange rates and the mixing rate. Such correlation would result in asymmetry of the distribution of the cross products about the mean value. The nature of the turbulence, cross correlation or randomness can be established by producing co-variance plots of the turbulent fluctuating components. Histograms of the distribution of instantaneous cross products and / or fluctuating component cross products can also be used to give an indication of the nature of any correlation. Log normal distributions, skewed towards higher magnitudes, indicate cross correlation between large magnitude turbulent events and strong momentum exchange. Normal distributions indicate a random nature to the turbulence, and no cross correlation in turbulence events.

Checks for cross-correlation have been performed with the time series data that was investigated for the noise removal exercise in Section 3.5.9.

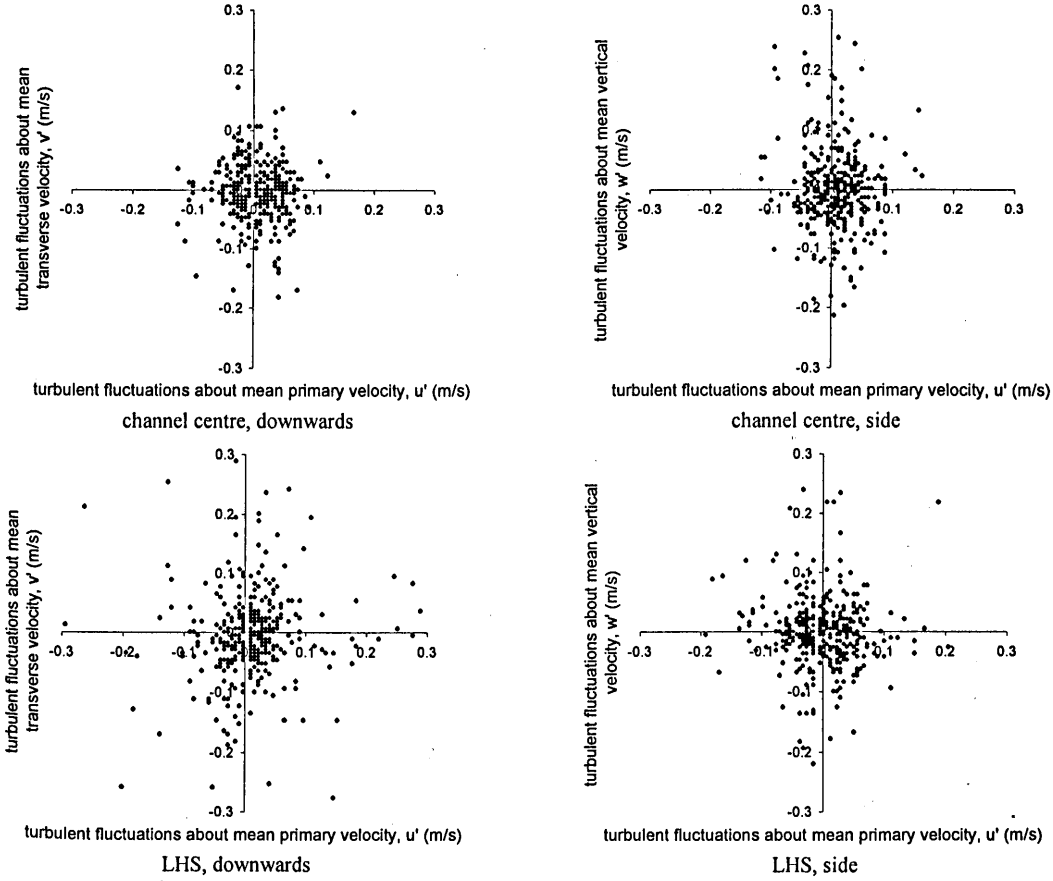

Figure 5.18 Cross correlation of turbulence events (same data as used in Section 3.9.5)

The cross correlation plots in Figure 5.18 show that there is no correlation between primary / vertical or primary / transverse for the eddy events which were measured. However, only the prime or fluctuating components have been investigated through this test. The derivation of Reynolds stress, as expressed by the cross product of the prime components alone, was shown valid only for two-dimensional flow conditions. Therefore, the potential nature of the cross correlation has been investigated by the histogram method suggested previously. This has been performed for both the instantaneous measurements and the fluctuating prime components, Figure 5.19.

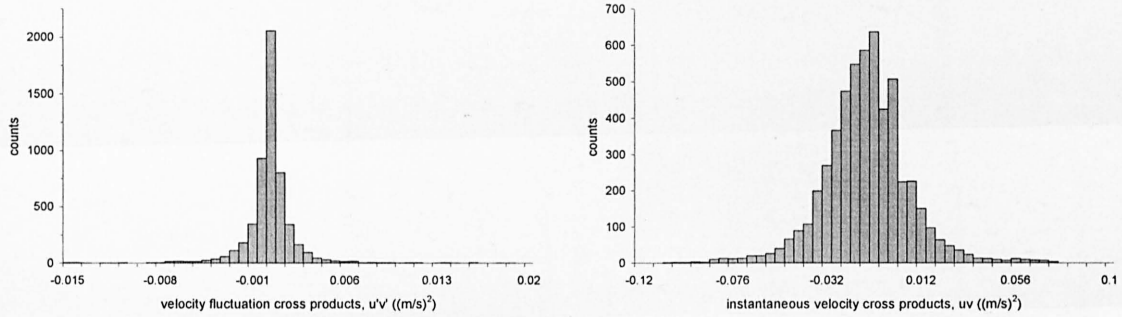

channel centre, down

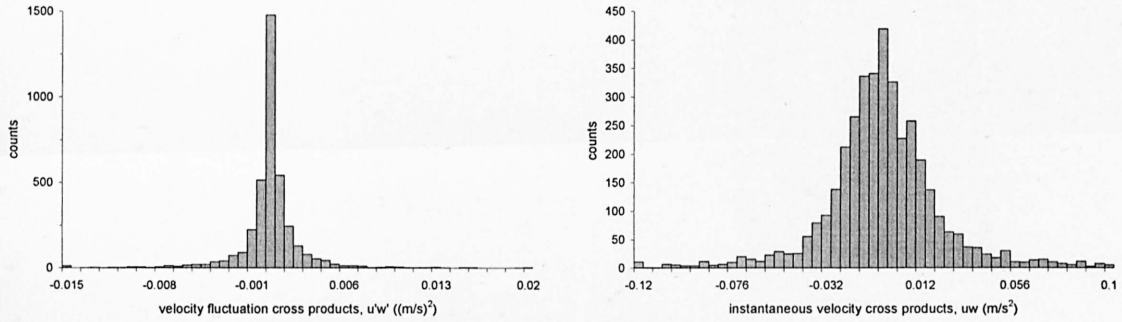

channel centre, side

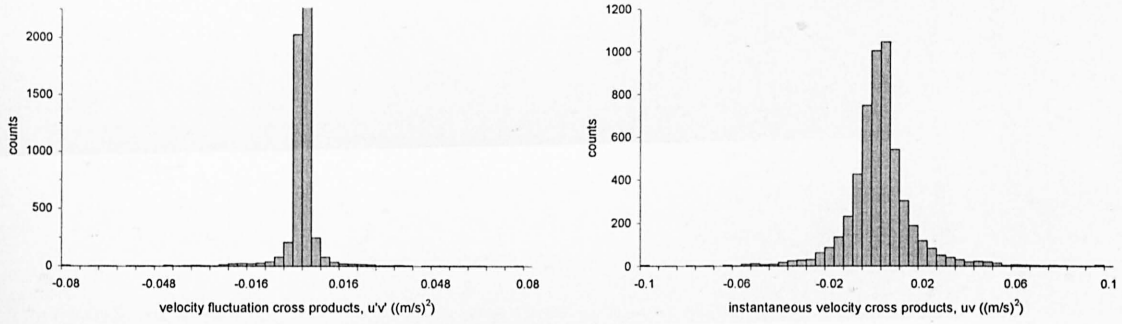

LHS, down

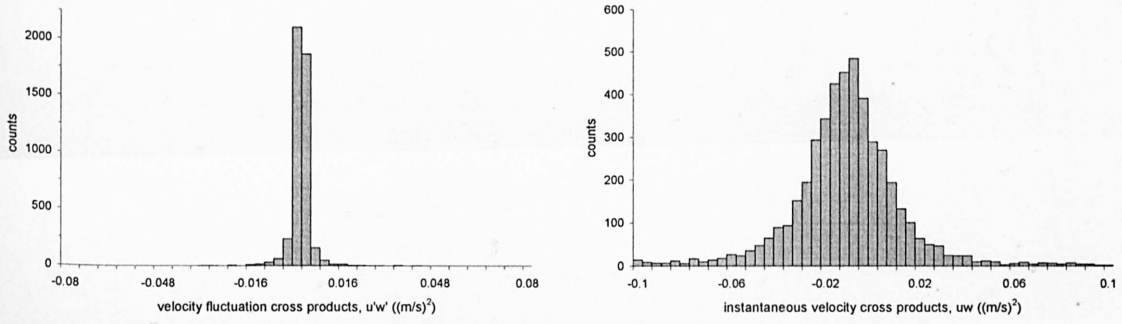

LHS, side

Figure 5.19 Investigation into nature of cross correlation of turbulence data
(same data as used in Section 3.9.5)

The normal distributions of the cross products of both the instantaneous measurements and the fluctuating components shown in Figure 5.19, suggests that there is little or no cross correlation in the turbulence events. This lack of cross correlation suggests that there is little advantage in calculation and expression of Reynolds stresses over the more simple expression of the Root Mean Square (RMS) value of the fluctuating element of each velocity component individually. The RMS value of the velocity fluctuations about the mean, the standard deviation of the time series, provides a good indication of the turbulence level, sufficient to perform qualitative assessment of the variation in turbulence levels.

5.3.2.2 Cross sectional variation

Depth average values of the calculated RMS values will be presented to investigate transverse variation in the turbulence level, so that it could be linked to transverse variation in mixing rate, Figure 5.20.

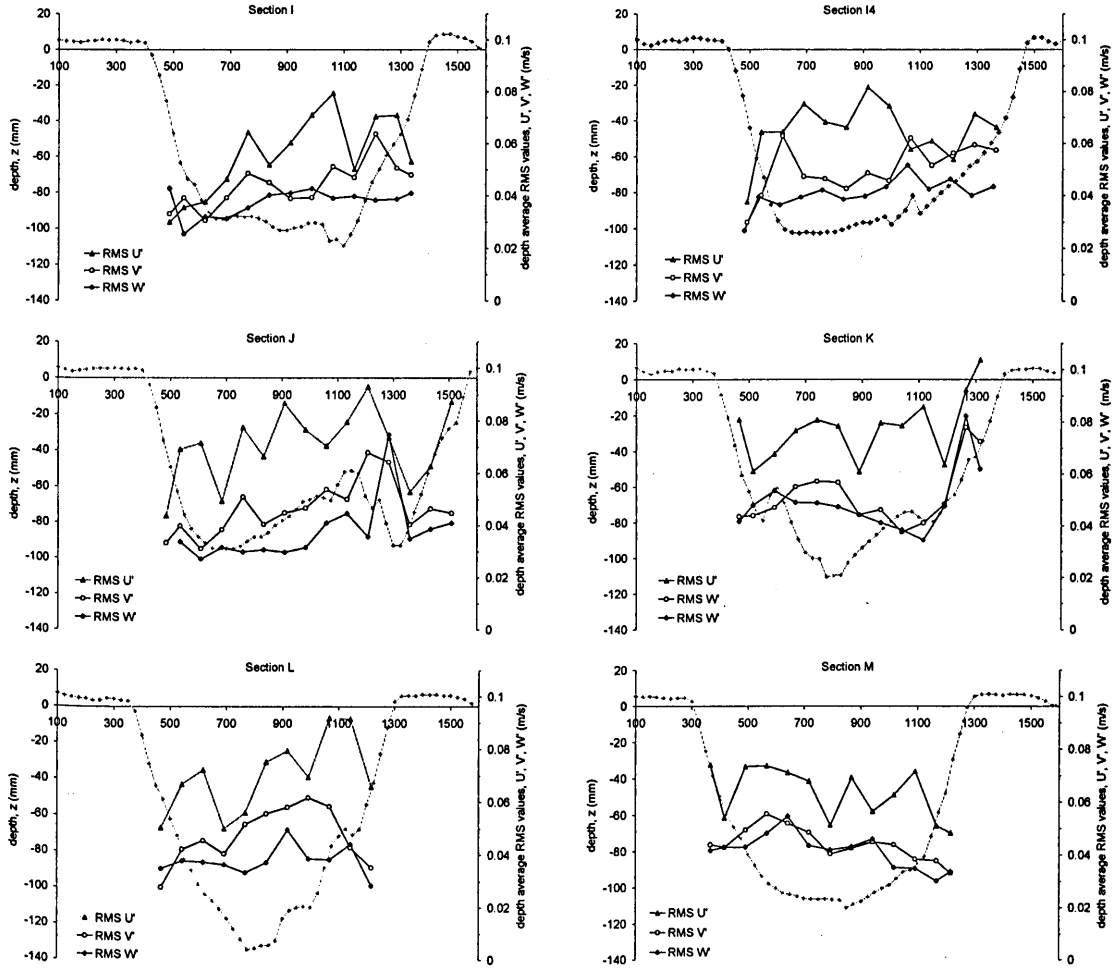

Figure 5.20 Transverse variation in depth average RMS velocity fluctuation about mean for each of the velocity components at each of the measured cross sections

The variability of the depth average values of RMS can be seen in Figure 5.20. Also highlighted is the lack of any strong trend in the variation over the channel width at any point in the meander half cycle. Figure 5.20 and Table 5.4 highlight the relative magnitude of the turbulence levels associated with each velocity components.

5.3.2.3 Longitudinal variation

Cross sectional average RMS values have also been calculated, to facilitate investigation of the variation of the turbulence levels in the longitudinal direction, Figure 5.21.

The RMS values of the transverse and vertical components show little longitudinal variation in magnitude, suggesting little change in the overall turbulence level. The magnitude of the cross sectional average of the RMS about the primary velocities shows a longitudinal variation. The RMS value reaches a peak at the straight section of the channel, and a minimum at the channel apex. This is the same trend exhibited by the cross sectional average primary velocity. Therefore, it may be surmised that the

magnitude of the fluctuations is directly related to the magnitude of the velocity. This has been suggested by many other investigators, for example Grass (1971). The longitudinal velocity RMS values normalised by the appropriate cross sectional average velocity yield a mean value of 0.2 with a standard deviation of only 0.018.

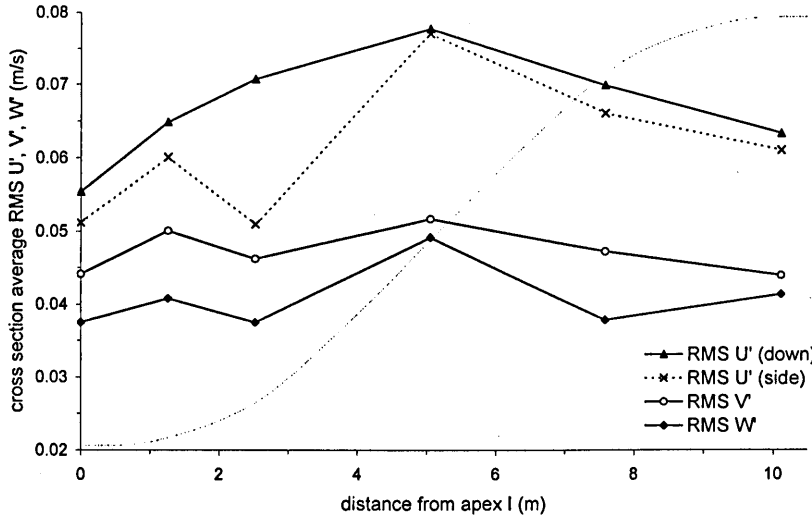

Figure 5.21 Longitudinal variation in cross sectional average RMS of velocity fluctuations about mean

U_{down} / U_{side} ratio =	1.096
V / U ratio =	0.705
W / U ratio =	0.607

Table 5.4 Comparison of reach average RMS values

Table 5.4 shows the relative magnitude of the fluctuations in the component directions, as well as a check on the data by comparison of RMS values for each of the sets of measurements of primary velocity.

5.4 *Transverse Dye Data*

The transverse dye dispersion tests were performed using a continuous injection system and a two minute sampling period at each point to negate temporal longitudinal mixing effects, leaving a study of the transverse and vertical mixing. The experiments were performed at four injection cross sections over the test half meander cycle, with up to four injection points within each cross section. These are detailed in Table 3.1.

In the following data the background concentrations associated with the recirculating system have been removed as detailed in section 3.4.5.3. The fluorometer calibrations have been applied and the distributions normalised by the relative injection concentration.

The aim of this section is to investigate transverse mixing, therefore the majority of the following work will deal only with depth average values of measured concentrations. It should be noted, however, that there was variation in the concentration over the vertical, particularly near the source. Vertical mixing was discussed in Chapter 2 and was shown to be predictable. The short length and time scales for vertical

mixing were discussed and, as explained, there is no need to model vertical mixing in the majority of river mixing situations.

Depth averaging of the concentration data has been performed on a depth-weighting basis, before any variance or change of moments calculations were performed. Other approaches to depth averaging were considered, such as calculating the variance of each depth profile and then averaging the variance. However, this would lead to significant problems in the application of the Generalised Method of Moments and stream tube ideas. The possibility of calculating the centroid of the distributions at each vertical height, aligning the centroids, and then depth averaging was also considered. This would have removed the transverse shearing effects, which is one of the processes to be quantified. Both suggested alternatives would give a biased result in the rate of transverse mixing and therefore not be applicable to standard two-dimensional predictive models, so were discounted. Depth weighted averaging is the method used in the vast majority of models and theoretical studies.

5.4.1 Data plots

Figure 5.22 to Figure 5.45 show the depth average dye concentration data collected from each of the injection points. Each figure shows a three-dimensional representation of the data over the channel. In these, the vertical scale has been exaggerated by a factor of 1.5 to highlight the bed forms. The mass flux in the centre line injection cases has been set to unity, for the side injection cases it has been set to one tenth. The contour shading has been set to highlight the relative concentration range of 0-0.1. The second plot for each injection case shows the dye data in a more technical format. The sampled cross sections are superimposed onto one graph. The x-axis represents cumulative discharge over each cross section, eliminating channel shape effects as discussed in Section 2.5, and the mass flux has been set to unity to aid visual inspection of the data. Note that the scale in the vertical is not constant between the plots.

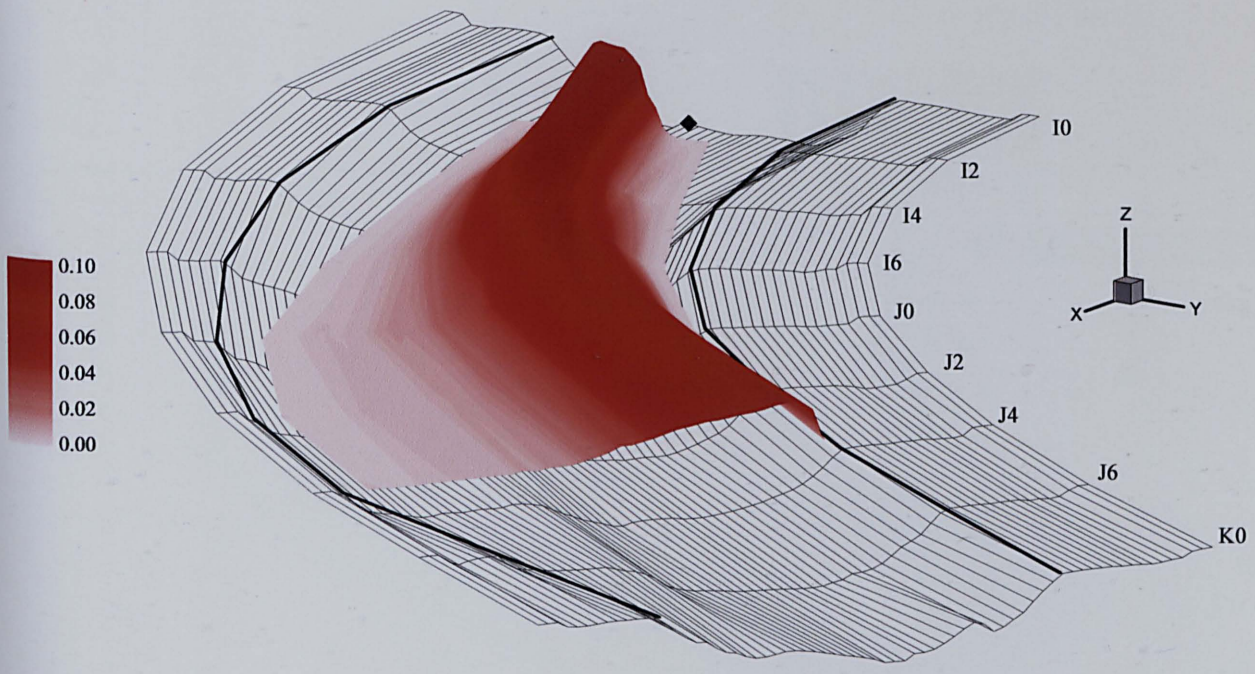

Figure 5.22 3D representation of transverse dye data below injection at I0 bed (looking upstream)

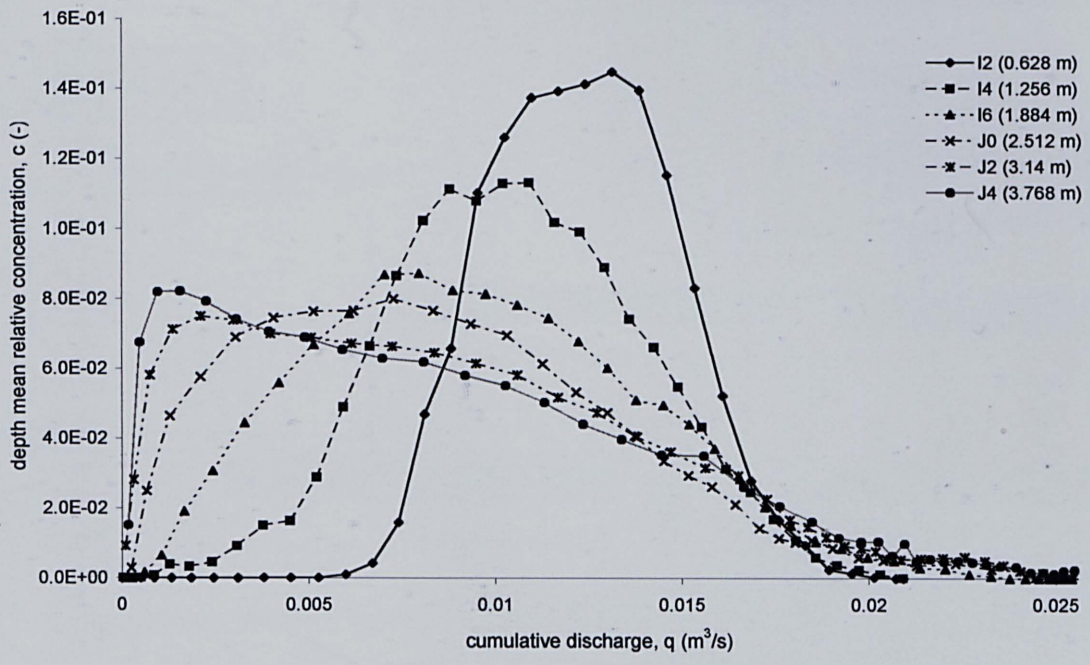

Figure 5.23 Transverse variation of depth mean concentrations, injection at I0 bed (looking downstream)

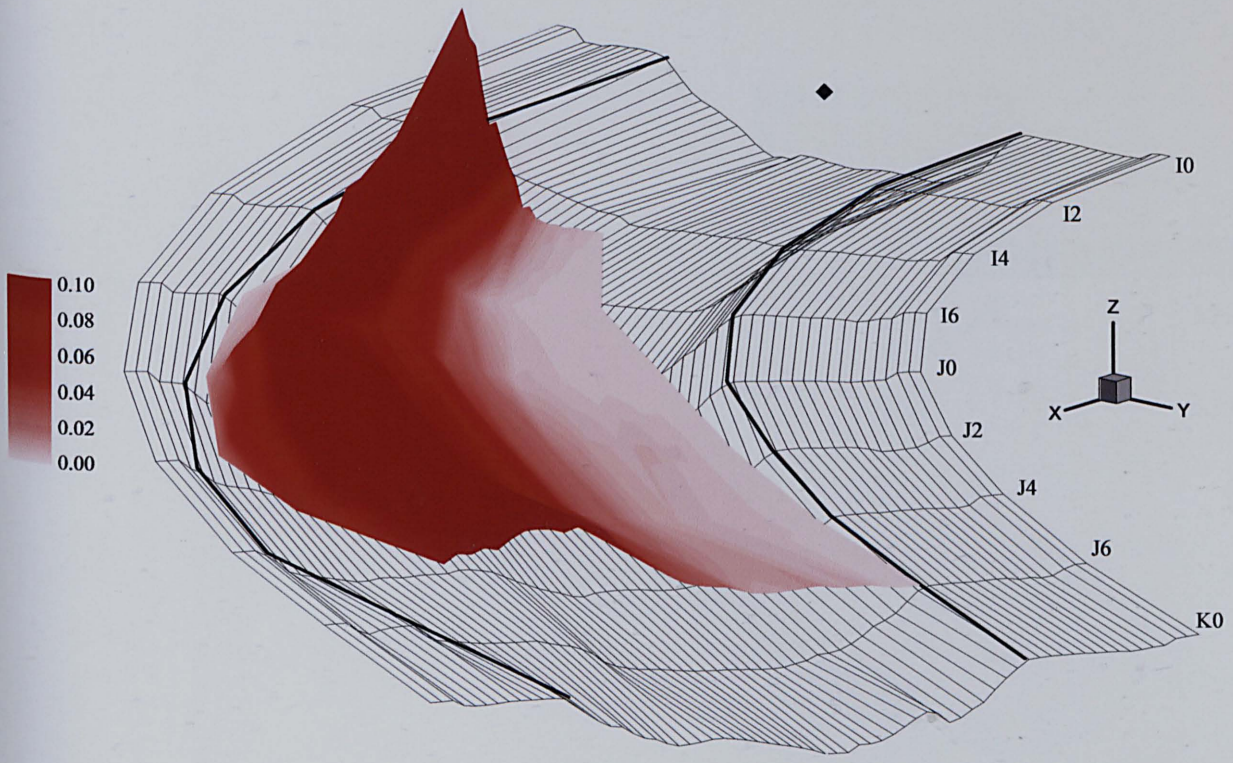

Figure 5.24 3D representation of transverse dye data below injection at I0 surface (looking upstream)

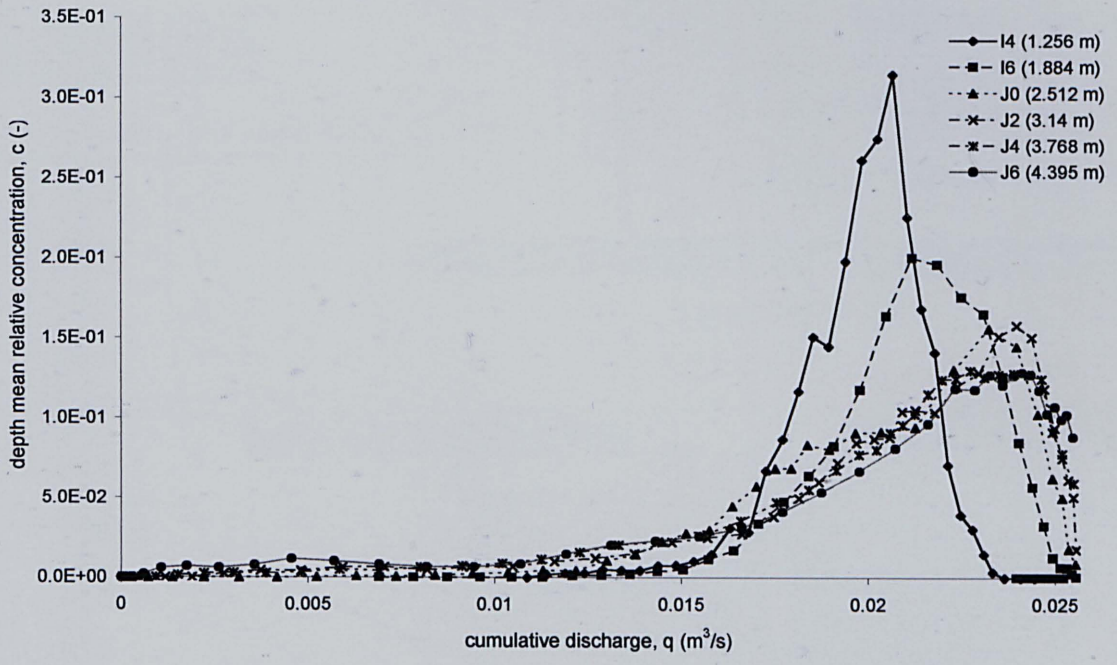

Figure 5.25 Transverse variation in depth mean concentrations, injection at I0 surface (looking downstream)

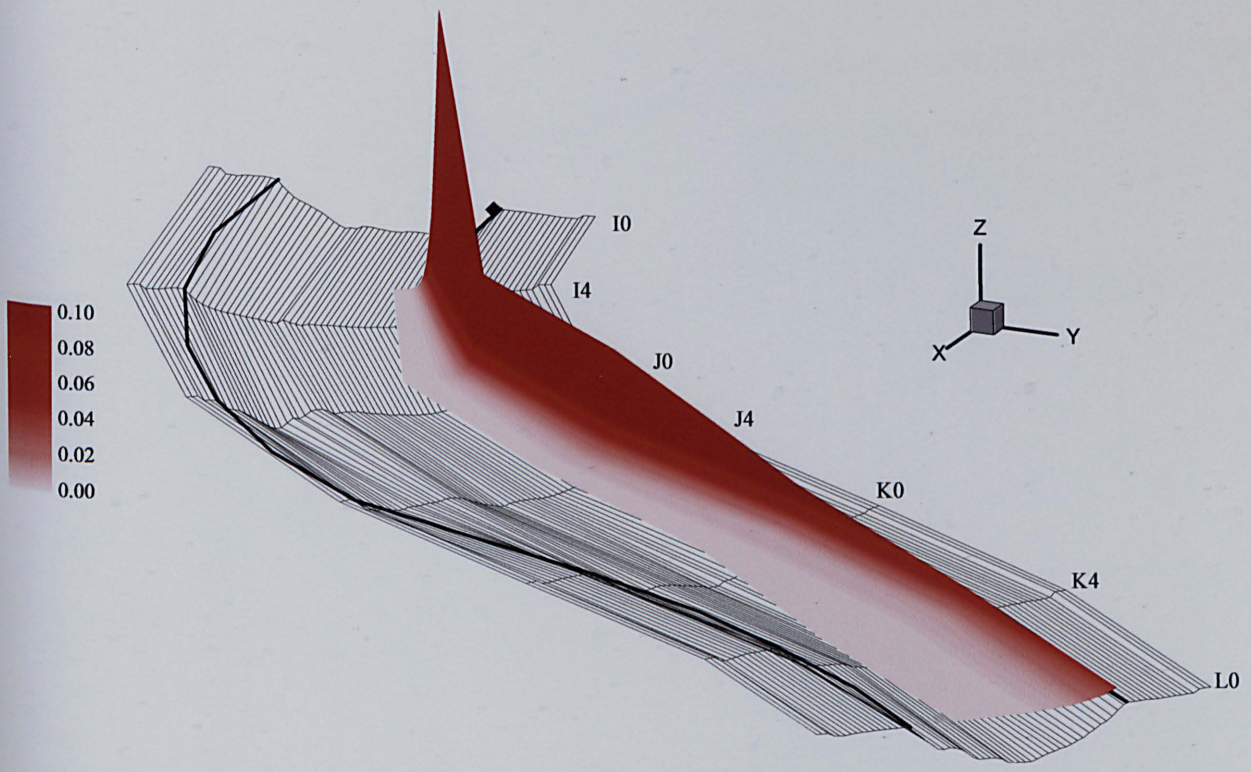

Figure 5.26 3D representation of transverse dye data below injection at I0 left (looking upstream)

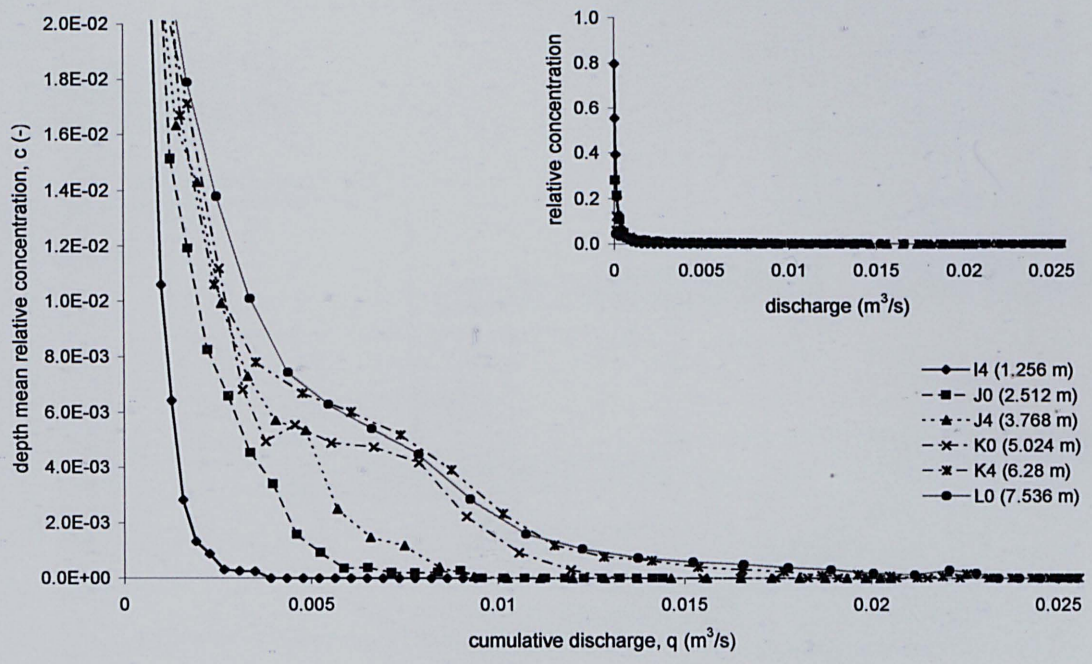

Figure 5.27 Transverse variation in depth mean concentrations, injection at I0 left (looking downstream)

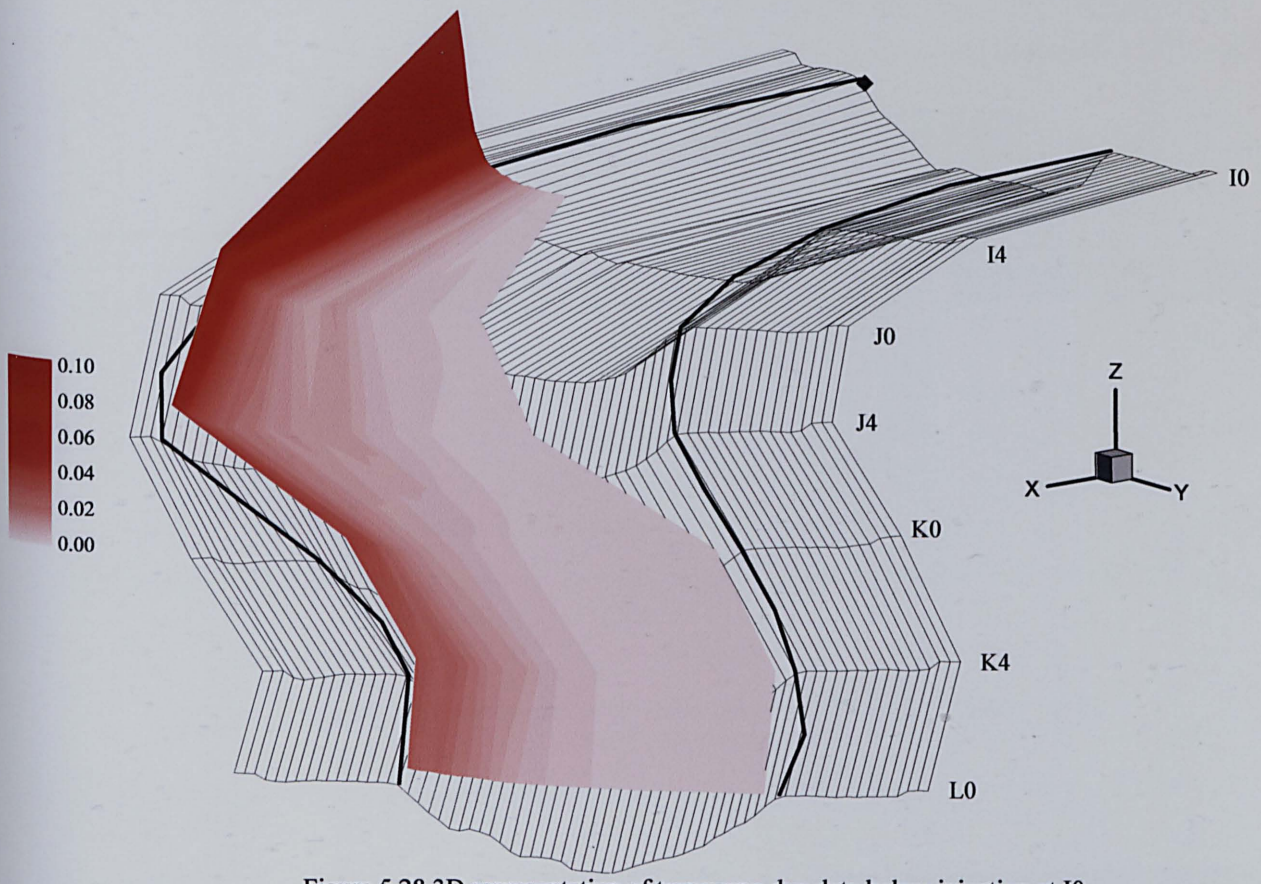

Figure 5.28 3D representation of transverse dye data below injection at I0 right (looking upstream)

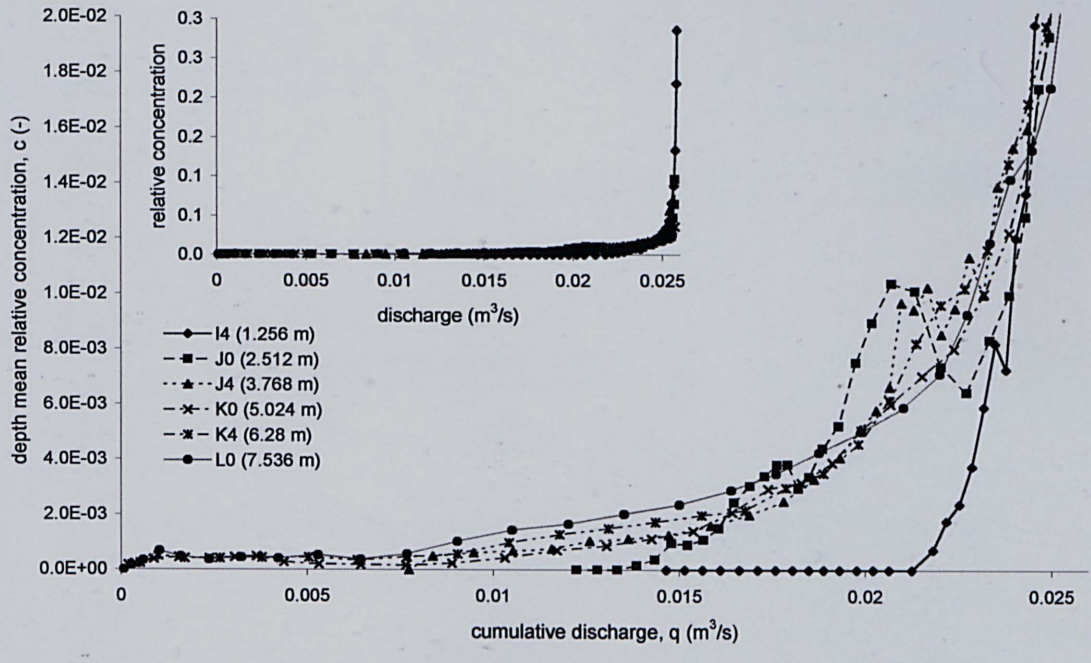

Figure 5.29 Transverse variation in depth mean concentrations, injection at I0 right (looking downstream)

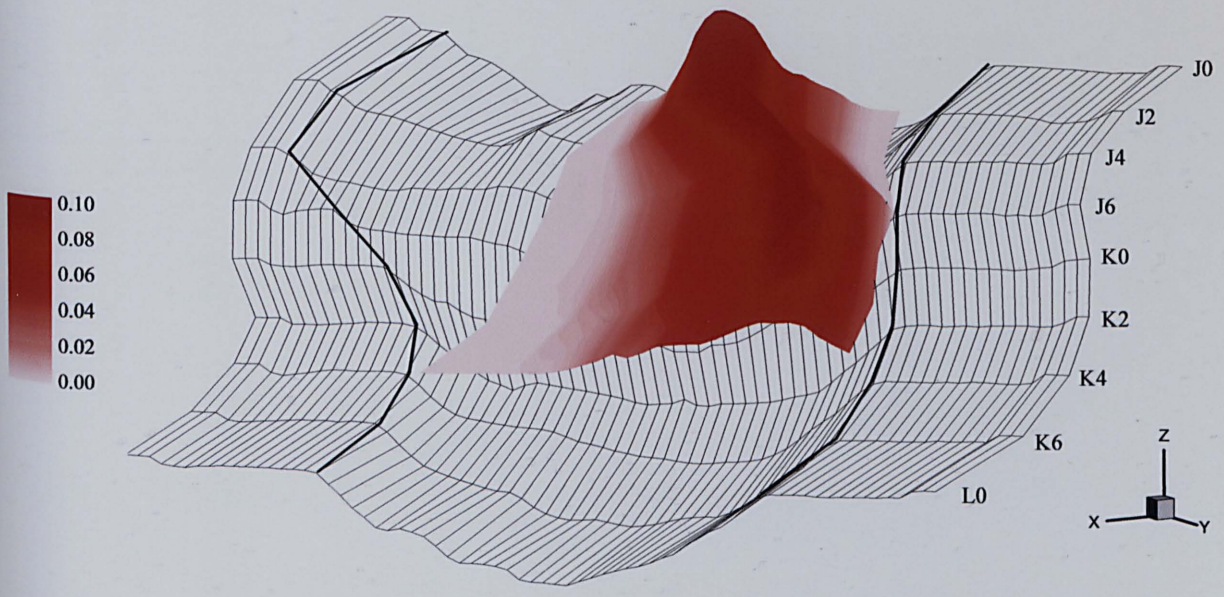

Figure 5.30 3D representation of transverse dye data below injection at J0 bed (looking upstream)

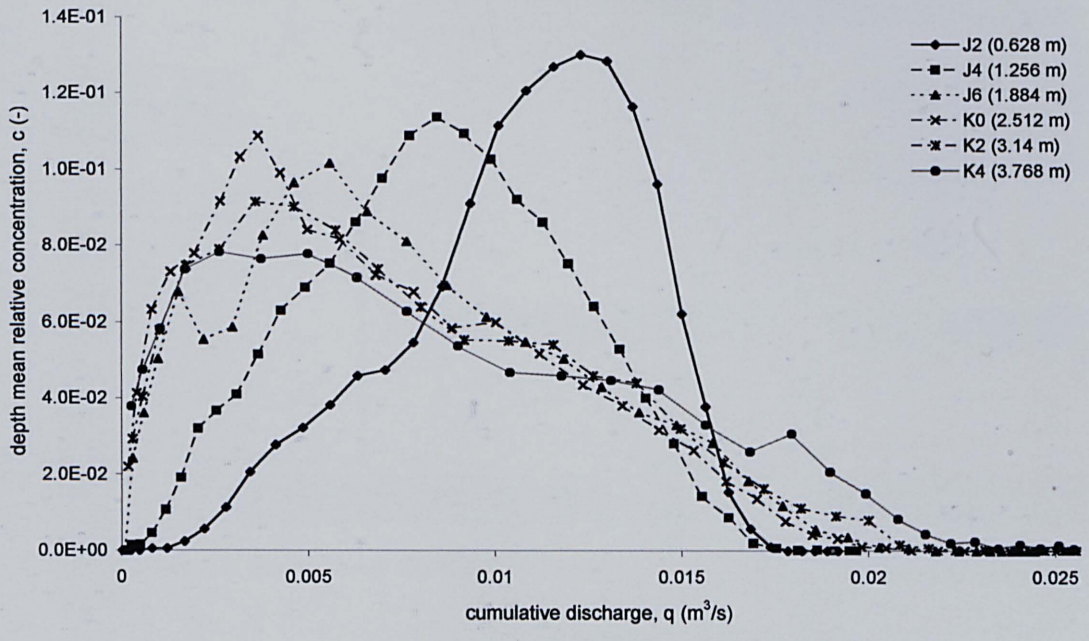

Figure 5.31 Transverse variation in depth mean concentrations, injection at J0 bed (looking downstream)

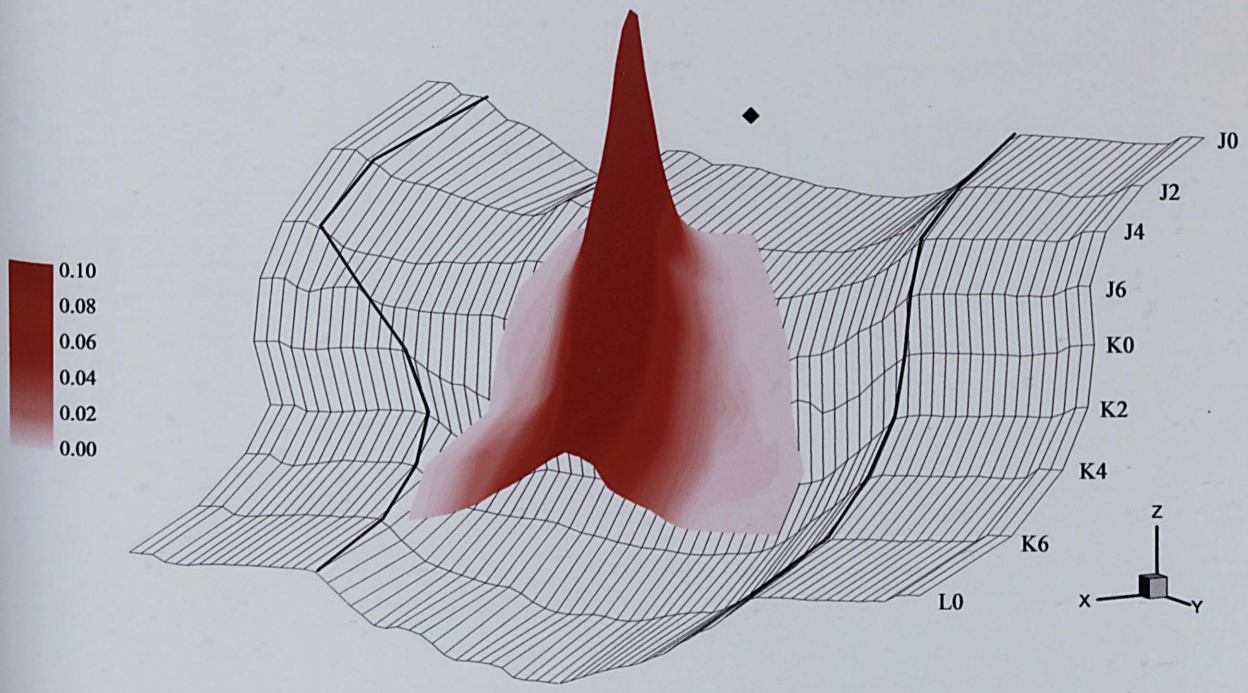

Figure 5.32 3D representation of transverse dye data below injection at J0 surface (looking upstream)

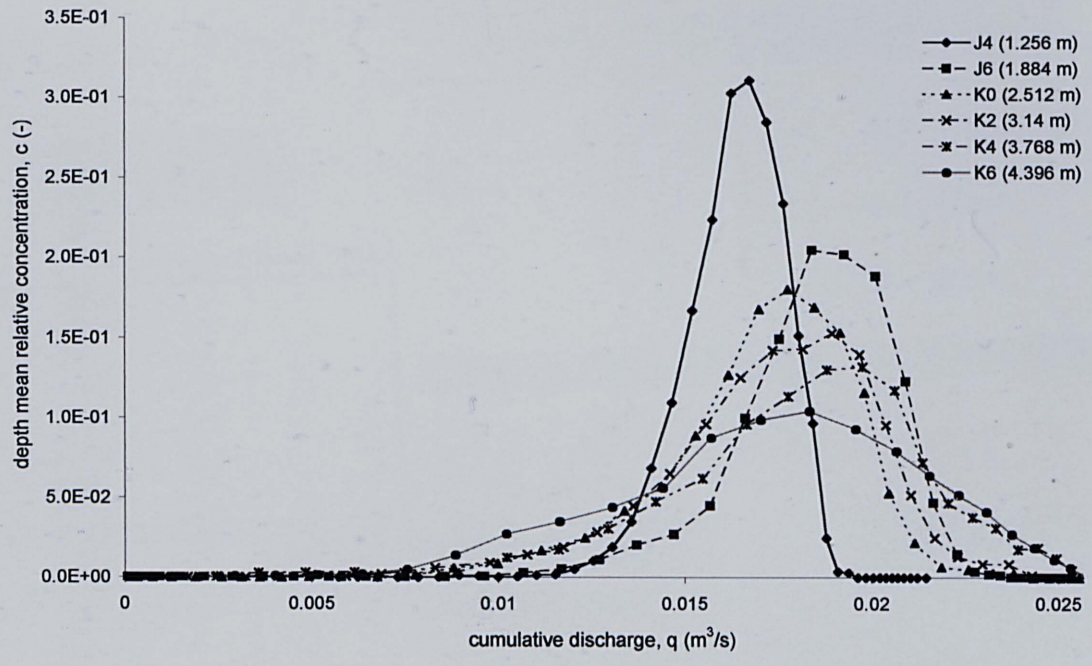

Figure 5.33 Transverse variation in depth mean concentrations, injection at J0 surface (looking downstream)

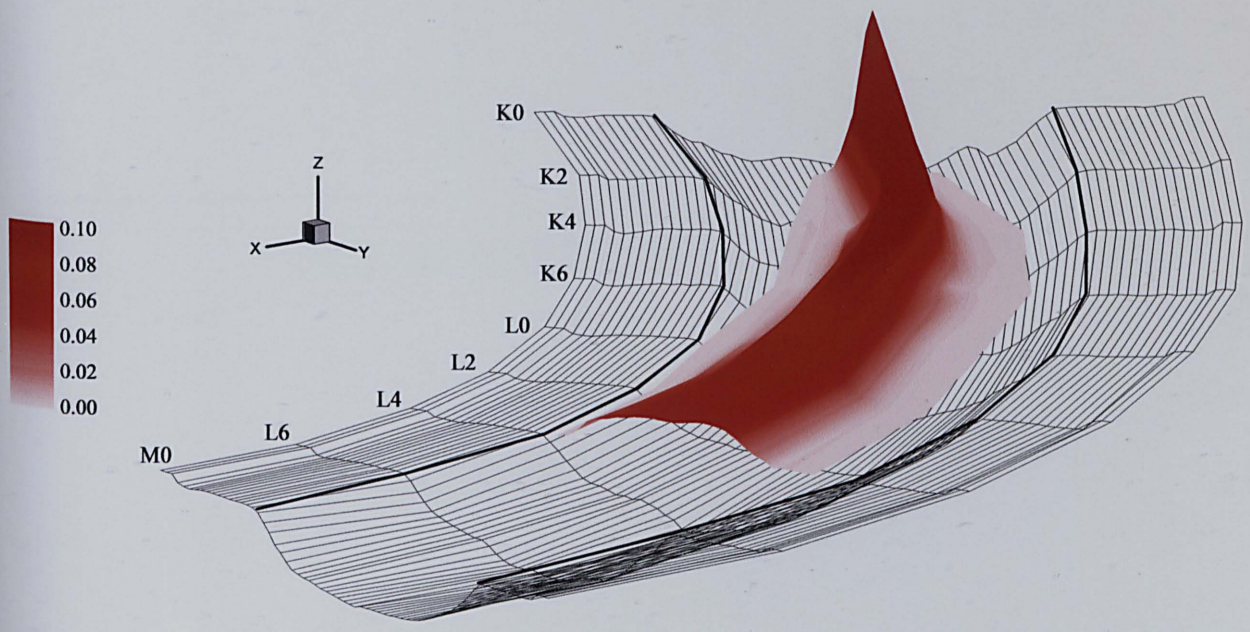

Figure 5.34 3D representation of transverse dye data below injection at K0 bed (looking upstream)

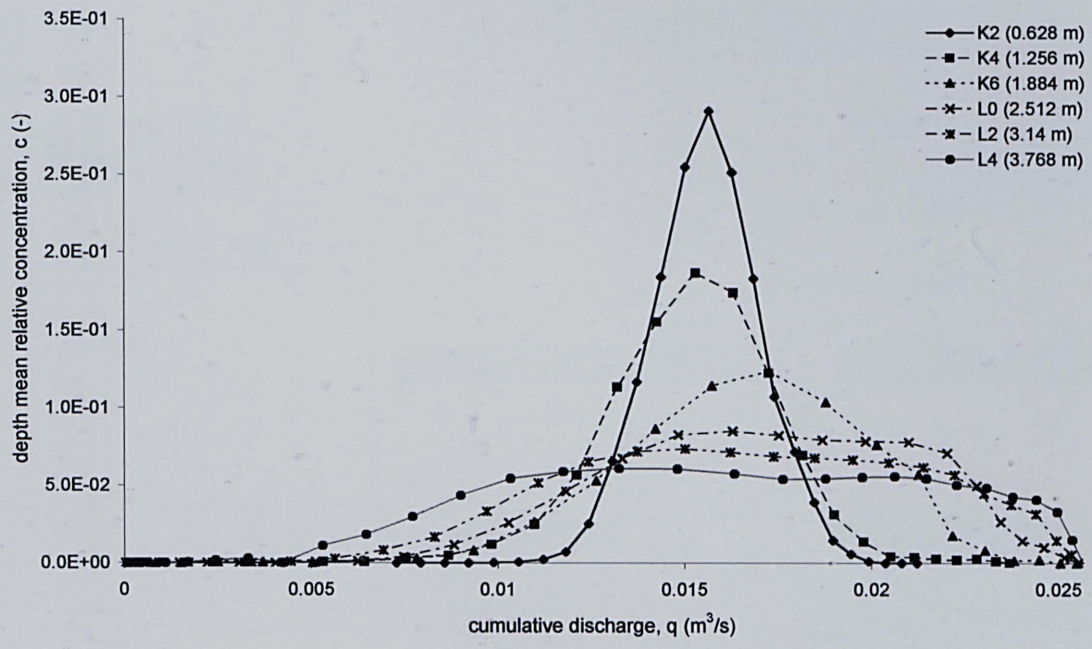

Figure 5.35 Transverse variation of depth mean concentrations, injection at K0 bed (looking downstream)

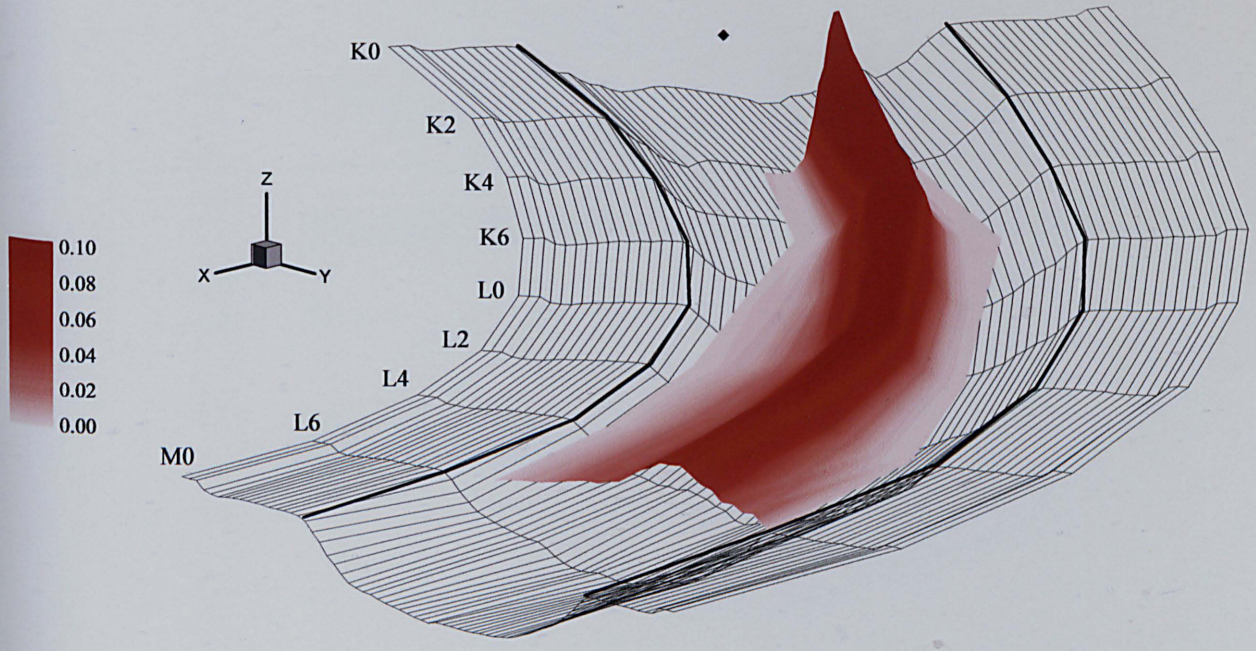

Figure 5.36 3D representation of transverse dye data below injection at K0 surface (looking upstream)

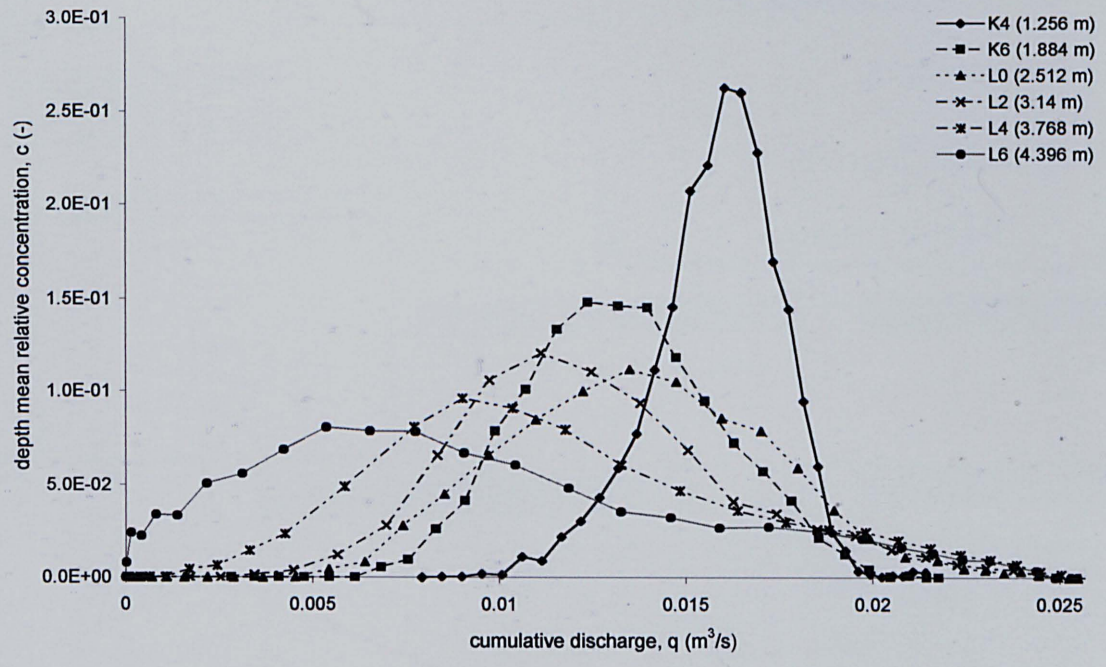

Figure 5.37 Transverse variation of depth mean concentration, injection at K0 surface (looking downstream)

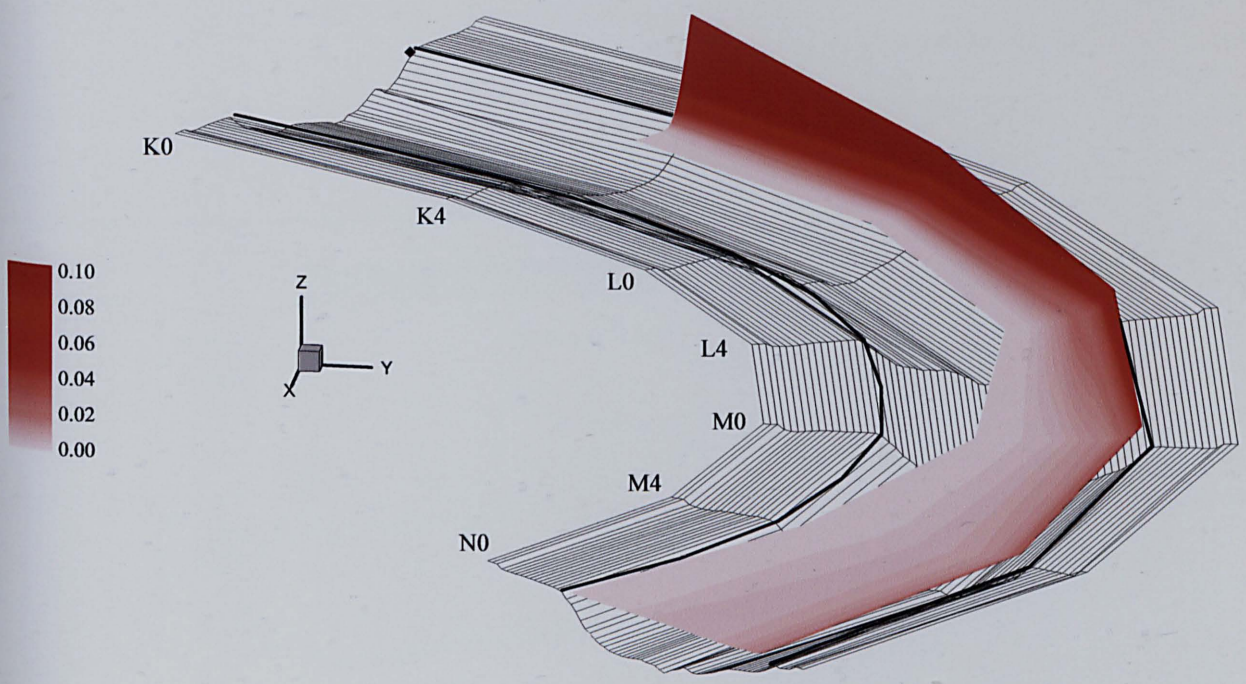

Figure 5.38 3D representation of transverse dye data below injection at K0 left (looking upstream)

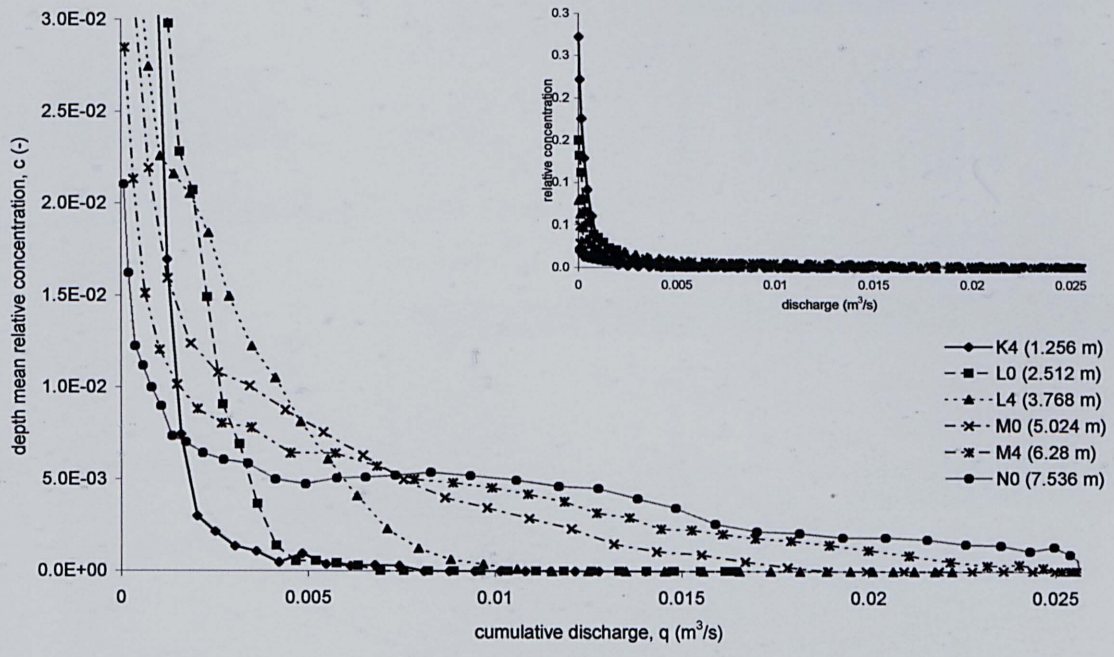

Figure 5.39 Transverse variation in depth mean concentration, injection at K0 left (looking downstream)

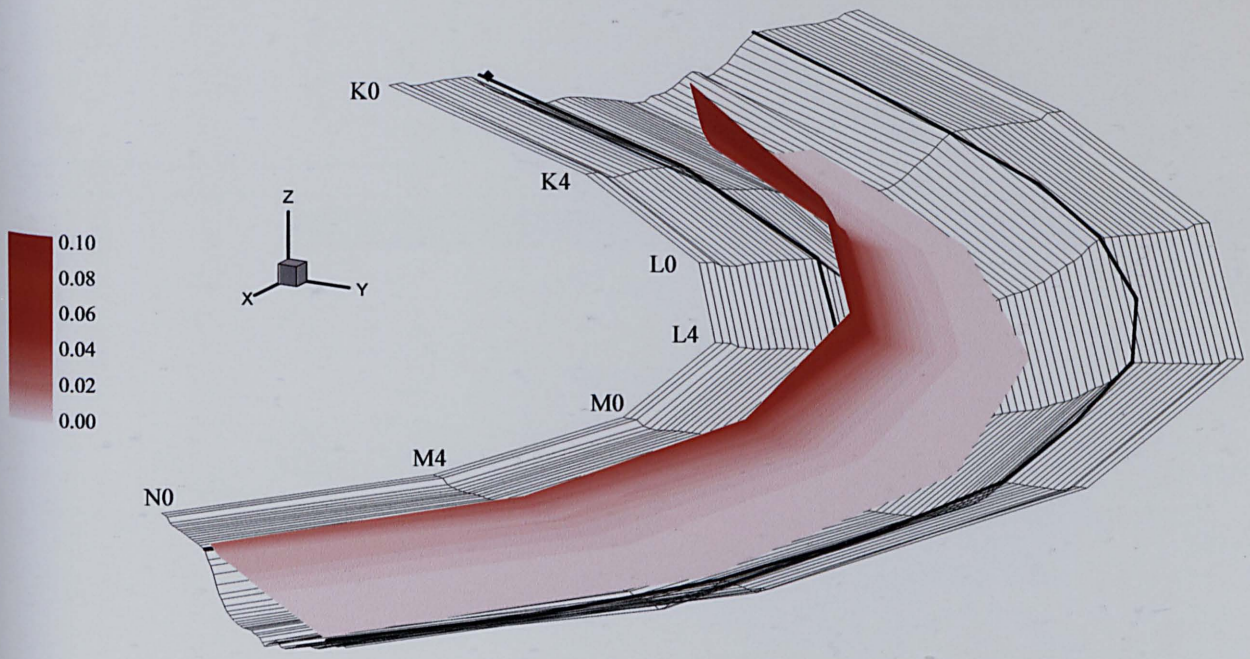

Figure 5.40 3D representation of transverse dye data below injection at K0 right (looking upstream)

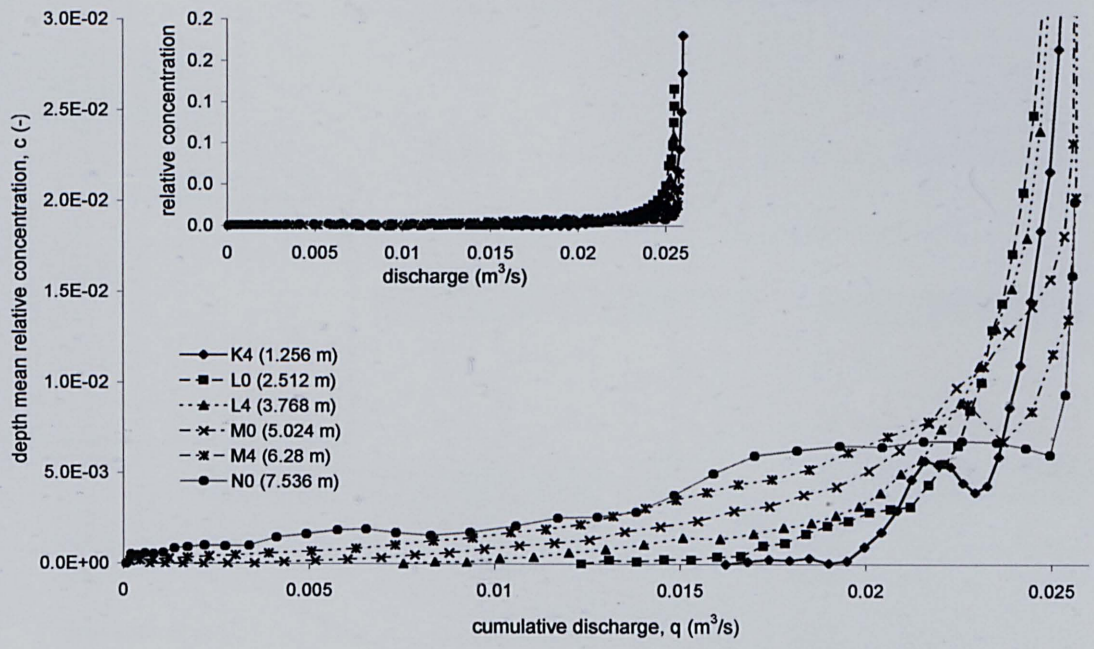

Figure 5.41 Transverse variation in depth mean concentration, injection at K0 right (looking downstream)

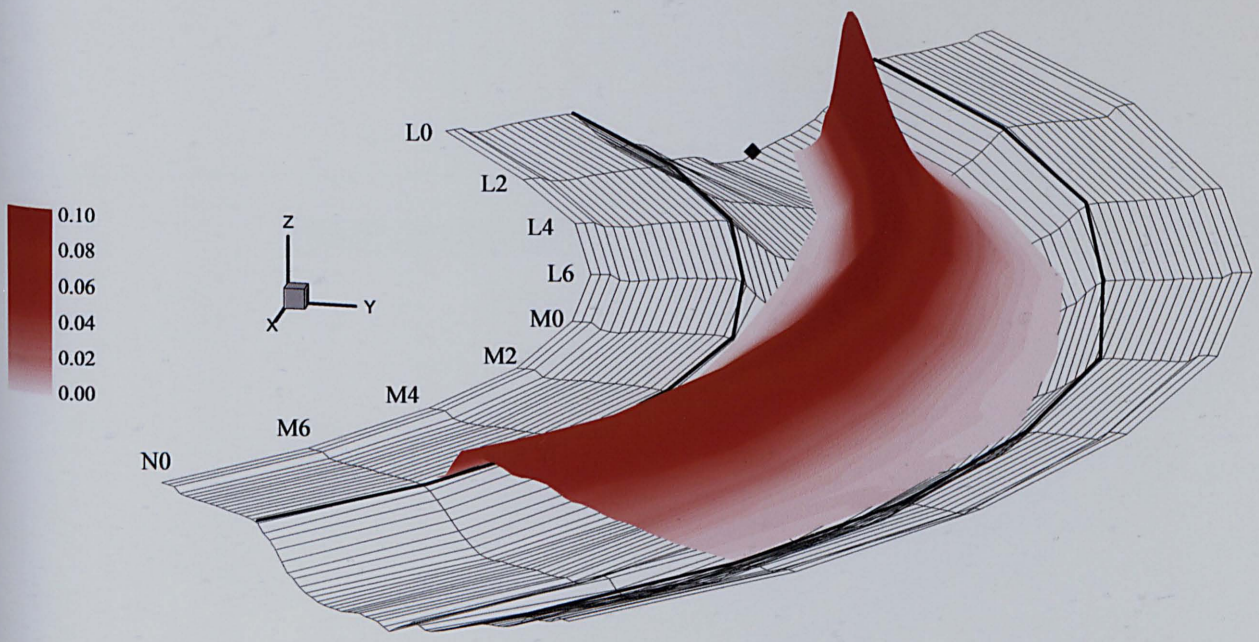

Figure 5.42 3D representation of transverse dye data below injection at L0 bed (looking upstream)

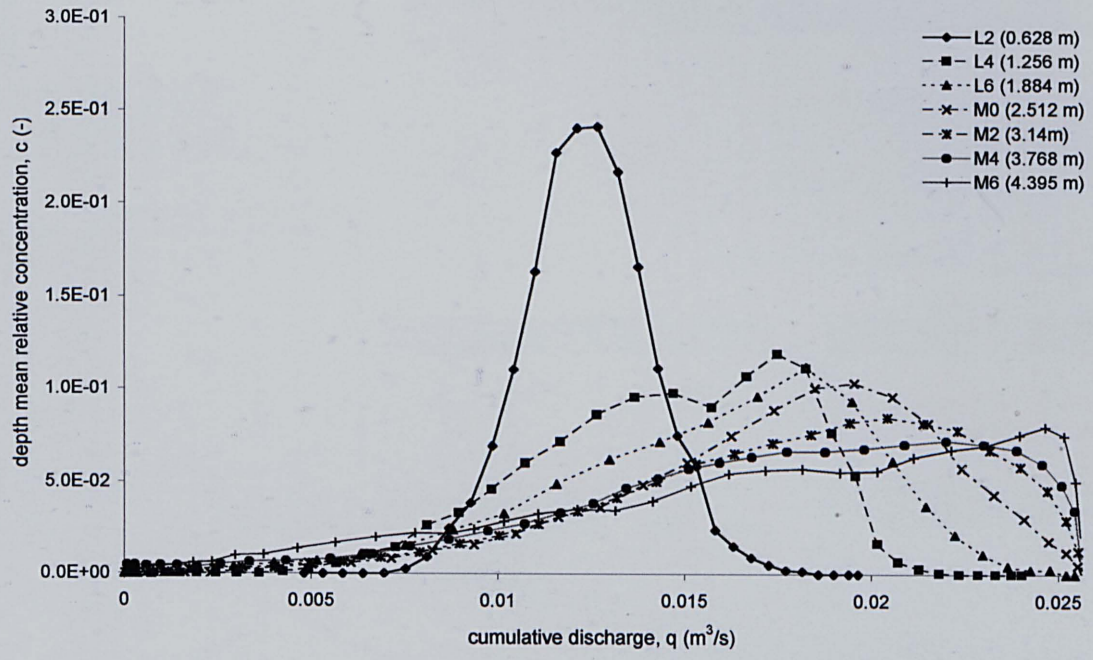

Figure 5.43 Transverse variation in depth mean concentration, injection at L0 bed (looking downstream)

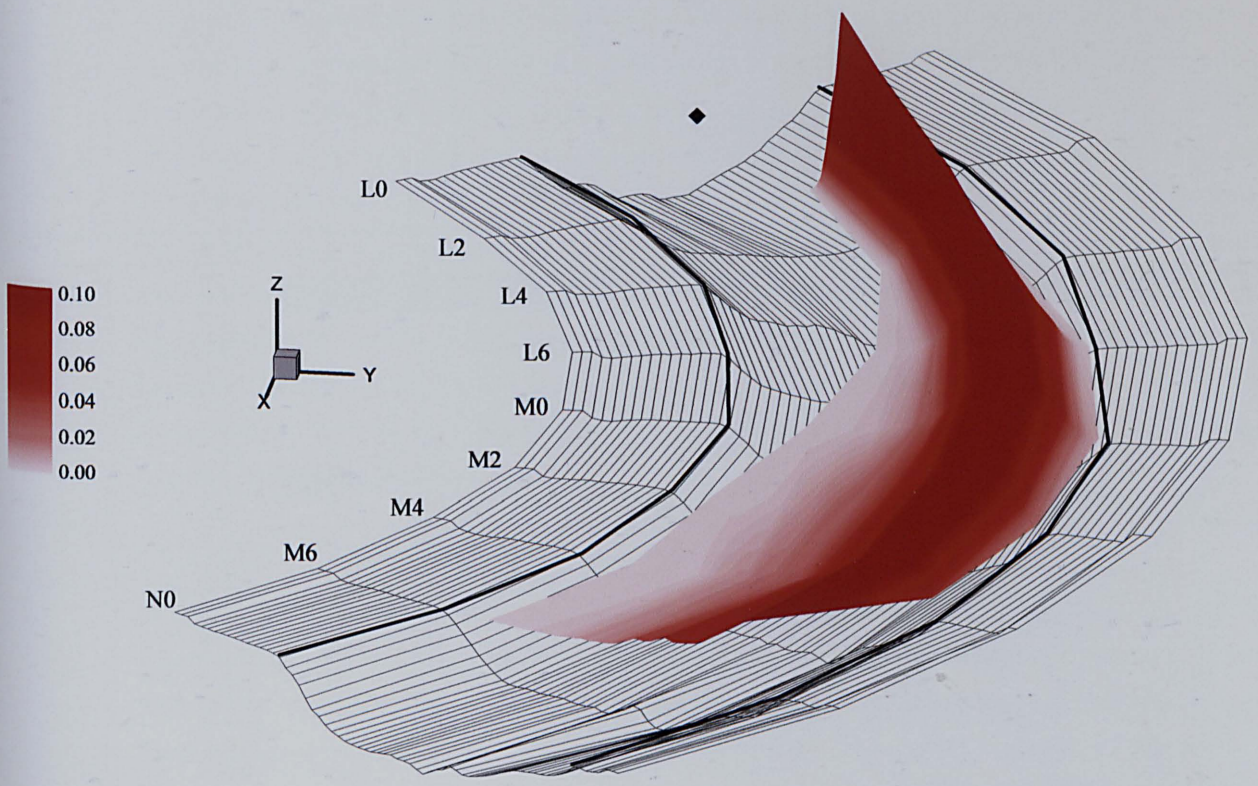

Figure 5.44 3D representation of transverse dye data below injection at L0 surface (looking upstream)

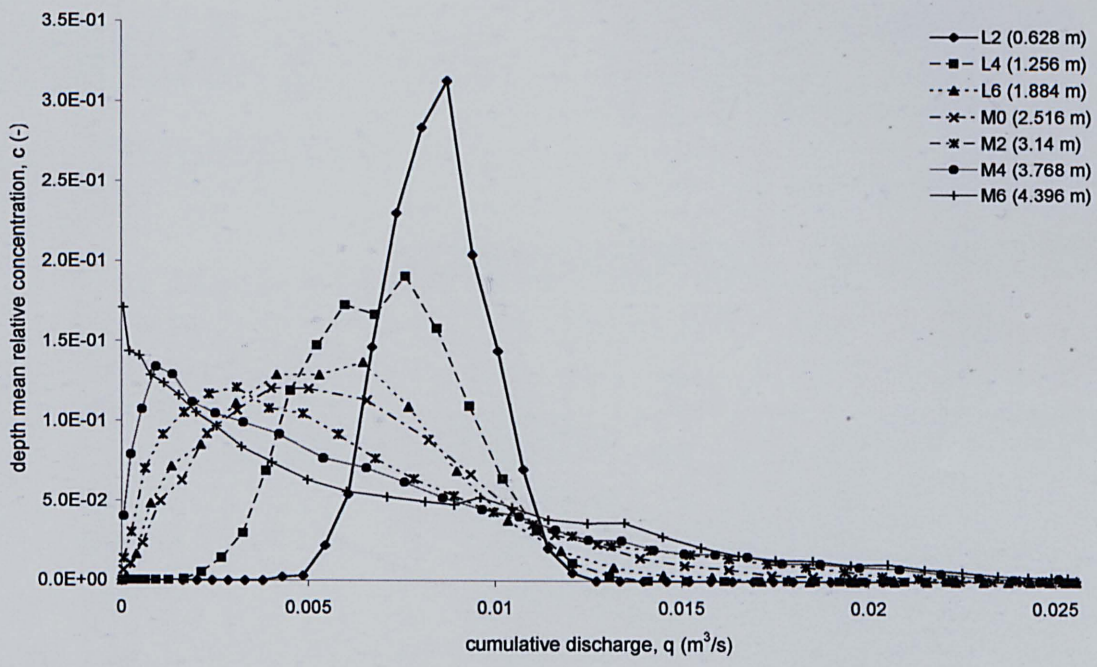

Figure 5.45 Transverse variation in depth mean concentration, injection at L0 surface (looking downstream)

5.4.2 Mass flux balance

It is possible to carry out checks on the quality of the tracer data by performing mass flux calculations. Calculation of the total mass of dye at a cross section is meaningless, flux is required to give a true representation of the amount of dye passing a given cross section. If the tracer is conservative, then the tracer mass flux through each cross section should be constant, assuming a steady injection rate and provided that normalisation by injection concentration has been correctly performed. To calculate mass flux, an evaluation of velocity is required. However, velocity measurements have only been made at six cross sections over the meander cycle, due to the time involved in the collection of this data and the short access period to the facility. Concentration measurements have been made at numerous cross sections, see Table 3.1. Calculations of mass flux based on measured concentration and velocity are limited to the few cross sections where the velocities have been measured. However, it may be possible to use predicted velocities to calculate depth average fluxes.

5.4.2.1 Mass flux balance, depth average

In Section 5.2.4.2 the prediction of depth average velocities from geometry data was discussed, and the use of Equation 2.130 shown to be accurate in predicting depth average velocity distributions. It was decided that a mass flux balance should be attempted using the predicted depth average velocity, and the depth average of the measured concentrations. The results of this are shown in Table 5.5 to Table 5.7.

I0 bed injection		J0 bed injection		K0 bed injection		L0 bed injection	
section	flux	section	flux	section	flux	section	flux
I2	5.47	J2	7.14	K2	5.00	L2	4.75
I4	4.59	J4	6.90	K4	4.71	L4	5.77
I6	5.38	J6	6.75	K6	3.74	L6	5.86
J0	4.95	K0	4.18	L0	3.08	M0	4.60
J2	5.06	K2	4.03	L2	2.22	M2	5.46
J4	4.83	K4	4.28	L4	2.90	M4	4.51
						M6	4.51
% err	17.82	% err	43.42	% err	55.64	% err	23.00

Table 5.5 Mass flux results for bed injection cases, fluxes from predicted depth average velocities (flux = 10^{-7} m^3/s)

I0 surface injection		J0 surface injection		K0 surface injection		L0 surface injection	
section	flux	section	flux	section	flux	section	flux
						L2	1.08
I4	2.19	J4	1.44	K4	2.00	L4	1.58
I6	2.54	J6	1.64	K6	2.08	L6	1.77
J0	2.06	K0	1.31	L0	1.09	M0	2.80
J2	1.48	K2	1.38	L2	2.85	M2	3.22
J4	2.31	K4	2.57	L4	1.65	M4	3.23
J6	2.13	K6	2.86	L6	1.25	M6	2.25
% err	41.78	% err	54.30	% err	61.65	% err	66.59

Table 5.6 Mass flux results for surface injection cases, fluxes from predicted depth average velocities (flux = 10^{-7} m^3/s)

I0 left injection		I0 right injection		K0 left injection		K0 right injection	
section	flux	section	flux	section	flux	section	flux
I4	6.59	I4	5.81	K4	8.05	K4	1.22
J0	6.25	J0	6.17	L0	7.55	L0	0.90
J4	3.82	J4	3.89	L4	5.03	L4	6.89
K0	5.69	K0	4.98	M0	2.88	M0	2.30
K4	6.52	K4	4.75	M4	3.68	M4	4.67
L0	4.90	L0	4.60	N0	3.33	N0	4.92
% err	46.54	% err	36.93	% err	65.46	% err	86.77

Table 5.7 Mass flux results for side injection cases, fluxes from predicted depth average velocities (flux = 10^{-7} m^3/s)

The figure obtained for mass flux should equate to the injection rate, because of the normalisation of concentration distributions by injection concentration. There is confidence in the consistency of the injection system because the constant head tank is a tried and tested system within the University of Sheffield, Mixing Studies Group. The injection rate was only directly checked during the set-up period and once around the middle of the testing period. On both occasions the injection rate was $4x10^{-7}$ m^3/s. Although only directly measured on these two occasions, the injection rate has also been checked from daily injection solution usage figures. The first and last sample times were used to give the duration of injection. The volume injected was found by weighing the injection solution drum at the start of each day and knowing the amount of water and neat dye used to make each day's injection solution. These calculations showed consistency in the injection rate within the bounds of error associated with the base figures, injection start time was always at least half and hour before the first sample time.

A study of the percentage errors in Table 5.5 to Table 5.7 reveals wide variation in the mass fluxes for each injection case. Even wider variation is evident over the complete data set. This may be attributed to a number of factors:

- Large discrepancies between the bed and surface injection mass fluxes are apparent. The fixed sand bed which was used has a degree of permeability associated with it. It was suggested that a loss of dye might occur due to transfer into the bed. It would be expected that this loss would be maximised with bed injection cases. However, the results in the above table suggest that the mass flux for the bed injection cases is around the injection rate, in many cases the mass flux appears to be an overestimate. This suggests that no significant transfer into the bed occurred.
- It was thought that a loss might be occurring due to residual levels of Rhodolite in the system, used to control background concentration levels, as detailed in Section 3.4.5.3. However, when the mass fluxes are examined with respect to time and dosing with Rhodolite there is no apparent trend.
- The accuracy of the predicted magnitude of depth average velocity information used in the mass flux calculations has errors associated with it, and these errors are carried through into these calculations.
- Potentially large errors have been introduced by using depth average figures. For example, consider concentration and velocity profiles as in Figure 5.46. The profile shapes are based on Equations 5.1. By integrating the velocity and concentration expressions over the depth and multiplying the products, an expression for the mass flux based on depth average terms can be derived. If the velocity and concentration expressions are multiplied and then integrated over the depth, an expression for the mass flux based on non-depth average values can be found.

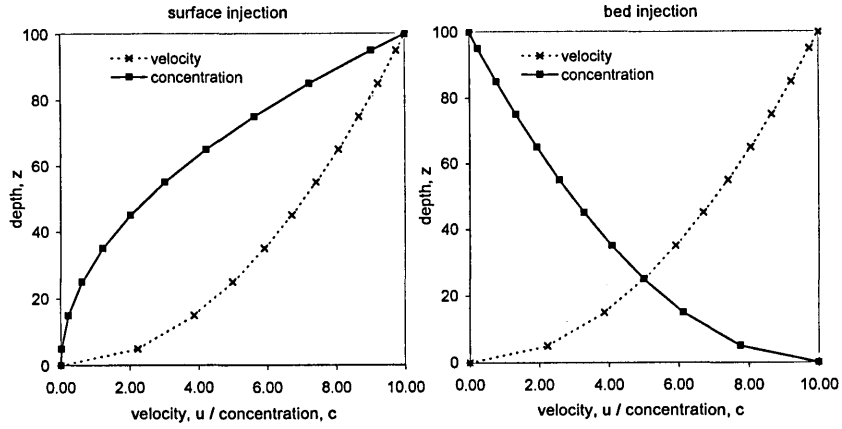

Figure 5.46 Idealised vertical velocity and concentration distribution predicted from Equations 5.1

$$u = az^{0.5} \qquad cs = bz^2 \qquad cb = h^{0.5} - z^{0.5} \qquad \text{Equations 5.1}$$

where cs is concentration from a surface injection and cb a bed injection, a and b are multiplication factors. The integral of these over the depth is:

$$u_h = \frac{2}{3}ah^{0.5} \qquad cs_h = \frac{1}{3}h^2b \qquad cb_h = \frac{1}{3}h^{0.5} \qquad \text{Equations 5.2}$$

Resulting in expressions for flux, based on depth average values:

$$cs_h u_h = \frac{2}{9}h^{2.5}ab \qquad cb_h u_h = \frac{2}{9}ah \qquad \text{Equations 5.3}$$

Multiplying the velocity and concentration expressions and then integrating over the depth leads to non-depth average expressions:

$$(cs.u)_h = \frac{2}{7}h^{2.5}ab \qquad (cb.u)_h = \frac{1}{6}ah \qquad \text{Equations 5.4}$$

By comparing the expressions in Equations 5.3 and Equations 5.4, it can be seen that the form of the depth and surface expressions is similar for depth averaging and non-depth averaging. However, the factors in the depth and non-depth average expressions are inconsistent. With the profiles specified, the surface case will under estimate flux by some 22% using depth average figures, whereas the bed case will result in an over estimate of around 25% for the given profiles. The lower the power used to describe the velocity and dye from bed injection, and the higher the power for the surface injection (the more curved the profiles) the greater these errors become. The results in Table 5.5 to Table 5.7 comply with this, as the mass fluxes from the bed injection cases is around twice the value for the bed cases.

It can be concluded that the calculation of mass flux, based on depth average concentrations and predicted depth average velocity profiles, is a poor check of the data.

5.4.2.2 Mass flux balance, non-depth average

Given the poor results of the mass flux balance calculations achieved using depth average concentrations and predicted depth average velocities, calculations which do not use depth average values should be attempted. In Section 5.2.4 the difficulties in predicting vertical distribution of primary velocities were mentioned. This leaves the situation as initially described in this section, that mass flux calculations can only be performed at the sections where velocity and concentration measurements coincide. The

requirement for cross correlation between velocity and concentration data was not foreseen during testing, therefore measurement points do not necessarily align. Hence, it was necessary to carry out linear interpolation between the velocity data points, both vertically and horizontally. The results of these mass flux calculations are shown in Table 5.8 to Table 5.10.

I0 bed injection		J0 bed injection		K0 bed injection		L0 bed injection	
section	flux	section	flux	section	flux	section	flux
I2	-	J2	-	K2	-	L2	-
I4	3.82	J4	-	K4	-	L4	-
I6	-	J6	-	K6	-	L6	-
J0	3.90	K0	3.85	L0	3.56	M0	3.89
J2	-	K2	-	L2	-	M2	-
J4	-	K4	-	L4	-	M4	-
						M6	-

Table 5.8 Mass flux results for bed injection cases, from interpolated velocity measurements (flux = 10^{-7} m^3/s)

I0 surface injection		J0 surface injection		K0 surface injection		L0 surface injection	
section	flux	section	flux	section	flux	section	flux
						L2	-
I4	2.88	J4	-	K4	-	L4	-
I6	-	J6	-	K6	-	L6	-
J0	2.12	K0	1.58	L0	1.44	M0	2.53
J2	-	K2	-	L2	-	M2	-
J4	-	K4	-	L4	-	M4	-
J6	-	K6	-	L6	-	M6	-

Table 5.9 Mass flux results for surface injection cases, from interpolated velocity measurements (flux = 10^{-7} m^3/s)

I0 left injection		I0 right injection		K0 left injection		K0 right injection	
section	flux	section	flux	section	flux	section	flux
I4	3.57	I4	3.79	K4	-	K4	-
J0	3.15	J0	3.97	L0	3.37	L0	1.23
J4	-	J4	-	L4	-	L4	-
K0	3.68	K0	3.86	M0	2.32	M0	2.44
K4	-	K4	-	M4	-	M4	-
L0	3.83	L0	4.00	N0	-	N0	-

Table 5.10 Mass flux results for side injection cases, from interpolated velocity measurements (flux = 10^{-7} m^3/s)

The results of these calculations show a vast improvement over the results of the calculations performed using the depth average values. The percentage error in the bed injection cases is 14.33, for the surface cases 50.01 and the side cases 69.28. It should be noted that this error in the side injection cases is also the error of the complete data set, and that the error stems particularly from the very low mass flux found for section K0. Overall errors for each set of injection cases for the depth average flux calculation was into hundreds of percent.

The bed injection cases and the I0 side injection cases show very good and consistent recovery ratios of dye. The surface cases and the K0 side cases are not as good. These errors may stem from a lack of definition of the dye data. The depth to first reading was 15mm, with sampling transects spaced every 18mm below this. The result is that the first reading is representative of the first 24mm and the other for

18mm steps, except near the bed where geometry constraints define the relative depth. In the case of surface injections, the vertical concentration gradient over the near surface region is high. Thus, the surface injection cases may have resulting underestimates of mass flux. This argument can also be extended to the side injection cases at section K0. In the region of K0, the secondary circulations have been shown low. Thus, below section K0 the dye may stay trapped near the surface and banks, resulting in high concentration gradients which are misrepresented.

These mass flux balance calculations have not conclusively proved the quality of the dye data. However, the fluxes include any errors in velocity measurement and interpolation, as well as concentration measurement errors, therefore these calculations have not shown the dye data to be of an unacceptable standard. It is therefore concluded that further analysis of the concentration data can be undertaken. The lack of mass balance from the depth average calculation should not be significant when using tools such as the Method of Moments. The change and development in shape of the distributions are important in quantifying the rate of mixing, not the mass fluxes.

5.5 *Transverse Variance Calculations*

The advection dispersion equation which was derived to explain and predict river mixing has solutions to enable the calculation of mixing coefficients, through the change of moments as introduced in Section 2.2.2. This requires the evaluation of variance of the measured distributions.

From the review of past work and theory there are two methods, or approaches, to the calculation of variance of transverse concentration distributions, variance can be calculated using transverse distance as detailed in the Method of Moments, Section 2.2.2, or based on cumulative discharge, as discussed in Section 2.5.3.

Mixing coefficients can be calculated from the change in these variances with distance. However, where bank impingement occurs the variance calculation will be affected so it is necessary to utilise the Generalised Method of Moments as introduced in Section 2.6.

5.5.1 Transverse distance calculations

The equations used to calculate variance are given in Section 2.2.2, Equations 2.19 a-d, Equation 2.20 and 2.21. Equations 2.19 a-d express moments as a function of longitudinal distance at given times. For transverse mixing, variance is required as a function of transverse distance at longitudinal positions. Therefore, Equations 2.19 a-d become:

$$M_0 = \int_{-\infty}^{\infty} c(y,x)dy \qquad \text{Equation 5.5 a}$$

$$M_1 = \int_{-\infty}^{\infty} yc(y,x)dy \qquad \text{b}$$

$$M_2 = \int_{-\infty}^{\infty} y^2c(y,x)dy \qquad \text{c}$$

$$\vdots$$

$$M_p = \int_{-\infty}^{\infty} y^p c(y,x)dy \qquad d$$

The centroid of a distribution can be found from the first moment over the zero moment, and the variance from the product of division of the second moment by the zero moment, minus the centroid squared.

Using these expressions, the variance of each transverse profile can be calculated as a function of longitudinal distance. Following this procedure the results presented in Figure 5.47 were obtained, the points on the x-axis mark injection sections.

In Section 2.2.2 it was shown that if the conditions and assumption of the derivation of the ADE were met, the increase in variance of the concentration distribution should be linear with distance. Later in Chapter 2 it was shown that for numerous transverse and longitudinal mixing experiments, both laboratory and field based, linear increase of variance with distance was obtained. However, Figure 5.47 clearly shows a lack of linearity in the nature of the variance distance calculations.

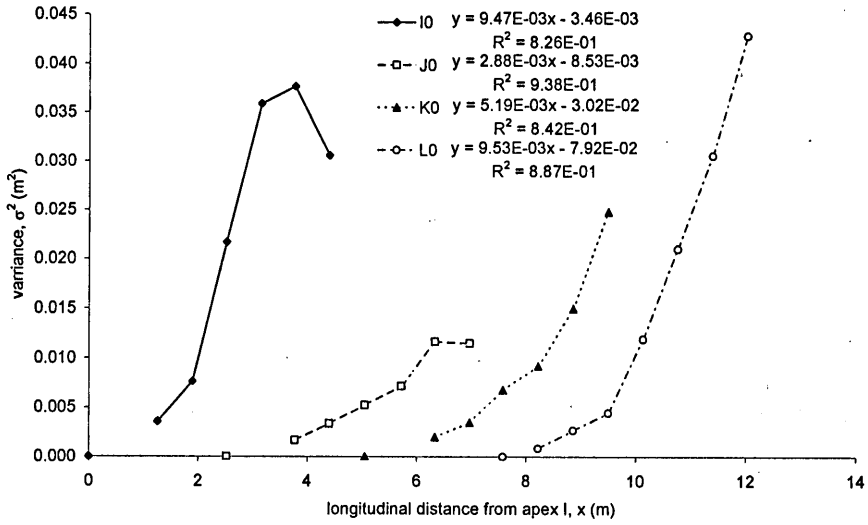

variance distance plots for surface injection cases

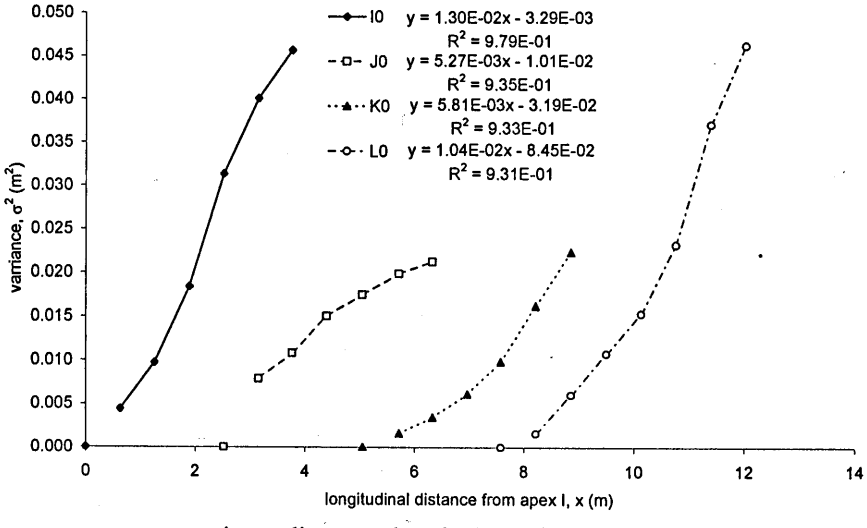

variance distance plots for bed injection cases

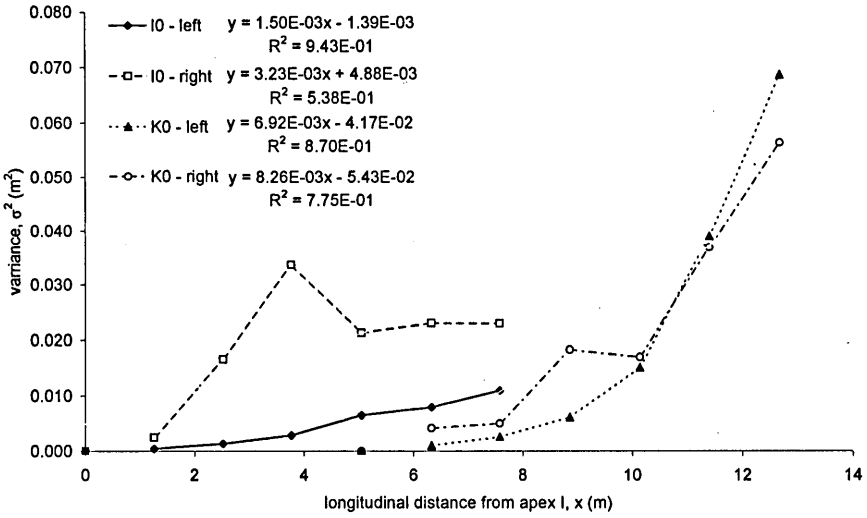

variance distance plots for side injection cases

Figure 5.47 Variance distance plots, calculations based on Cartesian co-ordinates

5.5.2 Cumulative discharge calculations

In section 2.5 it was suggested that natural channel configurations can have a significant effect on the variance calculations, through the incorrect interpretation of curvilinear distance, and the effects of mass movement brought about by changing channel cross section. The suggested solution to this, Yotsukura and Cobb (1972), is to convert the variance calculation to a cumulative discharge expression, or through Holley *et al* (1972) Generalised Method of Moments. In section 2.5, it was shown that the cumulative discharge approach offers a more robust and efficient solution than the Generalised Method of Moments in Cartesian co-ordinates, because it negates the need to evaluate net transverse drift velocities. The conversion to cumulative discharge and the resulting equations were given in Section 2.6. Using the cumulative discharge approach, the variances can be recalculated. However, to be able to replace transverse co-ordinates with a cumulative discharge expression it is necessary to have information of the flow distribution across the channel at every measurement cross section. This information is not available in sufficient detail from the velocity measurements, as they were made at only 6 cross sections over the test reach. However, in Section 5.2.4.2 it was shown that the transverse distribution of primary velocity and cumulative discharge could be accurately predicted by Equation 2.132 from profile data, which is available at all cross sections.

Figure 5.48 shows the effects of converting from transverse Cartesian co-ordinates to cumulative discharge terms on the measured tracer plume. Both the x-axis ranges have been set to show the full channel. This highlights the effect of removing skewness in the distributions.

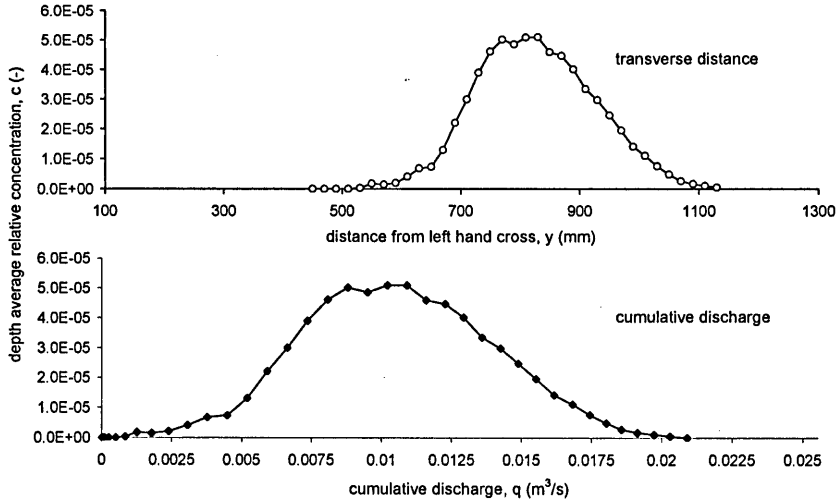

Figure 5.48 Effect on measured dye plume of converting from transverse distance co-ordinates to cumulative discharge terms, both X ranges set to cover the full channel (data from section I4 below injection at I0 bed)

Figure 5.49 shows the results of the variance distance calculation made using the predicted cumulative discharge distributions.

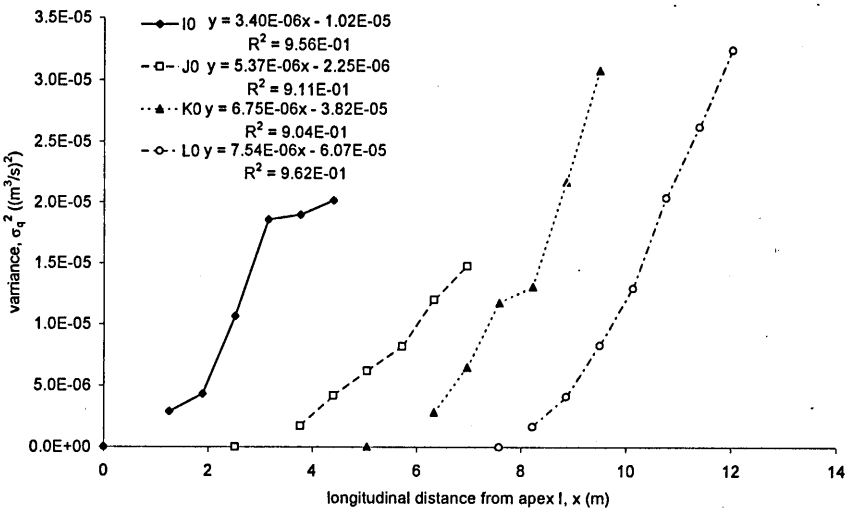

variance distance plots for surface injection cases

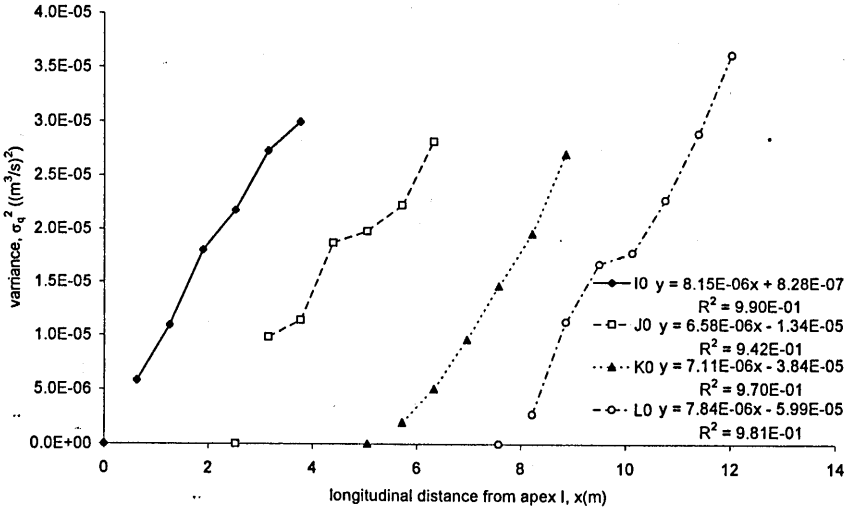

variance distance plots for bed injection cases

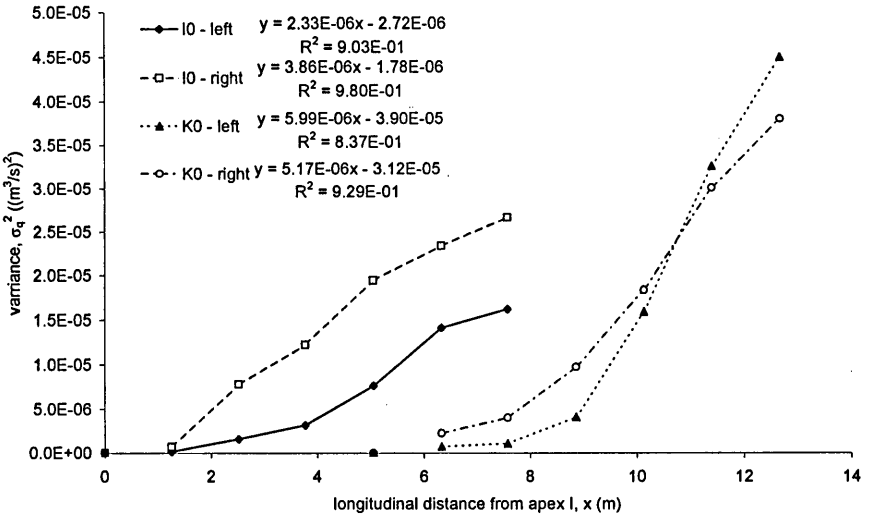

variance distance plots for side injection cases

Figure 5.49 Variance distance plots, calculations based on cumulative discharge

Comparison of Figure 5.47 and Figure 5.49 shows the dramatic effect that the cumulative discharge approach has had on the calculation of the change of moments. The improvement can be compared quantitatively by comparison of the R^2 values for the fit to a straight line, Table 5.11. The improvement is particularly pronounced for the side injection cases. In the near bank region the alteration between cumulative discharge and transverse distance is most pronounced.

	Surface				Bed				Side			
	I	J	K	L	I	J	K	L	I left	I right	K left	K right
R^2 cart.	0.83	0.94	0.84	0.87	0.98	0.94	0.93	0.93	0.94	0.54	0.87	0.78
R^2 cumu.	0.96	0.91	0.91	0.90	0.96	0.99	0.94	0.97	0.98	0.90	0.84	0.93

Table 5.11 Quality of fit to straight lines for variance distance plots

5.5.3 Generalised Method of Moments calculations

The variance of a transverse distribution can be significantly influenced by impingement of the dye concentration on the channel boundaries. Holley *et al* (1972) developed the Generalised Method of Moments to address the issues of channel boundary impingement and natural channel effects. However, as was explained in section 2.5 the natural channel effects are more simply accounted for with the cumulative discharge approach. In Section 2.6.2, the conversion of the Generalised Method of Moments to cumulative discharge terms was undertaken, thus cumulative discharge can be used to account for natural channel effects, and the Generalised Method of Moments for bank impingement. No significant results have been published using the Generalised Method of Moments in this form, therefore, it has been decided to carry out some checks on the method in both Cartesian and cumulative discharge forms, using simple analytic solutions.

5.5.3.1 Check of Generalised Method of Moments calculations

Concentration profiles were predicted using the following equation:

$$c_d(x,y) = \frac{m}{h\sqrt{4\pi k_y x u}} \exp\left(\frac{y^2 u}{4k_y x}\right) \qquad \text{Equation 5.6}$$

This equation, although simple to solve, for example on a spreadsheet, is only valid provided that tracer does not impinge on the banks. The ability of the Generalised Method of Moments to correctly account for bank side impingement is one of the main areas of investigation. To facilitate this, the idea of reflections has been used. The distribution from the above equation is evaluated at given longitudinal distances, for an infinitely wide channel. This distribution may then be 'folded up' within the desired channel width, by considering the channel boundaries as perfect reflectors. Thus, the distribution shown in the top half of Figure 5.50 is folded at ±0.6, then again at ±1.8 and then at ±3.0 etc, to produce the distribution shown in bottom half of Figure 5.50, that is a Gaussian distribution bounded within a 1.2m wide channel. Skewed distributions may be produced in the same way by shifting the location of the channel and the reflection points with respect to the initial distribution.

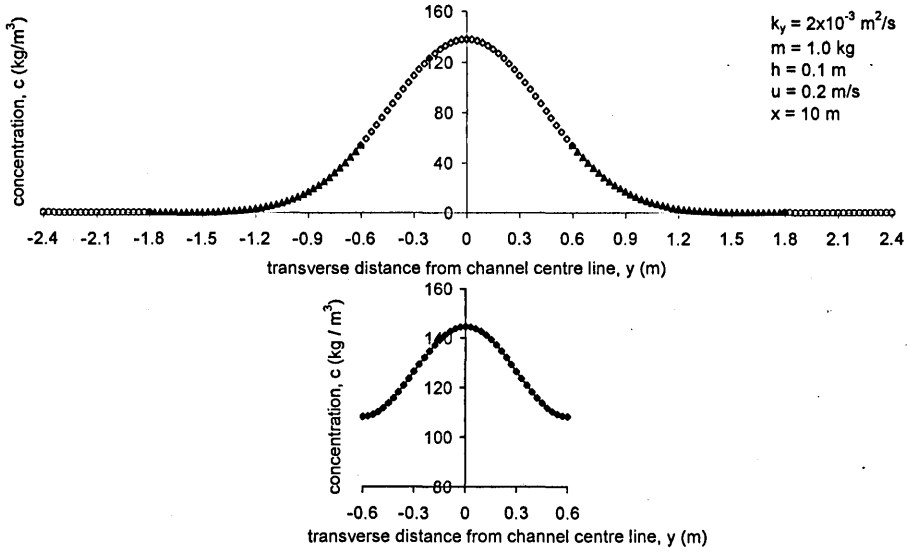

Figure 5.50 Graphs showing how reflected concentration distributions have been calculated

Initially, a rectangular channel was assumed, with a uniform velocity distribution. From this information a flow distribution can be determined across the channel, and calculation performed to evaluate the transverse mixing coefficient using the Generalised Method of Moments in Cartesian and cumulative discharge co-ordinates. Five injection points were simulated: centre line (no skew), right and left bank (full right / left) and the middle of the right and left hand sides (part left / right), shown graphically on Figure 5.51.

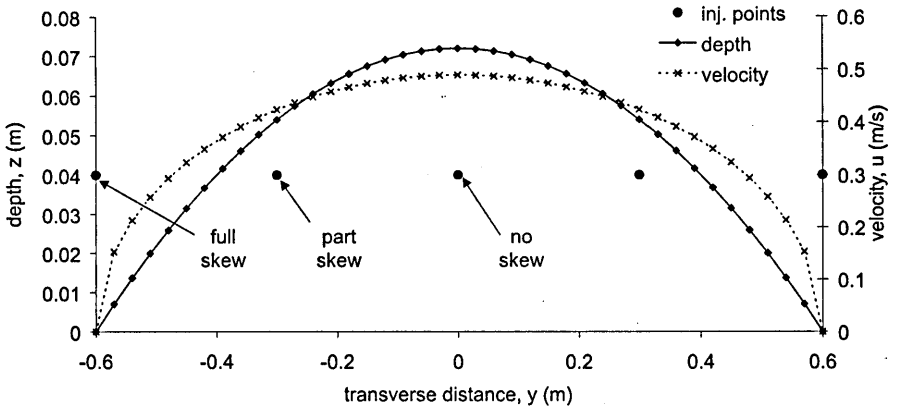

Figure 5.51 Parabolic depth and velocity distributions (also shown are the different injection points used)

The results in Table 5.12 show that for the case of rectangular channel shape and velocity distributions, the Generalised Method of Moments in either cumulative discharge or Cartesian co-ordinate systems appears to correctly evaluate the mixing coefficient. The input value of k_y was $2x10^{-3}$, the obtained values are all slight overestimates of this. It is believed that this is because of the way that the reflections were calculated. An R^2 (regression fit) value of one represents a perfect straight line, so it can be seen that the f(x) function is correctly accounting for bank impingement, this illustrated in Figure 5.52.

	no skew		full left		part left		full right		part right	
	k_y	R^2	k_y	R^2	k_y	R^2	k_y	R^2	k_y	R^2
Cartesian	$2.34x10^{-03}$	0.997	$2.20x10^{-03}$	0.995	$2.28x10^{-03}$	0.997	$2.22x10^{-03}$	0.991	$2.28x10^{-03}$	0.997
cumulative	$2.35x10^{-03}$	0.996	$2.21x10^{-03}$	0.995	$2.29x10^{-03}$	0.997	$2.20x10^{-03}$	0.991	$2.28x10^{-03}$	0.997

Table 5.12 Investigation into the accuracy of Generalised Method of Moments for a rectangular channel, with $\varphi = 1$ (h^2u being constant)

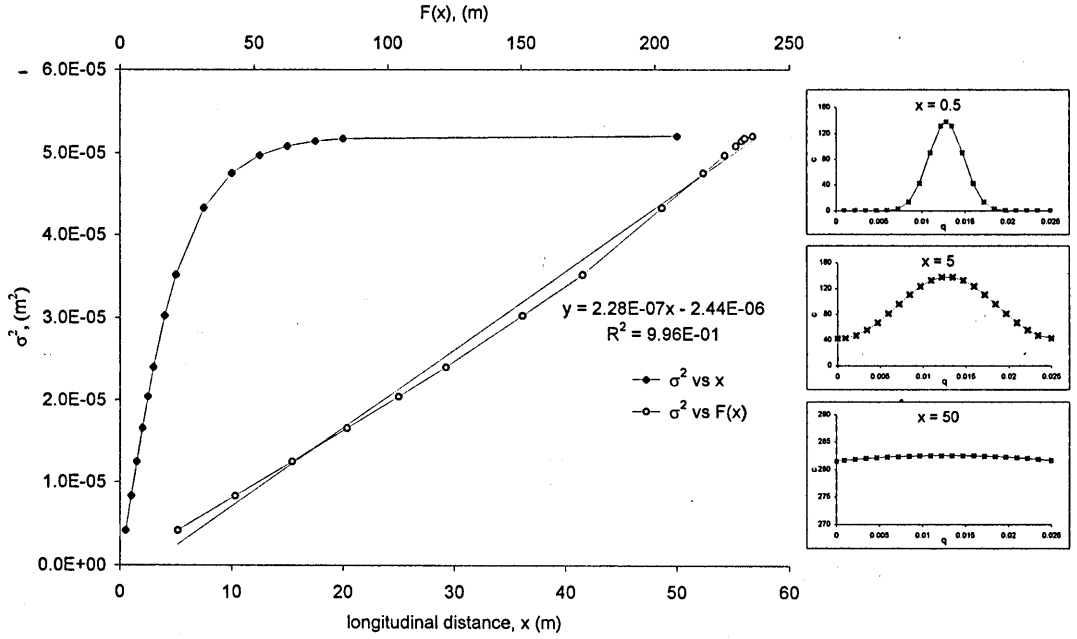

Figure 5.52 Graph showing variance distance plots results for Generalised Method of Moments calculations in cumulative discharge. Channel shape rectangular, no skew, $\varphi = 1$

The method was checked for a parabolic channel shape and velocity distribution, as in Figure 5.51. The same concentration distributions were used. Equation 5.6 is not truly valid for a parabolic channel or velocity distribution, nor is the method of 'folding' the distribution, as impingement will occur at different depths within the channel. However, the channel is very flat, 0.07m deep and 1.2m wide, and the investigation highlights the importance of the correct evaluation of the φ function in the near bank regions. The results of these calculations are shown in Table 5.13.

	no skew		full left		part left		full right		part right	
	k_y	R^2	k_y	R^2	k_y	R^2	k_y	R^2	k_y	R^2
cartesian (φ=1)	$1.34x10^{-03}$	0.969	$1.87x10^{-03}$	0.816	$1.55x10^{-03}$	0.996	$1.87x10^{-03}$	0.851	$1.55x10^{-03}$	0.996
cumulative (φ=1)	$1.82x10^{-03}$	0.991	$6.83x10^{-03}$	0.993	$2.96x10^{-03}$	0.996	$6.78x10^{-03}$	0.993	$3.04x10^{-03}$	0.996
cumulative (φ=uh^2)	$1.97x10^{-03}$	0.991	$2.29x10^{-03}$	0.996	$2.23x10^{-03}$	0.993	$2.41x10^{-03}$	0.995	$2.32x10^{-03}$	0.995

Table 5.13 Investigation into the accuracy of Generalised Method of Moments for a parabolic channel

From Table 5.13 it can be seen that with the Cartesian system there is a trend to underestimate the mixing coefficient, and also that in the full skew cases the straight line fit is poor, suggesting that the evaluation of f(x) is erroneous.

Following the conclusions of Lau and Krishnappen (1981) (working with predictive models) that averaging of (uh^2) had little effect, the cumulative discharge calculations were initially performed with φ = 1. The results of this show reasonable, although not excellent, agreement for the no skew and part skew cases, however, in the full skew case the coefficient is found to be very inconsistent. This originates from the situation where dye is concentrated near the bank. In this situation very high rates of change of concentration are coupled with very small rates of change of discharge, leading to a very large value in the f(x) term. The f(x) value should always be negative, as shown in Figure 5.53. However, with the full skew cases and φ = 1.0, positive values of f(x) were initially obtained as shown in Figure 5.54. This stems from an unequal affect of dc/dq and $q-\bar{q}$ in the near source region, when no extra weighting is given to the very low flow depths and velocities near the channel boundaries. It is essential that these effects are correctly included to ensure accuracy of predictive calculations. In the derivation of the Generalised Method of Moments in cumulative discharge terms, it was shown that the function φ should be equal to $m_x h^2 u$, Section 2.6.4.

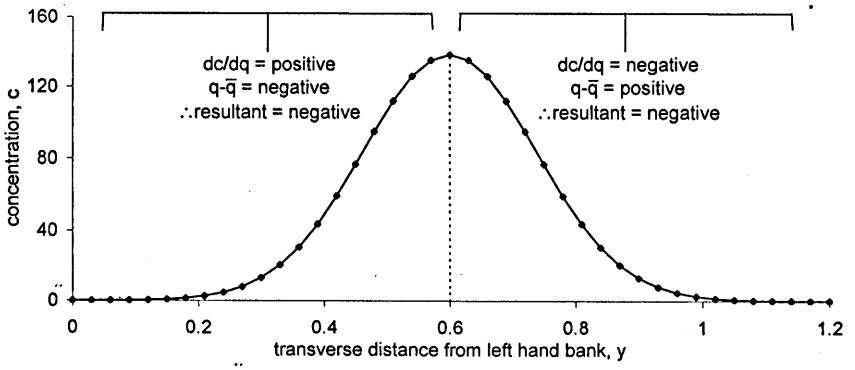

Figure 5.53 Graphic representation of f(x) always negative

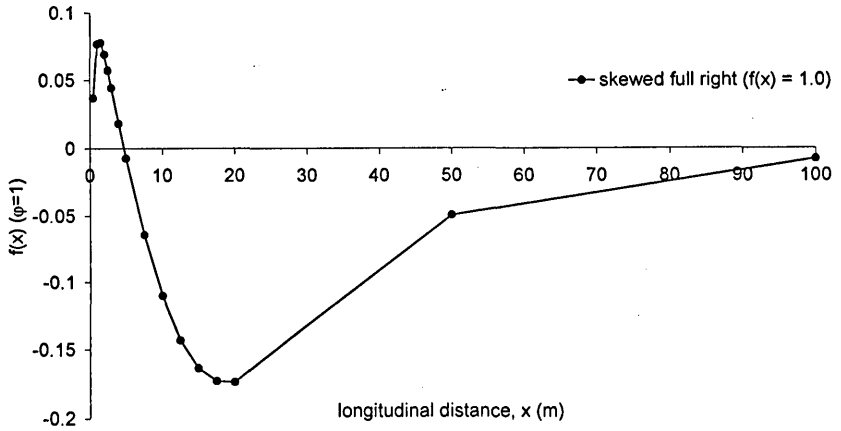

Figure 5.54 Longitudinal variation in f(x) with $\varphi = 1.0$ for parabolic channel

The stream tube data with $\varphi = h^2u$ in Table 5.13 shows an accurate prediction of k_y in all skew cases. A similar, but slight, over estimate of the mixing coefficients, as was obtained for the rectangular case, is again seen, although the no skew case does appear slightly low. Slight errors may be expected as the concentration distribution calculations from Equation 5.6 are not truly valid for cases of transversely varying depth or velocity. However, the ability of the Generalised Method of Moments to correctly account for the effect of bank side impingement has been demonstrated.

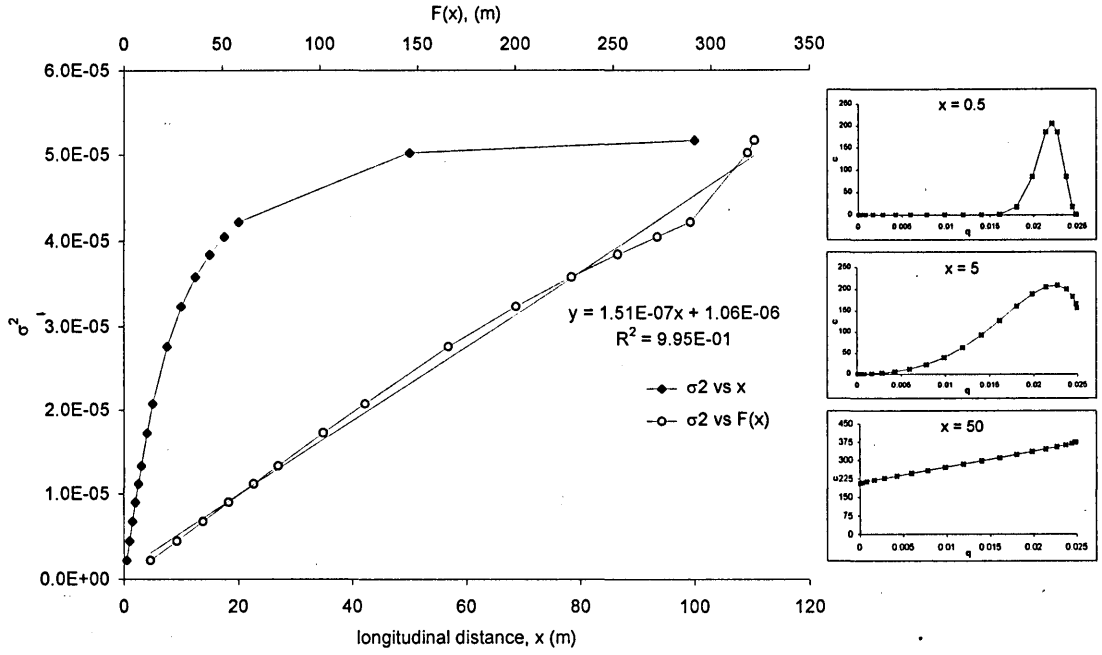

Figure 5.55 Graph of variance distance plots highlighting effectiveness of the Generalised Method of Moments in accounting for bank impingement (parabolic channel with a part right skew injection case)

Figure 5.52 and Figure 5.55 show plots of variance versus distance and variance versus F(x). From the figures it can easily be seen that the evaluation of the f(x) function with distance (F(x)) very effectively straightens the plot of variance versus distance. The line is not a perfect fit because of the sensitive nature of f(x) and its evaluation over distance. Figure 5.56 shows f(x) versus distance plots for three different skew cases within the parabolic channel. The non-linear and inconsistent (with skewness) nature of the

f(x) function can been seen. Skew to the left causes the same shape and values as right skew cases, as would be expected, and therefore is not illustrated.

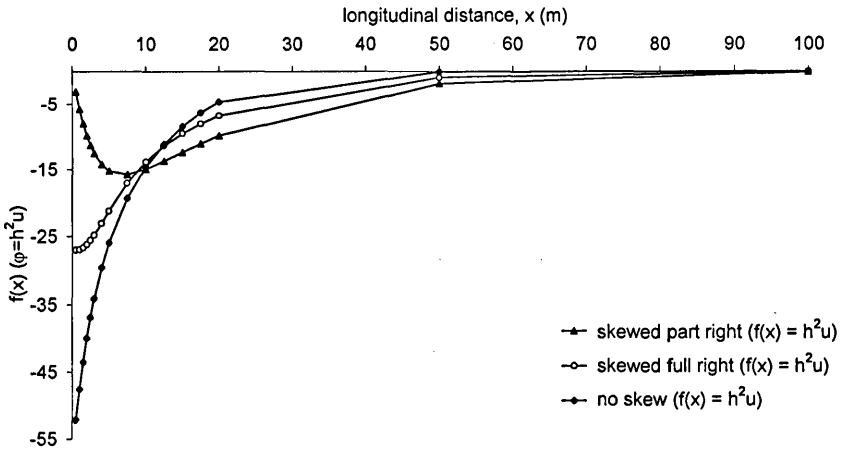

Figure 5.56 Graph showing longitudinal variation in f(x) for cumulative discharge calculations in parabolic channel

Figure 5.56 shows that at large distances the f(x) function approaches zero for all skew cases. This is because the tracer is becoming well mixed over the channel width and therefore the factor f(x) approaches zero to maintain a straight line fit when there is little or no change in variance.

The variation of F(x), the integral of f(x) with respect to distance, which is the area bounded by the curves in Figure 5.56, is shown in Figure 5.57. The non-linear nature of the of the f(x) function requires that for F(x) to be accurate f(x) must be evaluated as frequently as possible with distance, particularly in the near source area where the changes in f(x) are sudden. The slight deviation from a straight line exhibited in Figure 5.52 and Figure 5.55, σ^2 versus F(x), is due to too widely spaced assessment of f(x) particularly at the higher distances evaluated and the trapezium approximations used to evaluated F(x).

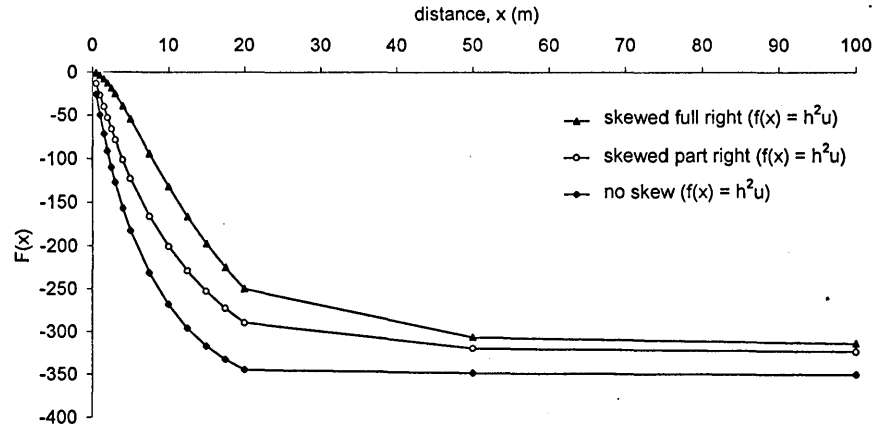

Figure 5.57 Graph showing longitudinal variation in F(x), cumulative discharge calculation in parabolic channel

Holley *et al.* (1972) and Lau and Krishnappen (1981) both showed through predictive models that the effects of using local or width average relationships to define φ have little, or no, effect on the predicted concentration distributions, other than in the near source region. However, this study has shown that when using the cumulative discharge model and the Generalised Method of Moments to estimate transverse

mixing coefficients, the correct stipulation of the relationship φ is essential. Values similar to that observed during experimentation were used during this check on the analysis method, except overall distances, which for this simulation, are extended to investigate far field effects.

5.5.3.2 Results from Generalised Method of Moments calculations

The calculations to verify the functioning of the Generalised Method of Moments resulted in the conclusions that the method can accurately account for effects of bank impingement. It is noted that the integral function φ needs careful evaluation. The calculations are also very sensitive to errors in concentration measurements. Calculations have been made using the Generalised Method of Moments, in cumulative discharge terms, for the measured data. The resulting variance versus F(x) plots are shown in Figure 5.58. Unlike Figure 5.47 and Figure 5.49, distance from apex I is not represented on the x-axis, in Figure 5.58 it is the modified distance, F(x), from injection for each case. Therefore, this figure should not be interpreted as representative of the variation in mixing coefficient with distance, as may be attempted with the previous plots.

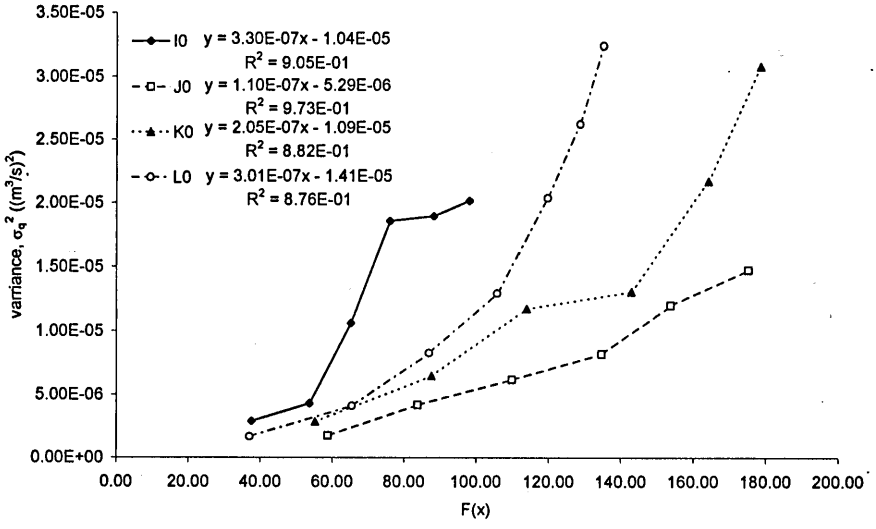

variance distance plots for surface injection cases

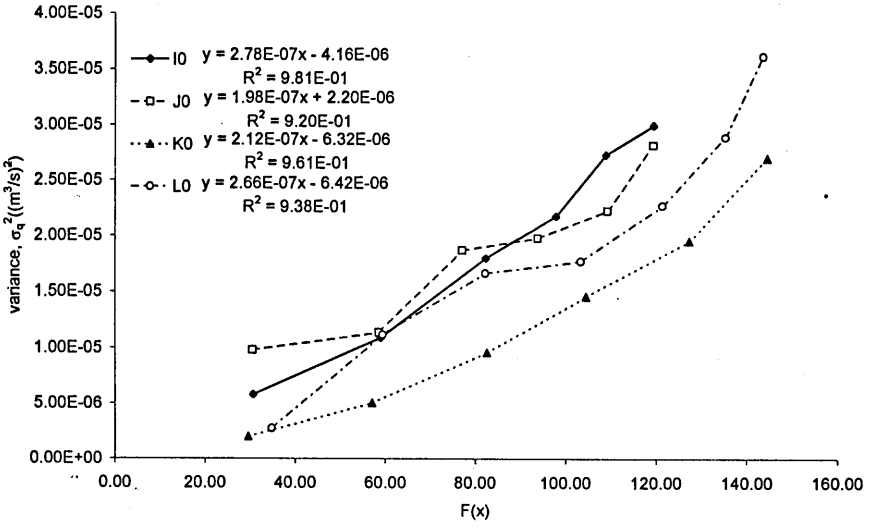

variance distance plots for bed injection cases

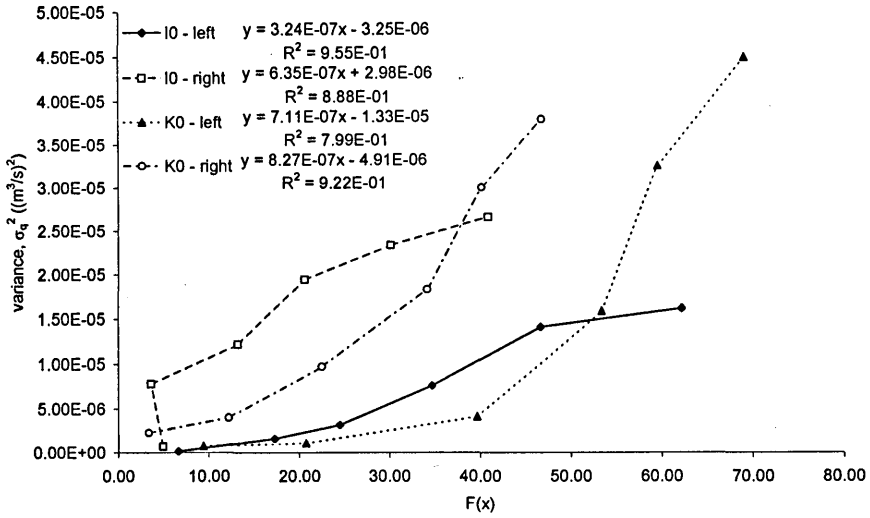

variance distance plots for side injection cases

Figure 5.58 Variance modified length factor plots, from Generalised Method of Moments calculations

There is a slight decrease in the quality of fit to a straight line shown in Figure 5.58, as compared to Figure 5.49. However, as demonstrated for idealised cases the Generalised Method of Moments calculation should take full account of bank impingement effects which were not accounted for in Figure 5.49. Assuming transverse mixing in this channel is predominately driven by secondary flows, and that these secondary flows vary over the measurement distances, it is questionable whether a straight line trend should be obtained.

5.6 Longitudinal Dispersion Data

In Section 2.9.5 the ADE and the ADZ models were introduced as the tools which form the basis for prediction of longitudinal dispersion and travel times in most river water quality models. These two models will be 'fitted' to the measured data using an optimisation procedure to obtain values for travel times, mixing coefficients and residence times. Details of the longitudinal dispersion tests performed using instantaneous injection and multiple monitoring points were given on Table 4.1.

5.6.1 Optimisation procedure

The following section gives details of the operation of the optimisation procedure which has been used to analyse the longitudinal mixing data. The purpose of the optimisation procedure is to remove variations in the prediction of travel time and dispersion parameters, resulting from inaccuracies in the calculation of variance, and location of first arrival times and centroids. A FORTRAN program was written to calculate the standard ADE and ADZ coefficients from a given pair of temporal concentration distributions, and then optimise the values. Further details on the development of this optimisation procedure and programming can be found, as applied to dispersion through manholes, in Dennis (2000).

The ADE and ADZ models require that mass be conserved. Therefore, it is necessary to mass balance the data. Mass balance principles assume a conservative tracer, constant river flow and measurement of the entire tracer mass at the upstream and downstream sites. To achieve mass balance the downstream data

points are each multiplied by a mass balance factor, calculated from the upstream tracer mass divided by the downstream tracer mass.

ADE and ADZ models require prediction of travel times, mixing coefficients and residence times. Calculations of area, centroid and variance were used to determine the standard coefficients, values of centroid travel time, $\bar{t}$, Dispersion coefficient, D_x, and reach time delay, τ .

These standard coefficients were then used in the ADE and ADZ equations to predict downstream concentration profiles from the upstream data. A measure of the goodness of fit between the profiles and the actual data, R_t^2, was calculated. The determination of R_t^2 is given by:

$$R_t^2 = 1 - \left[\frac{\sum_{t=1}^{n} (c_t - p_t)^2}{\sum_{t=1}^{n} c_t^2} \right] \qquad \text{Equation 5.7}$$

where c_t and p_t are the measured and predicted data values at time t.

Using this definition a prediction with an exact fit to the measured downstream data would give an R_t^2 value of one. A value of less than zero would indicate that the prediction fails to describe any part of the measured result.

The optimisation procedure for the ADE and ADZ equations was very similar and was included together in the same software. The programme performs a sequence of refining searches through combinations of parameters, travel time and dispersion coefficient values for the ADE, and travel time and time delay for the ADZ model, to determine the pair which give the optimum fit to the downstream concentration profile. A matrix system was employed to reduce the number of calculations required to reach the best fit solution. An 11 x 11 matrix was constructed, where the rows are headed by values of dispersion or time delay, and the columns are associated with travel times. For each combination of model parameters, a downstream profile is predicted from the upstream data, using the ADE or ADZ equation in the same way as the standard profiles were created. The R_t^2 value for this prediction is calculated, and assigned to the appropriate cell of the matrix. One hundred and twenty one combinations are required to fill the matrix.

The program sets maximum and minimum values for the pairs of parameters at the side of the matrix, based on the standard coefficients, and calculates step size and hence intermediate values along the matrix boundary. The range of the first matrix can be altered within the program. The best initial range depends on the data set. The optimisation procedure operates most efficiently if the pair of coefficients yielding the best fit prediction are close to the centre of the first matrix. In the discrete form of the ADZ model it is only possible to apply values of the time delay, τ , which are multiples of the data time step. The program has to ensure that all time delay values used along the matrix boundary are exact multiples of the time step.

At this stage the contents of the calculated optimisation matrix are examined, and the combination of coefficients giving the prediction with the best fit to the downstream data represented by the cell with the greatest R_t^2 value assigned to it is determined. A new matrix is then created by the programme which 'zooms in' towards the best fit coefficients. When the matrix cell representing the best fit coefficients is

not on the edge of the matrix, a new matrix is generated whose boundaries were defined by the coefficients immediately either side of the best fit values. This zooming procedure is shown diagrammatically in Figure 5.59. However, if the maximum R_t^2 is calculated to be on an edge of the matrix, then there is the possibility that a better downstream profile prediction might be achieved with coefficients out of the range of the current matrix. In this case a new matrix was generated which did not 'zoom in' further, but moved the matrix boundary coefficient values to translate the matrix, and, hence establish a maximum R_t^2 value within the boundaries.

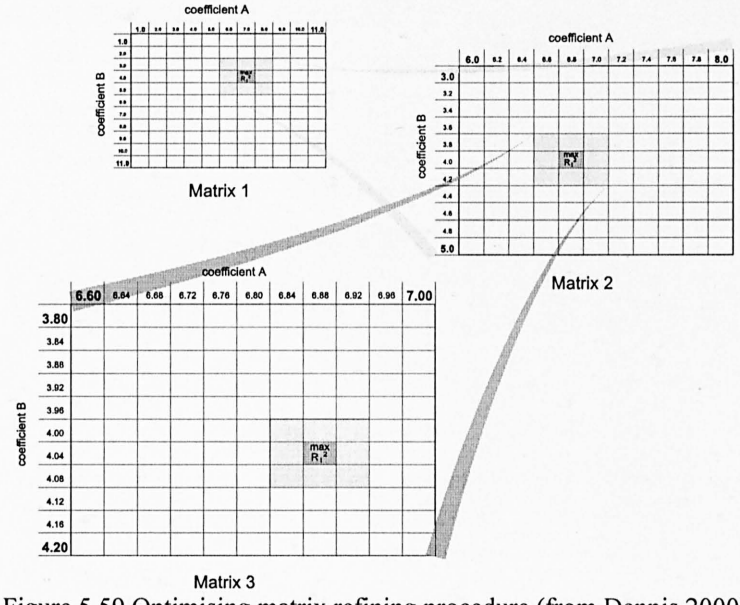

Figure 5.59 Optimising matrix refining procedure (from Dennis 2000)

The process of producing a new matrix was repeated until final resolution was reached. This was done by checking the step sizes between coefficients along the matrix edge each time a new matrix was generated. When the step size was reduced to pre-defined values for each coefficient, the ultimate best-fit prediction was reached. If the step between time delay values along the ADZ matrix became less than the data time step it was set as equal to the data time step, and the final resolution for time delay was said to have been reached.

The ultimate resolution of the refining matrix could be adjusted within the program, depending on requirements from the data being analysed. Settings used during analysis of this data are given in Table 5.14.

Coefficient	Accuracy
travel time steps	0.1 second
dispersion coefficient steps	0.0001 m^2/s
time delay steps	data time step (Δt) ~ 0.4 second

Table 5.14 Ultimate matrix resolution factors

When the optimum values have been found, an output file is created. Output information included the data filenames, measuring station distance and mass balance factor. The standard and optimised coefficients were given, along with the R_t^2 values for each case. The full data sets for time and

concentration were also output, enabling the upstream data, downstream data, standard and optimised predictions to be compared.

5.6.2 Checks on optimisation procedure

A number of factors and assumptions required careful consideration before analysis of the longitudinal dispersion data set could be attempting using the optimisation routine.

5.6.2.1 Mass balance

The upstream and downstream concentration distributions were mass balanced on the assumption of a conservative tracer. As with transverse mixing this stems from the fact that it is only the change and development of the plume shape which is critical in characterising mixing rates. Unlike the Generalised Method of Moments used in the analysis of the transverse data, the model fitting carried out here does not use normalisation by mass or even mass flux. However, the nature of the models is such that mass is conserved between the upstream trace and the downstream prediction. Therefore, it is logical that to obtain the optimum fit the downstream measured concentration profile must also have the same mass.

To investigate this, a set of data was selected and the mass balance factor between measured upstream and downstream data varied. Figure 5.60 shows the result of this investigation, clearly demonstrating that the optimum fit is only found when mass balance factors are correctly applied.

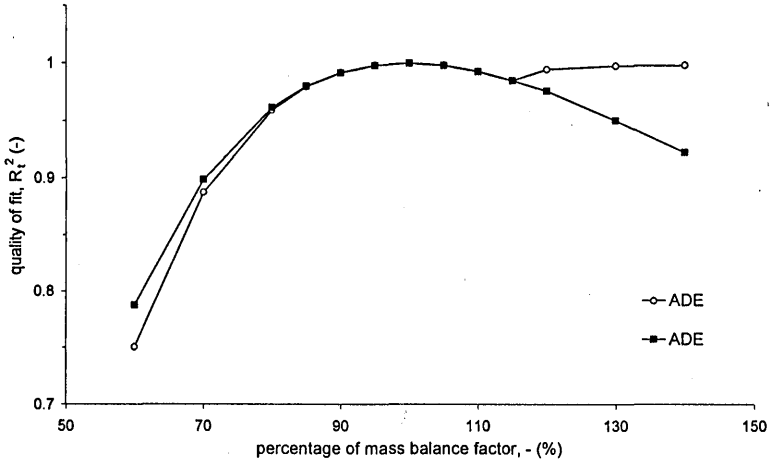

Figure 5.60 Effect of varying mass balance factor

5.6.2.2 Unique solution

To verify that the optimisation procedure was a reliable technique it was necessary to ensure that there was a unique pair of parameters which gave the best fit of prediction to the measured data. This was determined by examining the R_t^2 values over entire matrices, and ensuring that there was only one peak value. Figure 5.61 displays the results of this procedure for two matrices from optimisation of ADZ parameters. The base of the chart in the figure is composed of the travel time and time delay values used in the matrix. The three-dimensional surface represents the R_t^2 value for each travel time and time delay combination on the base. It is clear that there is a single peak, given by the parameter pairing providing the best fit.

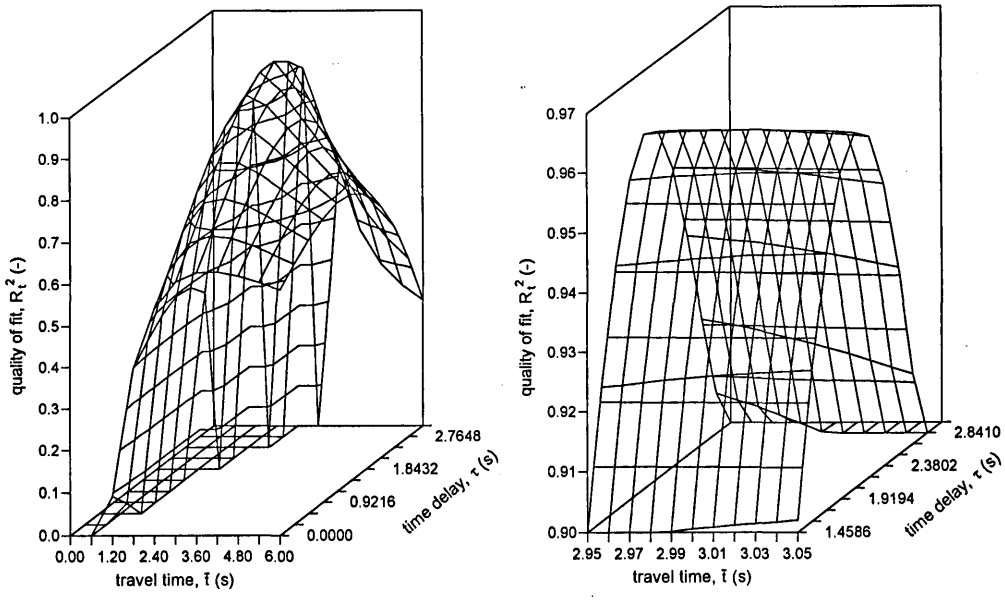

Figure 5.61 Surface plot representation of matrix optimisation results (from Dennis 2000)

5.6.2.3 Data cut off

In Section 4.4 the procedure for abstracting the data required for analysis from the logged data files was described. Within the procedure it was assumed that the concentration had returned to background when the variation in the peak concentration was less than 0.5 percent of the peak for 30 seconds. The effects on the optimisation procedure of using data cut off other than 0.5 percent were investigated. The results suggest that an accurate estimate of the coefficients could still be obtained with a cut off of up to 10 percent of the peak. However, it was decided to retain the 0.5 percent cut off for the sake of completeness and to ensure accurate background removal.

5.6.2.4 Noise

Noise was a problem with traditional methods as it had strong influences on location of start and end points and the calculation of variance. Some degree of noise may be present on the logged signal. This can be accommodated by the optimisation procedure. Assuming the noise is equally positive and negative about the true signal, then by minimising the errors the R_t^2 calculation will account for the effects. The majority of the data analysed had a level of noise associated with it, which led to variations in the non-optimised coefficients. The optimised values showed far less scatter.

5.6.2.5 Sampling rate

In section 3.4.2 the operating frequency of the fluorometers was given as 13 Hz, to cycle between reference, filters and readings, but with a final analogue output. Data logging was carried out at a rate greater than 13 Hz to ensure a complete record was obtained.

To minimise the run time of the optimisation program, the effects of data sampling were investigated. The large number of simulations required by the program meant that this could result in a considerable time saving. A test sample was investigated. The most sensitive sample was the one with the shortest over all

duration. The data set chosen was for the shortest reach, furthest upstream, at the highest flow rate. The data set had an initial sample rate of 50 Hz. The results of the analysis can be seen in Figure 5.62.

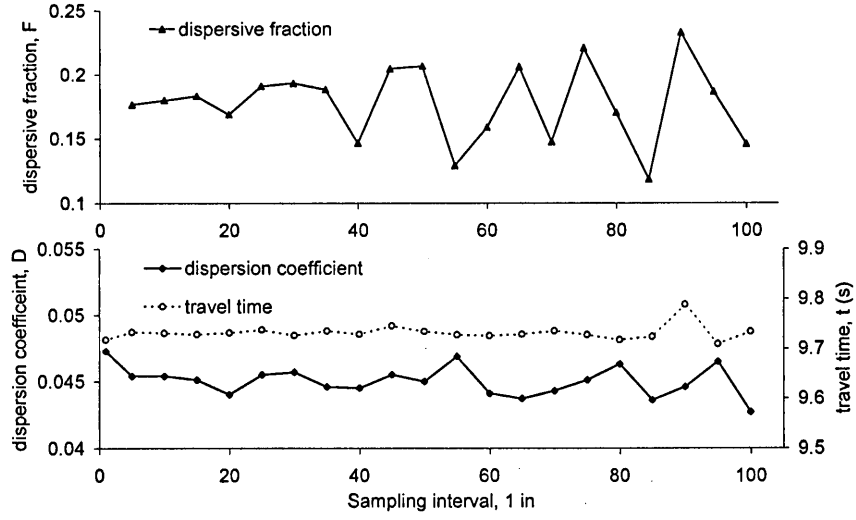

Figure 5.62 Results of sampling rate investigation

The ADE parameters of travel time and dispersion coefficient show remarkably little sensitivity to the sampling range which was investigated. However, the dispersive fraction, ADZ parameters, shows the introduction of error for a sample rate greater than 1 in 30. The dispersive fraction is calculated from travel time and reach time delay. To correctly solve the ADZ model, reach time delay must be a function of the time step of the data. This may lead to the errors in the dispersive fraction, rather than any loss of plume shape resolution. A maximum sampling rate of 1 in 20 for 50 Hz data, time step of 0.4 seconds was chosen based on this study.

5.6.2.6 Increasing concentration

When reviewing the results from analysing the past longitudinal dispersion data, it was noted that on some occasions the mass balanced downstream peak concentration was greater than the upstream peak concentration. Given the nature of mixing, it is physically impossible for the peak concentration to increase. However, the ADE element of the program managed to recreate the increasing concentration effect.

A situation requiring an increase in predicted peak concentration could have a number of sources, all relating to poor data. Truncated distributions, or traces including plume tail as background can result in an increase in peak concentration after mass balance. Alternatively, poor fluorometer location and incomplete cross sectional mixing can lead to the same apparent result. Any such data should be discounted. Given the mathematics involved it should be impossible to predict an increasing peak concentration, therefore some time was spent investigating the phenomena.

The principles of operation of ADE routing equation were shown graphically in Figure 2.27. Figure 5.63 represents the ADE prediction routine in a matrix form, for a zero dispersion case. The input distribution is given down the left-hand side, each discrete input time interval, $d\gamma$, is moved to downstream time by travel time (10) to t, but remains undispersed in a single time cell. Each time series column is then summed to give the predicted downstream distribution, across the bottom of the table.

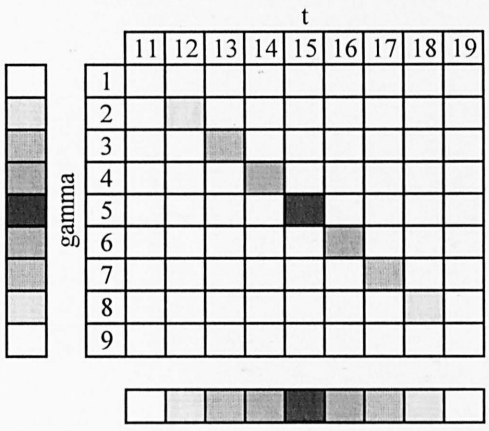

Figure 5.63 Matrix representation of ADE prediction

$$c_A(x_2,t) = \int_{\gamma=-\infty}^{\infty} \frac{c_A(x_1,\gamma)u}{\sqrt{4\pi D(\bar{t}_2-\bar{t}_1)}} \exp\left[-\frac{u^2(\bar{t}_2-\bar{t}_1-t+\gamma)^2}{4D(\bar{t}_2-\bar{t}_1)}\right] d\gamma \qquad \text{Equation 2.115}$$

For the zero dispersion situation, displayed in Figure 5.63, the exponential function of Equation 2.115 is equal to zero everywhere, except when $\bar{t}_2-\bar{t}_1-t+\gamma = 0$, along the diagonal of the matrix. In this case the distribution is moved downstream by an advection time delay, and not dispersed.

Error arises as the dispersion rate approaches zero, instead of each discrete $d\gamma$ block being advected and not spread, a very slight spread occurs. In this case an effect similar to that shown in Figure 5.64 occurs, in which the area bounded by the dashed line, representing the prediction, is greater than the area bounded by the solid line, advected and dispersed upstream data. Thus, it can be seen that it is through this special case that an increase in concentration can occur, that is, when advection is approaching zero and the travel time is a multiple of the time step, such that the prediction fits near the middle of a time step.

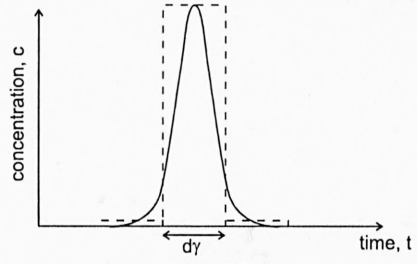

Figure 5.64 ADE error

An addition to the optimisation program was written to check for the occurrence of this condition. Ninety five percent of the area of a normal distribution is within four standard deviations. This spread may be found form the approximate solution:

$$4\sigma = 4\sqrt{2D_x(\bar{t}_2-\bar{t}_1)} \qquad \text{Equation 5.8}$$

By carrying out simulations with a sample set of data it was found that provided this spread was greater than twice the time step, an increase in concentration was not predicted. Therefore, it is possible to set a lower bound limit for the dispersion coefficient:

$$2d\gamma = 4\sqrt{2D_x\left(\bar{t}_2 - \bar{t}_1\right)}$$

$$D_{x\,min} = \left(\frac{d\gamma}{2}\right)^2 \Big/ 2\left(\bar{t}_2 - \bar{t}_1\right)$$

Equation 5.9

Inclusion of a statement to set D_x equal to zero and optimise only for travel time when D_x is less than or equal to D_{xmin}, prevents an increase in concentration being predicted.

5.6.3 Effect of optimisation

The overall improvement achieved by this optimisation technique was considerable for this data set. Figure 5.65 shows the improvement in fit for sample data with the ADE prediction.

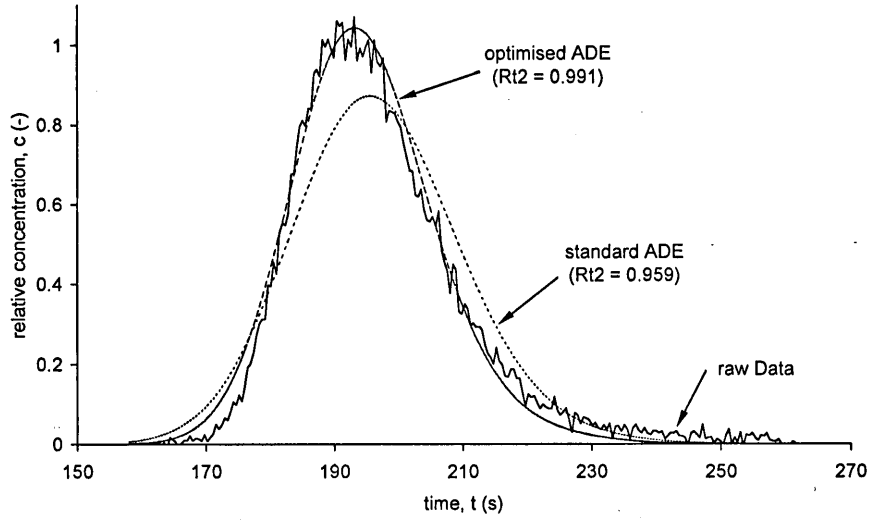

Figure 5.65 Example of improved fit through parameter optimisation (data from 25 l/s 1998, sections E-Q)

5.6.4 Longitudinal mixing analysis results

Having ascertained the reliability and validity of the optimisation procedure it is possible to process the data sets. Table 4.1 gave details of the flow rates, sampling points and potential reaches, for each of the channels. As stated 10-12 repeat injections were made for each flow case in each channel. All the results have been run through the splitting, background removal and calibration program and analysed using the optimisation procedure. As with the other data sets it is desirable to carry out some checks on the data quality before presenting the results.

As part of the optimisation it was necessary to mass balance the upstream and downstream traces for each reach, therefore, the mass balance factor was found. Using the mass balance factor and assuming conservative tracer it is possible to check the data. A summary of the mass balance figures is given in Table 5.15. The mass balance figures generally show good recovery of dye over all the reaches analysed, as can be seen in the table. However, occasional traces in each set showed wide variation in the mass balance. Poor mass balance figures suggest poor quality data such as incomplete traces, poor fluorometer location cross sectionally, or deviation from calibration.

Channel	Mean	S.D.
25 l/s 1998	0.9998	0.0242
25 l/s 1996	0.9989	0.0321
40 l/s	1.0169	0.0336
97l/s	1.0173	0.0601

Table 5.15 Summary mass balance figures for longitudinal dispersion tests

A number of factors resulted in reaches yielding coefficients with variation from the mean of their data set. In most cases, these results coincided with poor mass balance results, but not exclusively. Errors resulting in increasing concentration over the reach have been mentioned, reasons for the occurrence given, and a check for this added to the optimisation program. Some of the traces showed truncation of the data, primarily due to errors in starting or ending data logging. The presence of noise on some of the traces was mentioned, and the ability of the optimisation procedure to cope with a degree of noise noted. However, some traces show excessive distortion due to noise, or changes in noise level over the trace. Both of these result in uncharacteristic coefficient values. With some of the very early data there is a change in the fluorometer calibration over the testing period. This is not a problem for the analysis, because of the mass balance, although the mass balance figures may suggest error.

All the analysis results have been carefully checked for such errors, and any failures have been excluded from the results. The analysis results are presented in Figure 5.66 to Figure 5.74, showing dispersion coefficient and travel time for the ADE analysis and dispersive fraction for the ADZ analysis. The results of the analysis have been split into groupings, A-A is data from half meander cycle reaches, representing apex to apex. The quarter cycle reaches have been split into two, apex through to cross over (A-C) and cross over through to apex (C-A). This is in an attempt to investigate the variation in longitudinal mixing over the meander half cycle. For each point error bars plus and minus one standard deviation have been plotted to give an indication of the variation in values obtained for the 10-12 repeat injections and between reaches, after removal of erroneous results.

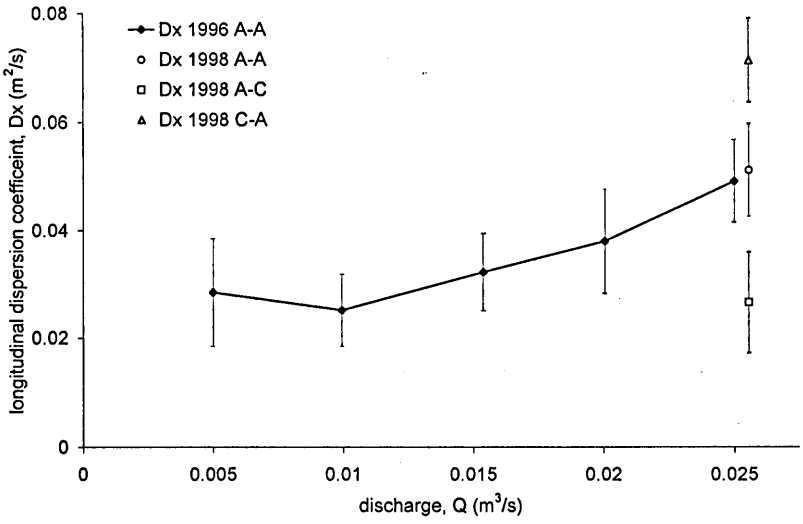

Figure 5.66 Variation in longitudinal dispersion coefficient with discharge for 25l/s channels

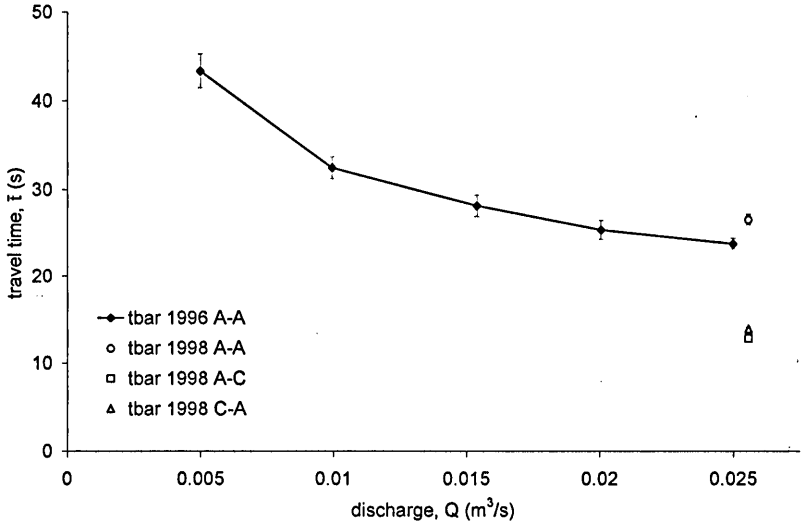

Figure 5.67 Variation in travel time (ADE) with discharge for 25l/s channels

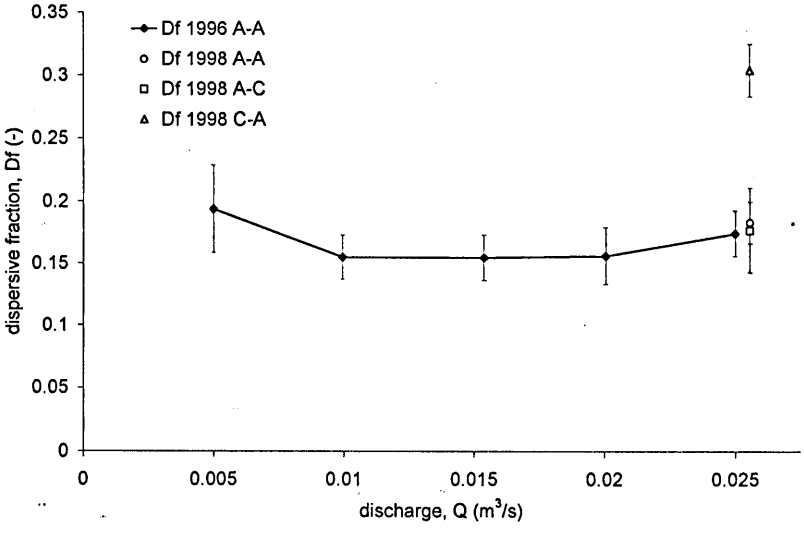

Figure 5.68 Variation in dispersive fraction with discharge for 25l/s channels

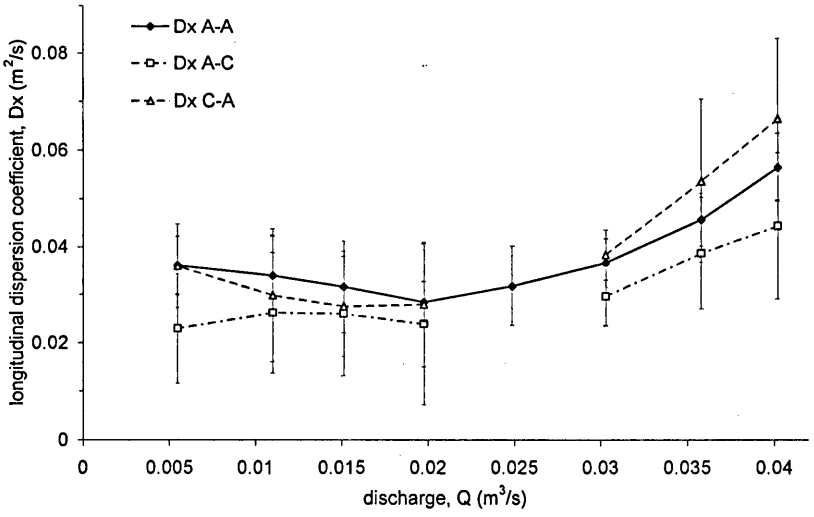

Figure 5.69 Variation in longitudinal dispersion coefficient with discharge for 40l/s channel

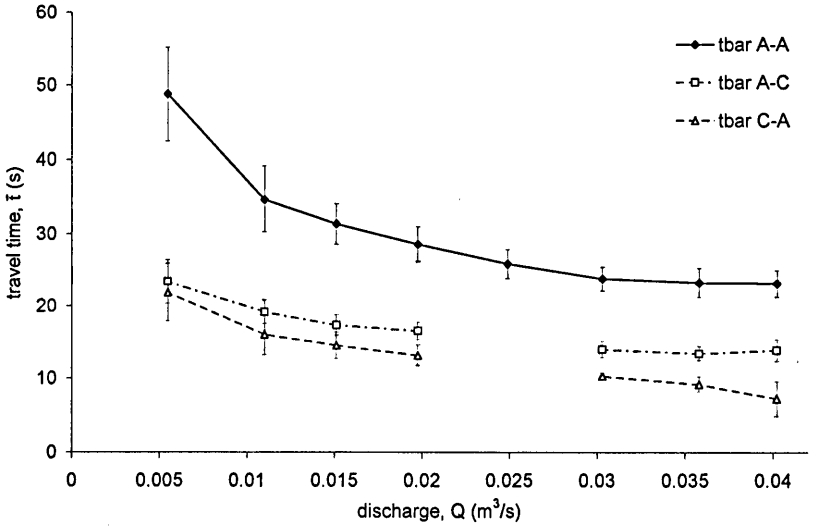

Figure 5.70 Variation in travel time (ADE) with discharge for 40l/s channel

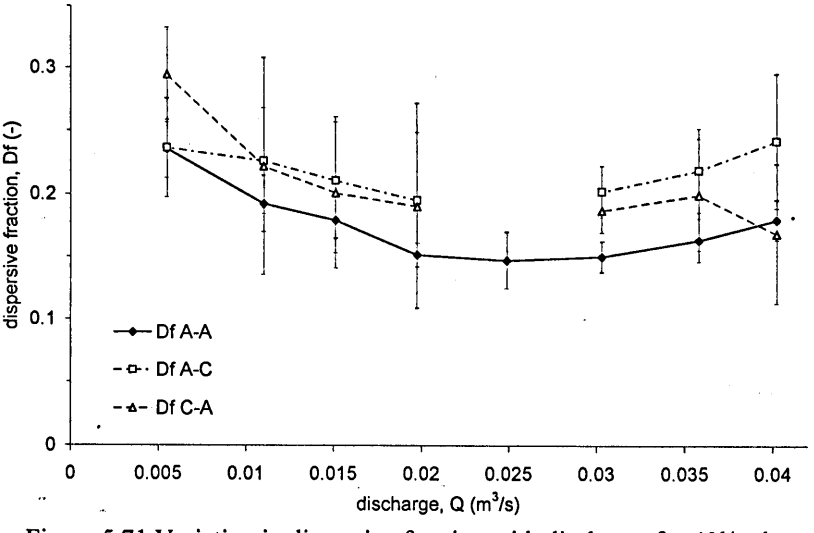

Figure 5.71 Variation in dispersive fraction with discharge for 40l/s channel

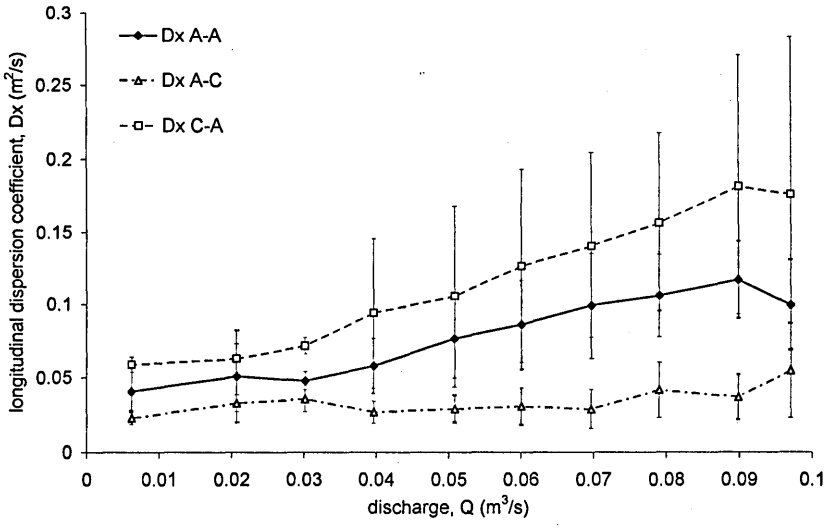

Figure 5.72 Variation in longitudinal dispersion coefficient with discharge for 97l/s channel

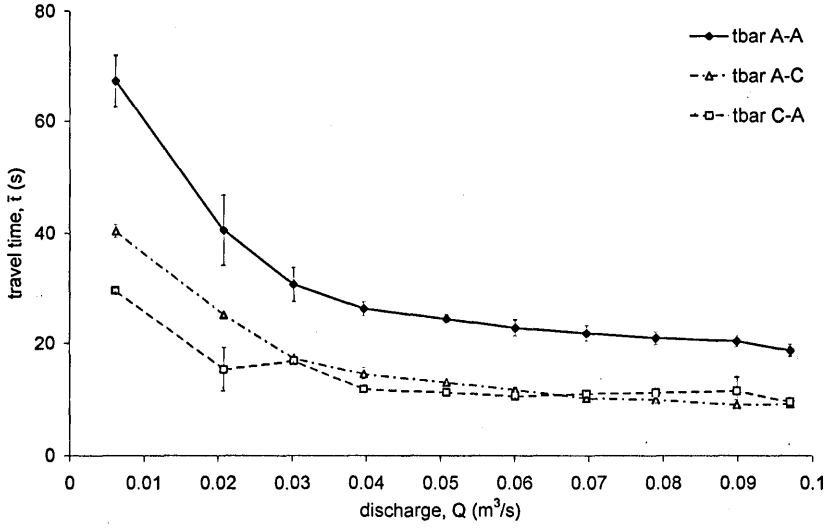

Figure 5.73 Variation in travel time (ADE) with discharge for 97l/s channel

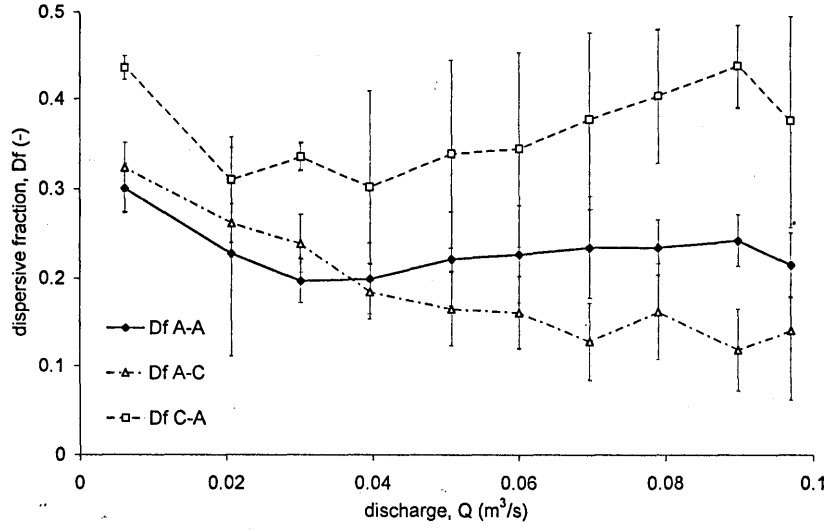

Figure 5.74 Variation in dispersive fraction with discharge for 97l/s channel

Chapter 6 Discussion

A detailed interpretation of the data and analysis which has been undertaken, with the aim of arriving at conclusions about the nature of mixing within the 'natural' channel forms that have been studied, are presented here. Methods of predicting mixing coefficients will also be investigated. Velocity and transverse mixing results are from the 25 l/s channel, longitudinal mixing results are based on this and three other channels formed at different flow rates.

6.1 Velocity Data

The velocity data which has been analysed and presented, provides an excellent indication of the overall flow field, and its change and development over the test meander half cycle. Variation in bed shear velocity, calculated by fitting log law profiles to the 'inner' region, and an indication of how turbulence levels vary over the test half meander cycle were presented. The data has been shown to be of good quality through mass balance and comparison tests.

Analysis has shown that simple equations are capable of accurately predicting cross sectional average velocities and transverse distributions of depth average velocity, although the equations over predict some of the finer effects associated with local bed features. The prediction of depth average velocities is valuable for establishing stream tube or cumulative discharge models. Prediction of cross section average bed shear velocity by simple equations was shown inaccurate, due to not accounting for the flow resistance of plan-form curvature. The transverse variation was shown to approximately relate to the local flow depth, with additional variation due to local features.

Through approximation of the channel plan-form geometry, it is possible to make accurate predictions of transverse velocities over the central region of the channel. This prediction is not limited to the fully developed stage, but can be extended to the build up and decay of the velocities with distance around and after a bend respectively. However, the predictions are only valid for the central region of the channel, and only predict a single circulation cell.

The simplicity, and quality of fit to measurements achieved by these predictions poses serious questions about the necessity to construct and develop complex computational fluid dynamics models for water quality simulations, associated with open channel flow in natural watercourses.

The turbulence data presented highlights the complexity of the information which is obtained, and the difficulty in establishing meaningful parameters from such measurements. The overall variation in turbulence levels has been illustrated. The turbulence has been shown to be a random isotropic function.

6.2 Transverse Dispersion

Transverse dye data have been presented. Visual inspection of the figures in Section 5.4 shows that the data is of excellent quality, with sufficient detail to provide a good description of transverse mixing over the half meander cycle. The mass flux balance calculations were inconclusive as proof of the quality of the data. However, the variance calculations undertaken are encouraging. All the work that has been

performed with the transverse tracer data is based on depth average values, because of the relative unimportance of vertical mixing, as presented in Section 2.7.

6.2.1 Evaluation of transverse mixing coefficients

Three methods, or approaches, to the calculation of variance of transverse dye concentration distributions were detailed in Section 5.5, and variance distance plot presented for each method. The methods lead to progressively more complex and scientific approaches to the evaluation of the transverse mixing coefficients.

6.2.1.1 Reach average coefficients

The traditional analysis to evaluate transverse mixing coefficients is based on the method of moments. Instead of calculating point by point values of mixing coefficient, a plot of variance against distance is produced and a best fit straight line found. It is possible to calculate the rate of transverse mixing from the gradient of such best fit straight lines. This method of evaluating mixing coefficients is valid, provided the rate of mixing is assumed constant over the measuring distance, or a reach average value of the mixing coefficient is required. Using a best fit straight line to a number of points on the variance distance relationship will smooth some of the errors associated with the evaluation of variance.

Each injection point has a set of six or seven measured tracer profiles below it. For each of these sets of profiles it is possible to calculate a mixing coefficient using the method above, an injection reach average coefficient. Injection reach average mixing coefficients have been calculated for the three methods of evaluating variance. The results of these calculations are shown in Figure 6.1. Each coefficient is plotted at mid-distance of its respective reach.

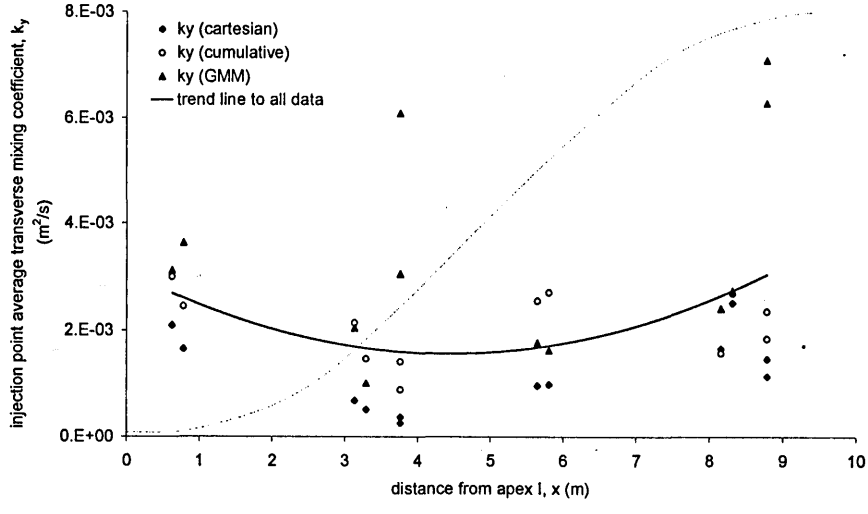

Figure 6.1 Injection reach average transverse mixing coefficients resulting from the three methods of evaluating variance

From Figure 6.1 it can be seen that there is a spread in the values of coefficients calculated by the different analysis methods. There is no pattern to the variation in values predicted by the different methods of evaluating variance. The three particularly high values are associated with the Generalised Method of Moments calculations for side injection cases.

Channel mean values of transverse mixing coefficient can be obtained by averaging the coefficients. These values can be non-dimensionalised by average flow depth and bed shear velocity, Table 6.1, such that they may be compared to the groupings presented in Table 2.3.

	Cartesian	Cumulative Discharge	GMM
k_y / hu*	0.786	1.315	1.300

Table 6.1 Normalised average transverse mixing coefficients

As can be seen in Table 6.1, the cumulative discharge and Generalised Method of Moments calculations yield very similar channel average values of transverse mixing coefficient, whilst the Cartesian approach results in a lower value. A value of 1.3 places this data set at the boundary between meandering and strongly curved channel classifications of Table 2.3.

The importance and dramatic impact that secondary currents can have on the rate of transverse mixing was shown in the review of background theory of transverse mixing. The velocity data, measurements and predictions have shown that strong secondary currents are present in this channel, and that they undergo a complete reversal over each half meander cycle.

Longitudinal variations in transverse mixing rate, attributable to secondary currents, have been investigated. Figure 6.1 shows a variation in the transverse mixing rate over the half meander cycle. There is a slight decrease in the reach average mixing coefficients around the straighter section of the channel, the values peak around the bend apex. This suggests a direct relation between mixing rate, secondary current and curvature. However, this trend is very slight for these injection reach average values of transverse mixing coefficient.

Given the rate of change of the secondary flow fields, compared to the reach length over which the mixing coefficients have been averaged, it is unsurprising that no strong relationship between mixing rate, secondary currents and curvature is highlighted. The transverse mixing coefficients should be evaluated over shorter distances to distinguish any such relationship.

6.2.1.2 Transverse mixing coefficients

Transverse mixing coefficients have been evaluated for successive pairings of variance below each injection point. Such calculation yields estimates of transverse mixing coefficient representative of the distance between pairs of measured cross sections, rather than reach average values for each injection point. The results of these calculations are given separately for each of the methods of evaluating variance.

Transverse mixing coefficients calculated from variances based on transverse distance are presented in Figure 6.2

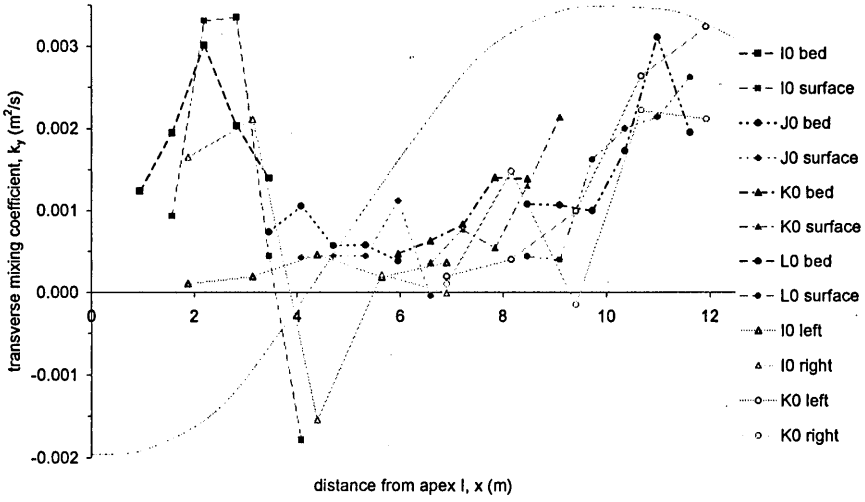

Figure 6.2 Transverse mixing coefficients from Cartesian variance calculations

Figure 6.2 shows a strong relation between mixing rate and degree of curvature, and therefore secondary flow. Although a trend is evident, little or no confidence is given to the values obtained using transverse distance because no account is made of channel curvature, net flow due to channel shape change, or bank side impingement.

It should be noted that Figure 6.2 includes negative mixing coefficients. This is due to a decrease in variance over the relevant reach, suggesting reduced transverse spread and increasing dye concentrations. This is a physical impossibility and confirms the unsuitability of this method for evaluation of transverse mixing in natural channels. The reasons for Cartesian based transverse variance calculations, potentially resulting in a decrease in variance, are a product of depth averaging. The effect was explained by Figure 2.8 when progressing from situation B to C. Increasing variance due to channel irregularities and depth averaging can be overcome by using cumulative discharge expressions.

Transverse mixing coefficients calculated from cumulative discharge based variances are presented in Figure 6.3.

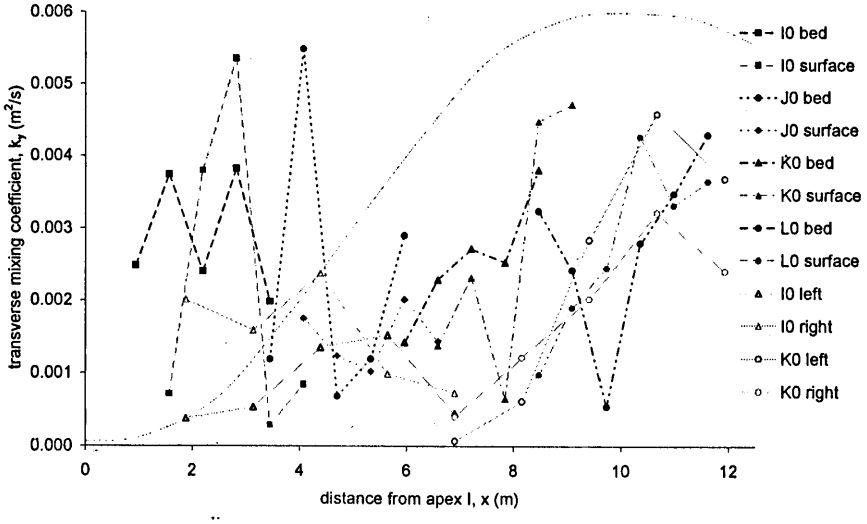

Figure 6.3 Transverse mixing coefficients from cumulative discharge variance calculations

Calculations of variance based on cumulative discharge should provide good estimates of transverse mixing coefficients as net transverse movements of water caused by curvature and shape variations are accommodated. The values of mixing coefficient in Figure 6.3 are all positive, suggesting that the natural channels effects have been correctly accounted for. However, the values of transverse mixing coefficients presented show a high level of noise, the trend between curvature, secondary flow and mixing rate is confused. The cumulative discharge approach does not account for the effects of bank side impingement, this may explain the variation in calculated values. It is difficult to isolate and remove the coefficient values affected by impingement because there is large error associated with locating the exact point where impingement first occurs, particularly with the irregular channel shape. Removal of all data where there is possible impingement would leave very few data points in Figure 6.3.

The Generalised Method of Moments may be used to account for the effects of bank side impingement on calculated variance. Transverse mixing coefficients calculated using the Generalised Method of Moments in cumulative discharge terms are presented in Figure 6.4.

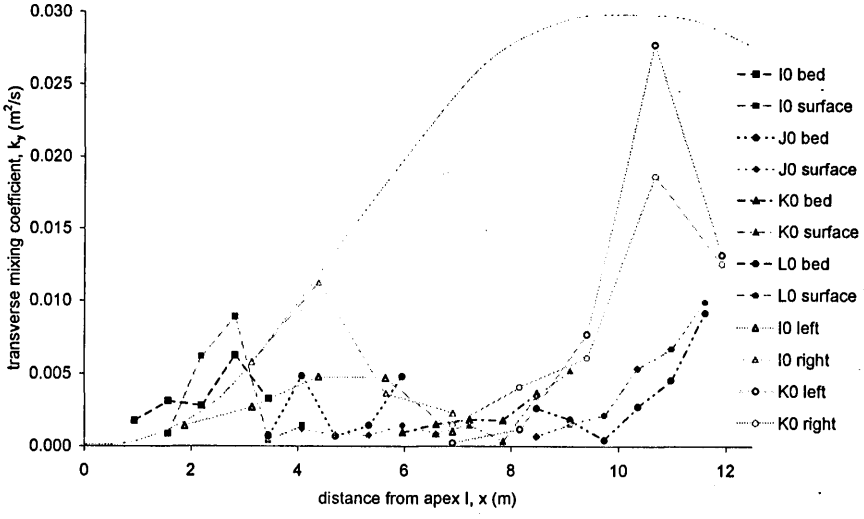

Figure 6.4 Transverse mixing coefficients from Generalised Method of Moments cumulative discharge calculations

Theoretically, only calculations utilising the Generalised Method of Moments correctly and fully account for the effects of curvature, net transverse flow, and bank impingement as shown in Section 5.5.3. Calculations using this method should provide the most accurate evaluation of transverse mixing coefficients. However, the data in Figure 6.4 appears inconclusive in establishing a link between the variation in mixing rate and channel curvature. Figure 6.4 is dominated by a few large values which were obtained for the side injection cases.

In the evaluation of the Generalised Method of Moments, Section 5.5.3.1, it was shown that the method is susceptible to errors when dealing with high concentration in the near bank vicinity. Such error is associated with the side injection cases. If these bank side injection cases are neglected, a strong relationship between curvature, secondary flow and mixing rate can be seen, as in Figure 6.5

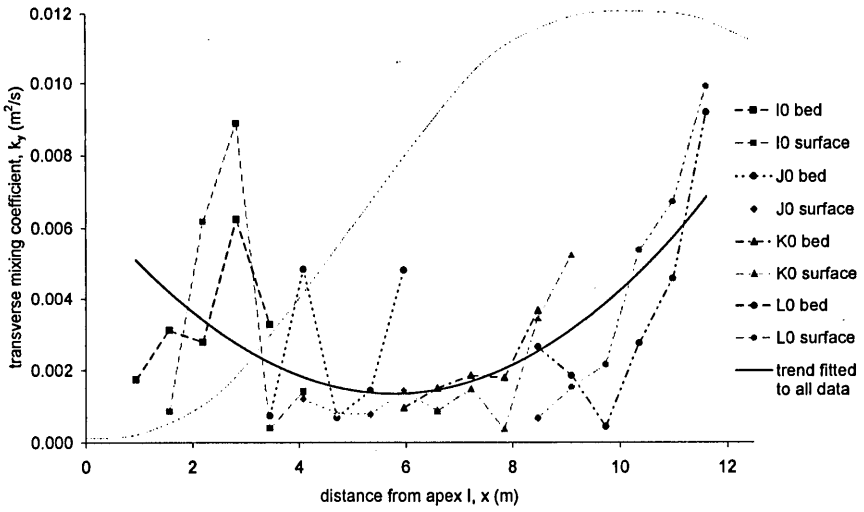

Figure 6.5 Transverse mixing coefficients from Generalised Method of Moments cumulative discharge calculations, centre line injection cases only

Through the Generalised Method of Moments it is possible to introduce factors to investigate transverse variations in the transverse mixing coefficient. However, this data is dominated by strong longitudinal variations. Transverse variations have therefore not been investigated.

6.3 Prediction of Transverse Mixing Coefficients

In the background theory review, two equations for the prediction of transverse mixing coefficients under strong secondary flow conditions were presented.

Fischer (1969) presented an expression to predict the rate of transverse mixing under fully developed secondary flow conditions. The equation was validated for an idealised laboratory channel, however, the application of the equation was shown to break down for a natural channel. Deficiencies in accounting for the build up and decay of secondary currents and approximation of channel geometries were given as the reasons for the inaccuracies in the prediction. The equation can be readily applied to the conditions in this study to make a prediction of the mixing coefficient. The required values can be found from Table 5.3 and a value of I can be found from the figures in Fischer (1969), or from the triple integration of the velocity distribution and a given vertical eddy diffusivity.

$$k_y = -\frac{u_x^2 h^3}{\kappa^5 r_c^2 u*} I \qquad \text{Equation 2.108}$$

$$k_y = -\frac{0.342^2 0.0735^3}{0.41^5 3.3^2 0.024}(-0.3) = 0.0046\ \text{m}^2/\text{s}$$

The derivation of Equation 2.108 was based on predicting a mixing coefficient under fully developed secondary flow conditions. Through comparison of this value with Figure 6.3 and Figure 6.5, it can be seen that this is an accurate assessment of the maximum transverse mixing coefficient found for the 25 l/s 1998 channel.

Fischer (1978) derived a 'tensor form of the bulk dispersion coefficient', Section 2.8.5, to predict transverse dispersion coefficients under uniform longitudinal and stepped transverse velocity profiles.

The equation enables the prediction of transverse mixing coefficients from idealised velocity distribution, assuming an eddy diffusivity. Fischer's final expression was:

$$k_y = \frac{(u_+ - u_-)^2 h^2}{48 e_z} + e_y \qquad \text{Equation 2.109}$$

The values required for the evaluation of this expression can be found in Table 5.3. Eddy diffusivity was taken as equal to 0.134du*, as found for transverse mixing in straight channels, Section 2.8.3. Table 5.3 gives two values of average magnitude of transverse velocities, fully developed maxima and a reach average value. From the maximum transverse velocity a transverse mixing coefficient of 0.0030 m^2/s is obtained. Assuming the reach average transverse velocity, a coefficient of 0.0013 m^2/s is found. Comparing these values with Figure 6.5 suggests that both the peak and average values are underestimated by this method. This is due to the approximation of the transverse velocity distribution as in Figure 2.18.

While the above equations provide simple methods of estimating transverse mixing rates they both have limitations. Fischer's (1969) equation provides an accurate estimate of the maximum transverse mixing coefficient, but is limited to prediction at fully developed conditions, occurring at large distance around bends. It is susceptible to errors in the evaluation of I or the triple integration of velocity distributions, and has been shown inaccurate against field data. Fischer (1978) allows for predictions at various locations, provided secondary flows can be predicted or have been measured, however, the final prediction is likely to be an underestimate.

6.3.1 Approximate solution

In Section 2.9.1.1 the numerical integration method of Chickwendu (1986) was presented. This method is a mathematical approximation which enables solution of the integration of velocity shear effects in the stream wise direction, such that estimates of mixing coefficients may be obtained. The method requires an estimation of eddy diffusivity. The approximation is similar to the trapezium, or Simpson rule, for integration. The solution can be readily programmed onto a spreadsheet.

6.3.1.1 Validation of method

Two known results will be considered to check the validity of the analytical method proposed by Chickwendu (1986).

In Section 2.7.1 an expression to evaluate the rate of vertical diffusion was derived. This was performed by assuming the eddy diffusivity equal to the eddy viscosity and the viscosity to vary linearly over the depth. Taking this with a log law distribution of the primary velocities over the vertical, the depth average vertical eddy diffusivity is given by 0.067du* (assuming $\kappa = 0.41$). In Section 2.9, Elder (1959) made use of this, and the vertical log law distribution of primary velocities, to derive an expression for longitudinal mixing coefficient, assuming $\kappa = 0.41$,

$$D_x = 5.93 h u^* \qquad \text{Equation 2.110}$$

Assuming values from Table 5.3, Elder's (1959) solution yields a value for longitudinal mixing of 0.0105 m^2/s. Using Chickwendu's (1986) solution with 100 zones, a zone thickness of 1mm, and making the same assumptions as Elder (1959) a value of 0.0105 is also obtained for D_x.

Chickwendu's (1986) solution was derived to provide estimates of longitudinal mixing coefficients. However, there is no reason why the solution cannot be adapted for transverse mixing situations, since the solution yields estimates of dispersion coefficient in the direction of a given velocity profile over the vertical. The solution is compared with that of Fischer (1978), used above, to check this assumption. The same input parameters and stepped velocity profile are used in both methods. The method of Chickwendu (1986) was again run with 100 zones. For the average and fully developed transverse velocities both methods yield identical results.

Through these two validation tests, it has been shown that the method of Chickwendu (1986) yields results within one percent accuracy of the analytical solutions. This accuracy was achieved using a 100 zone approximation. The checks also shows that the solution can be applied to situations of longitudinal or transverse mixing. Pearson (1999) used the solution to estimate transverse mixing coefficients under waves.

6.3.2 Predicting transverse mixing coefficients

Once a value of eddy viscosity has been assumed, it is possible to work from predictions of vertical distributions of transverse velocity to estimates of transverse mixing coefficient using the mathematical method of Chickwendu (1986). Predictions of the build up and decay of transverse velocities over the meander cycle have been made using the equations of Rozovskii (1957). It is therefore possible to make theoretical estimates of the variation in the transverse mixing.

Values for a number of potentially variable factors must be stipulated before predictions are made. The build up and decay of secondary velocities were predicted from the estimated fully developed transverse velocities, therefore, all velocities are based on the average parameters assumed for the fully developed conditions. Although the analysis method of Chickwendu (1986) allows some parameters to be varied, initial predictions were made using reach and depth average values, as given in Table 5.3. Eddy diffusivity was set to the value found during transverse mixing experiments in straight open channel flow, 0.134du*, Section 2.8.3. The bed shear velocity calculated from velocity measurements was used in preference to the value found from Equation 2.3 because of associated inaccuracies.

Figure 6.6 shows the predicted mixing coefficients as a function of longitudinal distance. It also shows the mixing coefficients found from the measured concentration profiles using the Generalised Method of Moments in cumulative discharge terms for the bed and surface centre line injection cases. Side injection cases have not been included because of potential errors associated with the near bank analysis, and because the predicted secondary velocities are only valid over the central region of the channel.

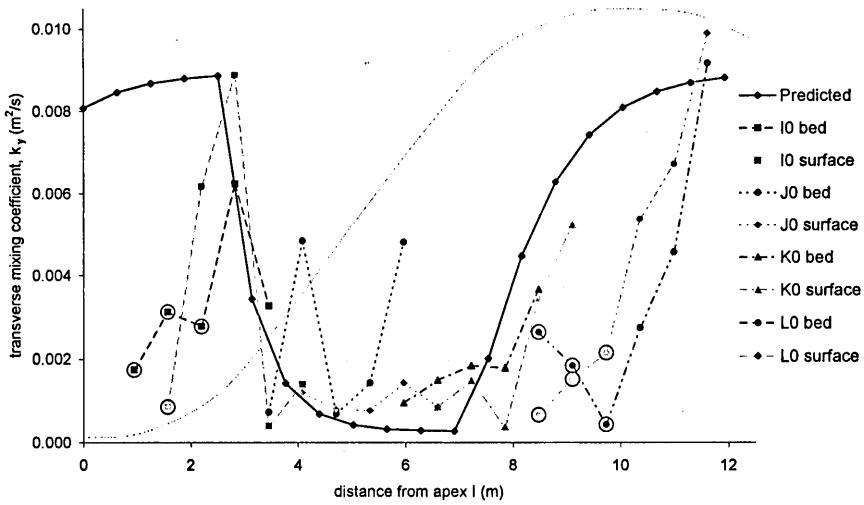

Figure 6.6 Comparison of predicted and measured values of transverse mixing coefficient

Figure 6.6 shows good agreement between the measured and predicted values, in terms of both magnitude and variation. Two main discrepancies in the fit can be seen, the near source mixing rate calculated from the dye measurements appears to be underestimated in the region of strong curvature (circled points) and the prediction to overestimate the decay / growth rates of coefficients around the bend straight interface regions. The errors in predicted mixing rate around the bend straight interfaces probably stem from the error in magnitude of predicted secondary velocities, resulting from the approximation of the plan form geometry. The error is small.

The injection cases which coincide with the predicted high mixing coefficients have a tendency to show an initial underestimate in the predicted mixing coefficient (circled points). This effect is analogous to the situation in longitudinal mixing where an initially skewed distribution may be obtained due to an imbalance in shear and diffusion processes, and incomplete cross sectional mixing, Section 2.9.1. In the transverse mixing experiments dye originates from a point source, rather than a vertical line source, as is assumed with the depth average form of this analysis. The dye will initially only experience local mixing processes. Therefore, the coefficient found from measurements in the near source region will be representative of the local mixing processes, predominately eddy diffusivity. Assuming eddy diffusion is uniform and isotropic (supported by the turbulence measurements), the dye will experience this degree of mixing in all locations, no matter how vertically or transversally mixed it becomes. This can be seen in Figure 6.6 where the initial underestimates are of the same order as the mixing rate found for the straighter channel section. Once the dye becomes sufficiently vertically mixed to experience the differential advection effects due to the secondary currents, the mixing rate dramatically increases because of strong shearing effects. This suggests that the data prior to vertically well mixed conditions is invalid.

The very high point values of transverse mixing coefficient which were obtained for the side injection cases at section K, Figure 6.4, can also be explained by vertical mixing effects, considering the growth of secondary circulation cell. Velocities at section K (measured Figure 5.2, and predicted Figure 5.13) show low secondary currents. The measured velocities show a very confused pattern of secondary flows, as

longitudinal distance increases from section K, the centre line injection cases at section K experience developing secondary currents. However, the side injection cases remain dominated by eddy diffusivity for a longer period, until the secondary circulation cell grows sufficiently to effect the channel edges and the dye. When it does, the circulation will suddenly cause dramatic mass movement of the dye across the surface, or the bed, of the channel, depending on the direction of circulation and injection side. This mass movement will result in a sudden change in variance, and hence high point values of mixing rates. This argument depends on the nature of the growth of secondary circulation.

The above explanation of why high point values of mixing rates result from the side injection cases at section K, requires secondary currents to propagate somewhere in the channel centre. It has often been suggested, for example Knight (1998), that for a series of alternating bends decaying circulation cells occur at the outside bank, while the new opposing circulation cells propagate at the inner bank, such that two counter rotating cells may be seen in the region of the crossover between the two bends. Unfortunately, the velocity data collected here is inconclusive in establishing the nature of the growth and decay of the circulation cells as it has insufficient longitudinal spatial resolution.

6.3.2.1 Sensitivity of predicted coefficients

Reach average values were assumed for the predictions of transverse mixing coefficients, and a good fit to measured values obtained. However, it is interesting to investigate the sensitivity of the solution to variation in the value assumed for eddy diffusivity. Figure 6.7 and Figure 6.8 show the effects of such variation.

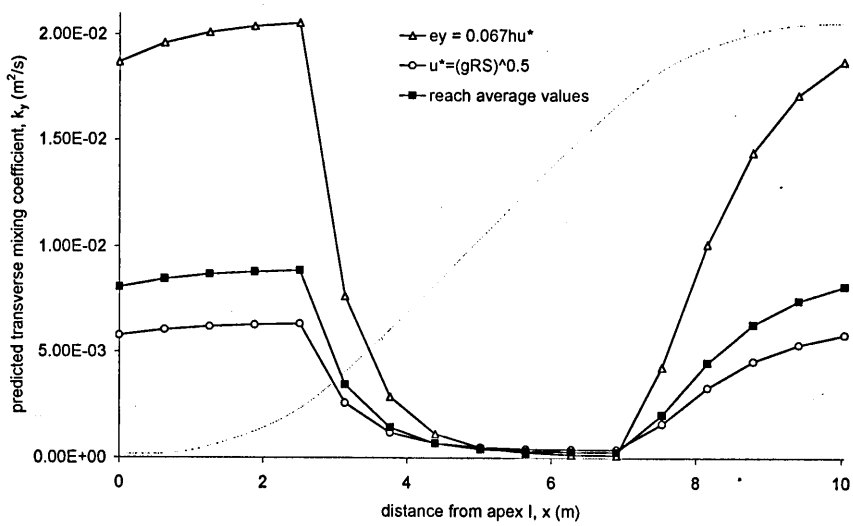

Figure 6.7 Sensitivity of predicted transverse mixing coefficients to input eddy diffusivity, longitudinally

Three sets of predictions are shown in Figure 6.7, the reach average value as used for the comparison above, a situation assuming that the eddy diffusivity is equal to the theoretical vertical rate, decreased diffusivity, and using the value of predicted bed shear velocity, increased diffusivity.

From Figure 6.7, it can be seen that the changes in the eddy diffusivity have little effect on the predicted mixing coefficient over the straight section where the mixing is dominated by eddy diffusivity. However, there is a significant effect on the predicted mixing coefficient where the shear effects are large. Figure

6.7 shows that decreasing eddy diffusivity results in an increased rate of shear dispersion. This is theoretically correct, when the diffusion rate is low the dye will remain in each distinct velocity regime longer, thus promoting the effects of differential advection or shear.

Figure 6.8 further highlights the nature of the relationship between eddy diffusivity and predicted mixing coefficients in the presence of strong secondary currents. If a very low estimate of diffusivity is used, the resulting predicted mixing coefficient will be greatly over estimated.

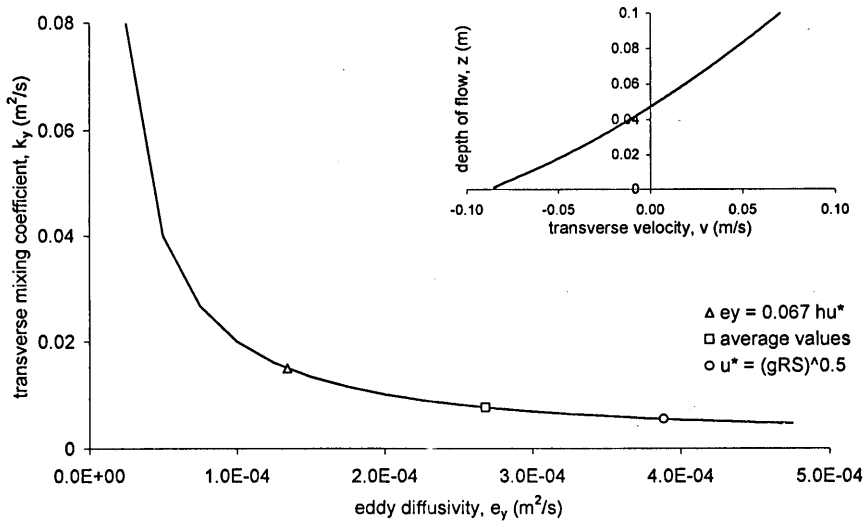

Figure 6.8 Sensitivity study of predicted transverse mixing coefficient to input eddy diffusivity, for the predicted fully developed transverse velocities

The method of Chickwendu (1986) allows for variation in diffusivity over the cross section. However, the investigation of variation in turbulence levels, Section 5.3, led to no clear reasoning to support variation in the rate of diffusivity over the cross section. The turbulence data suggests a longitudinal change in the level of turbulence and, therefore, diffusivity. The nature of the variation suggests reduced diffusivity over the curved section, increasing shear effects, alternatively, an increase in the diffusion rate in the straight section. It is not possible to directly calculate the eddy diffusivity from the turbulence information. Given these considerations, and the quality of the fit obtained in Figure 6.6, it is concluded that the variation in diffusivity, which may be inferred from the turbulence information, is inconsequential.

6.3.3 Comparison of predictions with published values of transverse mixing coefficient

The above investigation shows that accurate prediction of values and variation in transverse mixing coefficient in the presence of plan form curvature can be made. This is done using the method of Chickwendu (1986), in conjunction with the equations of Rozovskii (1957), and assuming transverse eddy diffusivity can be predicted by the equation found for two-dimensional plain turbulent open channel. This predictive method should be checked against other published values of transverse mixing coefficient. Three sources of published values of transverse mixing coefficient presented in Section 2.8 are applicable, Fischer (1969), Chang (1971), and Krishnappen and Lau (1977).

6.3.3.1 Fischer (1969)

Fischer (1969) presents transverse coefficients and channel data for a constant radius of curvature laboratory channel and from a field study of a long bend in the Missouri River.

Figure 6.9 shows the measured and predicted values of transverse mixing coefficient from Fischer (1969) laboratory study together with the predicted coefficients from the new method.

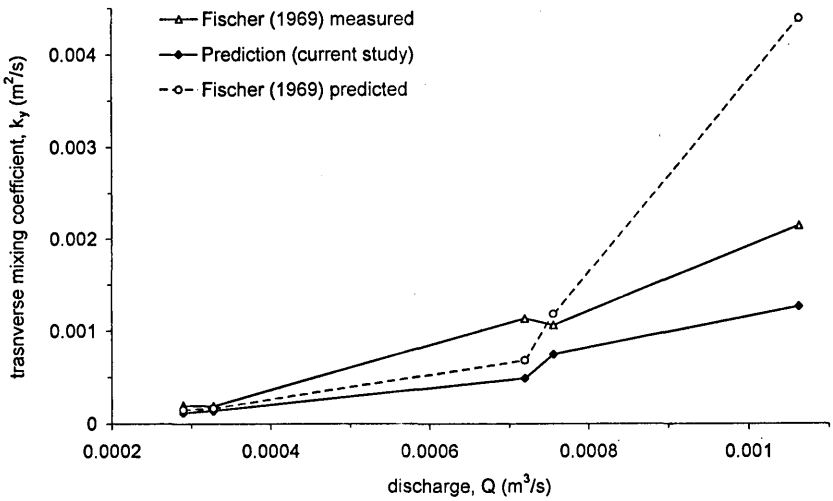

Figure 6.9 Comparison of measured and predicted values of laboratory study from Fischer (1969) with values predicted using the new method

Fischer's (1969) equation approximately predicts the measured values, but shows increasing error with increasing discharge. The new predictive method shows as good a fit to the measured values at low discharges, and does not show the same level of error at high discharges. To make these new predictions, fully developed secondary currents were assumed. It is surprising that the two predictions are not more similar, given that they both evaluate the integration of shear effects of fully developed secondary flows as predicted by the equations of Rozovskii (1957). It appears that some of the approximations assumed by Fischer in his expression of the solution lead to errors.

Table 6.2 shows the measured and predicted values of transverse mixing coefficient from Fischer (1969) field study, together with the predicted coefficients from the new method. This table clearly shows the deficiencies of Fischer's (1969) expression, and the ability of the new method to accurately predict the measured transverse mixing coefficient from the observed channel maximum properties.

values of channel property used to make predictions	k_y Fischer (1969) prediction m^2/s	k_y Fischer (1969) measured m^2/s	current k_y prediction m^2/s
average	0.002	0.120	0.028
maximum	0.274		0.114

Table 6.2 Comparison of measure and predicted values of field study from Fischer (1969) with values predicted using new method

6.3.3.2 Chang (1971)

In Section 2.8.5 transverse mixing coefficients found by Chang (1971) through fitting a stream tube model to measurements and integration of velocities distributions were presented, together with channel

data. However, the values and variation in coefficient presented by Chang (1971) were questioned, therefore, only average values will be compared.

Chang (1971) stream tube simulation k_y (m^2/s)	Chang (1971) integration of velocities, k_y (m^2/s)	new predictions k_y (m^2/s)
0.0106	0.0046	0.0017

Table 6.3 Comparison of values of transverse mixing coefficient from Chang (1971) and current predictive method

Comparison of the values in Table 6.3 suggests that the new method under predicts the transverse mixing coefficient. However, the methods used by Chang (1971) have already been seriously questioned in Section 2.8.5, so little weight is given to this result.

6.3.3.3 Krishnappen and Lau (1977)

Krishnappen and Lau (1977) present results from a study investigating the relationship between transverse mixing rate and channel meander amplitude. They used the Generalised Method of Moments in a Cartesian form to provide estimates of transverse mixing coefficient. In their analysis, the dependence of the transverse mixing rate on different parameters was investigated. Four different relationships were investigated. Krishnappen and Lau (1977) reach no conclusion as to the correct relationship for the variation in mixing rate. Four values of transverse mixing coefficient were presented for each plan form configuration studied. These four sets of values are represented by the dashed lines in Figure 6.10.

It can be seen from Figure 6.10 that the new predictive method accurately predicts the values of transverse mixing coefficient.

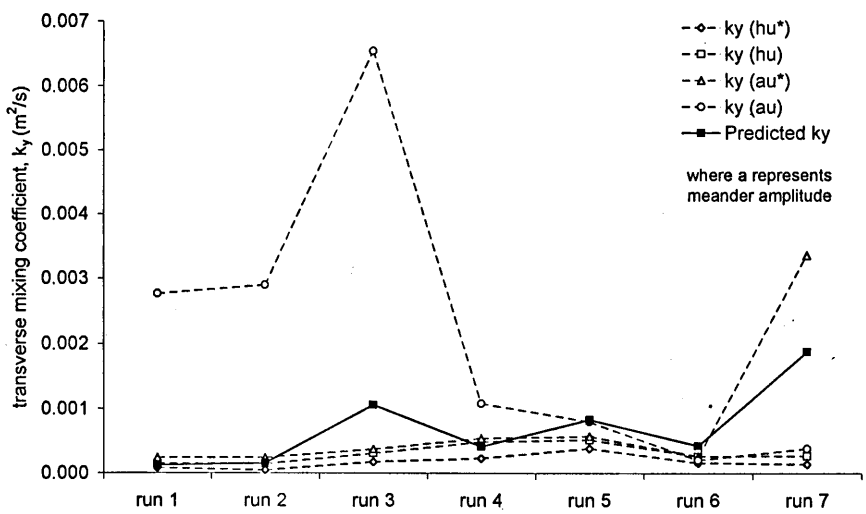

Figure 6.10 Comparison of values of transverse mixing coefficient from Krishnappen and Lau (1977) and new predictive method

6.4 *Longitudinal Dispersion*

A number of different aspects of longitudinal mixing can be investigated from the longitudinal dispersion data which has been analysed. Channel details, flow rates and measurement sections are given in Table

4.1. Details and validity of the analysis procedure, benefits of the optimisation procedure, and results were given in Section 5.6.

6.4.1 Trends with discharge

It is possible to investigate the trend with discharge of different longitudinal mixing parameters for this data set.

6.4.1.1 Travel time

Travel time is a coefficient required by both the ADE and ADZ models. However, the values which are obtained for the two models are not identical. The travel time providing the optimum fit to the ADZ model is always greater than that of the ADE model. The difference is constant at four percent. As mentioned in Section 2.9.5, the ADE model can not predict an increase in skewness, whilst the ADZ model does. It is believed that the skewness results in the difference in travel times.

Both ADE and ADZ travel times follow exactly the same trends with discharge. Figure 5.67, Figure 5.70 and Figure 5.73 show the travel times from the ADE model for the 25, 40 and 97 l/s channels respectively. Each of these figures shows the same trend between travel time and discharge. For engineering purposes, it is likely that travel time predictions would be made from reach lengths and velocity estimates. Velocity estimates may be obtained from discharge and cross sectional area measurements or flow resistance equations. However, such estimates are likely to be made for bank full conditions. This leaves the requirement of predicting the variation in velocity with discharge.

Figure 6.11 shows the velocity discharge relationships that were obtained for these three channels. Velocities were calculated from the optimised ADE travel times for the half cycle reach cases.

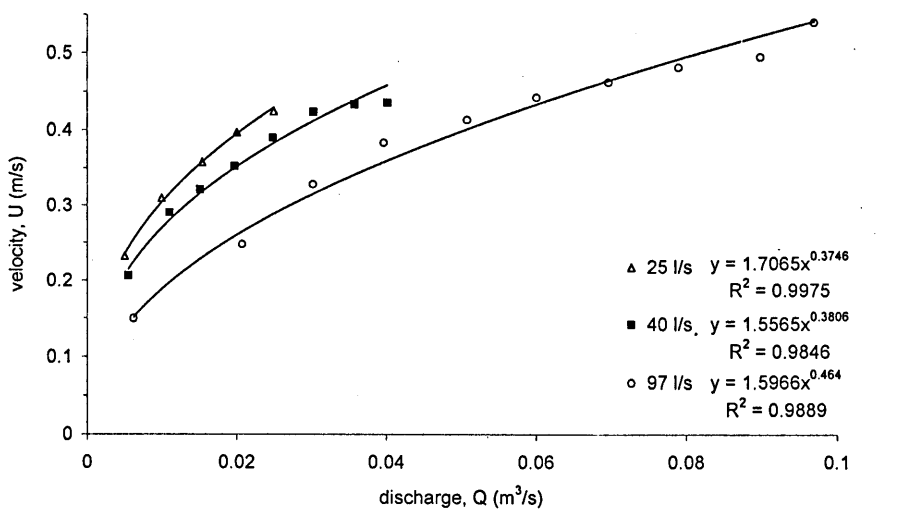

Figure 6.11 Velocity discharge relationship for the three channel configurations

The three curves in Figure 6.11 follow similar relationships between discharge and velocity, velocity approximately proportional to discharge to the power of one half. Relationships of this type have been suggested and used by the U.K. Environment Agency, however, no theoretical reason for the relationship has been suggested.

Normalisation of the velocities and discharges by the respective bank-full, or channel forming, values results in the curve shown in Figure 6.12.

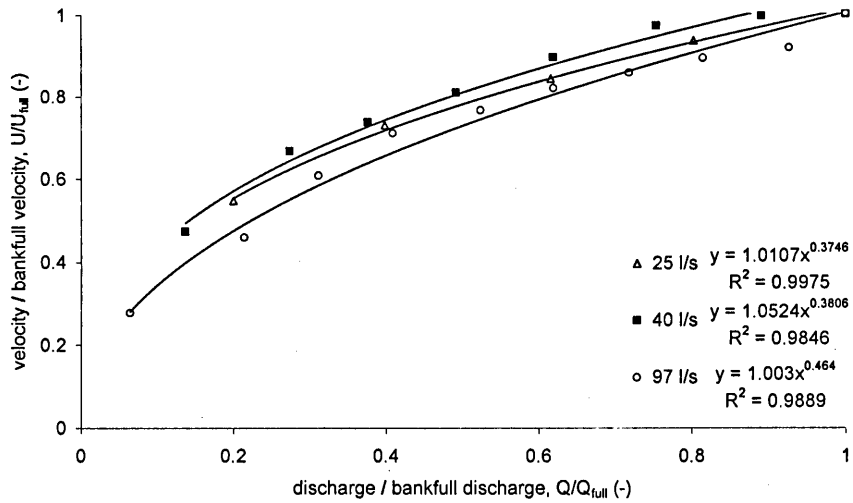

Figure 6.12 Normalised velocity discharge relationship for the three channel configurations

A single relationship can be used to describe the variation in velocity with discharge. This suggests that the variation of velocity with discharge is a universal function for the channels studied, related to the bank full properties. This suggests that the channel forming flow rate is vital in defining the variation and magnitude of the flow regime at less than bank full flow conditions.

6.4.1.2 Longitudinal dispersion coefficient

Unlike the relationship between discharge and velocity, and hence travel time, little work and no theory exists to quantify or suggest the trend of the relationship between discharge and longitudinal dispersion coefficient. The four data sets reported by Rutherford (1994), presented in Figure 2.23, and trends such as shown in Figure 2.22 and Figure 2.30, have led to attempts to derive predictive equations linking dispersion coefficient and discharge, such as in Section 2.9.7. These equations suggest that there is an overall increase in the rate of longitudinal mixing with discharge, and that the relationship is of a power form.

The relationship between discharge and dispersion coefficient for the three channels tested here is shown, Figure 5.66 for the 25 l/s channel, Figure 5.69 for the 40 l/s and Figure 5.72 for the 97 l/s channel. The 25 l/s and 40 l/s cases suggest an initial slight decrease, or plateau in the mixing rate, followed by an increase near bank full conditions. The 97 l/s case suggests an overall linear increase in the rate of longitudinal mixing. However, plotting the three channel cases together, as in Figure 6.13, for the half cycle reach cases, suggests that the overall trend with discharge of the three cases may be similar. A strong linear trend is shown, as characterised by the R^2 value of 0.9. This is different from the plots referenced in Section 2.9, as these all suggest a power relationship with a factor of around 0.5. A power relationship has also been fitted on Figure 6.13, the power is again around 0.5, but the data fit is poor, regression factor of 0.7.

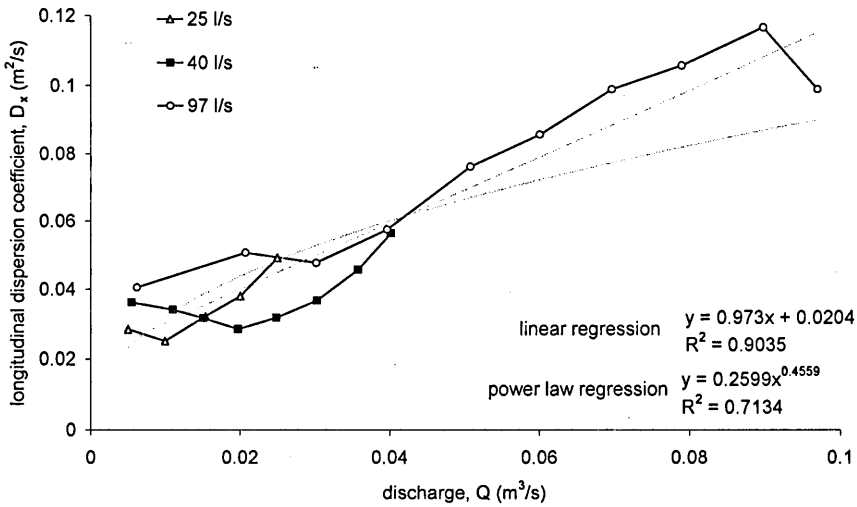

Figure 6.13 Variation in longitudinal mixing rate with discharge for the three channel cases

The overall increase in mixing rate may be due to increasing shear effects as the discharge increases because of more developed primary velocity profiles. Unfortunately, there is no velocity data available for any of the flow cases other than the 25 l/s bank full case studied in 1998 and presented in Section 5.2. Therefore, it is not possible to verify this hypothesis, or suggest how the velocity profiles develop with discharge. Equation 2.130, from Smith (1983) may be used suggest how the velocity profile changes, however there is no experimental check on the results of the equation.

6.4.1.3 Normalised longitudinal dispersion coefficient

In Section 2.8 and Section 2.9 normalisation of mixing coefficients by different factors was investigated. The most promising of these was the use of bed shear stress and hydraulic radius. The longitudinal dispersion coefficients from Figure 6.13 have been normalised by these factors and the results presented in Figure 6.14.

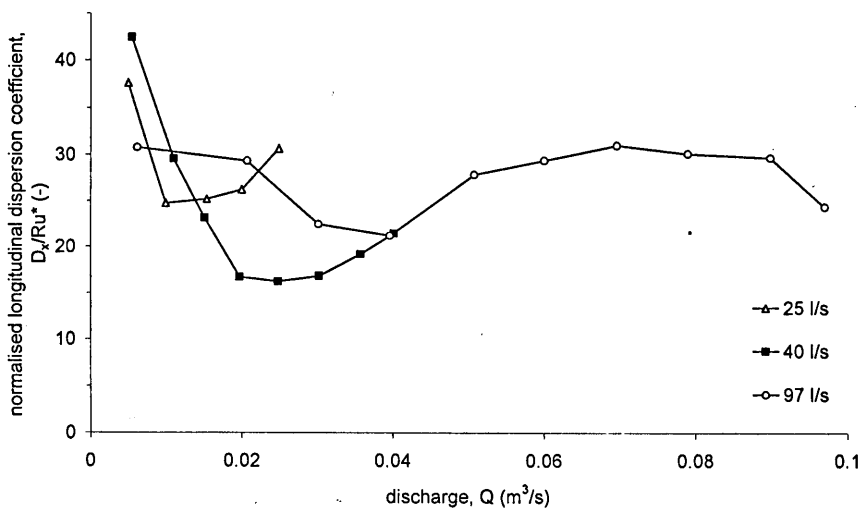

Figure 6.14 Variation in normalised longitudinal dispersion coefficient with discharge for the three channels

Normalisation has resulted in reduced range of values for the mixing coefficient. However, there is still considerable variation with discharge. The variation of normalised longitudinal mixing coefficient with discharge shows no clear trend. The hydraulic radius used was a reach average value calculated from profile and water surface data. The values of bed shear velocity are based on calculation from Equation 2.3. This equation has already been shown to be erroneous in the evaluation of bed shear stress in meandering channels, Section 5.2.4.2 and Table 5.3, therefore this may lead to errors with Figure 6.14.

6.4.1.4 Dispersive fraction

In Section 2.9.5 the dispersive fraction was introduced as a measure of the ratio between the residence time and the total time that tracer spends in a reach. Young and Wallis (1986) define the dispersive fraction, and suggest that it is immobile with discharge. Field data presented by Wallis, Young and Beven (1989a) supports the suggestion that the fraction is a constant with discharge. Figure 2.31 created from U.K. Environment Agency Time of Travel database, also suggests that the fraction is approximately constant with discharge, although very wide scatter is shown.

The variation of dispersive fraction with discharge for this data set is shown in Figure 5.68, Figure 5.71 and Figure 5.74 for the 25, 40 and 97 l/s channels respectively. These figures show that the dispersive fraction is not constant with discharge.

Figure 6.15 shows a composite plot of the variation of dispersive fraction with discharge for the three channels, again the results plotted are from the half meander reaches only.

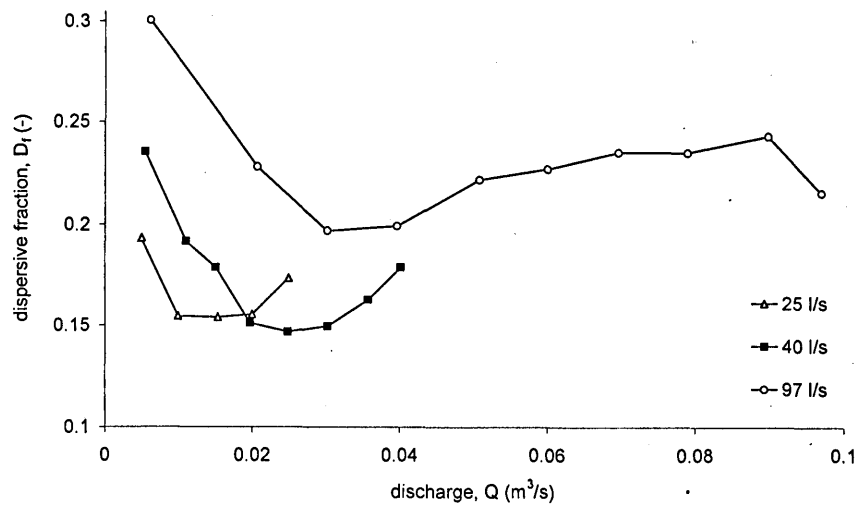

Figure 6.15 Variation in dispersive fraction with discharge for the three channels

Figure 6.15 shows little better definition of trend or relationship between the dispersive fractions than may be interpreted from the three cases individually. The results conclusively show that the fraction is not constant with discharge for these channels. The increase in dispersive fraction at low flow rates suggests that residence times increase more than the total time spent in the reach. This can be justified theoretically by considering dead zone effects. As the flow becomes very low in the channel, stagnant or back eddy zones are likely to increase, dramatically increasing the residence times. The increase in fraction towards bank full conditions, after a stable period around mid flow range, is harder to explain. The increase is

greater for the 25 and 40 l/s channels. A possible explanation, as with the increase in dispersion coefficient, is increasing shear effects in the primary velocity profile. The increase in shear would increase the mixing, modelled as increased dead zones. The suggestion of the immobile fraction is that the increasing shear is directly proportional to the increase in average velocity and travel time, rendering the fraction constant. Hence, different trends are expected for dispersive fraction and dispersion coefficient.

It is possible to normalise the dispersive fraction by the values at bank full conditions to attempt to render a single relationship, as was performed for the velocity data. The results of this can be seen in Figure 6.16.

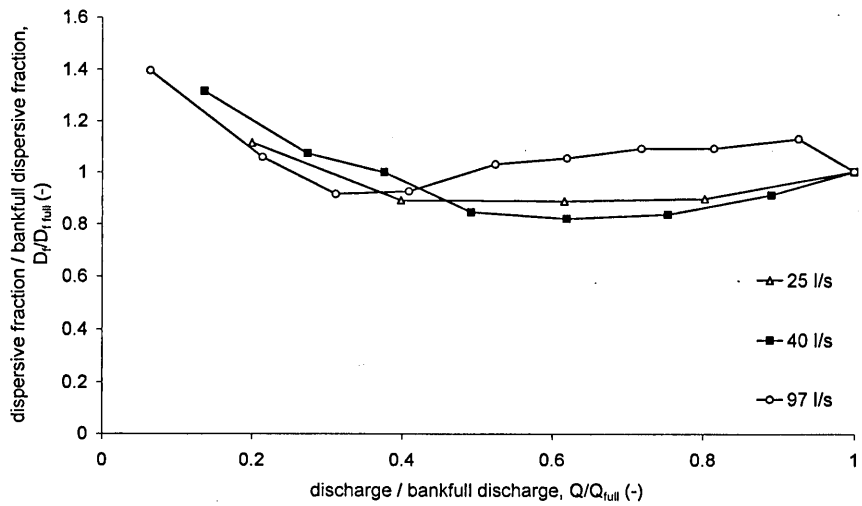

Figure 6.16 Variation in dispersive fraction with discharge, normalised by the channel forming values

From Figure 6.16 it can be seen that the normalised dispersive fraction for the three channels follows approximately the same relationship. It can still clearly be seen that the dispersive fraction is not constant with discharge for these channels. Although approximately a single relationship is found, there is no method to predict the value at bank full conditions, limiting the usefulness of this result. However, it does show the importance of the bank full conditions in defining the rates and values of parameters at other flow rates.

6.4.2 Half cycle trends

Figure 5.66 to Figure 5.74 show analysis results from the quarter meander cycle reaches which were detailed in Table 4.1. These quarter cycle reaches have been sorted into two categories, apex to crossover, representative of the first quarter of the test half cycle, e.g. I-K; and crossover to apex e.g. K-M, for the second quarter. This was to investigate the link between longitudinal mixing rates, secondary flow and transverse mixing conditions. Unfortunately, only apex sections were measured during the 25 l/s channel study in 1996, therefore no quarter cycle data is available.

6.4.2.1 Travel time

For the flow rates in all three channels, the travel times are approximately the same for both quarters, and half of travel time for the half cycle, Figures 5.67, 5.70 and 5.73 for the 25 40 and 97 l/s channels respectively.

6.4.2.2 Longitudinal dispersion coefficient

The trend of the dispersion coefficient is different for the two defined quarters of the meander cycle, for each of the channel cases. Irrespective of flow rate, the crossover to apex reach is always lower than the apex through to crossover reach. For the 1998 25 l/s channel this can be directly related to the rate of transverse mixing. From Figure 6.6 it can be seen that the A-C reach, 0-5m, has on average a higher rate of transverse mixing that the C-A reach, 5-10m. Thus, the inverse relationship between longitudinal and transverse mixing coefficients can clearly be seen.

Figure 5.72 for the 97 l/s channel shows that the longitudinal dispersion coefficient for the first quarter of the meander cycle remains approximately constant with discharge, while the second sector shows a linear increase in longitudinal mixing coefficient with discharge. The half cycle reaches yield coefficients that are the average of the first and second sectors. The trend of the two quarters may be explained by considering the primary shear and secondary currents. Secondary currents are low over the second quarter, hence as primary velocities increase with discharge, the primary velocity profile develops freely, resulting in greater primary shear. In the first quarter secondary currents are strong, particularly due to the approximately triangular cross sectional shape of the 97 l/s channel around the apex. These secondary currents promote transverse velocity shear, and through momentum exchange smooth the primary velocity profile, reducing the primary shear effects.

The 45 l/s channel, Figure 5.67, shows a more variable trend than the 97 l/s channel, possibly due to the smaller over all change in mixing rate, or poorer quality data. The quality of the data collected in this channel may be questioned when it is noted that at low flow rates the half cycle coefficient is greater than either the first or second quarters, rather than the average of the two quarters. In addition, at the flow rate of 25 l/s such a low number of quarter cycle analysis results were validated that the results at this point have to be neglected. The trend at higher discharges shows an increase in mixing coefficient for both the quarter cycle divisions, stronger in the second quarter. The increase in longitudinal mixing coefficient in the first quarter was not present in the 97l/s channel. The increasing longitudinal mixing coefficient in the first quarter for the 45 l/s channel is probably due to weaker secondary currents associated with the nearer parabolic channel shape, or an imbalance in the effects of increasing primary shear and increasing transverse mixing over the reach.

As stated, no quarter cycle data is available for the 1996 25 l/s channel. However, the 1998 study has longitudinal data at the quarter cycle level, together with extensive velocity and transverse mixing data, but only at bank full flow conditions. From this, it is possible to further investigate the trends between longitudinal and transverse mixing and secondary currents. It was suggested that primary shear effects might be greater in regions of weaker secondary mixing and currents. Figure 6.17 shows comparison of apex and crossover primary velocity profiles for the 1998 25 l/s channel. A transverse profile of the depth

average primary velocities and a vertical profile of primary velocities at channel centre line are shown. It can be seen that the velocity profiles at the crossover (K) have a greater change, and therefore greater shear, than at the apex (I). This effect may be due in part to the increased primary velocities at the crossover, due to reduced cross sectional area, and the reduced flow resistance associated with the lack of curvature. Unfortunately, no information is available to reach conclusions about the nature of the change in shear with discharge. The difference in longitudinal mixing coefficients resulting from the profiles in Figure 6.17, bank full in the 25 l/s channel, is very small compared to the change found in the 97 l/s channel at high flow rates.

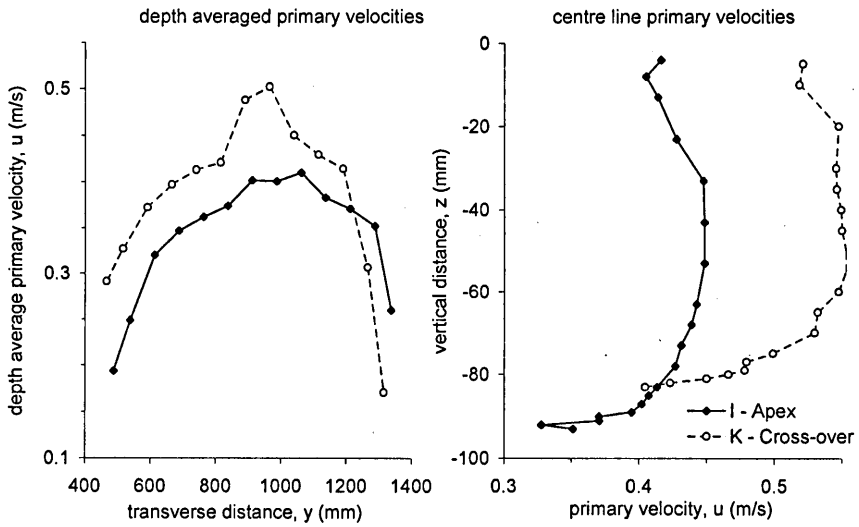

Figure 6.17 Change in primary shear between apex and crossover sections for 1998 25 l/s channel

At low flow rates, where the channels are approximately parabolic, there may be too little depth of flow for secondary currents to form. As the flow rate increases, secondary currents may develop. This effect could account for the initial drop in longitudinal mixing in the 25 and 45 l/s channels. The effect may not be present in the 97 l/s channel, as its unusual cross sectional geometry (approximately triangular at the apex) will promote secondary currents at low flow rates. Again, there is no velocity data to support this theory.

6.4.2.3 Dispersive fraction

The nature of the variation in dispersive fraction with discharge, at the quarter cycle level is confused. The calculation of dispersive fraction at short length scales appears to result in errors. At the quarter cycle level for the 97 l/s channel, Figure 5.74 shows similar trends for variation in dispersive fraction as for dispersion coefficient. The second quarter has a higher fraction than the first quarter, suggesting higher rates of longitudinal mixing in the second quarter than the first. This can be attributed to the same reasons as the change in dispersion coefficient. At low flow rates, the half cycle fraction is less than either the quarter cycle values. This is also the trend throughout Figure 5.71 for the 45 l/s channel and for the result from the 1998 25 l/s test.

6.5 Prediction of Longitudinal Mixing Coefficients

6.5.1 Empirical predictions

In section 2.9.7 several empirical relationships for the prediction of longitudinal mixing coefficients were presented. These relationships were used to predict values which were compared to the review data set. These formulae can be used to predict the coefficients found for each of the channels, and where possible the different discharges that have been tested during this study.

Equation 2.121 was derived specifically for sinusoidal channels, so is expected to yield reasonable estimates of the longitudinal mixing coefficients measured during this study. The equation predicts a reach average coefficient, normalised by hydraulic radius and bed shear velocity. For the three channels under consideration the radius of curvature and bend length are constant, therefore it is only possible to predict channel average values. No prediction of the variation with discharge is possible.

Channel	D_x / Ru* (predicted)	D_x / Ru* (from measurements)
25 l/s	32	30
40 l/s	26	23
97 l/s	15	28

Table 6.4 Longitudinal mixing coefficient from equation 2.121

Comparison of the values in Table 6.4 shows that the predictions from Equation 2.121 are of the correct order of magnitude. The predictions for the 25 and 40 l/s channels are very good, however the 97 l/s channel is underestimated. This may be because the 97 l/s channel does not have a freely developed shape, but was forced within concrete boundaries. The errors associated with these predictions are significant for water quality modelling considerations.

The second predictor has undergone a series of developments to arrive at the form presented in Equation 2.124, Lui (1977). The third is from Seo and Cheong (1998), Equation 2.126. Both equations are based on regression fits to field data and dimensional analysis.

Equation	Mean error ratio, prediction / measured	S.D. error ratio, prediction / measured
2.124, Lui (1977)	7.77	1.35
2.126, Seo and Cheong (1998)	40.56	15.23

Table 6.5 Errors in predicted values of longitudinal mixing coefficients

Table 6.5 shows that both Equations 2.124 and 2.126 exhibit considerable errors in providing estimates of measured longitudinal mixing coefficients. The results from these predictions are presented in Figure 6.18 and Figure 6.19. It should be noted that the predictions and measured values are on very different scales in both these figures.

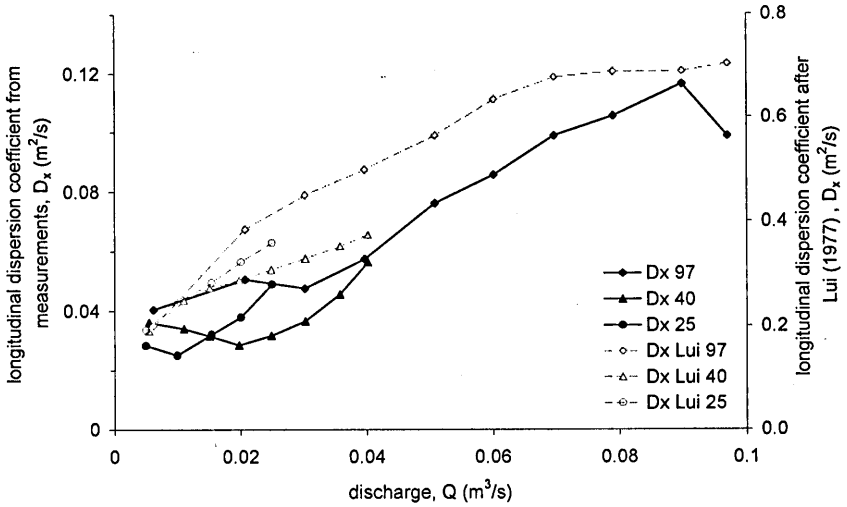

Figure 6.18 Comparison of predicted and measured values of longitudinal dispersion coefficient, after Lui (1977)

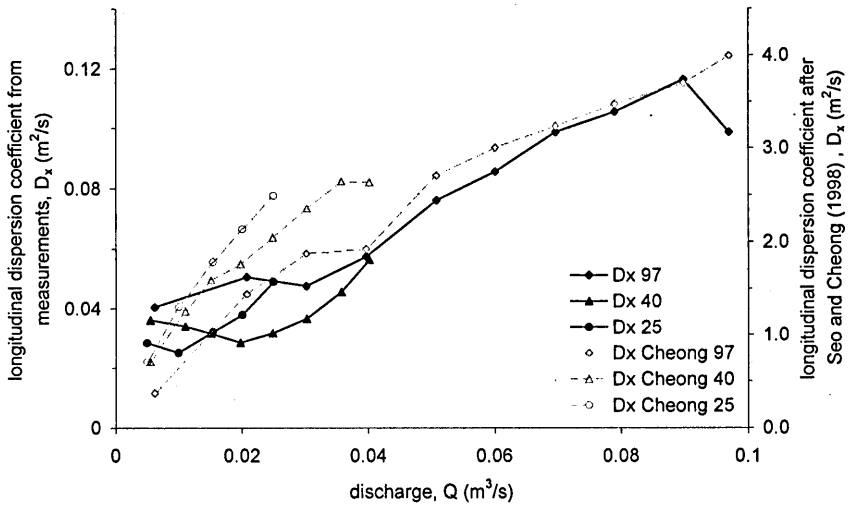

Figure 6.19 Comparison of predicted and measured values of longitudinal dispersion coefficient, after Seo and Cheong (1998)

Figure 6.18 and Figure 6.19 show that both equations approximately predict the change in mixing coefficient with discharge, but with a significant error in the magnitude of the value. Equation 2.124 correctly evaluates the relationship between the three channels, Equation 2.126 does not.

The error in the order of magnitude predicted by Equation 2.126 is large. Seo and Cheong (1998) present a modified form of the equation in which the constant values found from dimensional analysis were altered to optimise the fit to the data set. However, use of these modified values leads to a greater underestimate of the coefficients than the over estimates shown here.

The Flood Channel Facility is large scale for laboratory conditions, however, it is small scale when compared with river conditions. The Flood Channel Facility channels are similar to streams and brooks, rather than large rivers. Scaling errors may result from this, and explain the over estimates of Equations 2.124 and 2.126. Equations 2.126 particularly was derived with no reference to theory, but to provide the optimum fit to a set of field data through dimensional analysis.

Fischer (1969) and Jain (1976) both present expressions for longitudinal mixing predicted with relation to the transverse mixing rate, in the form of Equation 2.127. The equation relies on the selection of a coefficient, alpha, which Jain (1976) suggested should be within the range 0.001 to 0.016, and a transverse mixing coefficient. The use of Equation 2.127 has been investigated for the 25 l/s 1998 channel, where the transverse mixing coefficient has been measured. An alpha value of 0.0006 is required to correctly predict the longitudinal mixing coefficient. This is well outside the suggested range.

None of the methods for predicting rates of longitudinal mixing correctly evaluate the order of magnitude or variation with discharge of the longitudinal mixing coefficient measured in the channels at the flow rates tested.

6.5.2 Predictions from shear profiles

Fischer (1968) presented Equation 2.111, which suggests the complete integration of the primary velocity profile over a cross section, with a given rate of transverse mixing, should yield the longitudinal dispersion coefficient.

Elder (1959) used this approach in his derivation of an expression for longitudinal dispersion for plain two dimensional shear flow, based on a vertical velocity profile described by a logarithmic distribution. The well known result of this is $D_x = 5.93du^*$ (for $\kappa = 0.41$). Since flow depth is approximately equal to hydraulic radius, it is possible to compare this value of 5.93 with Figure 6.14. This shows that the dispersion coefficient estimated from an idealised vertical velocity profile significantly underestimates that found for these channels, indicating that the dominant dispersion process is primary velocity shear in the transverse direction.

6.5.2.1 Approximate solution

Using the method of Chickwendu (1986), it is possible to quantify the shear dispersion resulting from a given velocity distribution. This method has been checked and validated in Section 6.3.1.1. The method of Chickwendu (1986) was derived and presented for the evaluation of longitudinal shear dispersion, caused by vertical profiles of longitudinal velocities. In section 6.3.1.1, it was shown that the method could be adapted and applied to the prediction of transverse dispersion from a vertical profile of transverse velocities. The dominant shear process in longitudinal mixing is the transverse shear, resulting from transverse profiles of primary velocities. Chickwendu's method can be adapted to this situation. To modify the method for the evaluation of transverse shear effects it is necessary to convert depth to width terms and define a rate of mixing between horizontal rather than vertical fluid strips, a transverse mixing coefficient. Unfortunately, there are no complete solutions to check the validity of this adaptation of the mathematical method.

6.5.2.1.1 Predictions for the 25 l/s 1998 channel

It was shown in Section 5.2.4 that it is possible to accurately predict the depth average of the primary velocity measurements that were made in the 25 l/s 1998 channel. From such predictions of depth average velocities, evaluation of transverse mixing coefficient and using the modified method of Chickwendu (1986), it should be possible to estimate the longitudinal dispersion resulting from transverse velocity

profiles based solely on geometry information. It is also possible to make predictions using the depth average of the measured primary velocities.

Predictions of longitudinal mixing coefficient from geometry information have been made at each of the #0 and #4 subsections over the test half meander cycle. The evaluations of longitudinal mixing coefficient have been made using the predicted point values of transverse mixing coefficient, Section 6.3.2. Predictions using reach average and reach maximum values of transverse mixing coefficient have also been undertaken. The results of these predictions are shown in Figure 6.20 and Table 6.6.

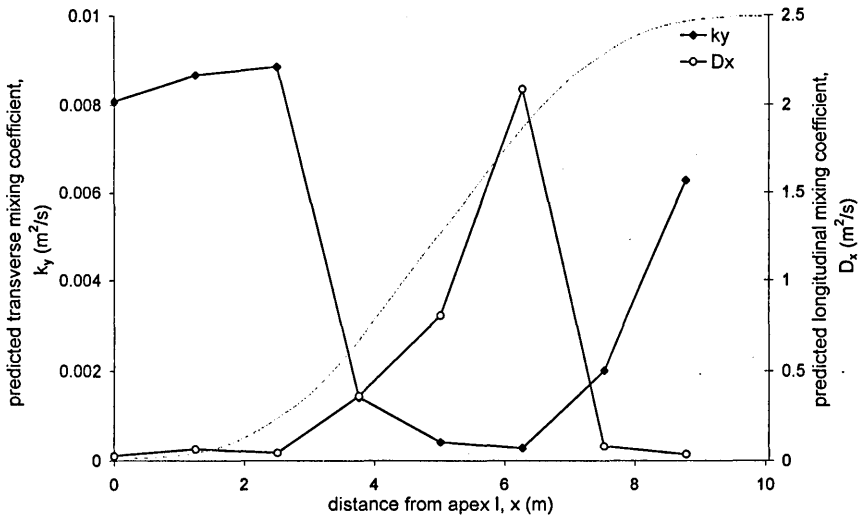

Figure 6.20 Predicted longitudinal mixing coefficient using point transverse mixing coefficient values and predicted primary velocities for the 25 l/s 1998 channel

From Figure 6.20 it can be seen that through the straighter section of the channel the predicted longitudinal mixing coefficient reaches a very high peak value. This is associated with low transverse mixing coefficient, approximately equal to the input transverse eddy diffusivity. This low value of transverse mixing coefficient is caused by weak transverse velocities in this region.

reach	measured values of D_x (m^2/s)	D_x calculated from point k_y value (m^2/s)	D_x calculated from average k_y (m^2/s)	D_x calculated from max k_y (m^2/s)
average	0.051	0.439	0.082	0.048
1st quarter	0.026	0.319	0.065	0.040
2nd quarter	0.071	0.558	0.098	0.056

Table 6.6 Results of prediction of longitudinal mixing coefficient from velocity shear effects for 1998 25 l/s channel

Table 6.6 shows a comparison of the predicted longitudinal mixing coefficients and the measured values for the 25 l/s 1998 channel. The predictions made using the point values of transverse mixing result in an over estimate of the mixing rate. The use of average or maximum, transverse mixing coefficients yield values of longitudinal mixing coefficient close to those measured. Both predictions reflect the variation in mixing coefficient over the quarter cycle that was measured. The values resulting from the maximum transverse mixing coefficient yield the best estimates, possibly due to the length scales of the mixing processes, or errors in the predicted primary velocity profile.

These predictions have been made using the transverse velocity profiles predicted by Equation 2.130. In Section 5.2.4 this was shown to be accurate for predicting the bulk transverse variations in depth average velocities, but of over emphasising the finer detailed variations due to local bed features. Predictions of longitudinal dispersion coefficients based on the depth average of measured primary velocities are shown in Table 6.7. The use of point values of predicted transverse mixing coefficients again result in an overestimate of the longitudinal mixing coefficient. For these predictions, using the measured velocities, it is the reach average value of transverse mixing coefficient that yields the best estimate of longitudinal mixing coefficient, not the reach maximum value as for the predicted velocity distributions. This suggests that the predicted velocity distributions over predict primary shear, and require a slight over estimate of the transverse mixing coefficient to counteract it. This over estimate is the result of over predicted primary velocity shear.

measured values of D_x (m^2/s)	D_x calculated from point k_y value (m^2/s)	D_x calculated from average k_y (m^2/s)	D_x calculated from max k_y (m^2/s)
0.051	0.191109	0.051042	0.037404

Table 6.7 Reach average values of longitudinal mixing coefficient calculated using depth average measured primary velocities

A study into the sensitivity of the predicted longitudinal mixing coefficient to the input transverse mixing coefficient was conducted, results are shown in Figure 6.21.

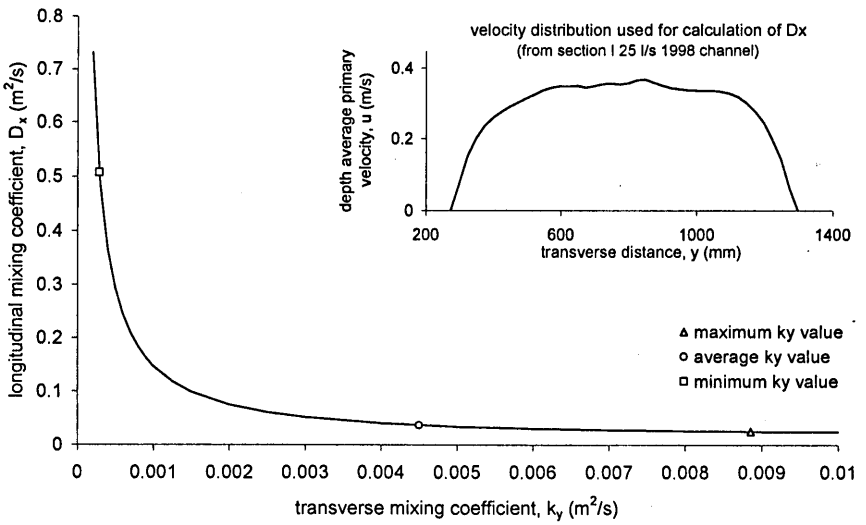

Figure 6.21 Results of sensitivity study into dependence of predicted longitudinal mixing coefficient on input transverse mixing coefficient

Figure 6.21 shows a similar trend to the one shown for the sensitivity study of transverse predictions, Figure 6.8. The potential range of input transverse mixing coefficients can lead to very dramatic changes in the predicted rate of longitudinal mixing, particularly at low input values. It should be noted that the longitudinal mixing coefficient predicted in Figure 6.21 for the minimum transverse mixing coefficient is less than the value shown in Figure 6.20. This is because the velocity function used is from the apex cross section.

Using point estimates of transverse mixing coefficient leads to over estimates in predicted longitudinal coefficient, due to very high peak values in longitudinal coefficient through the straight channel section. In Figure 6.6, it was shown that the predicted transverse mixing coefficients are accurate. However,

through the straighter section of the channel these predictions appear to be a slight underestimate of the measured values. This is concurrent with the right hand side of Figure 6.21, resulting in large over estimates of longitudinal mixing coefficient.

These predictions have been made using reach average values of transverse mixing coefficient. However the longitudinal shear effects have been evaluated at several points over the reach and then averaged. A prediction based on a reach average profile was attempted. The profile resulting from reach averaging was, however, very wide and shallow and produced a considerable overestimation of the shear effects.

Accurate predictions of reach average longitudinal mixing coefficients can be made using measured velocities and reach average transverse mixing coefficients for the 1998 25 l/s channel. Estimations made using the predicted primary velocities require reach maximum transverse mixing coefficient to counteract the over predicted shear effects, resulting from the velocity predictions over emphasising the finer features due to local bed features.

6.5.2.1.2 Prediction of longitudinal mixing coefficients for the other channels tested

The quality of fit between measured values of longitudinal mixing coefficient and values estimated from predicted depth average velocities and reach maximum transverse mixing coefficients are good for the 25 l/s 1998 channel. Using this technique, predictions of longitudinal mixing coefficients for the other channels were attempted. The results of these predictions, together with the measured values, are shown in Figure 6.22, Figure 6.23, and Figure 6.24 for the 25, 45 and 97 l/s channels respectively. It should be noted that these predictions were all made using the maximum bank full transverse mixing coefficient.

The quality of fit between predicted and measured longitudinal mixing coefficients in Figure 6.22 to Figure 6.24 is good. The predictions were made using spreadsheets and only required basic geometrical data, discharge and an estimate of Manning's n.

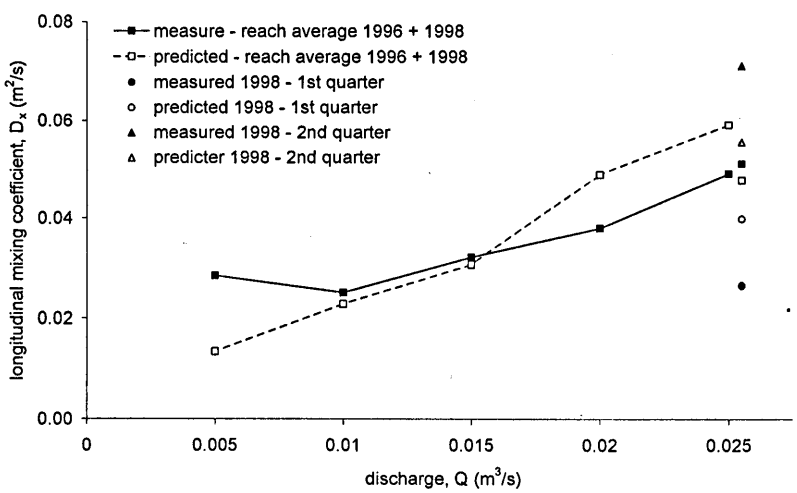

Figure 6.22 Comparison of measured and predicted longitudinal mixing coefficients for the 25 l/s 1996 and 1998 channels, made using maximum predicted transverse mixing coefficient

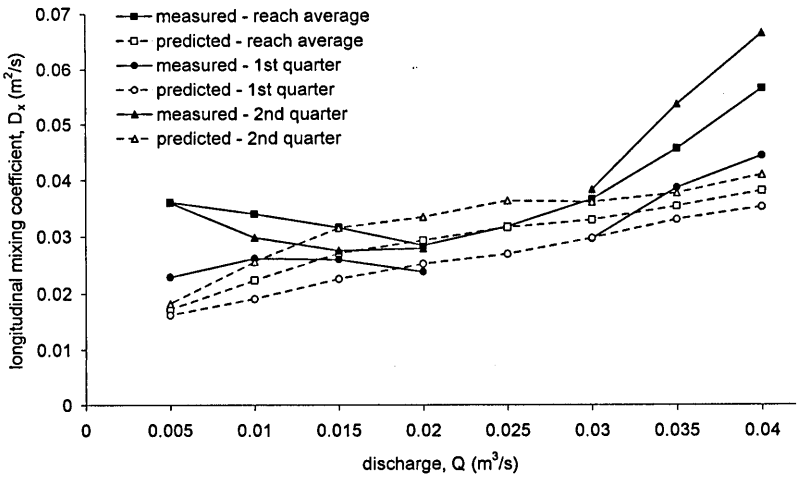

Figure 6.23 Comparison of measured and predicted longitudinal mixing coefficients for the 40 l/s 1996 channel, made using maximum predicted transverse mixing coefficient

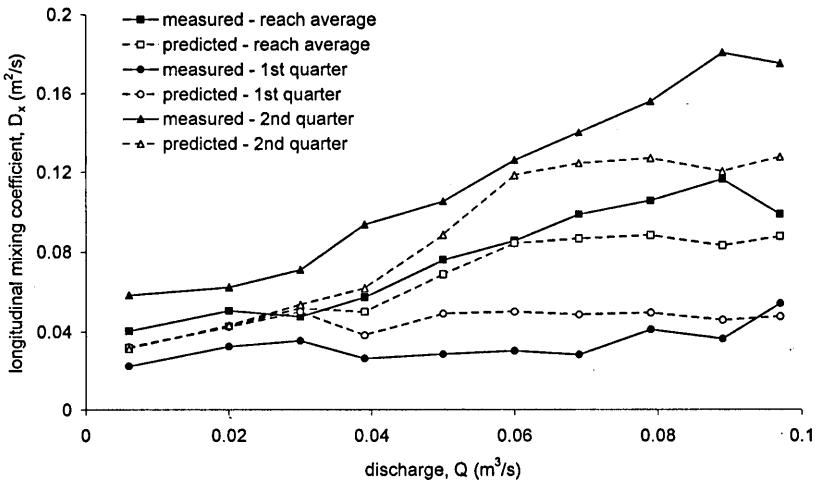

Figure 6.24 Comparison of measured and predicted longitudinal mixing coefficients for the 97 l/s 1996 channel, made using maximum predicted transverse mixing coefficient

The predictions of longitudinal mixing coefficients were made using the reach maximum value of predicted transverse mixing coefficient, at bank full flow conditions. Reach maximum values were shown to be required for the bank full 25 l/s 1998 channel to overcome inaccuracies in the predicted primary velocity profile, and because of the sensitivity of the predicted longitudinal mixing coefficient at low transverse mixing rates. When reach average transverse mixing coefficients, predicted at the relevant flow rates were used in the prediction of longitudinal coefficients, the results overestimated the measured values, suggesting that a higher rate of transverse mixing is required. The value obtained at bank full conditions gives the best fit.

The prediction of transverse velocities by Equations 2.139 and 2.140 and the resulting prediction of transverse mixing coefficients were earlier shown to be accurate for bank full flow conditions in the 25 l/s 1998 channel. However, there is no information about the accuracy of predicted transverse velocities or mixing coefficients at less than bank full conditions. Therefore, it could be inaccuracies in the predicted rate of transverse mixing at low flow rates which lead to the requirement of the bank full transverse

mixing coefficient for accurate prediction of longitudinal mixing coefficients. Alternatively the bank full channel forming conditions may govern the rate of transverse mixing, similar to the bank full conditions being required to normalise the prediction of velocities, Section 6.4.1.1, and dispersive fraction, Section 6.4.1.4.

There is insufficient data for any of the longitudinal mixing field data reviewed in Section 2.9 to make these types of prediction and thus further validate this predictive method.

Chapter 7 Conclusions

From the studies which have been undertaken it is possible to draw a number of conclusions, propose implications for engineering practice and make suggestions for further work.

7.1 Velocity Data

- The measured primary depth average velocities can be accurately predicted by relation to the local depth of flow, using the formulae of Smith (1983). However, the predictions over emphasise the detailed variations resulting from local bed features.
- The measured secondary circulations, together with their growth and decay, can be predicted by the formulae suggested by Rozovskii (1957). This is achieved from approximated plan form geometry and cross section profile data. The predictions are limited to a single cell and the central region of the channel.
- The complete vertical distribution of primary velocity cannot be predicted using log law or Cole's distributions because of the deviation from idealised two dimensional flow patterns, caused by plan form curvature and the associated secondary circulations. However, the log law distribution is valid over the inner region, defined as twenty percent of the depth to velocity maxima, and can be used to evaluate bed shear velocity.
- Bed shear velocities have been interpreted from the measurements of primary velocity. Through this the standard expression for bed shear velocity, Equation 2.3, has been shown inadequate in predicting longitudinal variation in bed shear velocity for curved channels. This deficiency is attributed to the fact that the derivation of the equation does not include flow resistance effects resulting from plan form curvature.
- Turbulence parameters have been investigated, although no strong conclusions are drawn due to questions over the quality of the data.
- Analysis of the measured time series velocity data has shown the turbulence fluctuations to be random and homogeneous about a stable time average component.

7.2 Transverse Mixing

- At the start of this research, there was considerable question over how to analyse transverse tracer measurements from natural channels and the effectiveness of such analysis. The work undertaken has shown conclusively that the cumulative discharge approach is able to account for the effects of changes in channel shape and curvature.
- The use of the Generalised Method of Moments, adapted to cumulative discharge terms, can efficiently account for the effects of bank side impingement in natural channels. However, this analysis method, as with the standard form of the Method of Moments, is susceptible to errors resulting from noise and inaccuracies at the edges of the measured tracer plume.
- It has been shown that the transverse mixing varies over the half meander cycle and that this variation is directly related to curvature, and therefore secondary circulations.

♦ From the predicted secondary circulations, and assuming an eddy viscosity equal to that found for two dimensional plain turbulent open channel flow, it is possible to make accurate predictions of the rate and variation in transverse mixing. These predictions are made using the mathematical method of Chickwendu (1986). The method was shown accurate for the measurements made in this work and for other published values from laboratory and field measurements.

7.3 Longitudinal Mixing

♦ The optimisation procedure used to analyse the longitudinal dispersion data is a new technique for laboratory scale, open channel flow mixing experiments. The application of the optimisation procedure has been verified and the improvement in model fit obtained by the procedure shown. This procedure has been invaluable in removing error in the evaluation of parameters resulting from the measurements. Trends which would otherwise have remained hidden within the spread of the estimated values, have been highlighted.

♦ Average velocities calculated from travel time data have been shown to follow a single power law relationship for all the channels, once normalised by the channel formation conditions. The relationship between normalised velocity and discharge was shown to have a gradient term approximately equal to one, and a power value of approximately one half. Field data is required to validate this.

♦ The longitudinal mixing rate was shown to increase with discharge, the relationship is approximately linear. The compiled data sets in Section 2.9 suggest a power law relationship between discharge and longitudinal mixing rate. The relationship suggested by this work results from multiple discharges in stable channel forms, and does not include any other channel differences or effects. It provides a more reliable estimation of the relationship.

♦ Normalisation of the longitudinal mixing coefficients by bed shear stress and hydraulic radius has been shown insufficient to render a single normalised value or relationship.

♦ The dispersive fraction has been shown to vary with discharge. This is inconsistent with the findings of Wallis, Young and Beven (1989a).

♦ Normalisation by channel formation values has rendered a single relationship between discharge and dispersive fraction for the three channels. However, this relationship is again not constant with discharge. The usefulness of this result is limited by an inability to predict the dispersive fraction at bank full or any other conditions.

♦ Longitudinal dispersion parameters have been investigated at the quarter meander cycle level. The first quarter always exhibited lower rates of longitudinal mixing than the second quarter. This has been directly linked to the effects of the transverse mixing rate and the change in primary shear resulting from the change in secondary circulations. This, together with the transverse mixing results, illustrates the inverse relationship between longitudinal and transverse mixing rates, through experimental measurement.

♦ Predictions of the measured longitudinal mixing coefficients using published empirical relationships have shown considerable error.

♦ Predictions of measured longitudinal mixing coefficients from transverse shear in the primary velocity have been shown accurate, and capable of predicting the variation with discharge. These

predictions were based on predicted depth average primary velocities, and channel maximum values of predicted transverse mixing coefficients, in a modified form of Chickwendu's (1986) method. The channel maximum value of transverse mixing is required for two reasons:

1. The reach average is required to compensate for errors in the predicted primary velocity profiles.
2. The bank full mixing coefficient is required as predictions of transverse velocities at lower flow rates are an unknown quantity, and the channel forming conditions are thought to dominate the process.

Validation of this method against field data is essential.

7.4 *Engineering Implications*

The main engineering implication resulting from this work is the ability to accurately quantify depth average transverse and longitudinal mixing coefficients from simple geometric channel properties, discharge and Manning's n.

7.4.1 Transverse mixing

Transverse mixing in channels with plan form curvature is dominated by vertical shear in transverse velocities, resulting from secondary circulations. To evaluate the transverse mixing coefficient in such situations the following steps should be followed:

- Approximate the channel plan form geometry to uniformly curved and straight sections, with an average channel centre line depth of flow, such that Equation 2.137 and Equation 2.138 from Rozovskii (1957) can be used to make predictions of the build and decay of secondary currents around the bends.
- Estimate eddy diffusivity from the equation found for plain turbulent two dimensional open channel flow, $e_y=0.134du^*$.
- Use the mathematical method of Chickwendu (1986) with the predicted transverse velocity profiles and eddy diffusivity to evaluate the transverse mixing coefficient at any given point over the approximated geometry.

It should be noted that the predicted secondary circulations are only valid over the central region of the channel, and only predict a single circulation cell. Transverse mixing coefficients tend be underestimated in straight sections of channel.

7.4.2 Longitudinal mixing

The process dominating longitudinal mixing in natural channels is transverse shear, resulting from transverse variations in primary velocities. To evaluate longitudinal mixing coefficients from transverse shear the following steps should be followed:

- Predict the transverse distribution of primary velocities using Equation 2.130. It should be noted that these predictions over emphasise the finer variations resulting from local bed features.

- The maximum bank full transverse mixing coefficient should be evaluated using the above method. The maximum bank full transverse mixing coefficient is required to counter the over predicted shear effects of Equation 2.130, and because the channel forming conditions govern the transverse mixing coefficient.
- Use the method of Chickwendu (1986), modified for shear in the transverse direction, to predict the longitudinal mixing coefficient from the velocity profiles and the transverse mixing coefficient. It is recommended that to yield a reach average value predictions should be made at a number of cross sections and then averaged. The averaging of cross sections prior to prediction leads to large errors.

All these calculations can be programmed onto a spreadsheet to enable fast and accurate predictions to be obtained.

The transverse predictive method has been tested and proved for a number of data sets, covering both field and laboratory conditions, and is therefore considered robust. It was only possible to validate the prediction of longitudinal mixing coefficients against the current data set, due to insufficient profile and plan form data with past studies. Further validation of this method is recommended.

7.5 Further Work

A number of logical progressions may be suggested to assist in reducing the bounds of uncertainty in the prediction of mixing coefficients.

Ideally, further work is required to fully validate the predictive methods for both transverse and longitudinal mixing coefficients. The transverse method has been validated against several sets of experimental results, but has only been evaluated against one set of field data. However, transverse mixing tests are expensive and difficult to carry out under field conditions. The predictive method for longitudinal mixing coefficients has only been validated against this data set, because of incomplete information to enable this type of prediction for past studies. However, it should be possible to identify the sites of a number of past studies and collect the required information to validate the method without having to repeat the tests. This is, therefore, an excellent possibility to be funded and undertaken as a small scale research project.

In Section 2.9.6 the compilation of, and some preliminary findings from, the Environment Agency's Time of Travel database were introduced. Further use and development of this database could lead to reduced uncertainty in the prediction of mixing coefficients and travel times, particularly through the grouping of river characteristics and parameters such as slope, curvature and bed material. However, considerable time and effort is required in areas of quality control checking of the database and cross-referencing with other data sources such as the Habitat Survey database, Global Imaging Systems and remote surveying information. Such work will probably result in the need for further laboratory or field studies to better define and quantify the factors identified, such as bed exchange rates. One of the major advantages of working from such data sources is that the resulting conclusions and practices should be readily accessible as the required information will be available.

During the testing period on the Flood Channel Facility at HR Wallingford some Laser Induced Fluorescence measurements were made. The ideas of Laser Induced Fluorescence have been around for some time, but have only recently become a viable measurement technique due to advances in equipment and technology. A measurement system has been developed over the past five years, within the Mixing Studies Group at Sheffield University. See Guymer and Harry (1996), and Harry, Guymer and Boxall (1998).

The principals of operation are similar to those of a fluorometer. Laser light is used to excite a fluorescent tracer, which then emits light of a different wavelength. A light sensitive device, fitted with an optical filter, can be used to record light intensity, which can be related to concentration. The system as set up at the Flood Channel Facility is shown in Figure 7.1. It was used in conjunction with instantaneous injections of dye, at different depths within nine cross sections.

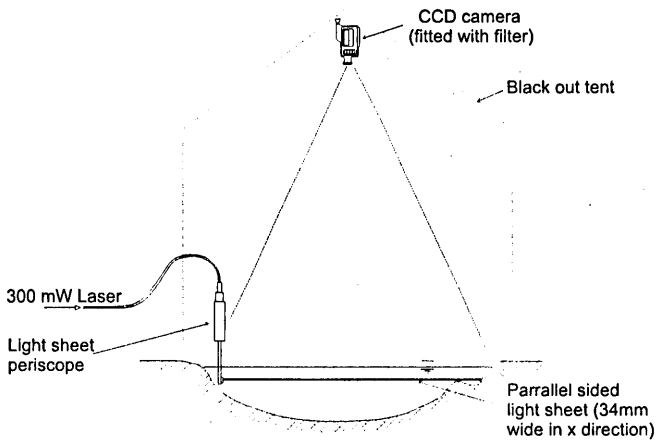

Figure 7.1 Sketch of Laser Induced Fluorescence apparatus configuration

Using a Laser Induced Fluorescence system has several advantages over more traditional Fluorometery measurements:

1. The system can be non-intrusive, depending on how the laser light sheet is introduced to the flow and camera location.
2. It is possible to obtain simultaneous measurements over a large area, limited by illumination power and visualisation area.
3. Unlike fluorometery work, concentration measurements are made in-situ, meaning that, depending on the speed of the image processing system, temporal and spatial fluctuations in concentration can be measured.

Although measurements have been made it is beyond the resources of the current project, in terms of both time and money, to undertake the development of an analysis system and the processing of this data. The data is currently stored on SVHS tapes, waiting for funding and development of analysis techniques. Data collected by the Laser Induced Fluorescence system in the 'natural' channel could potentially lead to improved understanding in several areas. Imaging over an area could lead to great insight into trapping and release effects of dead zones, which currently have only been investigated on a uniform, regular laboratory basis. Information about how the concentration level fluctuations change and develop over the plume could lead to great improvement in the understanding of the approximation of diffusive fluxes to gradient diffusion terms.

Acknowledgements

I would like to thank numerous people for their support and understanding while I have been undertaking this research, particularly Dr. Ian Guymer for his continual ideas and sarcastic comments, and my girlfriend Susan for her encouragement.

Funding to access the Flood Channel Facility at HR Wallingford Ltd. was provided by the EC Commission, Directorate General for Science, Research and Development as part of the program Training and Mobility of Researchers, Large Scale Facilities, under control number ERB FGME CT95 0082.

References

Bathurst, J. C. Thorne, C. R. and Hey, R. D. (1979) 'Secondary Flow and Shear Stress at River Bends' Journal of the Hydraulics Division, ASCE, October, HY 10, pp 1277-1295.

Beltaos, S. (1980) 'Longitudinal Dispersion in Rivers' Journal of the Hydraulics Division, ACSE, January, HY1, pp 151-172.

Beer, T. and Young, P. C. (1984) 'Longitudinal Dispersion in Natural Streams' Journal of the Environmental Engineers Division, ASCE, EE 109, pp 1049-1067.

Chadwick, A. and Morfett, J. (1994) 'Hydraulics in Civil and Environmental Engineering' E & FN Spon London England.

Chang, Y. C. (1971) 'Lateral Mixing in Meandering Channels' PhD Thesis, University of Iowa, U.S.A.

Chatwin, P. C. (1971) 'On the interpretation of some Longitudinal Dispersion Data', Journal of Fluid Mechanics, Vol. 48 (part 4), pp 689-702.

Chatwin, P. C. (1980) 'Presentation of Longitudinal Data' Journal of the Hydraulics division ASCE, January, Vol. 106, HY1, pp 71-83.

Chickwendu, S. C. (1986) 'Calculation of Longitudinal Shear Dispersivity using an N-zone model as N $\rightarrow \infty$' Journal of Fluid Mechanics, Vol. 167, pp 19-30.

Chow, V. T. (1959) 'Open Channel Hydraulics' McGraw-Hill, New York.

Day, T. J. (1975) 'Longitudinal Dispersion in Natural Channels' Water Resources Research, December, Vol. 11, No. 6, pp 909-918.

Demuren, A. O. and Rodi, W. (1986) 'Calculation of Flow and Pollutant Dispersion in Meandering Channels' Journal of Fluid Mechanics, Vol. 172, pp 63-92.

Denis, P. M. (2000) 'Longitudinal Dispersion Due to Surcharged Manholes' Ph.D. Thesis, University of Sheffield, U.K.

Drain, L.E. (1980) 'The Laser Doppler Technique', J. Wiley and Sons Ltd.

Elhadi, N., Harrington, A., Hill, I., Lau, Y. L. and Krishnappen, B. G. (1984) 'River Mixing – A State of the Art Report.' Canadian Journal of Civil Engineering, Vol. 11, pp 585-609.

Elder, J. W. (1959) 'The Dispersion of Marked Fluid in Turbulent Shear Flow' Journal of Fluid Mechanics, Vol. 5, pp 544-560.

Fischer, H. B. (1966) 'A note on the One-dimensional Dispersion Model' Air Water and Pollution, International Journal, Vol. 10, pp 443-452.

Fischer, H. B. (1967) 'The Mechanics of Dispersion in Natural Streams' Journal of the Hydraulics Division, ACSE, November, HY6, pp 187-215.

Fischer, H. B. (1968). 'Methods of Predicting Dispersion Coefficients in Natural Streams, with applications to lower reaches of the Green and Duwamish Rivers, Washington' U.S. Geological Survey Professional Paper, 582-A.

Fischer, H. B. (1969) 'The Effects of Bends on Dispersion in Streams' Water Resources Research, April, Vol. 5, No. 2, pp 496-506.

Fischer, H. B. (1975) 'Simple Method for Predicting Dispersion in Streams' Journal of the Environmental Engineering Division, ASCE, June, EE 3, pp 453-455.

Fischer, H. B. (1978) 'On the Tensor form of the Bulk Dispersion Coefficient in a Bounded Skew Shear Flow' Journal of Geophysical Research, May, Vol. 83, No. C5, pp 2373-2375.

Fischer, H. B., List, E. J., Koh, R. C. Y., Imberger, J. and Brookes, N. H. (1979), 'Mixing in Inland and Coastal Waters' Academic Press Inc. San Diego, California.

Fukuoka, S. and Sayer, W. W., (1973) 'Longitudinal Dispersion in Sinuous Channels' Journal of the Hydraulics Division, ASCE, January, Vol. 99, HY1, pp 195-217.

Graf, W. H. and Kironoto, B. A. (1994) 'Turbulence Characteristics in Rough Uniform Open Channel Flow' Proceedings Institution of Civil Engineers, Water, Maritime & Energy, December, Vol. 106, pp 333-344.

Grass, A. J., (1971) 'Structural Features of Turbulent Flow over Smooth and Rough Boundaries' Journal of Fluid Mechanics, Vol. 50, part 2, pp 233-255.

Green, H. M., Beven, K. J., Buckley, K. and Young, P. C. (1994), 'Pollution Incident Prediction with Uncertainty' Mixing and Transport in the Environment, edited by Beven, K.J. Chatwin, P.C. and Millbank, J.H., Wiley and Sons Ltd.

Guymer, I. and Harry, A. J. (1996) 'Use of Laser Induced Fluorescence and Video Imaging Techniques in an Investigation of the Mixing across the Dead Zone / Flow Zone Boundary' Proceedings of the Institution of Mechanical Engineers, C516/027, pp 419-428.

Guymer, I. (1998) 'Longitudinal Dispersion in a Sinuous Channel with Changes in Shape' Journal of Hydraulic Engineering, ASCE, Vol.124, No.1, pp.33-40.

Harry, A. J. Guymer, I. and Boxall, J. B. (1998) 'The use of Laser Measurement Techniques in an Investigation of the Mechanics of Solute Entrainment in Dead Zones' Flow modelling and turbulence measurements, ISFTM, October 5-8, Tainan, Taiwan.

Holley, E. R. Siemons, J. and Abraham, G. (1972) 'Some Aspects of Analysing Transverse Diffusion in Rivers' Journal of Hydraulic Research, No.1, pp 27-56.

Holley, E. R. and Abraham, G. (1973a) 'Laboratory Studies on Transverse Mixing in Rivers' Journal of Hydraulic Research, No.3, pp 219-252.

Holley, E. R. and Abraham, G. (1973b) 'Field tests on Transverse Mixing in Rivers' Journal of the Hydraulics Division, ASCE, December, Vol. 99, No. HY 12, pp 2313-2331.

Holley, F. M. and Nerat, G. (1983) 'Field Calibration of Stream-Tube Dispersion Model' Journal of Hydraulic Engineering, ASCE, August, Vol. 109, No 11, pp 1455-1470.

Jain, S. C. (1976) 'Longitudinal Dispersion Coefficients for Streams' Journal of the Environmental Engineering Division, ACSE, April, EE2, pp465-474.

Jobson, H. E. and Sayer W. W. (1970) 'Predicting Concentration Profiles in Open Channels' Journal of Hydraulic Engineering, ASCE, Vol. 96, HY 10, pp 1983-1996

Jobson, H. E. (1997) 'Predicting Travel Time and Dispersion in Rivers and Streams' Journal of Hydraulic Engineering, ASCE, November, pp 971-978.

Khalil, M. B. (1972) 'On Preserving the Sand Patterns in River Models' Journal of Hydraulic Research, IAHR, No. 10, pp 291-303.

Kironoto, B. A. and Graf, W. H. (1995) 'Turbulence Characteristics in Rough Uniform Open Channel Flow' Proceedings of the Institution Civil Engineers, Water Maritime & Energy, December, Vol. 106, pp 333-344.

Knight, D. (1998) 'Fluvial Forms and Processes: A New Perspective' J. Wiley and Sons Ltd.

Krishnappen, B. G. and Lau, Y. L. (1977) 'Transverse Dispersion in Meandering Channels' Canada, Inland Waters Branch, Scientific Series, No. 75.

Langbein, W. B. and Leopold, L. B. (1966) 'River Meanders – Theory of Minimum Variance' Geological Survey Professional Papers, 422-H.

Lau, Y. L. and Krishnappen, B. G. (1977) 'Transverse Dispersion in Rectangular Channels' Journal of Hydraulics Division, ASCE, October, Vol. 103, No 10, pp 1173-1189.

Lau, Y. L. and Krishnappen, B. G. (1981) 'Modelling Transverse Mixing in Natural Streams' Journal of Hydraulic Engineering, ASCE, February, HY2, pp 209-226.

Lui, H. (1977) 'Predicting Dispersion Coefficient of Streams' Environmental Engineering Division, ASCE, Vol. 103, Pt 1, pp 59-69.

Lui, H. and Cheng, A. H. D. (1980) 'Modified Fickian Model for Predicting Dispersion' Journal of the Hydraulics Division, ASCE, June, HY 6, pp 1021-1040.

Luk, G. K. Lau, Y. L. and Watt, W. E. (1990) 'Two-dimensional Mixing in Rivers with Unsteady Pollutant Source' Journal of Environmental Engineering, ASCE, February, Vol. 116, No. 1, pp 125-143.

Luk, G. K., (1991) 'Two-dimensional Time-dependent Pollution Dispersion Modelling' Proceedings IAHR Congress 1991. pp 453-458.

Magazine, M. K. Pathak, S. K. and Pande, P. K. 'Effect of Bed and Side Roughness on Dispersion in Open Channels' Journal of Hydraulic Engineering, ASCE, Vol. 114, No.7, pp.766-782.

McNulty, A. J. (1983) 'Dispersion of Continuos Point Source in Open Channel Flow' Ph.D. Thesis, University of Canterbury, Christchurch.

McQuivey, R. S. and Keefer, T. N. (1974) 'Simple Model for Predicting Dispersion in Streams' Journal of Environmental Engineers, ACSE, Vol. 100, EE4, pp 997-1011.

Nokes, R. I. (1986) 'Problems in Turbulent Dispersion' Ph.D. Thesis, University of Canterbury, Christchurch.

Nokes, J. R. and Wood, I. R. (1988) 'Vertical and Lateral Turbulent Dispersion: some Experimental Results' Journal of Fluid Mechanics, Vol. 187, pp 373-394.

Pearson, J. (1999) 'Mixing Under Waves' PhD Thesis, University of Sheffield U.K.

Potter, R. (1999) 'Transverse Mixing in the Presence of Transverse Depth Variations' PhD Thesis, University of Sheffield U.K.

Prandtl, L. (1952) 'Essentials of Fluid Dynamics' Hafner Publishing Company, New York, N.Y.

Rozovskii, I. L. (1957) 'Flow of Water in Bends of Open Channels' Originally in Russian, the Academy of Science of the Ukraine SSR, (Israel Program for Scientific Translation, Jerusalem, Israel 1961).

Rutherford, J. C. (1994) 'River Mixing' J. Wiley and Sons Ltd.

Seo, I. W. and Cheong, T. S. (1998) 'Predicting Longitudinal Dispersion Coefficients in Natural Streams' Journal of Hydraulics Engineering, ASCE, January, Vol. 124, No. 1, pp 25-32.

Shiono, K. Feng, T. and Muto, Y. (1998) 'Reynolds stress and Flux Measurements in Open Channel Flows' Flow modelling and turbulence measurements, ISFTM, October 5-8, Tainan, Taiwan.

Shiono, K. and Knight, D. W. (1991) 'Turbulent Open Channel Flows with Variable Depth Across the Channel' Journal of Fluid Mechanics, Vol. 222, pp 617-646.

Shiono, K. and West J. R. (1987) 'Turbulence Perturbations of Velocity in the Conway Estuary' Estuarine, Coastal and Shelf Science, Vol. 25, pp 533-553.

Smart, P. L. and Laidlaw, I. M. S. (1977) 'An Evaluation of some Fluorescent Dyes for Water Tracing' Water Resources Research, February, Vol. 13, No. 1, pp 161-172

Smith, R. (1983) 'Longitudinal Dispersion Coefficient for Varying Channels' Journal of Fluid Mechanics, Vol. 130, pp 299-314.

Smith, R. (1992) 'Physics of Dispersion' Coastal and Estuarine Pollution – Methods and Solutions' Technical sessions, Scottish hydraulics study group, One day seminar 3rd April, Glasgow.

Taylor, G. I. (1921) 'Diffusion by Continuos Movements' Proceedings London Maths Society, Series 2, Vol. 20, pp 196-212.

Taylor, G. I. (1953) 'Dispersion of Soluble Matter in Solvent Flowing Slowly through a Tube' Proceedings Royal Society, Series A, Vol. 219, pp 186-203.

Taylor, G. I. (1954a) 'The Dispersion of Matter in Turbulent Flow through a Pipe' Proceedings Royal Society, Series A, Vol. 223, pp 446-468.

Taylor, G. I. (1954b) 'Conditions under which Dispersion of a Solute in a Stream of Solvent can be used to Measure Molecular Diffusion' Proceedings Royal Society, Series A, Vol. 225, pp 473-477.

Verboon, G. K. (1973) 'Transverse Mixing in Rivers; a Numerical Approach' XVth IAHR Congress Istanbul, September 2-7.

Valentine, E. M. and Wood, I.R. (1977) 'Longitudinal Dispersion with Dead Zones' Journal of the Hydraulics Division, ACSE, September, HY9, pp 975-990.

Wallis, S. G. Young, P. C. and Beven, K. .J. (1989a) 'Experimental Investigation of the Aggregated Dead Zone Model for Longitudinal Solute Transport in Stream Channels' Proceedings Institution Civil Engineers, Part 2, March, Vol. 87, pp 1-22, Paper 9335.

Wallis, S. G. Guymer, I. and Bilgi, A. A. (1989b) 'Practical Approach to Modelling Longitudinal Dispersion' Proceedings of International conference on Hydraulic and Environmental Modelling of Coastal, Estuarine and River Waters, Bradford, England, September 19-21, pp 291-300.

Webel, G. and Schatzmann, M. (1984) 'Transverse Mixing in Open Channel Flow' Journal of Hydraulic Engineering, April, Vol. 110, No. 4, pp 423-435.

Yotsukura, N. and Cobb, E. D. (1972) 'Transverse Dispersion in Surface Water' Geological Survey Professional Paper, 582C.

Yotsukura, N. and Sayer, W. (1976) 'Transverse Mixing in Natural Channels' Water Resources Research, August, Vol. 12, No. 4, pp 695-704.

Young, P. C and Wallis S. G. (1986) 'The Aggregated Dead Zone Model for Dispersion in Rivers' International conference on Water Quality Modelling in the Inland Natural Environment, Bournemouth, England, L1, pp 421-433.